1996 International Workshop on Millimeter Waves

April 11 - 12, 1996

Palazzo del Capitano del Popolo
Orvieto, Italy

Organized by

MTT North Italy Chapter
MTT Center & South Italy Chapter
MTT Germany Chapter
MTT UK/Ireland Chapter
MTT France Chapter

Sponsored by

Alenia S.p.A.
Alenia Spazio
Andromeda Sistemi
CNET France
IEEE C&S Italy Section
IEEE MTT Society
U.S.A.R.D.S.G. European Research Office
University of Perugia

DISCLAIMER NOTICE

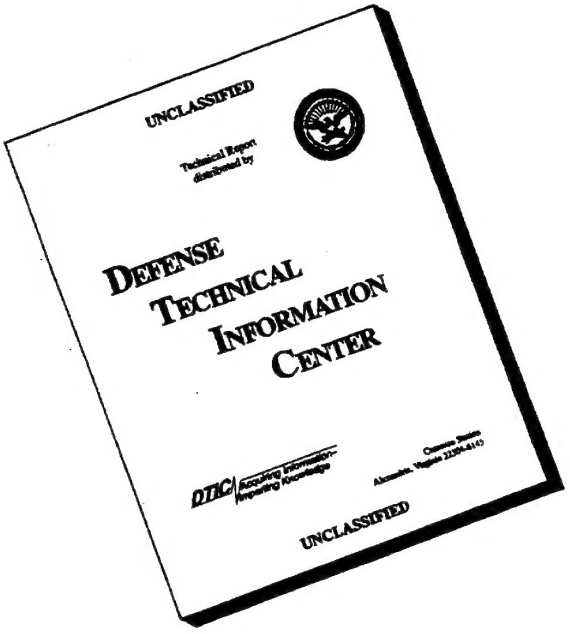

THIS DOCUMENT IS BEST QUALITY AVAILABLE. THE COPY FURNISHED TO DTIC CONTAINED A SIGNIFICANT NUMBER OF PAGES WHICH DO NOT REPRODUCE LEGIBLY.

Steering and Program Committee

Chairman

R. Sorrentino	University of Perugia • Italy

Co-chairman

P. Lampariello	University of Rome • Italy

P. Naldi	MTT North Italy Chapter
P. Bernardi	MTT Center & South Italy Chapter
N. Keen	MTT Germany Chapter
T. Oxley	MTT UK/Ireland Chapter
R. Adde	MTT France Chapter

Organizing Committee

S. Catena	University of Perugia • Italy
R. Giorgini	Itelco S.p.A. • Italy
M. Stovali	University of Perugia • Italy

Secretariat

R. Frontani	University of Perugia • Italy

Foreword

It is our pleasure and privilege to welcome you to the 1996 International Workshop on Millimeter Waves. This is the fourth of a series of millimeterwave workshops started in Rome in 1986, then followed by Perugia (1989) and Orvieto (1992). The workshop has been organized jointly by several European Chapters (Central & South Italy, North Italy, France, Germany, UK) of the IEEE Microwave Theory and Techniques Society.

Scope of the workshop is to provide a forum for discussion and assessment the latest advances in millimeterwave technology and applications. The two-day technical program includes 10 invited talks given by internationally recognized experts and 20 regular contributions. As in 1992, a Special Issue of the French journal Annales des Télécommunications, has planned, containing expanded versions of the invited papers.

The charming town of Orvieto, with its magnificent Cathedral and its picturesque medieval appearance has been chosen once again as the venue of the workshop. The thirteenth century Palazzo del Capitano del Popolo, recently transformed into a modern and efficient Convention Center, will be the site of the workshop.

The Mayor of the city of Orvieto has kindly allowed us to use the Teatro Mancinelli for a classical music trio concert that will be offered to all participants on Thursday evening. A banquet at Maurizio Restaurant is included in the social program.

We are confident that all of you will experience a productive and stimulating technical meeting and hope you will also have the opportunity to enjoy the many artistic beauties of Orvieto and its vicinities.

As usual, the generosity of our sponsors has made possible organizing this event. Special thanks must be given to the organizing committee for their invaluable job and dedicated service: Dr. Sergio Catena and Dr. Maria Stovali from the University of Perugia, and Dr. Rosanna Giorgini from ITELCO.

Roberto Sorrentino and Paolo Lampariello
Workshop Co-Chairmen

Table of Contents

Commercial Millimeter-Wave Applications

L. Raffaelli

Summary

- Introduction
- Wireless TV
- Short-haul Digital Radios
- Automotive Radars
- Other MMW applications
- Conclusions

The World's Hierarchy of Needs

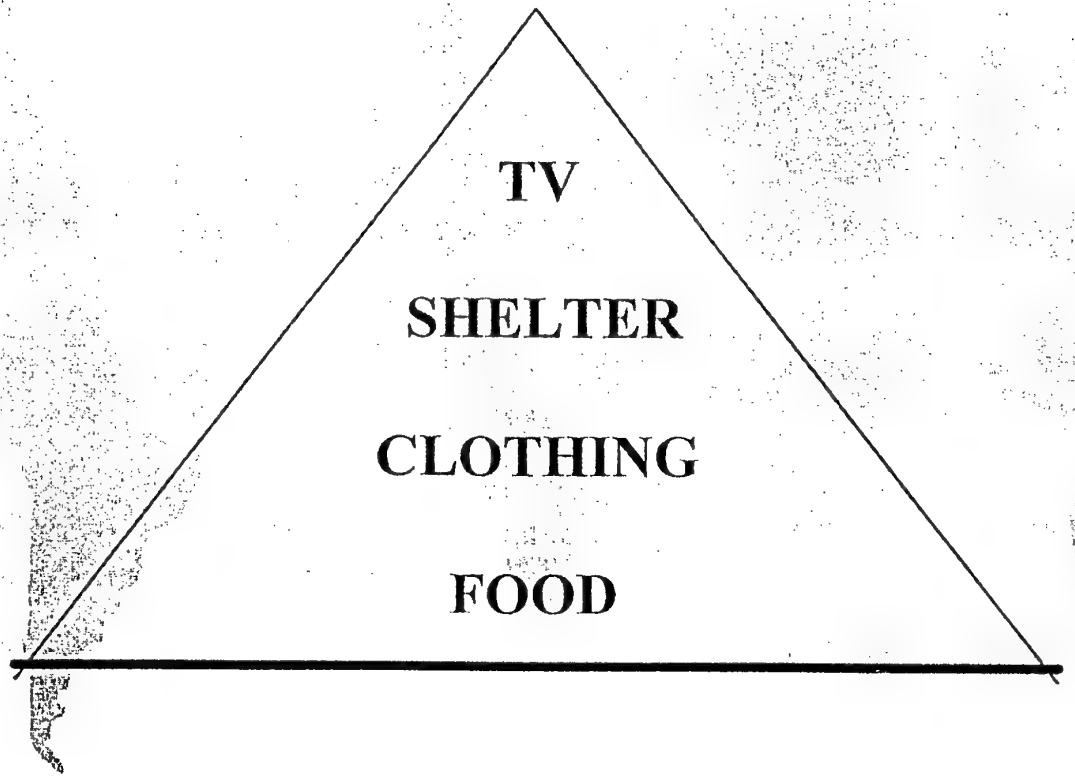

ARCOM

Household in China

With a Television : 55%

With a Telephone : 3%

Source : Paul Kagan Associates,
IEEE Communications Society

Commercial MMW applications

Lamberto Raffaelli

ARCOM,Inc.
No.Andover, MA

Video Delivery Systems

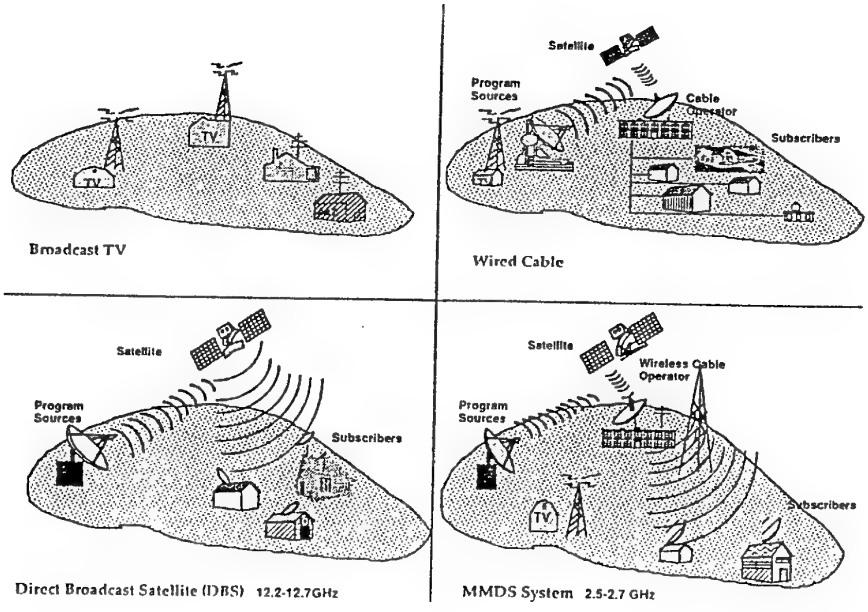

LMDS

Similar in concept to MMDS, operates today in the 27.5 to 29.5 GHz band

Suite 12 (CellularVision) of New York has patented the idea (US Pat. 4,747,160)

Greater channel capacity (200 channels) through digital compression and bandwidth

Interactive option in few channels for Video on Demand (VOD)

ARCOM

LMDS Receiver

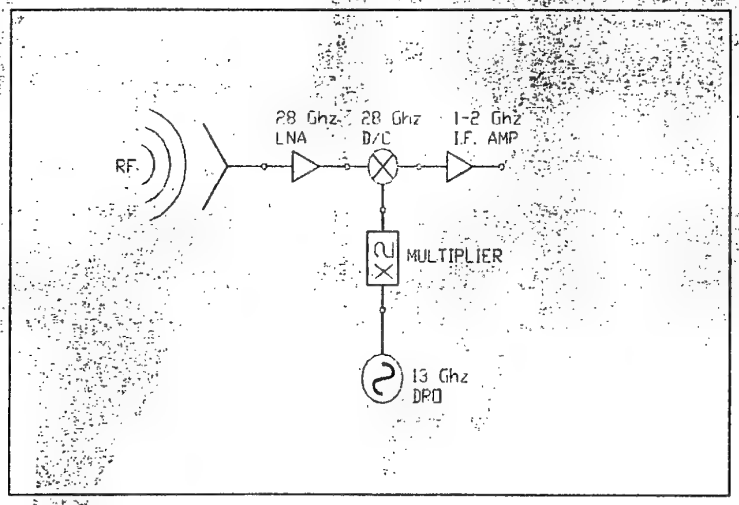

ARCOM

LMDS D/C Figure of Merit

FM=Ant.gain-NFrec.

Solution	4"Antenna (G=26dB)	6"Antenna (G=28dB)	Impr.6"Ant. (G=30dB)
No LNA D/C NF=7dB	19dB	21dB	23dB
4dB NF LNA D/C NF=5dB	21dB	23dB	25dB

ARCOM

LMDS issues

LO stability over temperature +/-3MHz

Planar antenna limited in sidelobes and efficiency

Price of D/C not to exceed $150 in100Kqty

Band could move at 42 GHz due to point-to-point (terrestrial and satellite) radio requirements

Still propagation issues to be resolved

ARCOM

Short-haul Radios

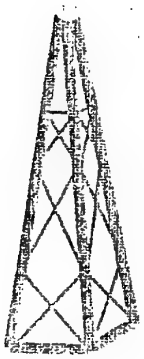

LR

The PCN Cellular Network

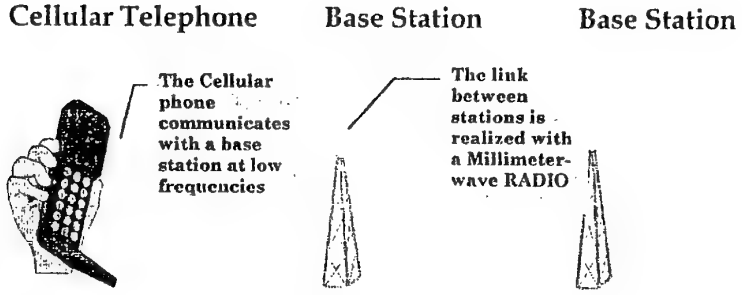

A Millimeter-wave (MMW) Radio

A Millimeter-wave Radio serves the same function as a copper wire or fiber optic cable : it connects (links) two ends.

A Radio includes a Modem/Processing unit and a Millimeter-wave Assembly including the antenna and the Front-end. The Modem processes the data (telephone channel) and moves it to the front-end that transmits and receives through the antenna.

Radios

Spectrum	MW	MMW
Distance	Long-haul < 25 Miles	Short-haul < 10 Miles
Pout	up to 10W	100-200 mW
Antenna	2 to 8 feet	1 to 2 feet
TX/RX locat.	On the Gnd	Behind Antenna
Band	up to 18 Ghz	23, 26, 28, 38, 60 GHz
Selling Price	up to $25K	< $5K
Microwave Content	20 to 30 %	30 to 40 %
Market	Flat	Growing (25-30 %/ yr)

LR

MMW Radios

Technology/ Transmitter	Strength	Weakness
Waveguide/ Gunn based	Mature Techn. Low NRE Phase Noise	Size Gunns Prod. Cost
Planar/ MIC/MMIC Fundamental	Size Prod. Cost Reliability	Band-width NRE Phase Noise
Planar/ MIC/MMIC Multiplied	Size Reliability Band-width	NRE Prod.Cost

LR

Radio Transmitter

Approach	**Cost**	**Phase Noise** at 38 Ghz (dBC/Hz at 100 KHz)	**Comment**
Fundamental P-Mesfet MMIC	Lowest	70	Requires 38 Ghz Harm. Mixer
Fundamental Planar Gunn	Good	80	It is still a Gunn
Multiplied Si-Bip/Fet/HBT	Fair	85	Prescaler available

LR

Multiplied Source

- Si-Bipolar Source at 4 GHz exhibits 98-105 dBC/Hz at 100 KHz.
- A X10 Multiplier will deteriorate phase noise by 20 dB MIN
- Resulting Phase Noise at 40 GHz in the 78 to 85 dBC/Hz at 100 KHz

LR

MMIC Opportunities

- PAs with P1dB up to 23 dBm
- LNAs with NF=4 dB at 38 GHz
- Multipliers (X2, X4, X8) and amplified multipliers
- Power Adjust and Muting function
- LNA/ IR Down Converters
- Up-Converters

LR

MMW Radios
MMIC Opportunities

Band	LNA NF	Psat (1st gen.)	P1dB (2d gen.)
23 Ghz	4 dB	23 dBm	23 dBm
28 Ghz	4.5 dB	22 dBm	22 dBm
38 Ghz	5 dB	21 dBm	21 dBm

LR

38 GHz Transmitter

ARCOM P/N 38TX-005

- Bandwidth 37 to 40 GHz
- Pout + 20 dBm
- Power Adj. 40 dB MIN
- Harmonics 20 dBC MIN
- Spurious 60 dBC MIN
- VSWR Out 2 : 1
- Bias 400 mA @ 12 V

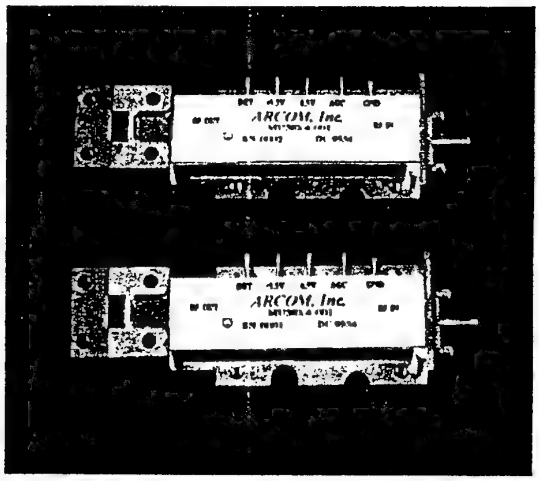

60 GHz Transceiver

ARCOM P/N 60TR005

- Bandwith 60 +/-0.5 GHz
- Output Power +13 dBm
- RX C. Loss 10 dB
- Tuning Speed 100 MHz
- Phase Noise 75 dBC/Hz @ 100 KHz
- VSWR 2 : 1 MAX
- Ref Input Level 15 dBm
- DC Current 1.2 A @ 6V

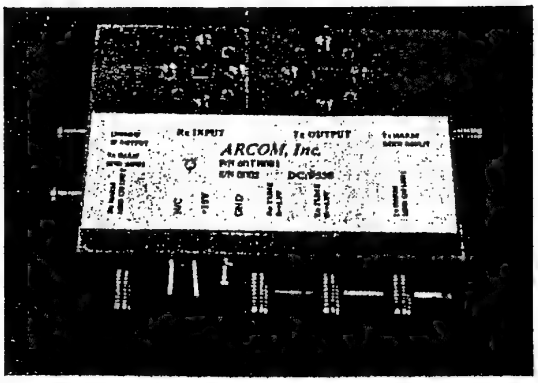

Automotive Sensors

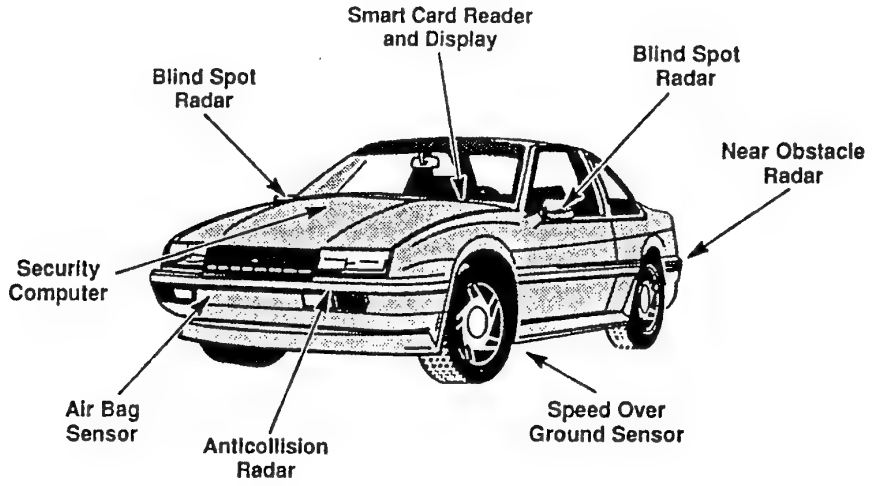

AUTOMOTIVE CRASHES

Source : George Parker, IVHS Review

- Highway crashes 6th leading cause of death in the USA
- #1 cause of death for people under 25
- Costs associated with 44,531 deaths and 5.4M injuries was $137B in 1990
- 93% of crashes due to human factors

LR

AUTOMOTIVE RADAR SYSTEMS
FRONT END REQUIREMENTS

- HIGH ANTENNA DIRECTIVITY
- SMALL SIZE/VOLUME
- OPERATE IN ADVERSE WEATHER
- HIGH RELIABILITY (MTBF=100,000 HRS)
- LOW COST ($100-$200 FOR 100K Units/Year)

→ *MMW RADAR*

Forward looking Radar
Frequency Band

● Europe	76 to 77 GHz
● USA	24, 77, 94 GHz and more
● Japan	60 GHz

LR

AUTOMOTIVE RADARS
SYSTEM TRADEOFFS

	FMCW	PULSED
OSCILLATOR	HIGHER COMPLEXITY Low Phase Noise Low Residual FM High Linearity (May Require Linearizer)	LOWER COMPLEXITY Mod Sense Stability
TRANSMIT POWER	HIGHER AVG POWER (5-10 mW)	HIGHER PEAK POWER (40 mW @ 0.1%)
T/R SWITCHING	NONE	FAST
ANTENNA(S)	DUAL ANTENNAS (OR DUPLEXER)	SINGLE ANTENNA
MICROWAVE POLLUTION	HIGHER	LOWER

Competing Technologies

Technology	Strength	Weakness
MMIC	Prod. Cost Size, Weight Reliability	Devel. Time and cost New technology
MIC	Quick turn around Mature technol.	Prod. cost Repeatability
Waveguide	Mature technol. Short Dev. time Low NRE	Prod. cost, Size Power Consumption

LR

Monolithic Technology Alternatives

Technology	Approach	Pros	Cons
0.15 Micron P-HEMT	Fundam. Source	Size/Cost Power Cons. Single chip	Not in prod. yet Phase Noise
0.25 Micron P-Mesfet	Multiplied Source	Mature process	Power Cons. Size/Cost
Schottky, PINs	Multiple Chips	Low Cost/mm Ideal for D\C and Switches	3 chips min

LR

Transmitter Source Device Technology

Solution	Phase Noise	Effic.	Reliab.	Cost
InP Gunns	Good	Fair	Fair/Poor	Poor
GaAs Gunns	Good	Poor	Fair	Good
Power Mesfet	Poor	Poor	Good	Fair
PHEMT	Poor	Good	Good	Good
HBT	Good	Good	N/A	N/A

LR

Active Device Parameters

Device/ Param.	Fmax	1/F Corner Fref.	Padd Effic. %
Gunn	100 Ghz	N/A	1
0.25μ Pmesfet	50 GHz	10 MHz	2
0.15μ PHEMT	100 GHz	> 10 MHz	5-10
1μ SiGe HBT	60 GHz	0.1-1 KHz	>10
2μ GaAs HBT	70 Ghz	1-10 KHz	>10

LR

Oscillator Technology

Solution	Phase Noise at 77 Ghz, at 100 Khz
WG Gunn	80-85 dBC/Hz
Planar Gunn	75-80 dBC/Hz
MMIC X2 Mesfet	60-65 dBC/Hz
MMIC PHEMT	55-60 dBC/Hz
HBT	70-80 dBC/Hz

LR

MMW Automotive Radars
Why MMICs

- **Low cost** in volume production
- Small size and weight
- Low power consumption
- High Reliability

LR

ANTENNAS

Type	Perform.	MB Cap.	Integrat.	Cost
Lens	Good	Good	Poor	Fair
Planar Array	Fair	Poor	Good	Good
Mech. Scanned	Good	Great	Fair	Poor

LR

Automotive Radars
Key Ingredients to succeed

- Link to Automotive Industry
- Radar Experience
- MMW Experience
- Semiconductor capability
- Large Volume Manufacturing capability
- Funding to support long term investment

LR

Automotive Radars
Why not !

- Large investment required for chip development and module manufacturing (4 to 10 $M)
- Difficult customers
- Any profit ?
- Teaming required
- Product Risk

LR

CONCLUSIONS

- The MMW commercial market is offering unprecedented volume opportunities to the Microwave Industry.
- This market is growing fast in the direction of consumer products : very large volume, very low cost, and very competitive.

Development of a Low-Cost 35 GHz Radar Sensor

A. A. Efanov, C. G. Diskus, A. Stelzer, H. W. Thim, K. Lübke and A. L. Springer

Development of a Low-Cost 35 GHz Radar Sensor

Andrew A. Efanov, Christian G. Diskus, *Member*, *IEEE*, Andreas Stelzer,
Hartwig W. Thim, *Senior Member*, *IEEE*, Kurt Lübke and Andreas L. Springer

Abstract - **A 35 GHz low-cost RF front-end unit suited for automotive applications has been constructed. The unit consists of both receiving and transmitting corporate-fed microstrip patch array antennas, a microstrip directional coupler, a monolithic GaAs FECTED oscillator and a single Schottky diode mixer. Inexpensive microstrip technology has been used yielding a good compromise between cost factor and technical performance.**

INTRODUCTION

Millimeter-wave radar sensor systems especially suited for the automotive applications were intensively developed during the last few years. Combination of a low-cost technology together with advanced electrical characteristics and high reliability is a cornerstone requirement for an application in the automotive industry. Since the microwave front-end unit is the key unit determining the system's performance and cost, it is the most crucial part of the whole system. This paper presents the results of the authors' solution of the problem, which yields a good compromise between the above mentioned contradictory requirements.

SYSTEM CONFIGURATION

The block diagram of the front-end unit is shown in Fig. 1. This configuration is suitable for both Doppler CW (continuous waveforms) as well as FM (frequency-modulated) CW radar systems. In the Doppler CW mode the oscillator generates unmodulated oscillations leading to an output IF frequency which is proportional to the relative velocity of a target. In the FM CW radar mode the frequency of the transmitted signal is varied as a function of time in some manner making the output IF frequency proportional to the distance between target and the radar.

During the course of this work two prototypes with different antennas have been designed. In order to minimize costs a microstrip technology has been used for both the passive and active parts of the front-end units. The prototypes have been fabricated and tested in the Doppler CW mode.

ANTENNAS

Depending on a specific application, various requirements can be specified for the transmitting and receiving antennas. Two linearly-polarized corporate-fed microstrip patch array antennas have been designed for the system. The first one is a 4x4 array antenna with 16 degrees beamwidth and 17.5 dB (isotropic) power gain. The second one is a 8x8 array antenna with 8 degrees beamwidth and 21.5dB (isotropic) power gain.

A relatively inexpensive RT/duroid 5880 (a trademark of Rogers Corp.) substrate material of 0.254 mm thickness has been used for the fabrication of the antennas and the 10-dB directional coupler. The passive part has been made using standard photolithography and etching-technology, and has been covered by a gold film in order to minimize losses. More detailed description of the antennas is given in (1). Fig. 2 shows a photograph of the 4x4 array antenna module.

This work was supported by the Austrian Science Foundation (FWF) under contract No. P8697.
A. A. Efanov is with the Aerospace Monitoring Center, Krylova St. 19, Lvov, 290044, Ukraine.
C. G. Diskus, A. Stelzer, H. W. Thim, K. Lübke and A. L. Springer are with the Microelectro-electronics Institute, University of Linz, Altenberger Strasse 69, A-4040 Linz, Austria

OSCILLATOR

In order to minimize costs a special planar Gunn diode has been used instead of a sophisticated transistor oscillator. This approach relaxes the demands on the resolution of the lithography. The device under question is a transferred electron device with a specially designed cathode contact, which suppresses the formation of travelling domains. This is accomplished by negatively biasing a Schottky gate contact which overlaps the cathode contact. The electron injection into the drift zone is controlled by the electric field underneath the gate, thus producing a stationary high field domain. Further details of this Field Effect Controlled Transferred Electron Device (FECTED) has been published in (2).

MIXER

Using the FECTED oscillator as a self-oscillating mixer an IF signal of about 1 mV_{eff} has been obtained with a moving metallic target at a distance of 2 - 3 meters. The RF signal received by the patch antenna was around 10 μW, the power output of the oscillator was 3.5 mW. The same sensitivity has been obtained, when a commercially available mixer diode was used. Eventually, a single GaAs Schottky mixer diode will be used in this module and this work is presently in progress.

CONCLUSION

An inexpensive configuration of the microwave part of a 35-GHz radar sensor system has been presented. The described approach makes it possible to achieve acceptable system performance with low-cost technology.These front-end units can be used in the velocity-distance radar systems with an operational range of several meters. A further reduction of the cost can be achieved by monolithically integrating the oscillator, mixer and directional coupler on a single chip.

ACKNOWLEDGEMENTS

The authors would like to thank G. Hofmann, J. Katzenmayer and G. Hinterberger for fabricating the devices. One of the authors (A.A.E.) thanks Prof. H. Thim for the invitation to participate in this project at the Microelectronics Institute of the University in Linz.

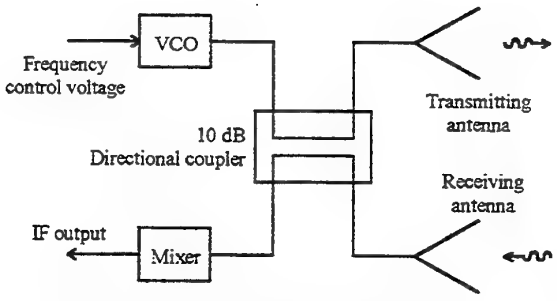

Fig. 1: Block diagram of the front-end unit

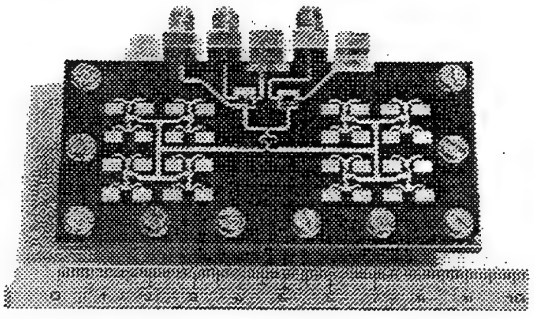

Fig. 2: Photograph of the front-end unit

(1) A. A. Efanov and H. W. Thim, „Corporate-Fed 2x2 Planar Microstrip Patch Sub-Array for the 35 GHz Band", Antennas and Propagation Magazine, vol. 37, no. 5, pp. 49-51, Oct. 1995

(2) K. Lübke, H. Scheiber and H. Thim, „A Voltage Tunable 35 GHz Monolithic GaAs FECTED oscillator", IEEE Microwave and Guided Wave Letters, vol.1 pp. 35-37, February 1991

A Short-Range, High-Resolution Millimetre-Wave-Surface Movement Radar

G. Galati, M. Ferri, M. Naldi and F. Marti

A short-range, high-resolution millimetre-wave Surface Movement Radar

by Gaspare GALATI (#), Mauro FERRI (*), Maurizio NALDI (#) and Fausto MARTI (#)

(#) Tor Vergata University, DISP, Via della Ricerca Scientifica, 00133 Roma, ITALY
(*) Oerlikon Contraves Italiana, Via Affile 102, 00131 Roma, ITALY

1) Airport surveillance requirements and the use of radar

Airport capacity is a bottleneck in air transport ; advanced Surface Movements Guidance and Control Systems (SMGCS) are being studied to guarantee a safe and expedite traffic of aircraft and other vehicles in busy airports to maximise their capacity in all weather conditions. The SMGCS functions are surveillance, guidance, monitoring and planning. The surveillance, object of this paper, aims to detect, locate and identify/classify vehicles and obstacles in the movement area , as an input to operational displays and to collision avoidance logic. Surveillance requires data fusion from different sources , the main sensor being the Surface Movement Radar (SMR) which is capable to detect non co-operating targets and obstacles.
Moreover, advanced SMR's are expected to supply high resolution radar images of aircraft for classification and aid in the tracking process.
The main radar requirements are :

- Probability of detection equal to 90% (with a probability of false alarm equal to 10^{-6}) for a target having, in the X band (around 9 GHz), a radar cross section of 1 sq. metre ; this performance should apply to all the movement area and for all weather conditions, including fog and rain up to 16 mm/hr .
- Data renewal interval not greater than 1 second .
- Resolution better than 6 metres.

2) Rationale for a millimetre-wave radar

Present-day SMR's, mostly operating in the X or K_u band (around 16 GHz) suffer from : (i) limited coverage with masking effects due to obstacles, (ii) large antenna dimensions (e.g. 6 m or more) for the assigned resolution with difficult and costly installation, (iii) unfavourable cost/effectiveness ratio.
To overcome these problems, a new solution has been studied and developed under the auspices of the Italian Research Plan on Transportation (PFT2) of the Council of Research (CNR). This solution is based on a network of short-range SMR's (S-MRN : Surface- Miniradar Network) based on MMW technology to reduce dimension and weight [1], [2].
The use of multiple sensors in the network (in most cases, from 2 to 4 sensors, according to the layout of the airport) avoids masking effects and allows to reduce the maximum range to 1.5 Km in the worst weather conditions (instead of 5 or 6 Km) ; hence, low power radar (miniradar) can be used.
Choice of the operating frequency of the miniradar [3] has been made as a trade-off between the cost and the performance of various solutions. The frequencies around 35 GHz , 77 GHz and 95 GHz (W band) have been taken into account according to the WARC (World Administrative Radio Conference) 1992 . Evaluations have been done for:

- both clear and rainy weather (16 mm/h rainfall) ;
- same antenna dimensions and same transmitted power ;
- radar cross-section variable with the frequency according to the inverse of the wavelength (the increase of the RCS with the frequency has been also demonstrated in W-band by Oerlikon Contraves in field measurements).

Under clear weather condition, the range performance at 95 GHz is somewhat better than the others (as an example it is : 3 km at 95 GHz , 2.5 km at 77 GHz, 1.6 km at 35 GHz).
On the other hand, in case of rainy weather propagation with 16 mm/h rainfall, the differences among the three performances are minimal, especially at short range (as example for 3 km at 95 GHz it is still about 3 km at 77 GHz and 4 km at 35 GHz). This effect is mainly due to the fact that the increase of the propagation losses for the higher frequencies is compensated by the increase of the RCS, at least up to 1500 m, where the performance in rain is nearly the same. Therefore, the choice of the frequency has been based on antenna dimension. In order to satisfy the stringent resolution requirement (< 0.2° azimuth beamwidth), a larger and expensive antenna would be necessary at the lower frequencies. Considering that the cost of a W-band solid state transmitter (the solid state solution being possible because of the short range) is considerably less than that of to a large antenna at 35 GHz, the W band results as the best choice. By using this higher frequency, it is possible to satisfy the resolution requirements with an antenna having very small dimensions resulting in reduced installation problems.

3) *Characteristics of the miniradar*

The main characteristics of the MMW miniradar (Fig 1), which must operate in frequency diversity in the W band, are :

- Antenna : with inverted $cosec^2$ pattern in elevation (with near field focusing) , narrow (less than 0.2 degrees) in azimuth , circular polarisation against rain . The technical solution is an offset-fed reflector not exceeding 1mx1m and rotating, with the RxTx box, at 60 RPM .
- Transmitter : pulse length equal to 0.2 μ s, peak power not less than 20 W , pulse repetition frequency between 40 and 70 KHz. The solution is solid state , based on an IMPATT devices.
- Receiver : superheterodyne, with a logarithmic final amplifier (input dynamic range : greater than 90 dB)..
- Radar Processor : digital, with non-coherent integration of pulses, Constant False Alarm Rate (CFAR) threshold, plot extractor .
- Central Processor : with multiple radar fusion and image processing to extract shape , centroid and orientation angle of the aircraft.

An engineering model of this sensor will be tested in house and in an airport during 1996, to check the design choices.

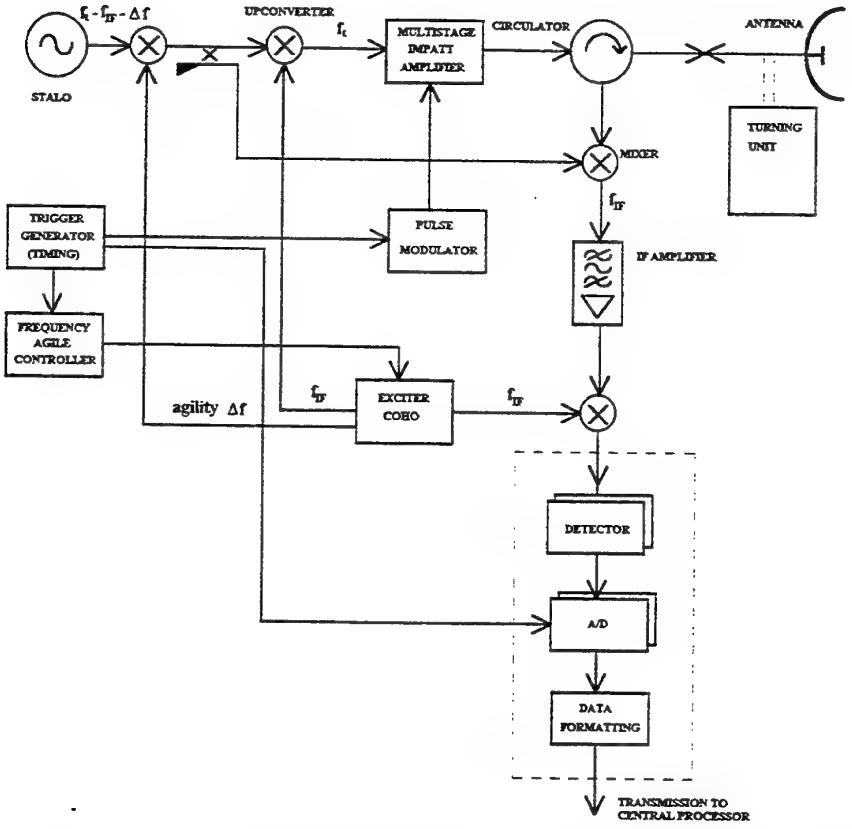

Figure 1 : Block diagram of the W-band miniradar of the S-MRN . The whole part is rotating with the antenna.

REFERENCES

[1] M. Ferri, G. Galati, F. Marti: "Advanced Radar Techniques for the Air Transport System: the Surface Movement Miniradar Concept"; IEEE National Telesystem Conference, S. Diego (USA) May 26-28 1994.

[2] G. Galati , M. Ferri , F. Marti, M. Naldi:"A distributed Surveillance System for Surface Movement Guidance and Control", Advanced Workshop on Air Traffic Management ATM 95, Capri, Italy October 2-6 1995

[3] M. Ferri, G. Galati, F. Marti:" Distributed advanced surveillance for SMGCS", ECAC APATSI and EC Workshop on SMGCS, Frankfurt, 6-8 April 1994.

Millimeter-Wave Indoor Lan Transceiver Development

Y. Takimoto

MILLIMETER-WAVE INDOOR LAN TRANSCEIVER DEVELOPMENT

Yukio Takimoto
Advanced Millimeter Wave Technologies Co. Ltd.
(YBP, Hodogaya, Yokohama, Japan)

1. INTRODUCTION

Various millimeter-wave communications systems for commercial use are under development in many countries. Short range, very compact, low to ultra-high speed data transmission systems including local area network (LAN) are mostly expected to be realized.

This paper shows basic configuration of transceivers and MMICs used in the Minimum Delay Spread LAN we have proposed and fabricated, after the short talk on the development of millimeter-wave communication systems in Japan.

2. MILLIMETER-WAVE COMMUNICATIONS IN JAPAN

2.1 Development History

The research and development of millimeter-wave band in Japan started in 1950s along with the development of a millimeter-wave mass volume communication system using over-size circular waveguides after the Bell Telephone Laboratories.

The Wireless System Laboratory of NTT vigorously promoted research into millimeter-wave band and systems and, in 1972, constructed a 23-km length circular waveguide line between Mito city and Tokai village in Ibaragi prefecture for practical testes. However, due to the prompt development of much economical optical fiber communications, this practical research was terminated at the completion of experimental millimeter-wave communication system in 1975.

After this, frequency enhancement effort in Japan rapidly moved into the optical fiber field, and serious research into millimeter-wave communication systems and device technologies were consequently sluggish for long time.

Since 1980s, research and development of millimeter-wave device technologies have been advancing again in Japan. The millimeter-wave technologies have been used in not only short-distance sensing systems and short-distance communication systems, but also scientific and commercial use not for military. In addition, the possible future shortage of lower frequency spectrum have forced to develop the commercial millimeter-wave application systems in Japan.

As shown in Table 1, the Ministry of Posts and Telecommunications (MPT) has initiated its subsidiary institutes to make efforts in millimeter-wave development since 1977[1]. Of those activities, the MPT and the millimeter-wave sensing system study and research committee ('84-'91) significantly worked in general applications system study[2], which produced four R&D projects. One is Robotech Laboratory Co. devoted on the vehicular locating and control system ('87-'93), another is Advanced Millimeter-Wave Technologies Co. taking in the millimeter-wave communication system and MMIC device development during '91 to '96, the third is millimeter-wave indoor communications study committee ('91-'93), and the last one is the establishment of Association for the Promotion of Millimeter-wave Development and Utilization (APMDU) organized with more than 80 private sector members in 1991.

In 1994, the Hokkaido (northern Japan) section of the MPT have organized a study committee on millimeter-wave applications for snow lands, and are conducting several experiments on the effectiveness of automotive radar sensors, and on the fundamental millimeter-wave characteristics of snow and ice.

Meanwhile, the MPT settled the frequency guide-lines in November 1992, in order to advance the nation-wide development activities: 59-60 GHz is assigned experimental frequency band, and 59-64 is specified a to-be-developed band for broad applications. With this

Table 1 R&D Activities of Millimeter-Waves in Japan

	'77	'83	'84	'85	'86	'87	'88	'89	'90	'91	'92	'93	'94	'95
CRL	77-85 Atmospheric propagation study				86-91 Scattering characteristics of materials						92- Indoor communication technologies			
MPT	77- System study and research			Sensors, Key technologies		Automotive sensors	ID card	Building application		Indoor propagation	92 Allocation of experimental band in 60 GHz		94-96 Committee on MM-wave applications for snow lands	
MKK			84-91 Millimeter-wave sensing system study and research committee							91-93 Millimeter-wave indoor communication study committee				
RCR							88-90 MMW application study			91- MMW development & application promotion council				
KTC						87-93 Robotech Laboratory Co., Ltd Application on vehicular locating & control				91-96 Advanced MMW Tech. Co. Very small comm. system & MMICs				

CRL: Communications Research Laboratory,
MKK: Radio Equipment Inspection and Certification Institute,
RCR: Research and Development Center for Radio Systems,
MPT: Ministry of Posts and Telecommunications,
KTC: Japan Key Technology Center.

assignment, the MPT simplifies the radio application documents and procedure necessary for the license. This conception aimed so that every R&D effort is focused on a single band, and every millimeter system planner can get various devices and technologies so easy and at low cost.

In 1995, the MPT decided a technical standard for automotive radar in 60.0–61.0 GHz, 10 milli-watt, and antenna with 40 dB maximum gain, and is then planning to decide a technical standard for millimeter-wave local area network (LAN).

2.2 Currently Used Commercial Systems

50 GHz Simple Radio System as shown in Fig. 1 has been in-use since 1985, and the operating systems arecounted over four thousands. The main features are listed in Table 2, and capable of bi-directionally transmitting an analog TV signal with two voice channels or 6.3 Mbit/s data signal. This system features: (a) a licensed operator is not demanded, (b) easy application procedure for radio station license, (c) fixed and mobile stations, (d) no cable engineering required, (e) rainfall attenuation limits the span in several kilometers.

This system is also worthwhile when used in the following applications, (a) video-phone meeting, private telephone or data network of an enterprise among its separate buildings, (b) wide area TV monitoring such as dams, construction sites and parking lots, (c) TV news-gathering signal links, (d) CATV networks, etc.

Table 2 Simple Radio System

Frequency	50 GHz, FM or FSK
Capacity	one TV or 6.3 Mbps data
Output Power	<15mW
Span	<3km is recommended.

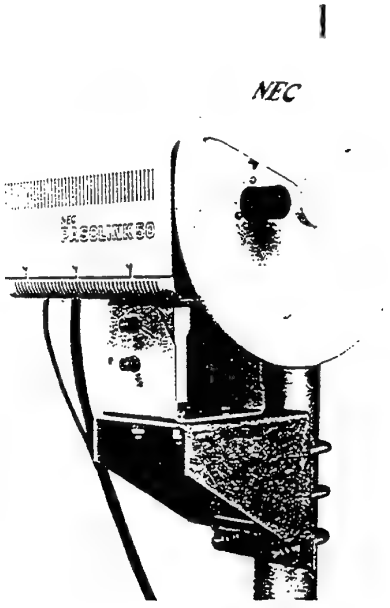

Fig. 1 50 GHz Simple Radio System

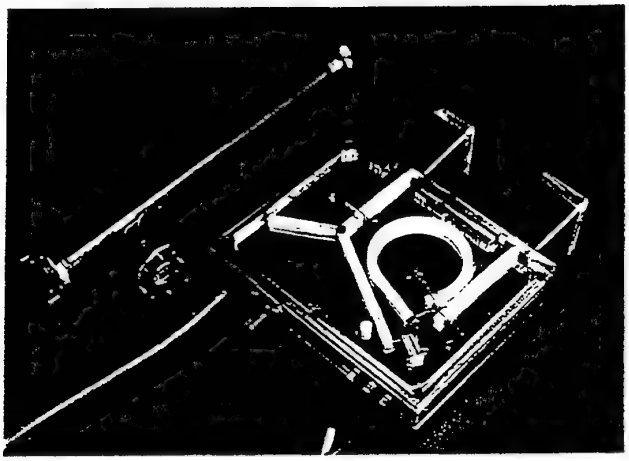

Fig. 2 60 GHz NRD Guide Transceiver

Table 3 NRD Transceiver

Oscillation	Gunn Dioide (+17.5dBm)
Freq.	59.2, 59.7 GHz
Modulation	AM (>15dB), PIN diode
Mod. Sig.	100 Mbs data,
Receiver	Diode balanced mixer
	8.5 dB loss at 500MHz IF
size	80mm x 100mm

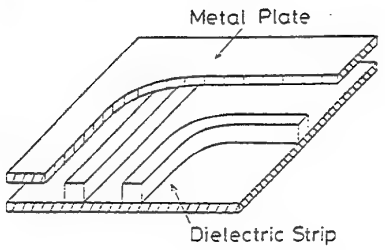

Fig. 3 NRD Guide

Fig. 2 shows 60 GHz compact transceivers using MIC modules and NRD (Non-Radiative Dielectric) guide technologies[3], being able to transmit 155 Mbit/s data over more than 100 meters (Table 3). NRD guide consists of square rods sandwiched between two parallel metal plates, with slightly shorter gap than a half wavelength as shown in Fig. 3. This guide features very small transmission loss of about 4 dB/m comparing to microstrip line (several tens dB/m), and easy to fabricate 60 GHz millimeter-wave circuits.

2.3 Principal Development of Future Millimeter-Wave Communications

As well known, the millimeter-wave technology makes it possible to transmit very wide or high-speed signals over short distances. Therefore, most principal development is to provide broader bandwidth for multimedia transmissions to the latest introduced personal communication systems (PCS) and to the wireless local area networks.

As well as the PCS terminal is effective only within a microcell, the millimeter-wave mobile telephone does also effective only in a picocell of much shorter radius. On the back of all picocell zones where the central station and the base stations are assigned, a fixed distribution network is necessary to be provided as shown in Fig. 4[4] which can transmit higher data rate sufficient for the summed data rate corresponding to a maximum number of terminals operating simultaneously in each picocell. Although this distribution network could be realized by the fixed millimeter-wave radio links, the fiber optical network is recommended in cost and easiness.

At the base stations, the recently grown interaction technology between microwave/millimeter-wave and optics will be important to interface fiber-optics with millimeter-waves.

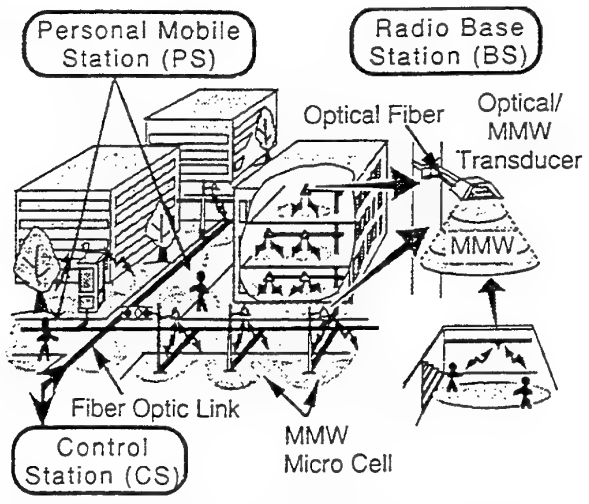

Fig. 4 Future Image of Personal Mobile System

Currently, wireless LAN systems of 2.4 GHz and 19 GHz bands as well as

of infrared regions are available for commercial products in Japan. The data handling rates of these systems are as high as 10 Mbit/s, which is compatible with that of the wired-Ethernet system widely used. The 2.4 GHz wireless LAN is not influenced by shadowing and reflected waves owing to low frequency and the spread spectrum modulation. However, the 19 GHz system managed to get rid of those inconveniences through route diversity using six sector antennas in both hub and user terminals applying in the horizontal propagation system.

The latter system produces merits of delay equalizer omission and of antenna pointing easiness. However, it has drawbacks of complexity and expenses due to route diversity configuration, and need to provide higher sensitive or higher output power transceivers making-up-for power reduction of reflected waves.

The two major laboratories of NTT and CRL in Japan are studying and developing the same horizontal propagation system[5], with simulating ray-tracing method and experimenting modem characteristics against reflected power ratio.

In contrast to indoor horizontal propagation, the AMWT proposed rather vertical propagation system, named Minimum Delay Spread (MDS) LAN which is shown in the following sections.

3. MINIMUM DELAY SPREAD LAN

3.1 System Configuration

In an office transmission, where the millimeter-wave propagates straightly just like a light wave, the shadowing possibility is high due to moving element or worker's walking. In addition, the millimeter-wave propagates in complicated way of reflections by the movement of doors and window shades. And those reflections cause frequency selective fading or inter-symbol interferences, which deteriorate the bit error rate characteristics of digital signal transmission.

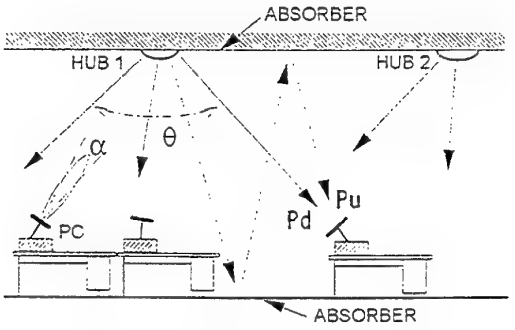

Fig. 5 MDS LAN Configuration

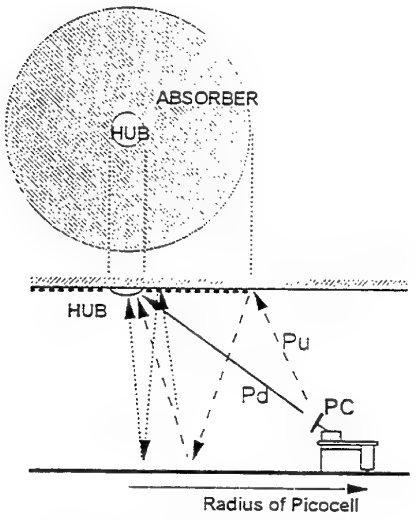

Fig. 6 Effective Absorber Area

The proposed MDS indoor LAN shown in Fig. 5 [6] organizes pico-cell zones of about 10 meter diameter, provided with a broad angle hub station antenna attached to the ceiling in the center of the each zone and several wireless subsidiary terminal stations with sharp directional beam antennas in the zone. The limited use of line-of-sight millimeter-wave, propagating in rather vertical direction, is effective to reduce the shadowing possibility which may be caused by the worker's moving, and to reduce the undesired signal reception.

In order to reduce the multi-path interferences, partial usage of radio wave absorber is useful. Our system considerations[7] resulted the absorber area is sufficient to partially cover the ceiling around the hub station antenna, if the system uses directional beam antennas in the subsidiary wireless terminals (Fig. 6). The ratio of the desired signal power to the undesired interference power can be estimated more than 26 dB in the above system, which is enough power ratio to demodulate QPSK signal in less than 10^{-5} bit error rate.

The system parameters of the MDS LAN are listed in Table 4.

Table 4 System Parameters of Minimum Delay Spread LAN

Information	100 Mbps
Direction	bi-lateral
Zone Diameter	8 meter
Ceiling Height	3 meter
Frequency	59-60 GHz
Modulation	FSK
Output Power	10 mW
Noise Figure	8 dB
Ant. Gain(Hub)	3 dBi
Ant. Gain(User)	20 dBi
Receiv. Level	-49 dBm
Noise Level	-79.9 dBm
Interference	-75.8 dBm

This system configuration brings simple circuit configuration, that means reduction of the route diversity, diplexer, adaptive delay equalizer, FEC codec, and system cost finally.

3.2 Brass-Board Models of 60 GHz LAN Transceivers

As shown in Fig. 7, the AMWT has fabricated and is testing the brass-board models[8] of 60 GHz wireless LAN transmitting 100 through 155 Mbit/s ultra-high speed data, using 60 GHz MMIC chip-sets they have developed.

The AMWT have also developed two types of 10 Mbit/s Ethernet packet signal transmitting wireless LAN systems operating in 60 GHz band. One model employs a preassigned TDMA/TDD(Time Division Multiple Access/ Time Division Duplex) scheme with FSK modulation as shown in Fig. 8, and the other model uses CSMA/CD (Carrier Sense Multiple Access / Collision Detection) with FDD (Frequency Division Duplex) scheme. In both models, circular polarized antennas are used for the easiness of polarization angle alignment, and those antennas are equipped separately for the transmission and the reception.

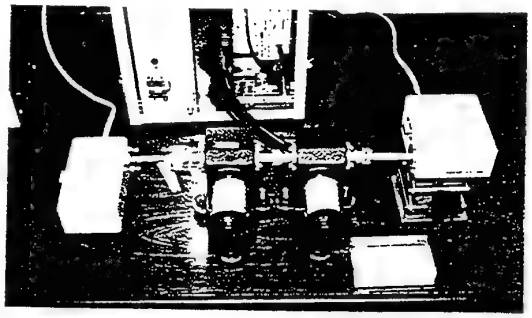

Fig. 7 60GHz/100Mbps TX and RX (A)

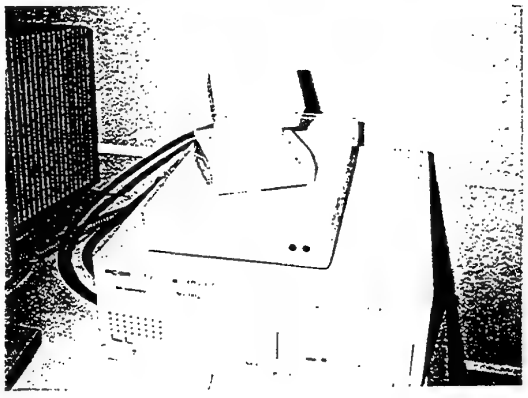

Fig. 8 60GHz 10Mbps Transceiver (B)

The RF transmitter applies 60 GHz direct frequency modulation using a VCO stabilized with a dielectric resonator, and the RF receiver features a simple filter-less RF circuit using image-rejection down-conversion technique. Those brass board system parameters are realized as shown in Table 5.

3.3 Developed MMICs for Transceivers

High performance 60 GHz MMICs based on pseudomorphic heterojunction technologies have been developed also by the AMWT. They are dielectrically stabilized oscillators for 60 GHz carrier sources and modulators, a wide-band power amplifier, a low noise down-converter and so forth [9].

In the oscillators and power amplifiers, 0.15 μm gate N-AlGaAs/InGaAs/N-AlGaAs HEMTs are adopted. The HEMT with a 100 μm (50 μm x 2) width gate has 240 GHz fmax and 500 mA/mm maximum drain current. In the low noise MMICs, 0.1 μm gate N-InGaP / InGaAs / GaAs pseudomorphic HEMTs are adopted, where the MSG is 10.4 dB at 60 GHz in 100 μm width gate.

The representative MMICs are listed in Table 6.

The oscillator which

Table 5 Main Specifications of Brass-Board Model

BB Model	High Speed Wireless LAN		Ultra-High Speed WLAN	
	Type A	Type B	Type A	Type B
Comm. Systm	TDMA/TDD	Full Duplex/FDD	One Way	One Way
Modulation	2-FSK	2-FSK	QPSK	8-DPSK
Trans. Sig.	10 Mbps	10 Mbps	100 Mbps	155 Mbps
Trans. Power	10 dBm	3 dBm	6 dBm	-10 dBm
NF	12 dB	6 dB	12 dB	6 dB
Ant. Gain(Hub)	0 dBi	5 dBi	0 dBi	5 dBi
(Terminal)	15 dBi	19 dBi	15 dBi	19 dBi

Table 6 Features of Developed MMICs

	DR-OSC	DR-VCO	WB Power Amp.	Low Noise Down-Conv.
Chip size:	2.22x3.37mm^2	2.22x2.22	1.07x2.22	1.7x3.45
Freqyency:	59.55 GHz	60.0 GHz	52.5 - 62.5 GHz	59 - 61 GHz
Output power:	10.1 dBm	6.6+/-0.3dBm	16.5 dBm	+20.7 dB(Conv. Gain)
Phase Noise: (100kHz off carrier)	-90dBc/Hz	-80dBc/Hz	-	3.6 dB(Noise Figure)
Linear Gain	-	-	14 dB	25dB(LNA gain)
Sensitivity	-	55 MHz/V	-	IF:140 MHz
Stability:	1.6 ppm/deg.C	-4.1 ppm/deg.C	-	-

frequency is stabilized with dielectric resonator (DRO) exhibits 10.1 dBm output power, low phase noise of -90 dBc/Hz at 100 kHz off-carrier, and high stability of 1.6 ppm/deg.C [10].

The FM/FSK modulator ia realized by a Dielectric Resonator stabilized Voltage Controlled Oscillator (DRVCO), which features 55 MHz/volt at 60 GHz, 6.6 dBm output, -80 dBc/Hz phase noise, and -4.1 ppm/deg.C frequency stability[11].

The power amplifiers shows 14 dB gain and 16.5 dBm output power over the frequency range of 52.5 though 62.5 GHz [12].

A low noise downconverter consisting of a four-stage LNA and a single-balanced image-rejection active drain mixer has been developed. It features higher than 20.7 dB conversion gain and less than 3.6 dB noise figure from 59 to 61 GHz [13].

3.4 Radio Absorbable Construction Materials

Radio absorbable construction materials have been studied under the test using reflection ratio measurement shown in Fig. 9[7]. Both transmitting and receiving antennas are attached to the wooden arch, a material under test on a small table is placed at the center of the arch, radio waves swept from 50 to 75 GHz are radiated sharply to the material, and the reflected signal is received at the RX antenna and analyzed at the network analyzer.

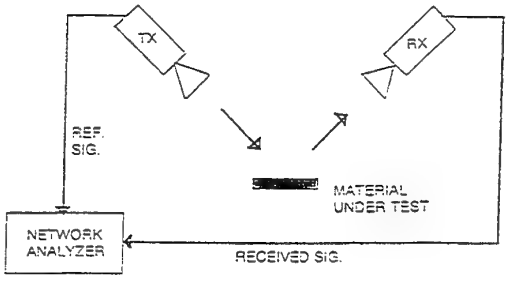

Fig. 9 Reflection Loss Measurment

It has been proved that concrete, pulp cement board, and fireproof cement excelsior board have reflection losses of from 8 to 20 dB. In the meantime, a wide band $\lambda/4$ thick absorber of about 1 mm thick sheet has also been proved that the frequency bandwidth of more than 20 dB loss is about 10 percent at 60 GHz.

Those absorbers are expected to be applied to the MDS LAN of Fig. 5.

6. CONCLUSIONS

The first part of this paper described the development history of Japan, including frequency allocation, standardization, commercial use millimeter-wave application system such as 50 GHz simple radios and NRD guide transceivers, and activities of wireless LAN development.

The latter part shows details of Minimum Delay Spread LAN the author proposed, fabricated and tested.

REFERENCES

[1] Y.Takimoto and A.Inoue, "Millimeter-wave communications development in Japan," MIOP'95 (Sindelfingen, Germany), pp.539-543, June 1995.

[2] Y.Takimoto and M.Kotaki, "Millimeter-wave and development of sensing technology," MWE'92 Microwave Workshop Digest (Tokyo, Japan), pp.313-318, Sept. 1992.

[3] F.Kuroki and T.Yoneyama, "Nonradiative dielectric waveguide digital transceiver at 60 GHz band," 1994 IR & MM Waves, (Sendai, Japan), Th2.5, pp.437-438, Oct. 1994.
[4] E.Ogawa, "Millimeter-wave distribution over fiber optic link for personal mobile communications," 7th World Telecommunication Forum, Telecom'95 (Geneva), pp.791-795, Oct.1995.
[5] T.Ihara, "Research and development activities on millimeter-wave short-range application systems in Japan," Proc. of Microwaves and RF, (London), pp.203-208, Oct. 1995.
[6] Y.Takimoto, "Recent activities on millimeter-wave indoor LAN system development in Japan," 1995 IEEE MTT-S International Microwave Symposium (Orlando, USA), WE1D, pp.405-408, May 1995.
[7] Y.Takimoto and A.Inoue, "Study on minimum delay spread condition for millimeter-wave indoor local area network," Proc. of Microwaves '94, (London) pp.386-391, Oct. 1994.
[8] Y.Takimoto, "Development of 60 GHz short range communication systems," MWE'95, Microwave Workshop Digest, (Yokohama, Japan), pp.231-236, Dec. 1995.
[9] K.Ohata and T.Saito, "Millimeter-wave MMICs for wireless communication systems," MWE'95 Microwave Workshop Digest, (Yokohama, Japan), pp.305-310, Dec. 1995.
[10] M.Funabashi et al., "A V-band AlGaAs/InGaAs heterojunction FET MMIC dielectric resonator oscillator," 1994 GaAs IC Symp. Digest, pp.30-33.
[11] T.Inoue et al., "60 GHz dielectrically stabilized monolithic voltage controlled oscillator," 1995 European Microwave Conference. Proc., pp.281-284.
[12] M.Funabashi et al., "A 50-70 GHz band heterojunction FET MMIC power amplifier," 1994 IR & MM Wave Digest, (Sendai, Japan), pp.433-434, Oct.1994.
[13] T.Saito et al., "60 GHz MMIC image-rejection downconverter using InGaP/InGaAs HEMT," 1995 GaAs IC Symp. Digest, (San Diego), pp.222-225, Oct.1995.

Millimeter-Wave Communications

B. Rembold

International Workshop on Millimeter Waves
Orvieto, Italy
April 11-12, 1996

MM-WAVE COMMUNICATIONS

B. Rembold [1]

Abstract:

The discussion about the use of frequencies beyond 30 GHz for commercial radio communications reaches back to about 20 years, when first studies had been made for intersatellite communications and for mm-wave radio links to trains. Supported by individual R&D funds from national ministeries in the last years investigations were mostly focused on mm-wave technology and propagation measurement for finding a low cost mm-wave-circuitry as well as more insight in propagation behavior of mm-waves due to precipitation, fading, intersymbol interference, reflexion and obstacle penetration. In parallel to these works questions for frequency-allocation and -assignment came up and are in discussion right now.

Today some new groups in the European Telecommunications Standards Institute ETSI are investigating standards for the transmission for various applications. The frequency range 37 - 39.5 GHz has been allocated for fixed systems (private radio relays). About 2000 links at 38 GHz have been installed in Germany for connecting the base-transceiver-stations (BTS) with the basestation-controller, for the DCS 1800 as well as for GSM. Some 1000 additional links will be expected in the next years. The magnetic leviation train *Transrapid* in the northern part of Germany as well as the japanese Maglev of the *Miyazaki Test Track* make use of a 39 GHz data link in order to provide a secure train operation. In Japan are about 700 point-to-point radio stations in the 50 GHz-band in operation, as already published 1986.
The possible market demand for wireless access to the future ATM-networks (mobile Multimedia) will give an impact to the mm-wave technology. The paper presents an overview about the state-of-the-art of existing mm-wave systems, and will point to possible new applications and to the most important areas of technology which have to be investigated in the next future.

[1] Institut für Hochfrequenztechnik, RWTH Aachen, Germany

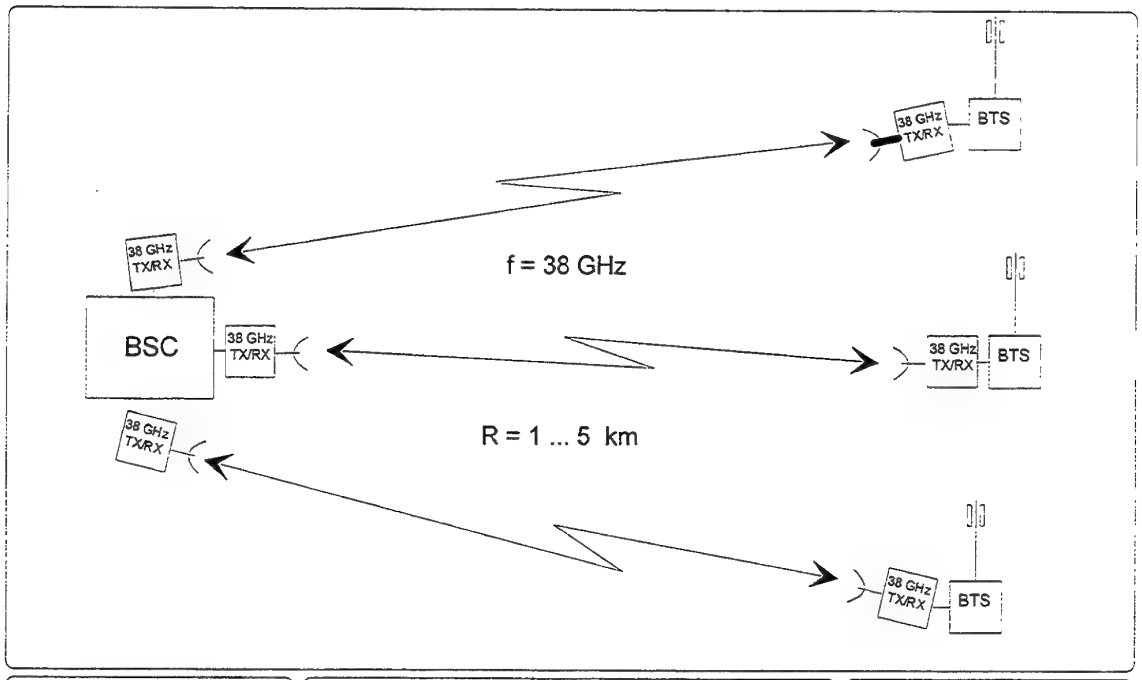

Institut für Hochfrequenztechnik RWTH Aachen B. Rembold	BSC - BTS - mm - wave - links for DCS 1800	

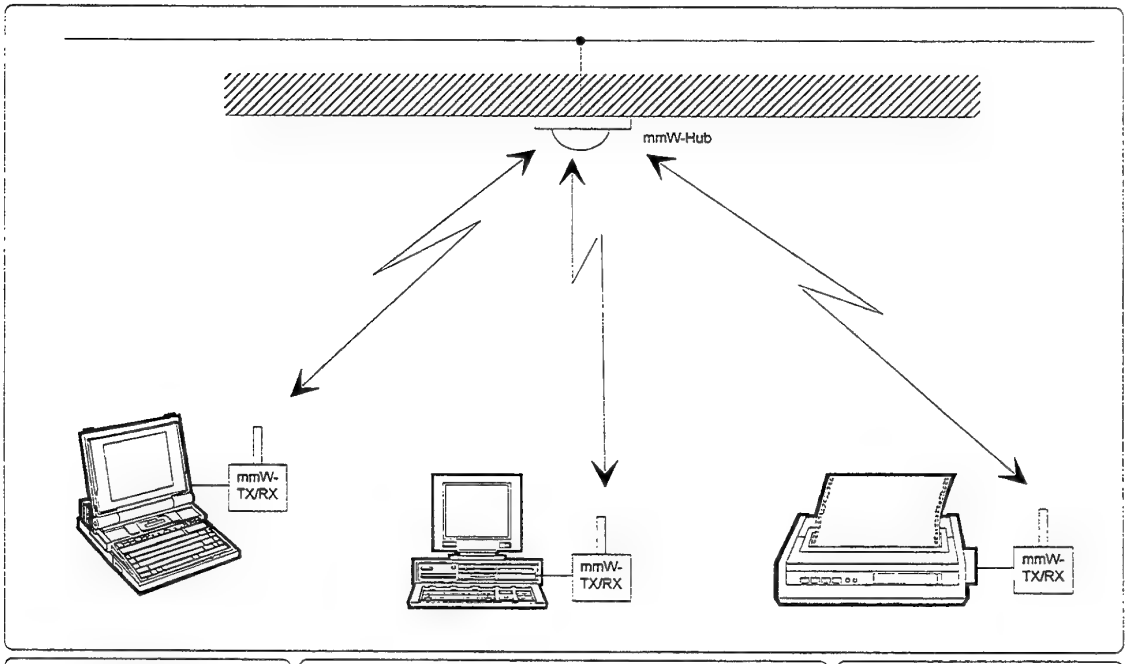

Institut für Hochfrequenztechnik RWTH Aachen B. Rembold	Wireless LAN at mm-Waves for indoor communications	

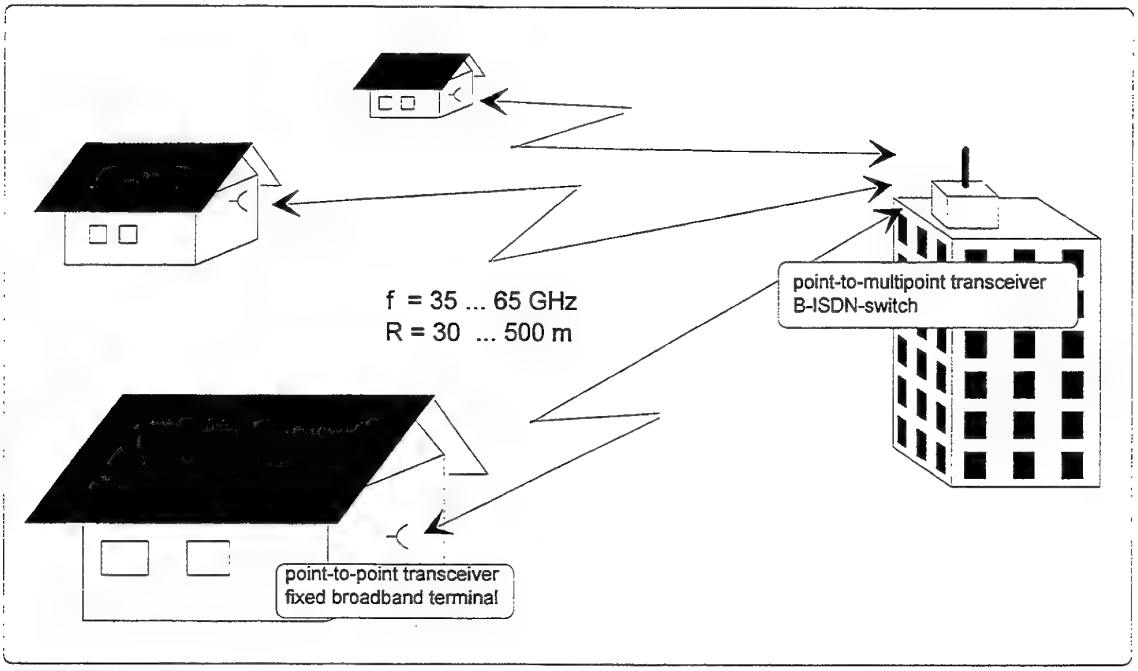

Institut für Hochfrequenztechnik
RWTH Aachen
B. Rembold

ATM-Radio in the Local Loop

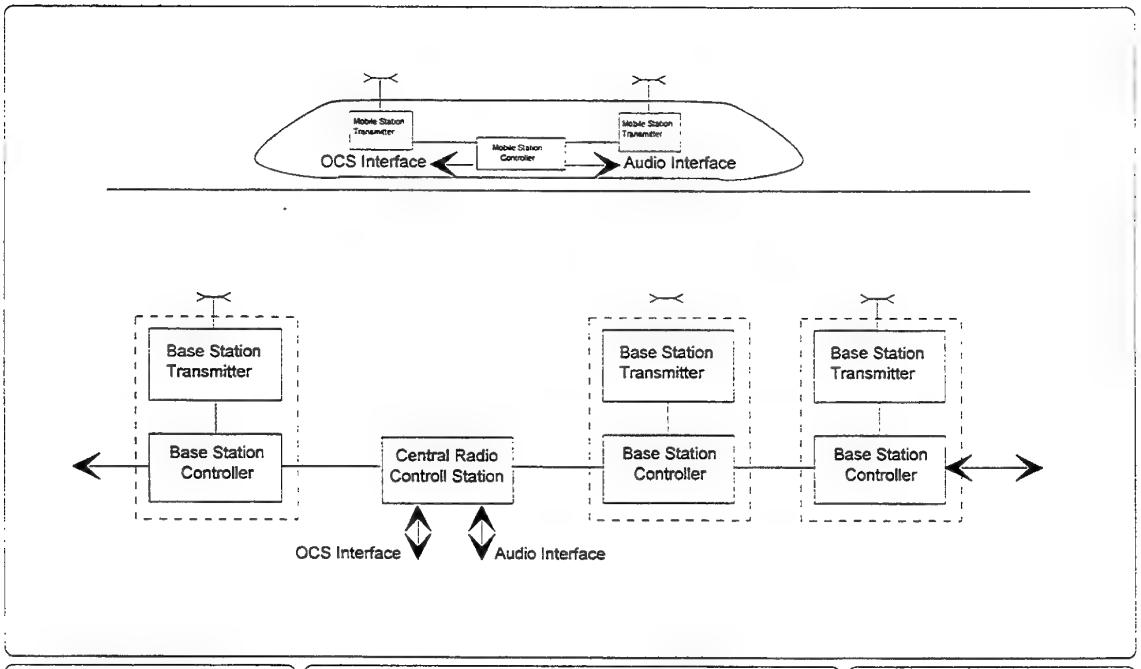

Institut für Hochfrequenztechnik
RWTH Aachen
B. Rembold

Transrapid 39 GHz Communication Link
System Overview

MAGLEV train TR07 with mmwave Base Station

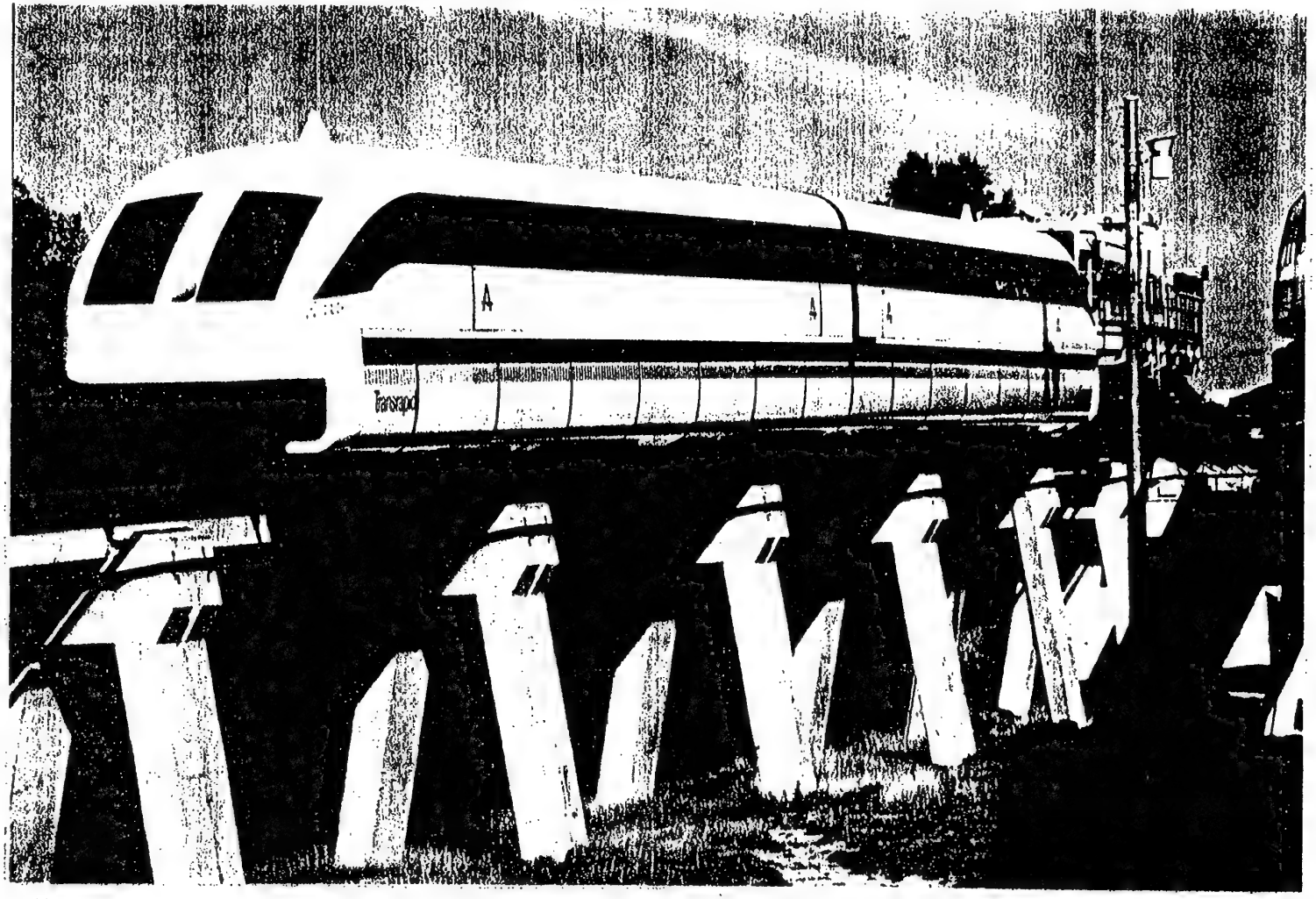

mmwave Communication System for MAGLEV

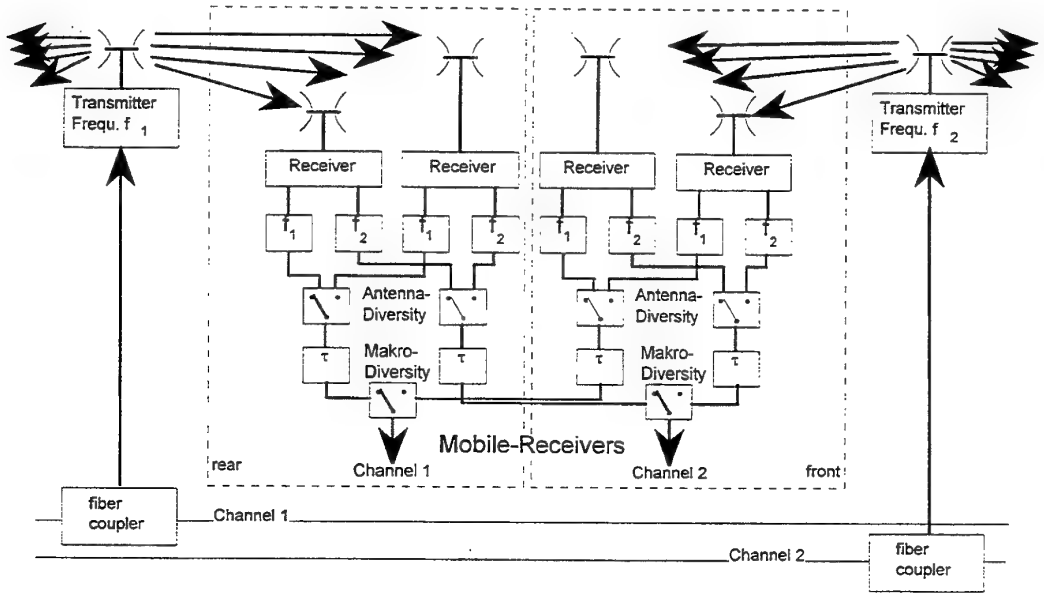

Diversity-Concept Base-to-Mobile-Station

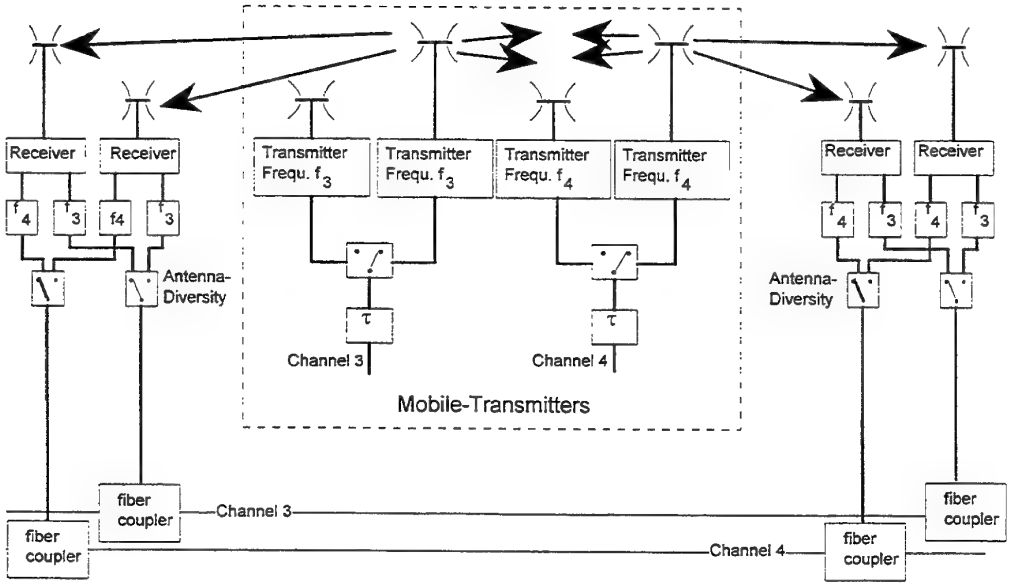

Diversity-Concept Mobile-to-Base-Station

Transrapid Diversity-Concept

1. Two parallel channels in each direction between Transrapid and Control-Center:

   Channel 1
   Channel 2 for BS to MS

   Channel 3
   Channel 4 for MS to BS

2. Each channel transmitts on its individual frequency
3. Each frequency is received by two stations (makro diversity)
4. Each station is provided with two receiver-chains (antenna diversity)

→ eight "air-links" in parallel

Sensorsysteme Daimler Benz Aer

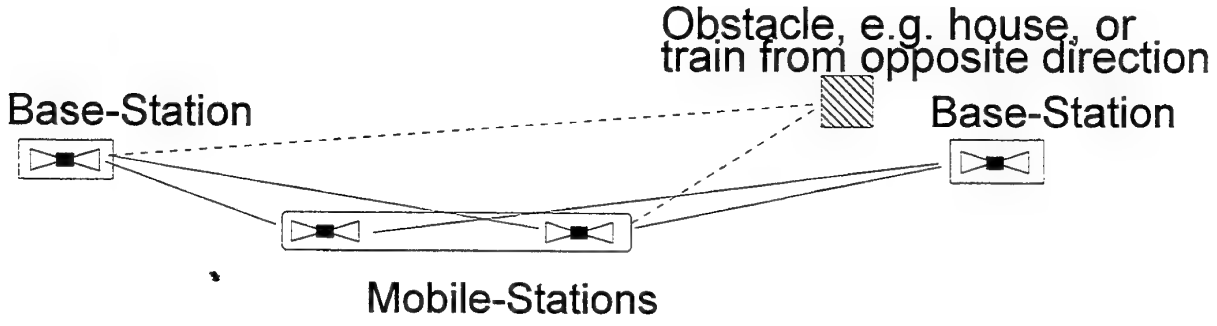

Circular Polarisation against multipath propagation

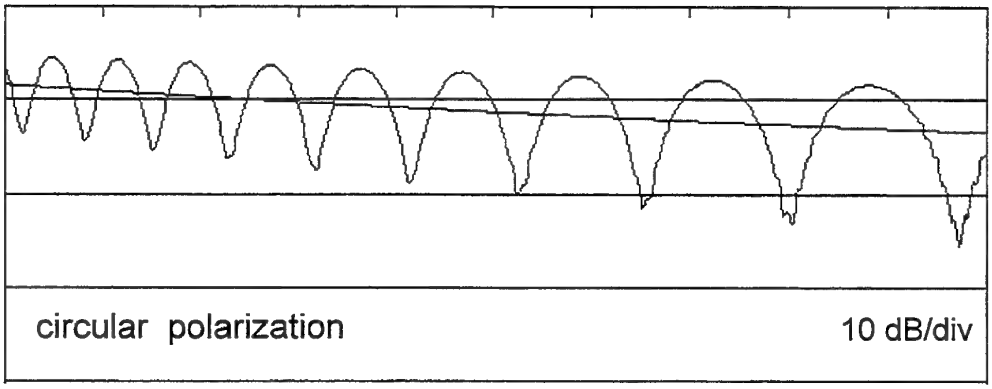

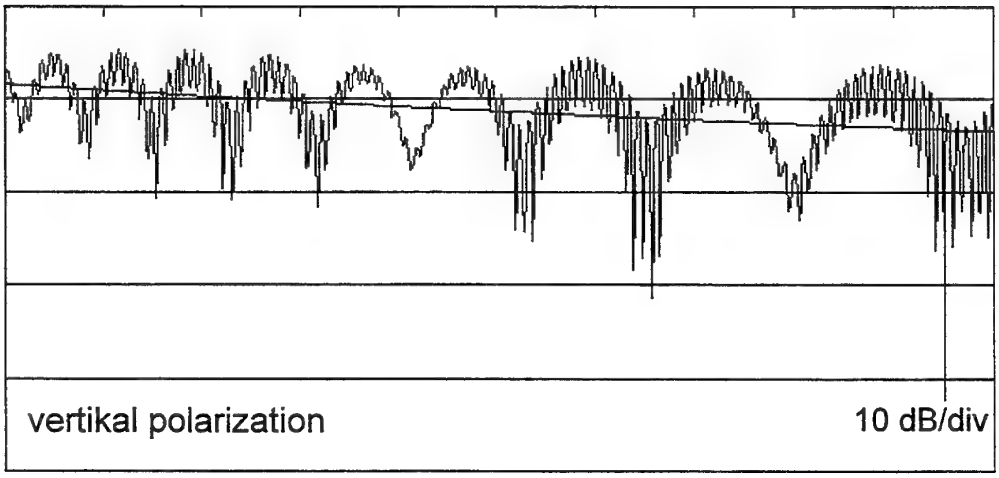

Simulation of oncoming train,
superposition of reflexions from ground
and from train
f = 40 GHz, length = 40 m

MMIC's:

Linear Power Amplifiers
Low Noise Amplifiers
DRO's

Modems:

COFDM for PA's with "medium Linearity"
Channel Equalizer for sequential modems

System Aspects:

Diversity Methods
Polarizations
Intelligent mmW-Antennas

Narrowband Characterization of 60 GHz Radio Propagation in Indoor Environment

V. Degli-Esposti, M. Frullone, G. Riva

NARROWBAND CHARACTERIZATION OF 60 GHZ RADIO PROPAGATION IN INDOOR ENVIRONMENT

Vittorio DEGLI-ESPOSTI**, Mario FRULLONE*, Guido RIVA*

* Fondazione Ugo Bordoni, Bologna
** Università degli studi di Bologna
Villa Griffone , 40044 Pontecchio Marconi , Bologna
Tel: +39 51 846854; Fax: +39 51 845758; e-mail: vdegliesposti@deis.unibo.it

Summary

Mobile communication networks evolution is rapidly moving toward a widespread use of indoor wireless transmission and in particular of high-speed data and multimedia services, which are very demanding in terms of bitrate and thus bandwidth. The 60 GHz band, offering a large amount of free bandwidth, is being considered recently as a good choice for future wireless LANs by several authors [1, and references therein]. This band is also very attractive due to the oxygen attenuation peak (about 15 dB/Km of excess attenuation) which could contribute minimising interference between adjacent LANs.

In order to ensure a reliable and error free radio transmission at 100 Mbit/s or more in an adverse multipath propagation environment such as the indoor one, diversity schemes, equalisers and proper radio port placement will be needed. To this end, an accurate propagation channel characterisation represents a major concern. Since experimental sounding is very expensive and time-consuming, computer models represent a valid alternative. In the present work, a narrowband 60 GHz propagation characterisation method which adopts a three dimensional ray model (or ray tracing model) is presented. A vertically polarised, omnidirectional antenna have been modelled and placed as a radiating element in a typical indoor environment; then, the field strength distribution as well as the statistical characteristics of the resulting multipath fading have been analysed and the corresponding results are reported in the paper.

The ray model

Ray models have been recently acknowledged as the most suitable tools for indoor microwave radio propagation modelling. As will be clear further, the validity of the ray approach could be put into question when the wavelength is comparable with the size of the environment and/or of its disomogeneities (i.e: walls, furniture, etc.), which is the case of UHF radio. On the contrary, in the millimeter wave case the ray approach represents certainly the most appropriate.

The starting point is the representation of the electromagnetic field generated by an antenna. If the antenna is comparable in size with the wavelength λ, then an observation point is said to be located in the *far field region* if its distance r from the source satisfies the relation $r >> \lambda$; a distance $r = 10\lambda$ is large enough for most purposes. In the far field region, as stated by the *stationary phase principle* [2], the field generated by the antenna can be represented as a spherical wave whose field is

$$(1) \qquad \mathbf{E}(r,\vartheta,\varphi) = \sqrt{\frac{\eta}{2\pi} P G}\ \mathbf{f}(\vartheta,\varphi)\ \frac{e^{-jkr}}{r},$$

where $\mathbf{f}(\vartheta,\varphi)$ is the antenna's radiation vector, P is the transmitted power, G the gain of the antenna, $k = 2\pi / \lambda$ is the wavenumber and $\eta = 377\ \Omega$ is the intrinsic impedance of vacuum.

In the ray approach, the spherical wave is represented as a set of straight rays having their origin in the antenna site. Each ray can be associated a *local plane wave* which is the local approximation of the spherical wave. Rays can experience reflection, transmission and diffraction actions due to the presence of obstacles. Since diffraction contribution at millimeter wave frequencies is very small it has been neglected here. In the present work we take into account walls, floors, ceilings, doors, windows, columns, etc. Every obstacle is modelled as a set of basic plane walls producing reflection and transmission. Each wall is a slab described by its electromagnetic properties (dielectric constant, magnetic permeability, conductivity) and is assumed to have a smooth surface. If the wavelength is much smaller than the wall, then the *local field principle* holds [3] and the field associated with a reflected or transmitted ray can be computed by applying the usual Fresnel's reflection and transmission coefficients [3]. Thanks to the high frequency involved, multiple reflection effects into the slab have been neglected [4]. Letting $\hat{\varepsilon}_r k^2 = b - ja$ and t_w be the thickness of the wall, we calculate the additional field attenuation A_w due to material losses by using the formula:

$$(2) \qquad A_w = \exp\left(-a\,\frac{t_w}{\cos\vartheta}\right),$$

where $t_w/\cos\vartheta$ is the ray path length inside the wall. Each ray impinging on a wall splits in two: the reflected ray and the transmitted ray. Each ray can experience an arbitrary number of reflections, transmissions or diffractions along its path: in this way a ray-tree is produced in which each node is a wall (or the receiver), each branch a sub-ray and the root is the transmitter. All the rays whose paths reach the receiver location should be considered when calculating the received signal, and all the corresponding field contributions at the receiver must be weighted with the receiving antenna's radiation characteristics and added according to their relative amplitudes and phases. The depth of the tree is theoretically infinite. However, since each scattering action results in a power loss, tree depth can be truncated by setting an upper limit N_{max} to the number of successive scattering actions a ray can experience, determining the total number of traced

rays and computation time. The computations presented in this paper were performed with $N_{max} = 4$, which has been found to give stable results in all cases.

Results

Results refer to a 15x20x3 m indoor environment corresponding to the second floor of Villa Griffone (where Marconi performed his first radio transmission experiment). The Tx and the Rx are equipped with omnidirectional antennas having a gain of about 2.2 dB. Radiated power is 10 mW and Tx height is 2.8 m. In Fig. 1 the received power on a plane located at a height of 1.1 m is shown. It is evident that the attenuation introduced by internal walls is so strong (about 20 dB) that each single room and door can be singled out. Being the wavelength 0.5 cm, fast fading fluctuations cannot be seen. Where a strong direct or reflected path is present also one floor-reflected path and one ceiling-reflected path are present: this is the reason for the visible field ripple, which is similar to the what can be seen in an outdoor radio link [5].

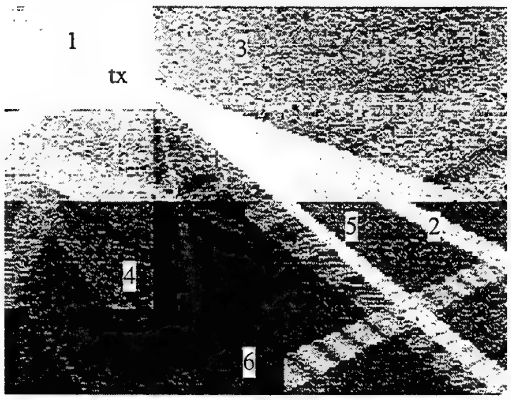

Fig. 1 - Received power in the second floor of Villa Griffone. Brightest colour: -64 dBm, darkest colour: -180 dBm

Location	P_{mean} (dBm)	Logn.	Rice	Ray-leigh
1	-92	0.62	**3.0e-2**	12.94
2	-104.58	2.32	**1.75**	57.58
3	-115.82	1.14	**0.10**	5.73
4	-138.55	0.54	**0.13**	**0.13**
5	-124.88	0.14	**2.9e-2**	47.59
6	-139.36	0.16	**3.0e-2**	50.15

Table 1 - mean power (first column) and χ^2 for some best-fits relative to the 6 locations shown in Fig. 1.

The similarity between 60GHz indoor and outdoor propagation is evident also from Table 1, where the mean square deviations of some best-fitted statistical distributions relative to the fast fading distribution [6] computed in six locations are reported. Since probably a dominant path almost always exists, the best approximation to fast fading distribution is always Rice. This is very different from 900 indoor propagation behaviour, as can be seen in [6].

Another peculiarity of 60 GHz indoor propagation seems to resemble outdoor propagation: due to the very small wavelength with respect to environment dimensions, field fluctuations can be easily classified either as "fast" or "slow". In Fig. 2 the FFT of two field scans along a line at 1800 MHz and at 60 GHz are compared (scan line is not the same); before making the FFT, the distance has been normalised with respect to the wavelength. It is evident that in the 1880 MHz case fast and slow fading are not separable. In the 60 GHz case the separated fast fading peak is clearly visible.

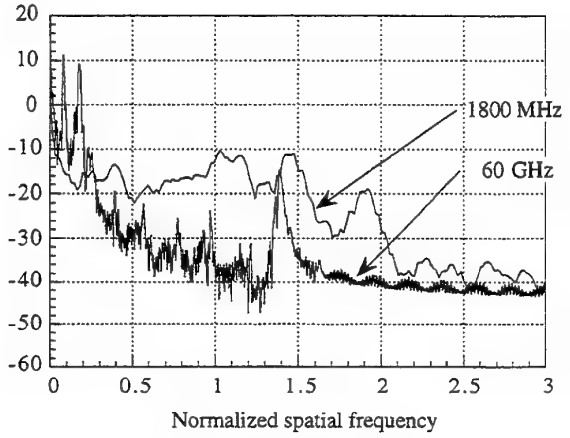

Fig. 2 - FFT transforms of electric field module scans along two lines (not same scale)

References

[1] - A. M. Hammoudeh and G. Allen, "Millimetric wavelengths radiowave propagation for line-of-sight indoor microcellular mobile communications," IEEE Trans. Veh. Tech., vol. 44, No. 3, pp. 449 - 460, August, 1995.

[2] - R. H. Clarke and J. Brown, *Diffraction theory and antennas*, Ellis Norwood Limited Publishers, Chichester, 1980.

[3] - G. Conciauro, *Introduzione alle onde elettromagnetiche*, McGraw Hill, Milano, 1993. (english version available)

[4] - L. Correia and P. O. Frances, "Estimation of material characteristics from power measurements at 60 GHz," COST 231 document TD(94) 129, Darmstadt, September 6-8, 1994.

[5] - J. D. Parsons, *The mobile radio propagation channel*, Pentech Press, London, 1992.

[6] - Pietro Daniele, Vittorio Degli-Esposti, Gabriele Falciasecca, Guido Riva, "Field prediction tools for wireless communications in outdoor and indoor environments", IEEE MTT-S European Topical Congress "Technologies for Wireless Applications", Turin, Italy, November 2-4, 1994.

Packaging of Millimeter Wave Circuits

W. Menzel

Packaging of Millimeter Wave Circuits

Wolfgang Menzel
Microwave Techniques, University of Ulm, Germany
Tel: ++49-731-502 6350
Fax : ++49-731-502 6359
E-mail: menzel@mwt.e-technik.uni-ulm.de

I. Introduction

Packaging of micro- and mm-wave MICs, MMICs, components or subsystems has to provide protection against mechanical stress, environmental loads like moisture and chemicals, and, possibly, against EMI. In addition, the complete assembly must operate in a wide temperature range, and it must allow the removal of heat generated in its interior /1/, /2/.
On the other hand, packaging includes aspects like interconnects between different circuits (possibly between different types of transmission lines, too), feed-through elements into and out of the package, choice of materials, or front-end architecture (Fig. 1). With increasing mass applications like phased arrays /2/ or traffic applications /3/, packages have to be fabricated and assembled easily and quickly based on reliable processes at reasonable cost. All these problems are increasingly relevant for applications at mm-wave frequencies.

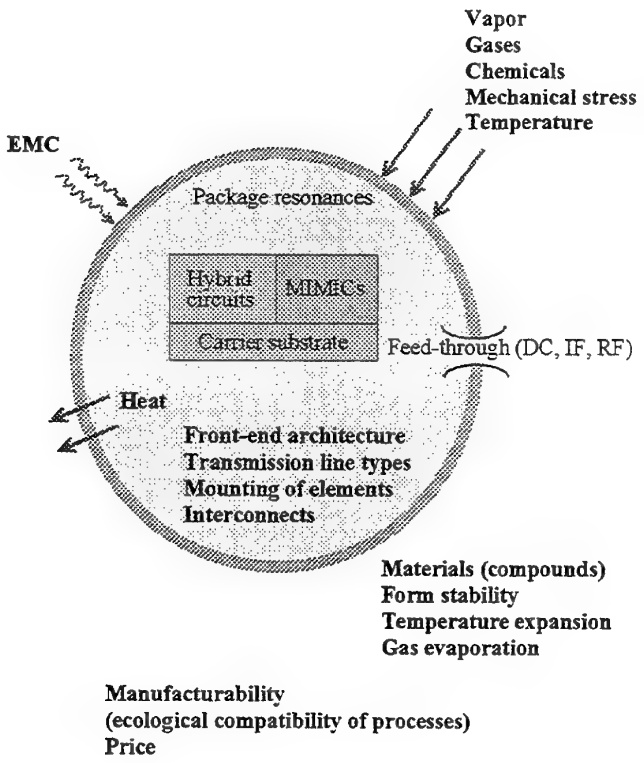

Fig. 1: Interconnect and packaging problems.

Therefore, this contribution will address topics like

- Front-end architecture for mm-wave circuits based on different transmission line media
- Package materials [(metallized) plastic, powder injection moulding, metal injection moulding]
- Circuit interconnects (flip-chip, adaptive bonding, electromagnetic field coupling)
- Feed-through elements (coaxial and compensated planar structures, electromagnetic field coupling, antennas)

II. Front-end architecture

While at lower frequencies, single devices or single MMICs are placed into a package, this mostly is not effective at millimeter wave frequencies. Even a single MIMIC is no longer small compared to wavelengths resulting in package resonance problems, and the cumulating effects of the interconnects from the MIMIC to the package feed-through, out of the package and from one packaged component to the other will add to high insertion and return losses. Therefore, carefully designed assemblies of MIMICs, passive components, radiating structures and other elements have to be combined to subsystems or "supercomponents" and will be placed together on a metal or dielectric carrier, shielded by a single package with special precautions against package resonances. The combination of components will be determined by

- good functionality
- short interconnects
- low number of package feed-through elements
- limitation of interferences between single components
- limitation of gain within one package (feedback prevention)
- sufficient removal of heat generated by active devices
- separation of power and low noise elements etc.

A metal carrier for the circuits can easily remove heat generated by active elements; another solution consists of placing all circuits on a dielectric carrier substrate which, at the same time, can carry the necessary interconnect lines, passive components or antenna elements /6/, /7/; this concept partly is called "substrate integrated packaging". As carrier substrate, even multilayer substrates for high density packaging and interconnects are investigated /7/-/9/.

MIMICs, passive components, radiating elements, or interconnect lines may be based on different transmission line media like microstrip or coplanar waveguide. Coplanar lines allow the realization of rather small circuits as, for a given transmission line impedance, both line and slot width can be adjusted resulting in very small transmission line cross sections. As the ground plane is on the same side of the substrate, its shielding effect allows a closer spacing of adjacent lines, too. No substrate thinning is necessary, and no vias are required for ground contacts. All this leads to a reduced circuit size with less process steps compared to microstrip and thus to a cost reduction. On the other hand, a rather small transmission line cross section leads to increased losses.
The different ground plane position of microstrip and coplanar line may lead to some problems for interconnects between these types of lines, this may be used, however, favourably for some specific arrangements (see Sect. IV).
In some applications, the circuits within the package have to be connected to coaxial or even waveguide feed-through elements /4/,/5/. With respect to hermetic sealing, an electromagnetic coupling of the millimeter wave signal to the outside world via antennas or broadside coupling between transmission line structures on opposite sides of a carrier substrate may be a good solution /6/, /7/. Future systems - work is presently done for phased array applications - will include optical interfaces, too.

III. Package materials

Metal as material for at least part of a package shows optimal properties concerning thermal conductivity, electromagnetic shielding, mechanical and thermal stability. For low thermal expansion, best match to semiconductor and ceramic materials can be achieved with special composites like invar or kovar. These, however, are difficult to machine and therefore expensive. Copper tungsten or copper molybdenum provide good thermal conductivity with high stability. Standard materials with good electrical and thermal conductivity like aluminium or brass (mostly plated with a less corrosive layer), are cheaper for these applications, but special precautions have to be taken due to their higher thermal expansion.
Fabrication of metal package parts may be done using standard machining procedures or injection casting; new techniques like metal powder sintering and metal injection moulding may pave the way for reduced production cost.
Ceramic materials are applied both as parts of the package as well as for substrates carrying RF transmission lines. To this end, and to provide electromagnetic shielding, these materials (partly) have to be metallized. Beryllia (poisonous), aluminium nitride, or aluminium silicon carbide show best thermal conductivity and are therefore applied in high power applications, while alumina is well known from standard microwave applications. They typically show low thermal expansion sufficiently matched to semiconductors. Ceramic parts typically are fabricated from fine powder, pressed to the required form and sintered at high temperatures. The sintering leads to a considerable shrinking of the dimensions which has to be taken into account during the design.
In some applications, even **quartz** /10/ with its relatively low dielectric constant or **silicon** which can be formed with micromachining techniques /11/ are used.
Plastic materials are cheapest in material and production cost; pure plastic provides, however, a number of challenges concerning mechanical and thermal stability and thermal expansion. Even as substrate material, PTFE is enforced by fillings like glass fiber of ceramic powder. At lower frequencies, leadframes are used as stabilizing elements /8/.
As a relative stable material for packages, polymers with special fillings of ceramic powder, glass or carbon fibers or even metal powder have been investigated /4/, /12/. These **composite materials** are engineered for high stability and low thermal expansion, they can withstand temperatures up to 200° C, and they may be easily fabricated employing powder or metal injection techniques. Metal inserts are used to remove heat from active areas. Liquid crystal polymers with their anisotropic behaviour may be of interest for a low thermal expansion in one plane /12/. Special care has to be taken using plastic materials with respect to hermeticity; in most cases, a metallization will be used to keep penetration of vapour low enough; this improves, at the same time, the electromagnetic shielding of the package.

IV. Circuit interconnects

At mm-wave frequencies, interconnects between different MMIC chips or to an additional substrate with either hybrid circuits or interconnect lines behave more and more as strong discontinuities. Dye bonding as well as the interconnects themselves require tight tolerances, but in spite of this, the respective production processes should be easy and low cost.
Therefore, the choice of the best interconnect technique, a good model for the microwave (and possibly thermal) behaviour, and a tolerance oriented optimisation is necessary.
Equivalent circuit models as well as full wave calculations of different types of interconnects therefore are investigated.

IV.1 Microstrip - microstrip

A great part of the present MMICs are based on microstrip. Therefore, an interconnect between two chips or between one chip and a hybrid circuit placed side by side is of great importance. Due to tolerances in chip size, non vertical edges of the chips, and possible thermal expansion, some gap will remain between the two substrates, and the bonding structure must include some kind of loop. This, however, leads to a pronounced low pass behaviour of the interconnect (Fig. 2) resulting in increased difficulties with increasing frequencies.

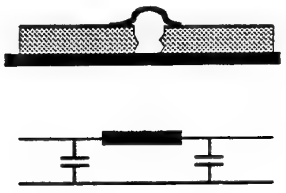

Fig. 2: Microstrip - microstrip bonding and equivalent circuit.

One proposal is based on as bonding elements, one or two wires (at the edges of the lines), bond tapes, or special tapes integrated on thin dielectric carriers (TAB: tape automated bonding, /13/) are employed.
At mm-wave frequencies, however, some compensation of the low pass performance of such transitions is necessary. a theoretical model of bond wire interconnects /14/ and a flexible compensation network as shown in Fig. 3. Depending on the gap between two circuits, the distance of two bonds is modified such that a good transmission performance is maintained up to about 100 GHz /4/, /12/. The distance between the chips is monitored by a camera, and by a suitable algorithm, bond wire positions and loop height are adjusted and controlled automatically. Up to 100 GHz, a return loss of better than 20 dB is predicted theoretically including reasonable ranges of gap widths as well as dye and loop bonding tolerances.

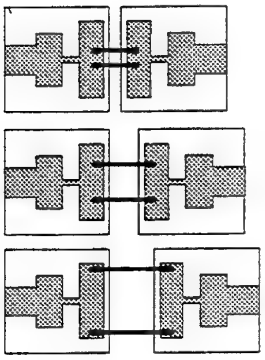

Fig. 3: Compensated two-wire bonding interconnects /12/.

IV.2 Coplanar - coplanar waveguide

As coplanar circuits are gaining increasing interest (see section II), great efforts are done developing effective interconnect techniques for this type of transmission line, too. Placing two coplanar circuits side by side ends up in even more severe problems compared to microstrip, as the ground plane has to be bonded together, too. Therefore, flip-chip techniques have been introduced consisting of bumps fabricated (with galvanic processes) on top of the circuit metallization (Fig. 4). The MMIC - or even a single device like a FET - then is placed top down on a carrier substrate and bonded to an equivalent transmission line structure. The same technique can be used to remove the heat of active elements via bumps placed directly at the FET source region /15/. The height of the bumps should be about three times the coplanar slot width to prevent interactions with the carrier substrate; typical values are 30 ... 75 µm. At mm-wave frequencies, some concern has to be made about the inductance of the bumps /16/, but in any case, flip-chip mounting provides an effective and economical interconnect technique in the mm-wave range /6/, /12/, /25/.

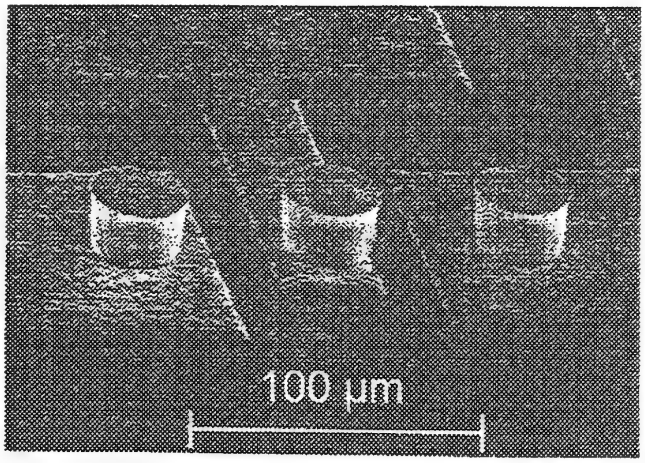

Fig. 4: Bumps on a coplanar waveguide for flip-chip mounting.

IV.3 Mixed interconnects

For some applications, microstrip MMICs may favourably be placed on top of a carrier substrate using coplanar interconnect lines (Fig. 5). The ground planes of both circuits then are in the same plane, and as typically, the microstrip substrate height is relatively small, a galvanic interconnect from the microstrip line to the center coplanar line is feasible. A more elegant solution uses electromagnetic field coupling on the bases of quarter wave structures /5/, /17/. At mm-wave frequencies, quarter wave structure on GaAs measure only a few tenths of a mm being compatible with the size of MMICs. The microstrip circuit must have a gap in the ground metallization in the coupling area; this, however should not be any problem as some back side structuring is done anyway to enable dye separation. As an example of this technique, the results of a 35 GHz test amplifier with electromagnetic coupling is presented in Fig. 6 in comparison with a direct on-wafer measurement.

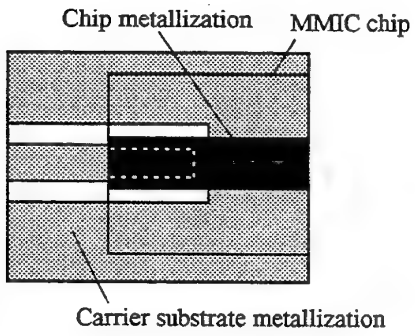

Fig. 5: Microstrip chip placed on a coplanar carrier substrate.

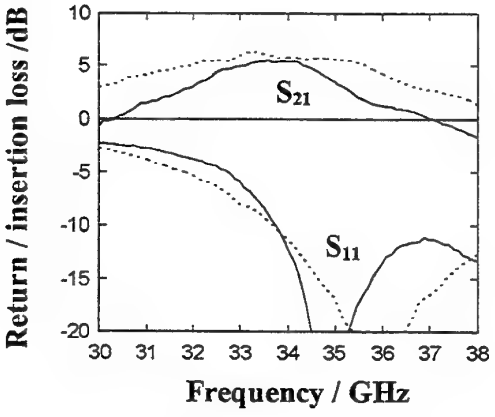

Fig. 6: S-parameters of a test amplifier measured using on-wafer probing (---) and electromagnetic coupling (—).
(The coplanar lines on the carrier substrate were connected to the measurement sytem by wafer-probing, too).

V. Package feed-through elements

A package feed-through structure has to provide an electrical interconnect into or out of the package maintaining a good seal and mechanical as well as thermal stability.
With increasing frequencies, the width of a package wall, especially in conjunction with a material of high dielectric constant like ceramics, is no longer small compared to wavelength. Regarding possible discontinuities of the interfaces at the package wall edges, strong reflections may occur, and some compensation has to be included.

V.1 Coaxial feed-through elements

For measurement purposes, coaxial cables and connector systems have been pushed into the mm-wave frequency region. Consequently, efforts are made to extend these systems to packaging techniques. Basically, it is rather straightforward using glass beads soldered into holes in a package wall. For examples, investigations on a 1mm coaxial cable and connector system are reported in /12/. The coaxial systems, however, require very stringent tolerances (a few µm only), and above 40 GHz, they pose severe problems with the transition to planar circuits within the package.

V.2 Planar feed-through elements

Using microstrip lines on a carrier substrate serving, at the same time, as package carrier, the lines could easily be extended out of the package. Suitable compensating and matching structures have to be included to compensate the involved discontinuities /18/, /20/. In addition, attention has to be paid to possible resonances of the feed-through structure /18/. Similar features can be expected for coplanar feed-through structures. Detailed work on this is described in /18/, a sketch of such an element is shown in Fig. 7 together with its return loss. Without compensation, a return loss of up to -12 dB is found which can be improved using a impedance-matched width of the center conductor /12/.

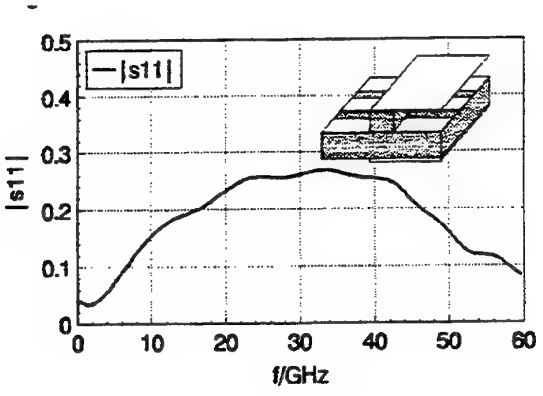

Fig. 7: Sketch and return loss of a coplanar feed-through element (from /18/).

V.3 Feed-through elements to waveguide

For ease of production and low cost, planar circuits are preferred if possible. For some application, however, waveguides are still necessary due to their low losses (e. g. for filters, resonators, oscillators) or a better compatibility with some types of antennas. A number of transitions from planar circuits to waveguide are well known like the probe coupled transition

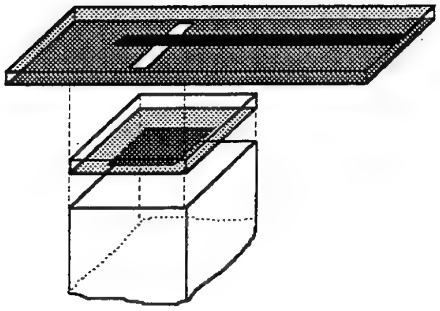

Fig. 8: Patch-coupled microstrip to waveguide transition

/18/, /21/ - /22/. Such a transition is used, too, in a packaging concept for mm-wave MMICs presented in /23/. With these types of transition, however, some waveguide structure, typically a short-circuited quarter-wave section, has to be placed on the opposite side of the waveguide port. This can be avoided by a novel concept presented in /5/ which is sketched in Fig. 8. From the microstrip line, the power is fed via a slot to a patch radiating into the waveguide. In this way, no waveguide structure is necessary on top of the planar circuit which, therefore, can extend independently of the transition. Results around 75 GHz for two transitions placed back to back, connected by 21 mm of microstrip line are given in Fig. 9. Taking into account a microstrip loss of 0.8 dB/cm, an insertion loss of about 0.3 dB per transition results in this frequency range.

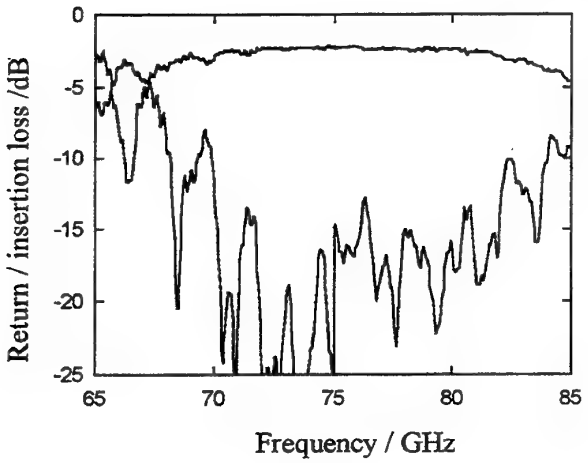

Fig. 9: Return and insertion loss of two microstrip to waveguide transition (Fig. 8) placed back to back and connected by a 21 mm microstrip line .

V.4 Antennas

Another elegant way to couple microwave signals out of a package is by radiation. To this end, antenna elements may be integrated into a package; in this case the package must have at least a transparent section. Alternatively, an integrated carrier substrate may include an antenna on its outer side; then some coupling either by galvanic or electromagnetic means has to be provided. In /6/ and /12/, a galvanic feed-through is used to feed a conventional planar array antenna. Another solution is a slot coupled patch antenna; this even could be directly connected and optimally matched to active elements as demonstrated in /25/ resulting in improved low noise receiving performance and wider bandwidth.

VI. References:

/1/ B. Berson: Strategies for microwave and millimeter wave packaging today. IEPS, Proc. Of the techn. Program, 9th Annual Intern. Electronics Packaging Conf., San Diego, USA, 1989, Vol. 1, 697 - 720.

/2/ H. Bierman: Designers strive for low cost packages. Microw. J., Sept. 1992, 100 - 106.

/3/ H. Daembkes, J. F. Luy: Millimetrewave components and systems for automotive applications. 25th European Microw. Conf., 1995, Bologna, Italy, INV.8.

/4/ M. Boheim, U. Goebel: Low Cost Packages for Micro- and Millimeterwave Circuits. 24th European Microw. Conf., 1994, Cannes, France, 122 - 132.

/5/ Grabherr, W.; Huder, B.; Menzel, W.: Microstrip to waveguide transition compatible with mm-wave integrated circuits. IEEE Trans. on MTT, September 1994, 1842-1843.

/6/ Baumann, G. et al.: 51 GHz Frontend with Flip Chip and Wire Bond Interconnections from GaAs MMICs to a Planar Patch Antenna. IEEE Intern. Microw. Symp. MTT-S, 1995, Orlando, USA, 1639 - 1641.

/7/ Strauß, G.; Menzel, W.: A novel concept for mm-wave MMIC interconnects and packaging. IEEE Int. Microw. Symp. MTT-S, 1994, San Diego, 1141-1144.

/8/ C. Nagy et al.: Advanced Manufacturing and Packaging Technologies for Military and Commercial Markets. Microw. J., Aug. 1995, 22 - 36.

/9/ Session on High Density Microwave Packaging Program. Proc. Of IEEE Intern. Microw. Symp. MTT-S, 1995, Orlando, USA, 169 - 184.

/10/ Shih, Y. C. et al: A High Performance Quartz Package for Millimeter-Wave Applications. IEEE Intern. Microw. Symp. MTT-S, 1991, Boston, USA, 1063 - 1066.

/11/ Robertson, S. V. et al.: Micromachined Self-Packaged W-Band Bandpass Filter. IEEE Intern. Microw. Symp. MTT-S, 1995, Orlando, USA, 1543 - 1546.

/12/ Final presentation of the projects „System Technologies for Micro- and Millimeterwave Circuits“ and „Mounting and Interconnect Techniques as Basis for Electrical and Optical Microsystems“ (in German), German Ministry of Research, Berlin, Nov. 30th and Dec. 1st, 1995.

/13/ Reichel, H.: Packaging aspects of single and multichip modules. EuPac '94, 1st European Conference on Electronic Packaging Technology & 7th Intern. Conference on Interconnection Technology in Electronics, 1994, 6 - 9.

/14/ Alimenti, F. et al.: Quasi Static Analysis of Microstrip Bondwire Interconnects. IEEE Intern. Microw. Symp. MTT-S, 1995, Orlando, USA, 679 - 682.

/15/ L. M. Felton: High yield GaAs Flip-Chip MMICs Lead to Low Cost T/R Modules. IEEE Intern. Microw. Symp. MTT-S, 1994, San Diego, USA, 1707 - 1710.

/16/ Jin, H. et al.: Rigorous Field Theory Analysis of Flip-Chip Interconnections in MMICs Using the FDTLM Method. IEEE Intern. Microw. Symp. MTT-S, 1994, San Diego, USA, 1711 - 1714.

/17/ Strauß, G., Menzel, W.: Millimeter-Wave Monolithic Integrated Circuit Interconnects Using Electromagnetic Field Coupling. Accepted for publication in the IEEE Trans. on CPMT, 1996.

/18/ Rittweger, M. et al.: 3D FDTD Analysis Applied to the Investigation of the Resonant Behavior of Ceramic Feedthrus. IEEE Intern. Microw. Symp. MTT-S, 1994, San Diego, USA, 1719 - 1722.

/19/ Grabherr, W., Menzel, W. : Active low noise transition from rectangular waveguide to microstrip line. IEEE Intern. Microw. Symp. MTT-S, 1995, Orlando, Fl., 1403 - 1406.

/20/ Christ, A.: S-parameter calculations using three-dimensional finite differences for microwave chip interconnects (in German), PhD Thesis, Techn. Univ. Darmstadt, Germany, 1988.

/21/ Shih, Y. C. et al.: Waveguide-to-microstrip transitions for millimeter-wave applications. IEEE Intern. Microw. Symp. MTT-S, 1988, 473 - 475.

/22/ Machac, J.; Menzel, W.: On the design of waveguide-to-microstrip and waveguide-to-coplanar line transitions. 23rd Europ. Microw. Conf., 1993, Madrid, Spain, 615-616.

/23/ Lohrmann, R., Ehrlinger, W.: Packaging of millimeterwave-MMICs for communication system applications. MIOP '93, Sindelfingen, Germany, 237 - 241.

/24/ Sakai, H. et al.: A novel millimeter-wave IC on Si substrate using flip-chip bonding technology. IEEE Intern. Microw. Symp. MTT-S, 1994, San Diego, 1763 - 1766.

/25/ Grabherr, W.; Menzel, W.: Broadband, low-noise active receiving microstrip antenna. 24th European Microw. Conf., September 1994, Cannes, 1785-1790.

MMW Leaky-Wave Antenna

T. Itoh

MMW Leaky-Wave Antenna

Tatsuo Itoh

UCLA
Department of Electrical Engineering
66-147 A. Engineering IV
405 Hilgard Avenue
Los Angeles, CA 90095-1594 - USA
Ph.: +1-310-206-4820, Fax: +1-310-206-4819
E-mail: itoh@ee.ucla.edu

MMW LEAKY-WAVE ANTENNA

- **Technical background of Passive Ultra-Compact Imaging (PUCI) Technology**
  - **Physics of thermal imaging:** energy emission of objects at nonzero temp.
  - **MMW penetration superior to IR:** MMW can "see" 20 to 50 times than IR through fog, clouds, smoke, and haze.
  - **MMW imagers previously too large, expensive.**
- **Potential applications for PUCI technology:**

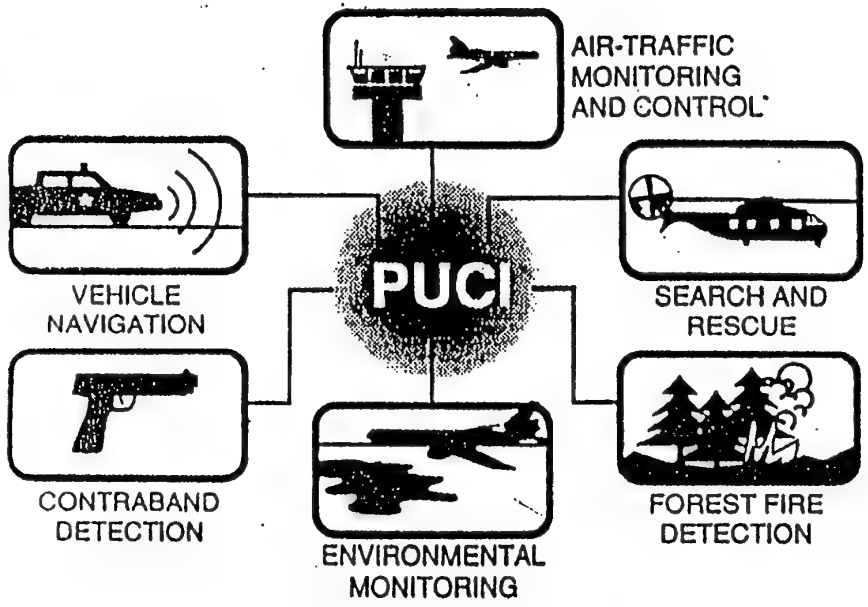

Some Dielectric Waveguide based Leaky Wave Antennas Previously tried

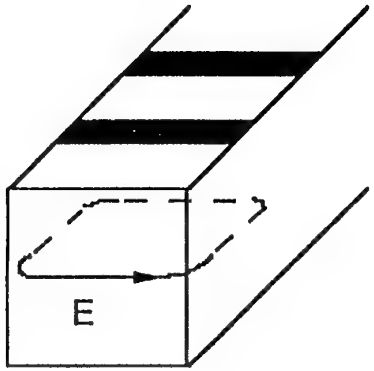

E_x radiated

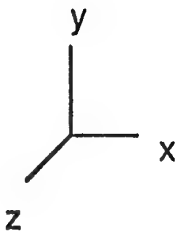

E_z radiated

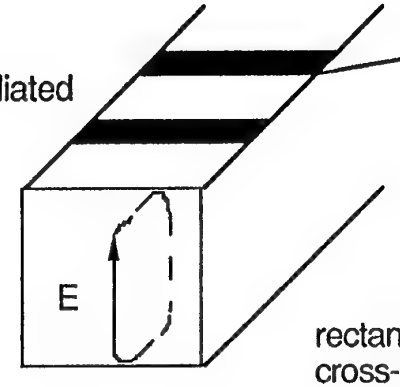

metallization (radiating elements)

rectangular/square cross-section dielectric wave-guide

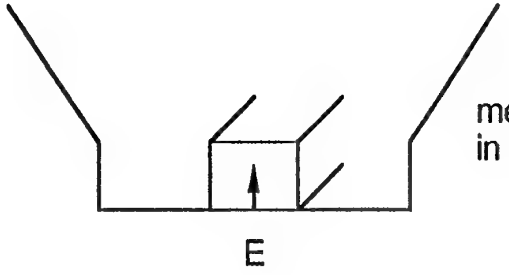

metal horn enhances directivity in x-y plane

MMW LEAKY-WAVE ANTENNA

- **Antenna configuration:**

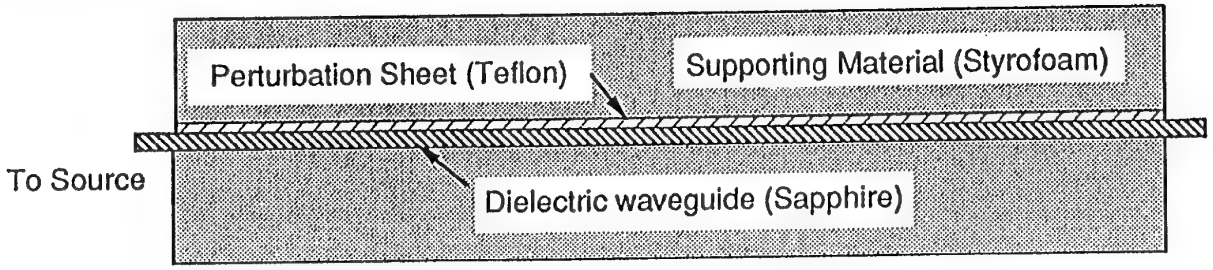

Side View

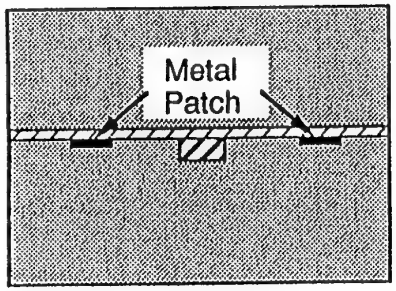

Cross Section

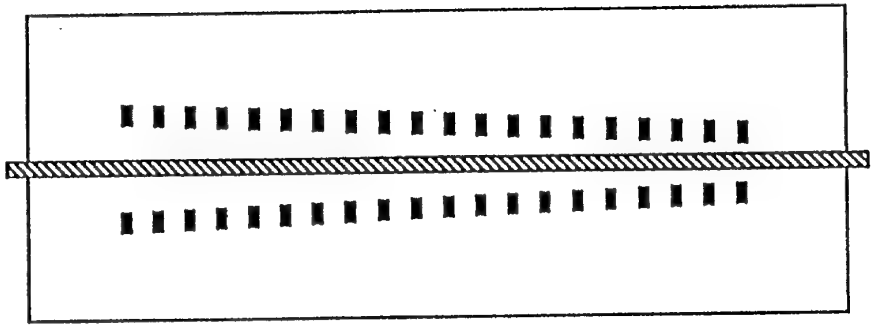

Top View

MMW LEAKY-WAVE ANTENNA

• Simulated and measured antenna performance

- $\theta = \mathrm{Sin}^{-1}\left(\frac{\beta}{k_0} - \frac{2\pi}{d}\right)$

- Theoretical and measured data agree well.

- Scanning range from 91 to 97 GHz
  - 16.5 degree for 80-mil period.
  - 24.5 degree for 50-mil period.

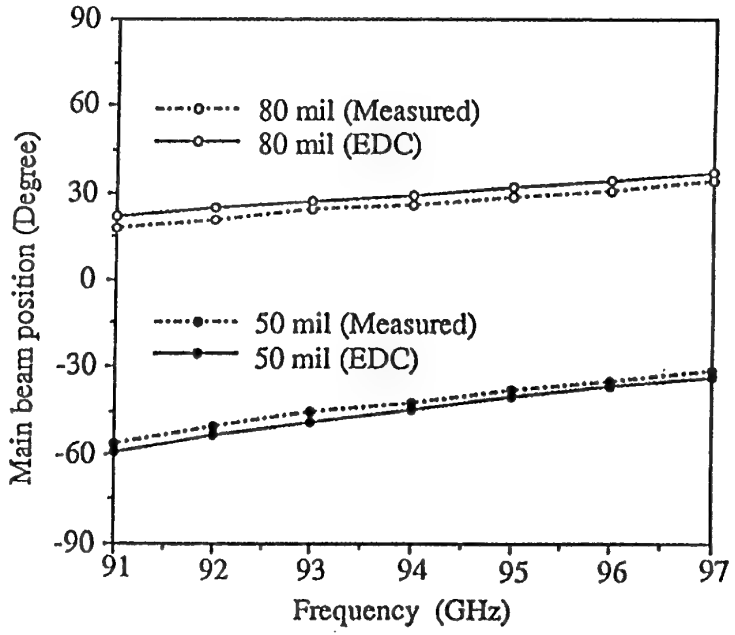

LEAKY WAVE ANTENNA

NEAR FIELD MEASUREMENT:

The amplitude distribution of the near field is measured by a network analyzer, and the phase is extrapolated from the main beam position. This data is then transformed into far-field pattern.

Beam -width=0.6deg, since only 1/3 of the aperture is used

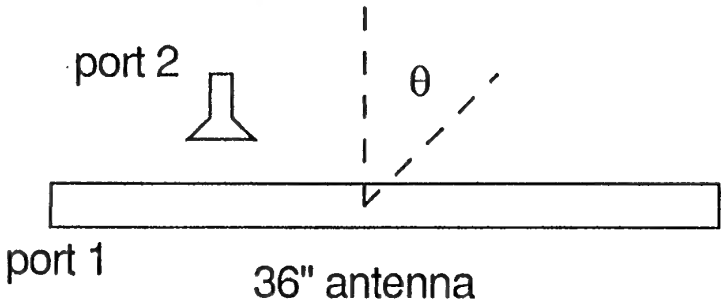

36" antenna

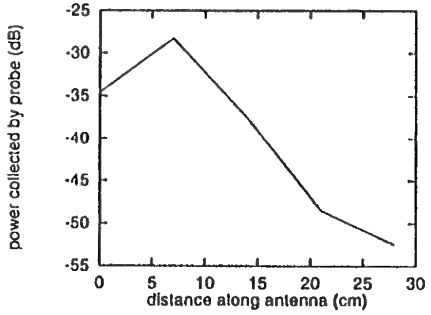

Near field amplitude

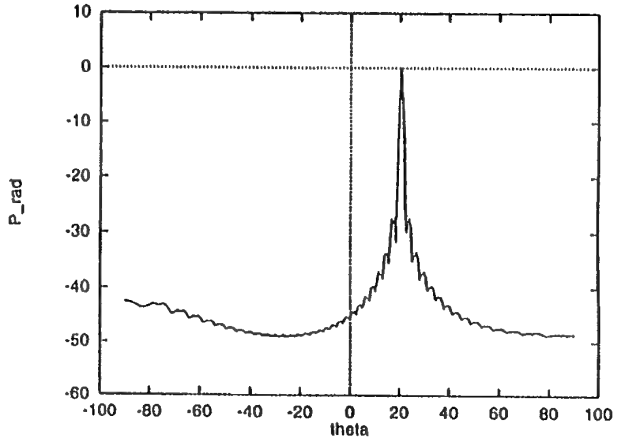

Far field pattern

Time Domain Techniques (FDTD)

COMPARE F.D.T.D. RESULT TO EXPERIMENT:
29 strips, spacing 0.67 λ, 50% duty cycle.
substrate : 0.39λ thick, permittivity:2.46.
Freq. 80 GHz.
(Experimental results published by Raj Mittra and
R.Kastner in IEEE Transactions on AP, July,1981)

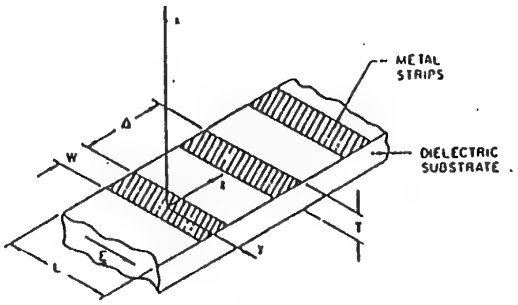

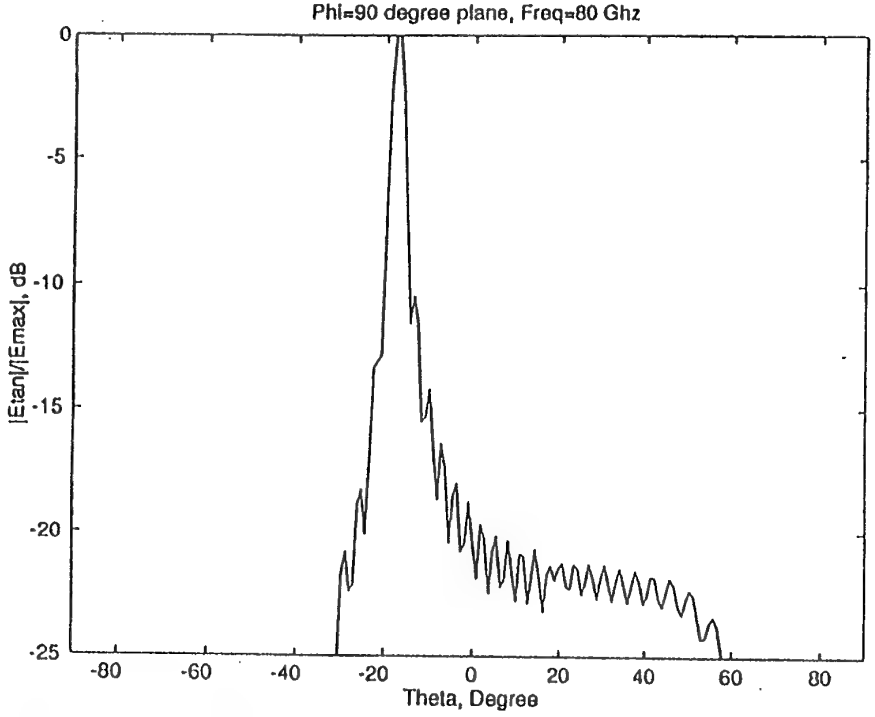

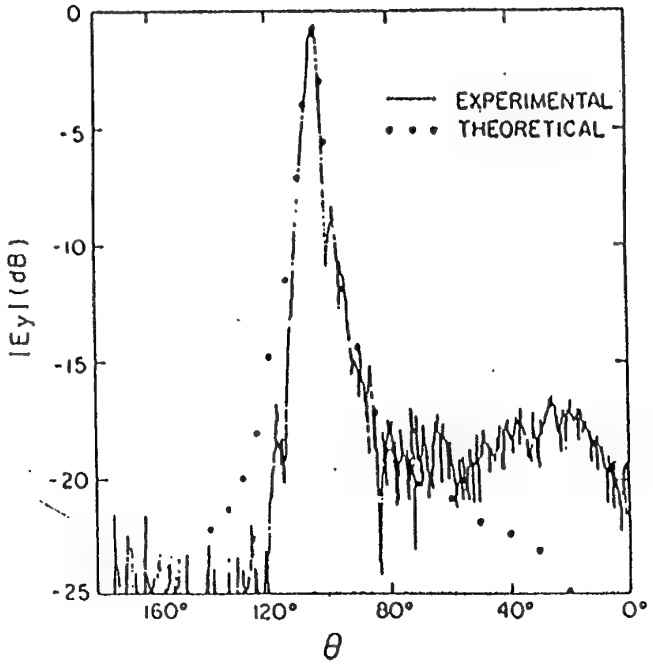

LEAKY WAVE ANTENNA

PLANNED STRUCTURE FOR 212GHZ

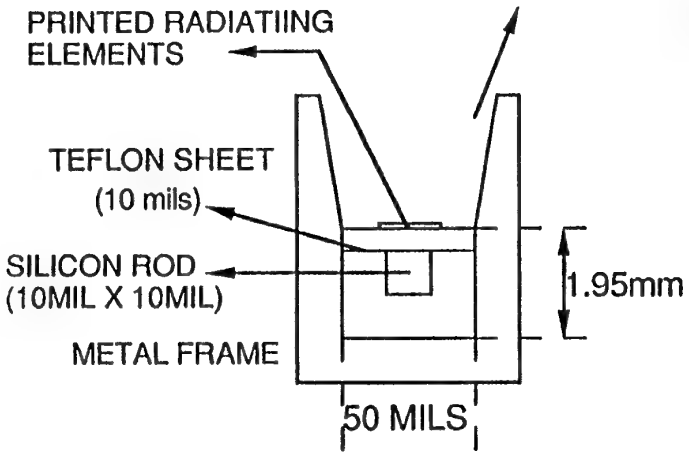

CROSS-SECTION

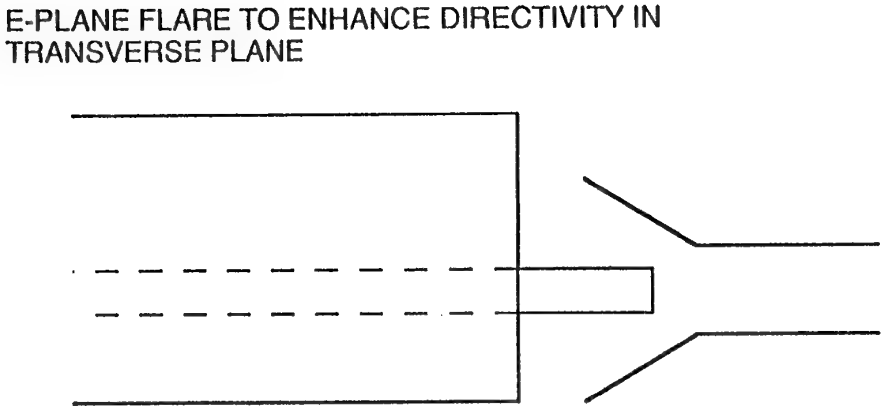

TRANSITION TO WR-5 WAVEGUIDE

TOP VIEW SHOWING POLARIZATION
(INPUT AND RADIATED)

A Novel Active Leaky-Wave Antenna

- Active devices within antenna compensate waveguide loss due to radiation, conductor, and dielectric material.
- Effective aperture is increased as compared to a similarly designed passive antenna. Gain is improved and the beam width is narrowed.
- Overcomes the problem of high loss typically encountered in millimeter-wave applications, thereby improving the antenna performance.
- Prototype is built on a low-cost substrate, the PC board, which suggests an inexpensive alternative to PTFE-based substrates for microwave applications.

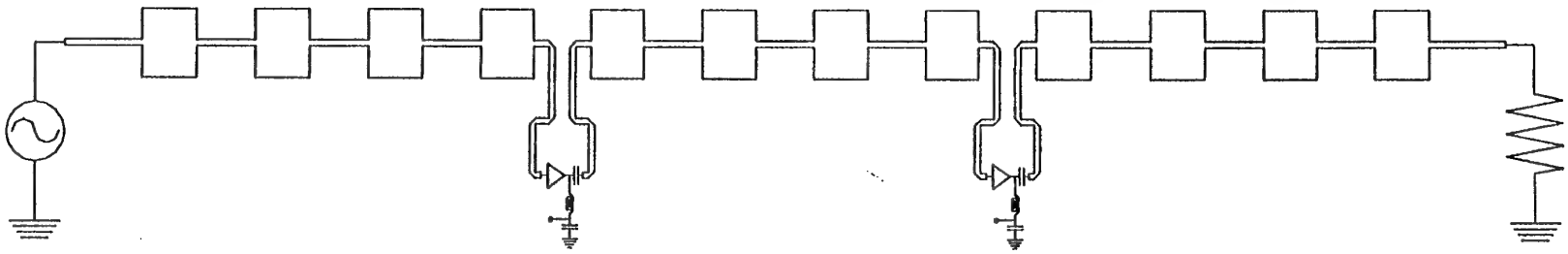

Schematic Diagram of the Active Antenna

A Novel Active Leaky-Wave Antenna

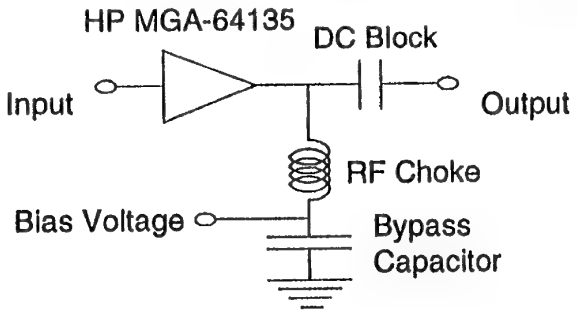

Schematic Diagram of the Active Circuit

Theoretical Comparison Between Passive and Active Antennas

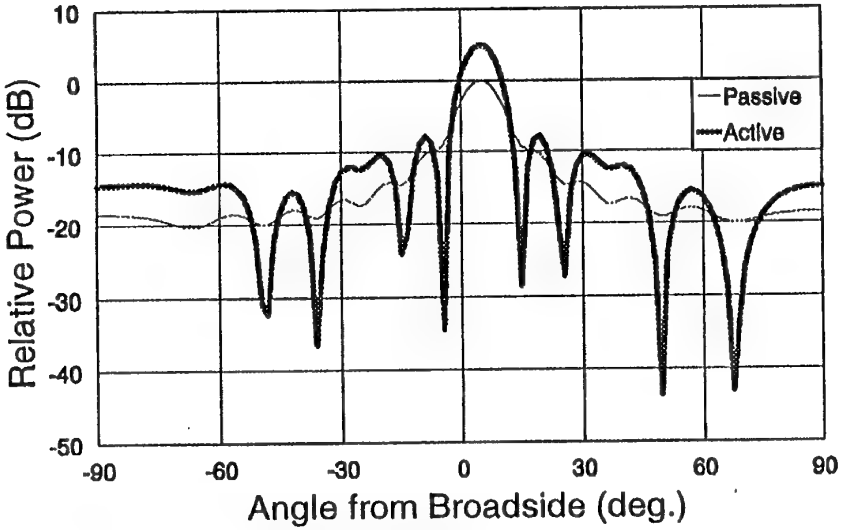

Measured Comparison Between Passive and Active Antennas

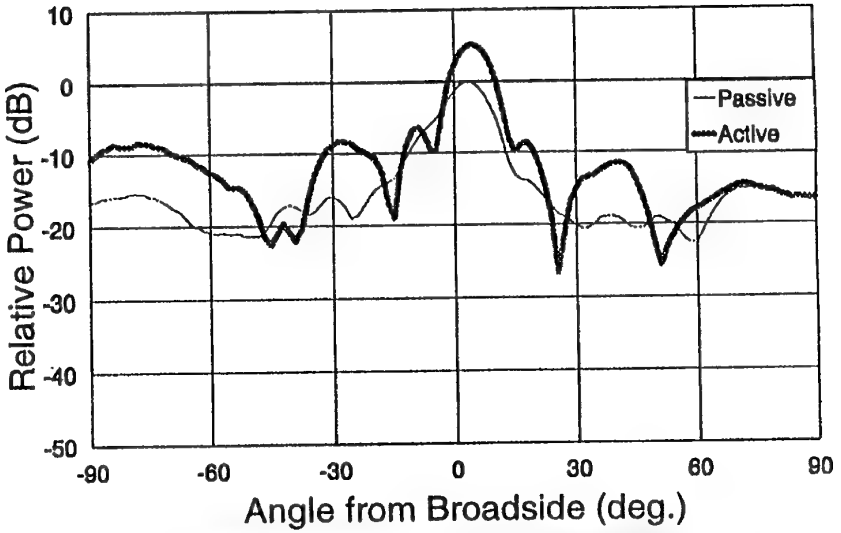

SLAB-BEAM LENS AMPLIFIER

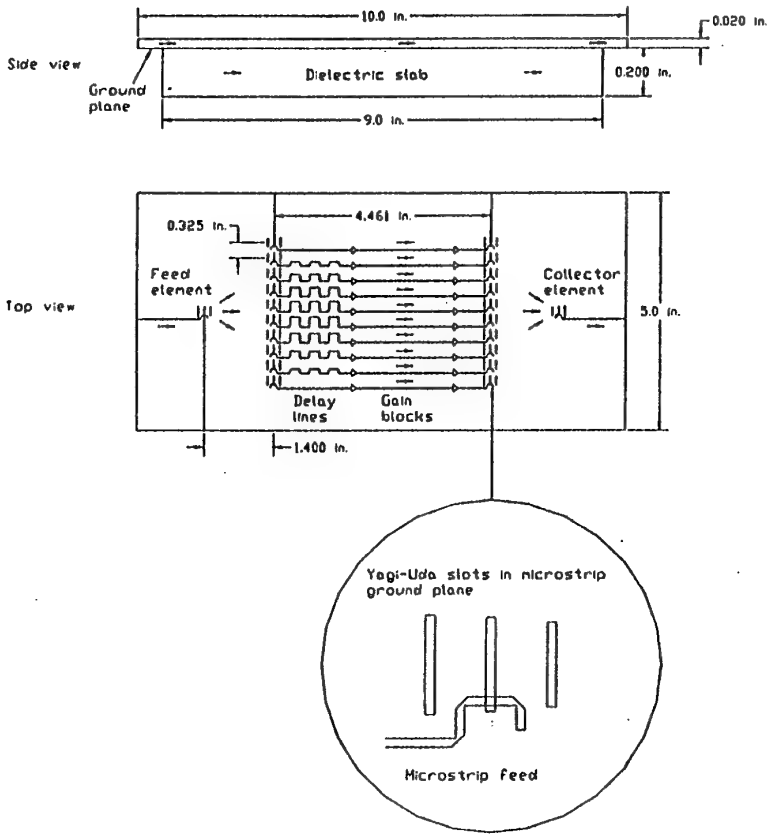

- Construction compatible with palanar fabrication technology
- Gain blocks and microstrip lines are on top side of thin substrate on top of dielectric slab
- Yagi-Uda slot arrays are on the common ground plane

NOVEL USE OF THE YAGI-UDA ARRAY

SLAB-BEAM LENS AMPLIFIER GAIN VERSUS FREQUENCY

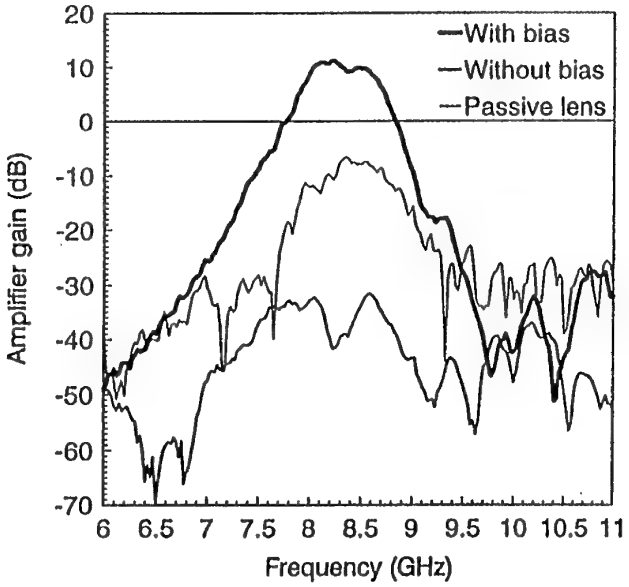

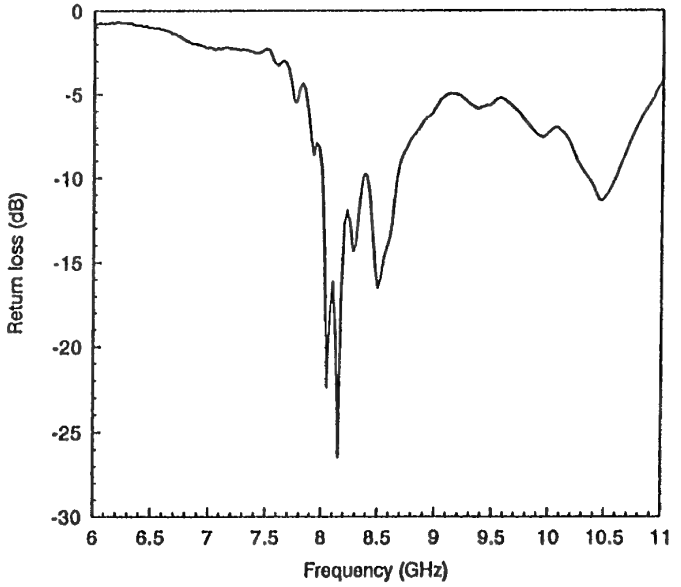

- **Peak gain is 11 dB at 8.25 GHz**
- **3-dB gain bandwidth is 0.65 GHz**
- **Antenna element pass-band matches slab-beam lens amplifier pass-band**

HIGH DEVICE PACKING DENSITY QUASI-OPTICAL ACTIVE ANTENNA

- At millimeter-wave spectrum, generated power per active device is low
- To increase output power in quasi-optical amplifier, high device packing density active antenna is used
- Power combining at circuit level must be simple and does not increase the real-estate significantly
- Here, broadband microstrip-to-slotline transition is used to couple signal to the antenna and power combine/divide to/from the amplifiers
- This results in a 3dB-gain bandwidth of 17.3%

CIRCUIT AND RESULT

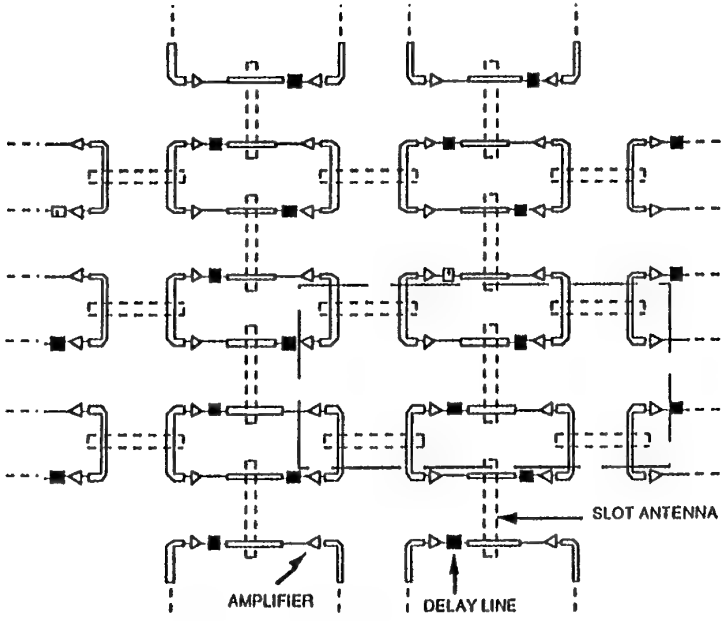

Schematic diagram of the array

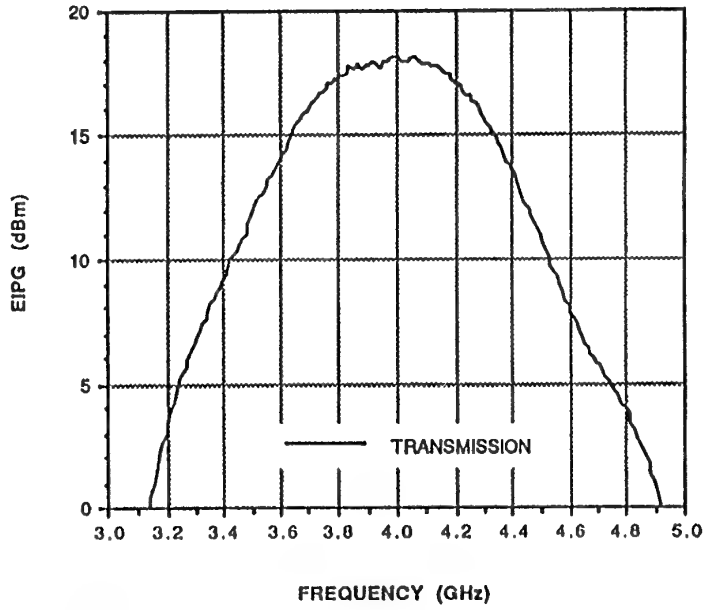

Measured EIPG of a single unit (marked dotted in schematic diagram)

MONOLITHIC 155 GHz AND 215GHz QUASI-OPTICAL SLOT OSCILLATORS

- Advances in device technology have also allowed design of quasi-optical active antenna to be implemented at millimeter-wave frequency

- An InP based HFET is used as the active device :

Gate length	:	0.05 μm
Gate width	:	10 μm
Unity voltage gain transitionfrequency	:	544 GHz
Maximum oscillating frequency	:	738 GHz

- Slot antenna is used with CPW as the transmission lines
  CPW is chosen to elliminate parastics of bonding

- This work is conducted by University of Michigan and Hughes Malibu Research Laboratory

CIRCUIT LAYOUT AND RESULTS

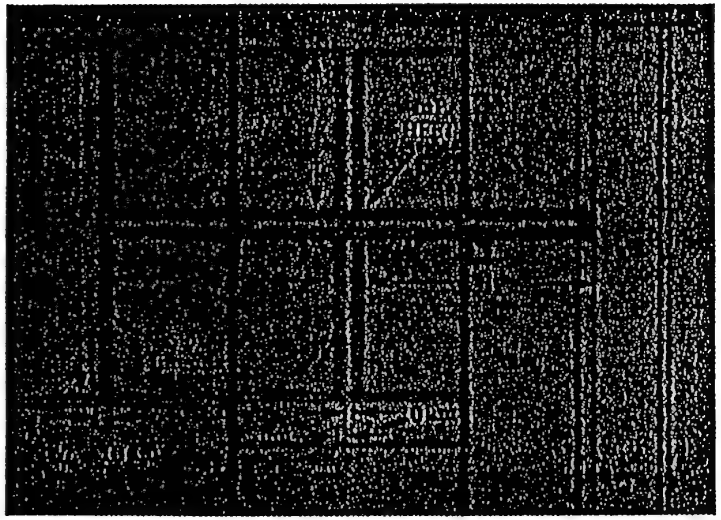

CIRCUIT LAYOUT

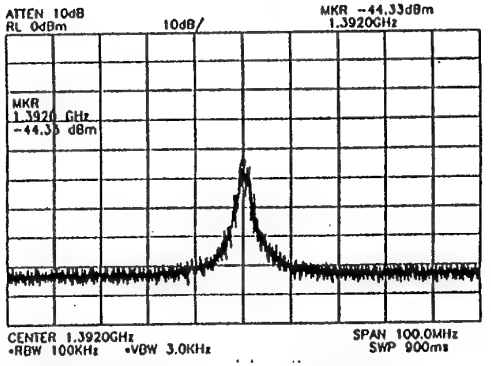

MEASURED CONVERTED SPECTRUM OF 155 GHz

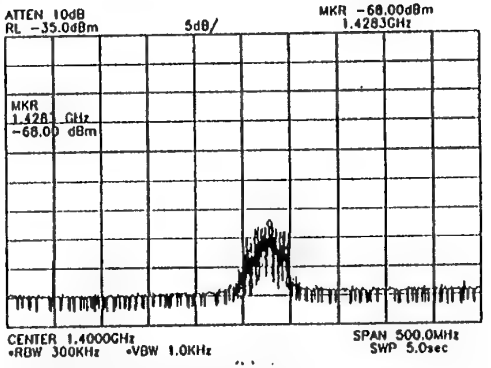

MEASURED CONVERTED SPECTRUM OF 215 GHz

20 GHz quasi-optical oscillator

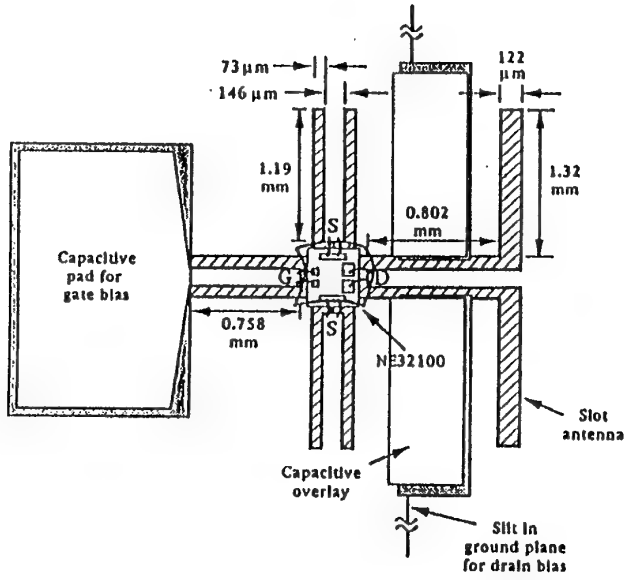

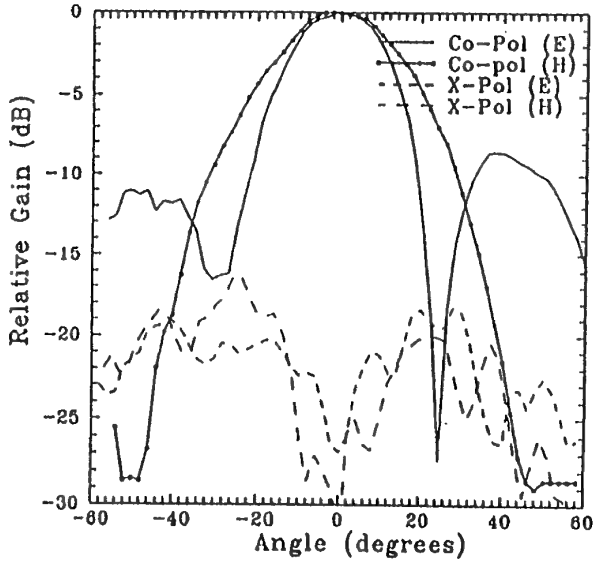

- CPW-fed slot antenna with FET
- Stubs provide resonant feedback

Radiation pattern of oscillator on 2.6 cm silicon substrate lens

(after Kormanyos et al., *IEEE Trans. MTT*, April 1994)

Quasi-optical oscillator with Gaussian output beam

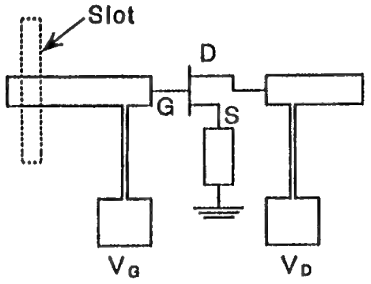

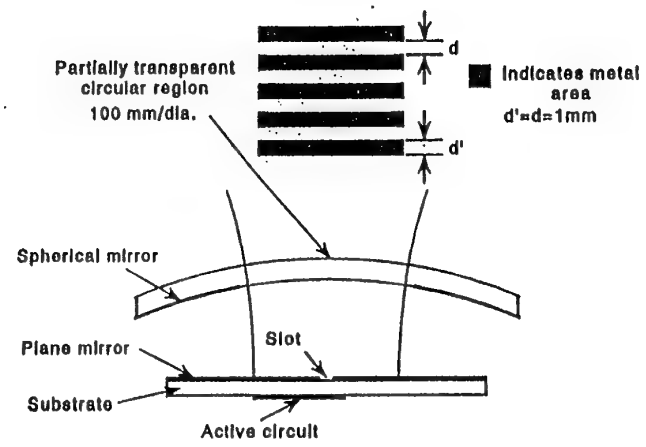

- Microstrip-fed slot antenna
- Ground plane serves as plane mirror to to form resonator with spherical mirror

(after Kiyokawa and Matsui, *IEEE Microwave Guided Wave Lett.*, May 1994)

Multi-slot antennas for quasi-optical circuits

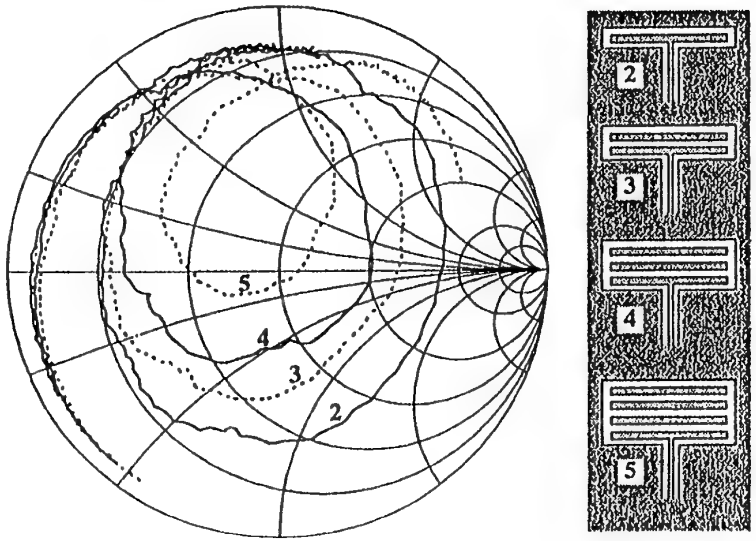

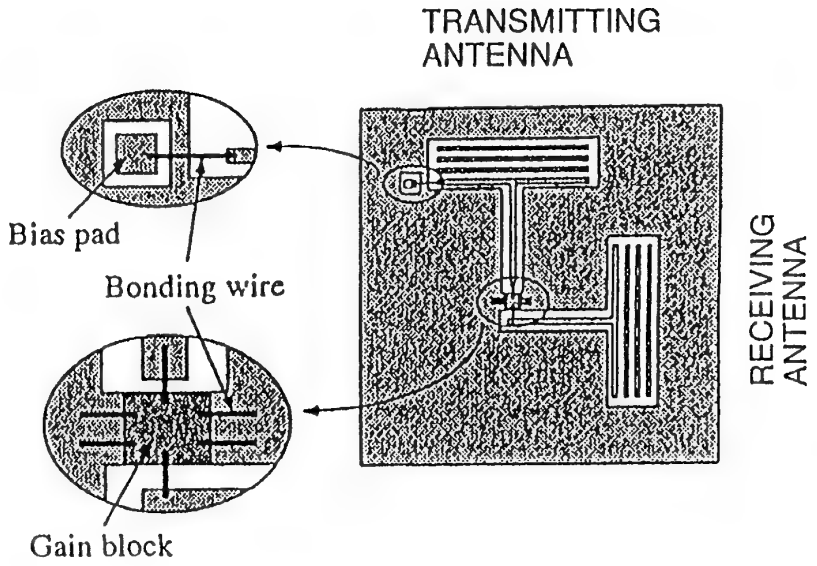

- Impedance of multi-slot antenna approaches 50Ω for 5-slot element
- Wide-bandwidth amplifier

(after Tsai and York, *IEEE Microwave Guided Wave Lett.*, June 1995)

Planar Quasi-optical SIS Receiver at 230 GHz

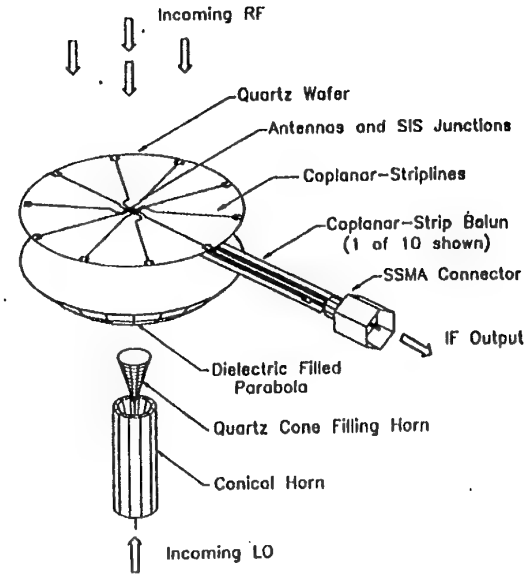

Schematic showing parabola used to focus incoming radiation on planar circuit

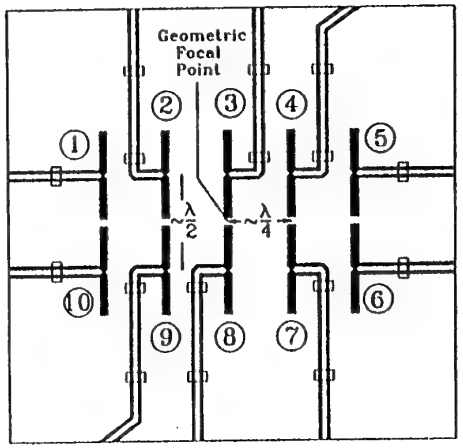

Layout of the 10 printed dipole antennas

(Stimson et al, IEE transactions on MTT, April, 1993)

FOCAL PLANE IMAGING ARRAY BUILT IN SILICON

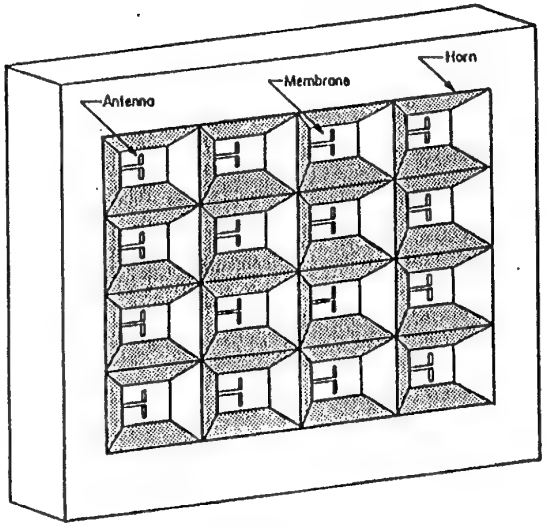

STRUCTURE OF ETCHED SILICON HORN ARRAY

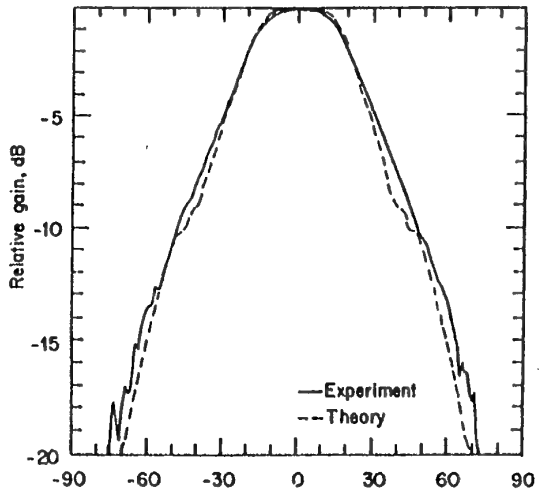

H-PLANE RADIATION PATTERN FOR 9X9 242GHZ ARRAY

G.Rebeiz et al., IEEE Transactions on AP, Sept,1990

Multisources Active Annular Slot Antenna

F. Baudrand, D. Bajon, B. Souny, H. Baudrand

Multisources active annular slot antenna

F. BAUDRAND*, D. BAJON**, B. SOUNY***, H. BAUDRAND*

* *ENSEEIHT, 2 rue C. Camichel, 31071 TOULOUSE CEDEX, FRANCE*
** *ENSAE, 10 avenue E. BELIN, 31055 TOULOUSE CEDEX, FRANCE*
*** *ENAC, 5 avenue E. BELIN, 31071 TOULOUSE CEDEX, FRANCE*

A complete electromagnetic analysis of the structure shown in Figure 1 with or without back cavity is undertaken. Four field effect transistors are inserted directly as active commandable current sources in the slot providing interesting symmetry properties in some scanning applications.
The analysis of the bandwidth and radiation pattern includes the study of the effect of finite internal impedance and real spatial extension and connections of the current sources. The influence of radom is also included in this analysis and experimental confrontation will be presented during the talk.

Analysis

Considering cylindrical symmetry of the structure , the antenna is viewed as an uniaxial discontinuity between two half spaces, one of them being bounded if a back cavity is introduced. The formulation of the boundary value problem is readily obtained by inspection of the formal equivalent network representation of the continuity conditions given in Figure 2. The introduction of the admittance operator $\hat{Y}_S$ is the key point of this work. $\hat{Y}_S$ expresses the local relationship between magnetic and electric fields in the slot. In this way it represents as well the internal impedance of the sources as any lumped element inserted in the slot like short point as considered in [1-2]. In free space, the continuous modal expansion of the fields is carried out by Hankel transform [3]. In the slot, a set of functions defined on the entire domain is chosen to perform the Galerkin's procedure. It should be noticed that the definition domain of these functions overlaps the definition domain of the functions associated to the sources. This point allows a realistic and versatile description of the feeding conditions of the antenna.

Numerical results

As an example of numerical results, the radiation impedance is reported in Fig 3 a-b for the three basic excitation conditions (1 1 1 1), (1 j -1 -j) and (1 -1 1 -1) resulting from symmetry considerations applied to the four sources fed antenna. The upper half-space being loaded with a dielectric lens,.the comparison between Fig 3-a and 3-b highlights the influence of the back cavity on the resonance frequencies.
The effect of the internal impedance of the feeding current sources on the power radiation pattern is given in Figure 4 for the (1 j 1 j) excitation condition. For this same excitation, Figure 5 illustrates the far field normalized power pattern.

Conclusion

This analysis allows a complete and precise description of the realistic topology of an actively loaded slot antenna, including passive elements related to the connexions. Staying in the frame of integral methods, this analysis provides all the fundamental characteristics of the antena with few computation effort.

REFERENCES

[1] C.E. TONG and R. BLUNDELL, « An Annular Slot Antenna on a Dielectric Half-Space », IEEE Trans. on Antennas and Propag., vol AP-42, pp 967-974, Jul 1994.
[2] H. MORISHITA and K. HIRASAWA « Analysis of a Cavity-Backed Annular Slot Antenna with one Point Short », IEEE Trans. on Antennas and Propag., vol AP-39, pp 1472-1478, Oct 1991.
[3] K. ARAKI and T. ITOH, « Hankel transform Analysis of Open Circular Microstrip Radiating Structures», IEEE Trans. on Antennas and Propag., vol AP-29, pp 84-89, Jan 1981.

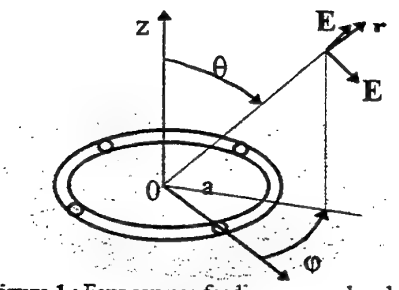

Figure 1 : Four sources feeding an annular slot antenna

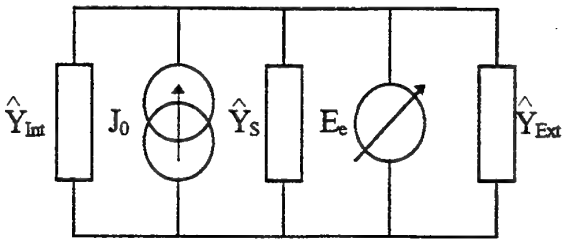

Figure 2 : Equivalent network representation of the boundary value problem.

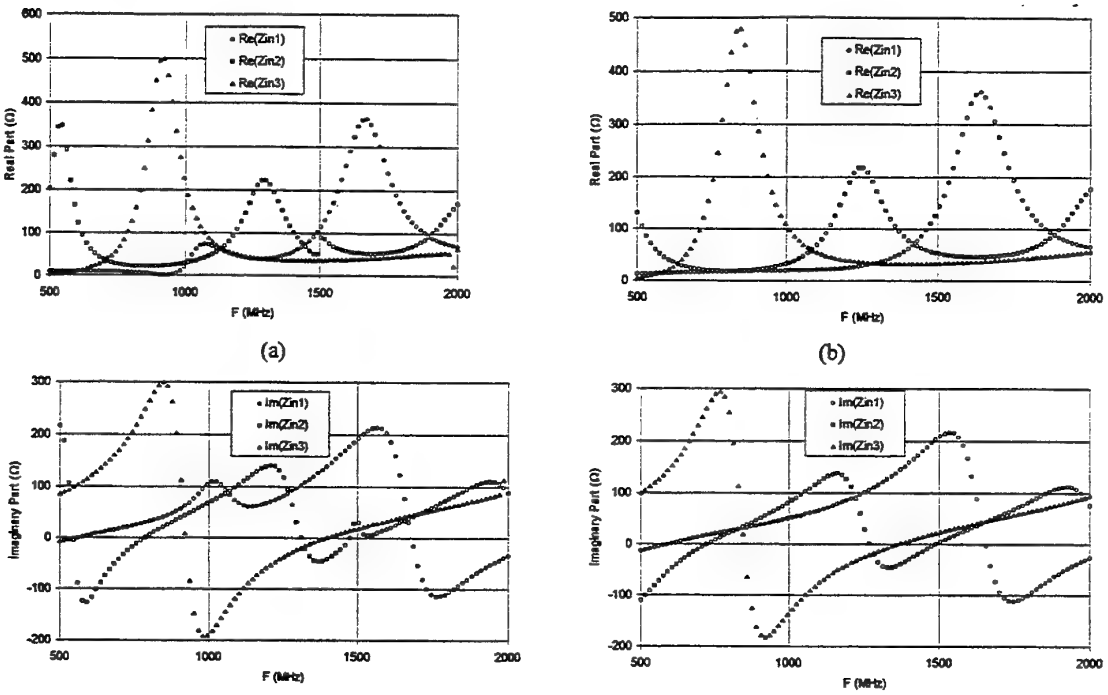

Figure 3 : Input impedance of sources (a) with (b) without back cavity.
The index 1-2-3 refer to (1, 1, 1, 1), (1, j, 1, j) and (1, -1, 1, -1) excitation conditions respectively.

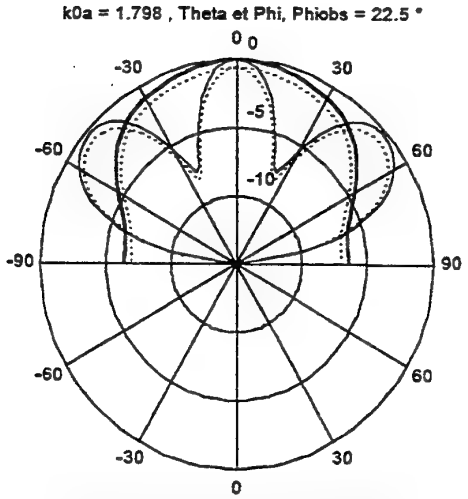

Figure 4 : Polar power radiation pattern for configuration #2 with 3° extended sources.
—— infinite internal impedance
····· finite internal impedance : R = 1kΩ, C = 1 pF

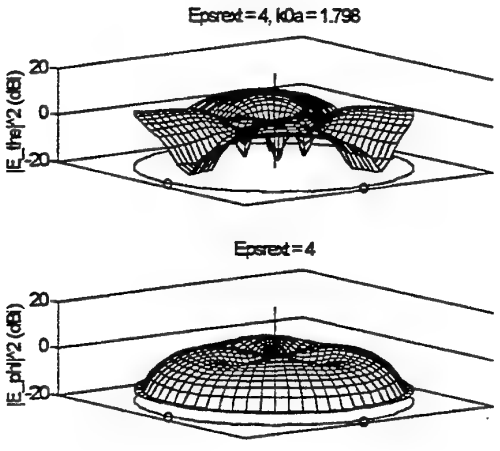

Figure 5 : Far field radiation pattern for configuration #2 in polar coordinates.

Spinning-Grating MMW Scanning Antenna

V. A. Manasson, L. S. Sadovnik and R. Mino

SPINNING-GRATING MMW SCANNING ANTENNA

V.A. Manasson, L. S. Sadovnik and R. Mino
WaveBand Corporation, 375 Van Ness Ave., Suite 1105, Torrance, California 90501
Telephone: (310)212-7808, FAX: (310)212-7726
E-mail: manasson@aol.com

Cost reduction is one of the most important considerations in millimeter-wave (MMW) radar development. Hardware, especially the phase-shifters, for electronic beam scanning in the MMW band presents complex fabrication challenges that dramatically raise the device cost. A typical mechanically-scanning antenna contains one or more hinged parts (lenses, mirrors or feeds). In operation they experience strong mechanical accelerations, and other forces that sharply limit the scanning speed. We propose a solution to this problem.

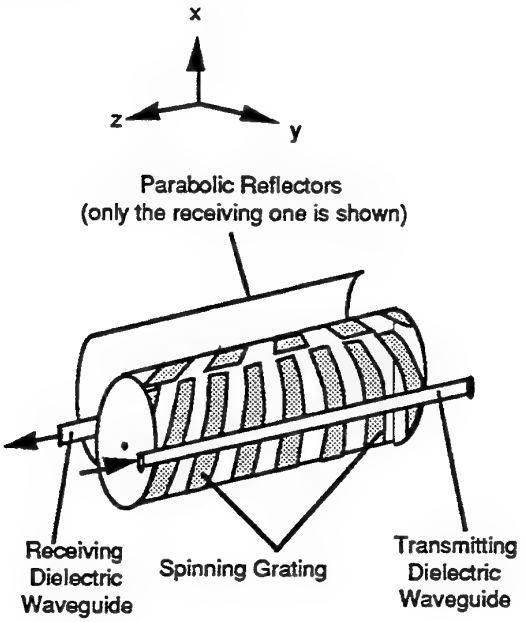

Figure 1
The spinning grating consists of two identical semi-cylinders. The grating periods in the immediate proximity of the two waveguides are exactly the same.

The proposed antenna (see Figure 1) consists of two dielectric waveguides, two parabolic reflectors, and a spinning metal grating that perturbs the propagation of the evanescent wave along the waveguide and controls the diffraction of the MMW out of the waveguide. Beam tracing is shown in Figure 2 for the y-z plane and in Figure 3 for the x-y plane.

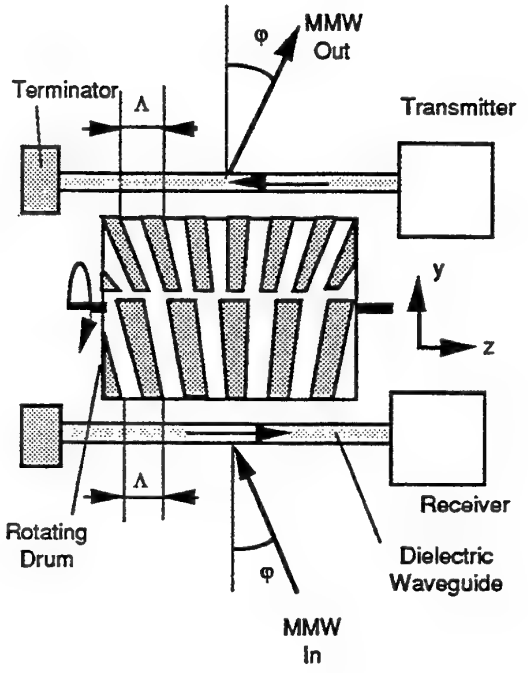

Figure 2
Beam tracing in the y-z plane. The angle φ of emission and of reception is determined by the instantaneous value of the grating period Λ, which varies along the circumference of the drum.

The period Λ of the grating close to the waveguide at any given time is a function of the angular position of the drum at that instant. The coupling angle φ is determined by Λ (see Figure 2). Rotation of the drum steers the beam. The cylindrical grating consists of two identical semi-cylinders with identical grating patterns. The identical pattern on the two semi-cylinders ensures that the grating period Λ facing the waveguides will be the same for both waveguides, as will the coupling angles φ (in accordance with the reciprocity principle). Parabolic mirrors redirect the beams in the x-direction (see Figure 3) and confine them in the y-direction.

The angle of the outgoing radiation φ is determined by the equation

$$\sin\varphi=\beta/k_0-p\lambda/\Lambda, \qquad (1)$$

where β is the propagation constant, λ and $k_0=2\pi/\lambda$ are, respectively, the wavelength and the wave vector in free space, p is an integer, and Λ is the grating period. β depends on the waveguide material, its profile, size, and mode order. Equation (1) indicates that φ depends on Λ. This dependence forms the basis for the scanning capability. In the proposed architecture, Λ varies continuously as the cylinder rotates.

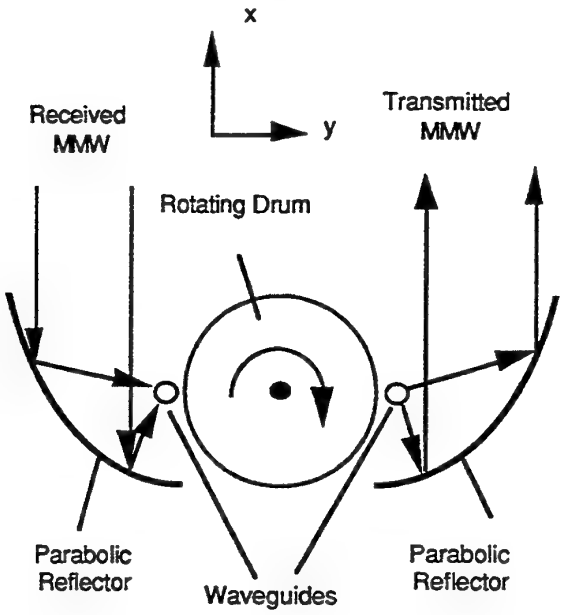

Figure 3
Parabolic mirrors direct and shape the beams in the x-y plane.

We fabricated the antenna and tested it using near-field technique at a frequency of 94 GHz.

The scanning range (30 degrees) and the beamwidth in both dimensions (0.5 and 5 degrees, respectively) was close to the design numbers. The far-field patterns obtained from the near-field measurements for one position of the grating are shown in Figures 4 and 5 for the H-plane and E-plane, respectively.

Conclusion

We demonstrated a new antenna with a high potential for fast rate scanning. It has a 30 degree scanning range, and 0.5 degree beam-width in the scanning plane. The first prototype of the new antenna suffers from higher than expected side-lobes. Numerical modeling revealed several factors contributing to this effect. The solution for this problem has been found and its implementation is underway.

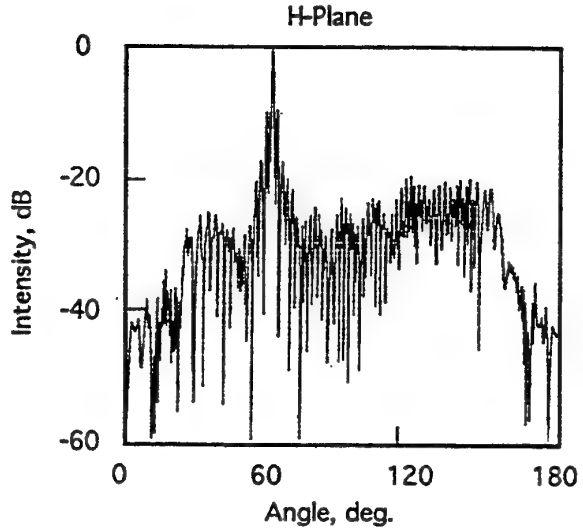

Figure 4

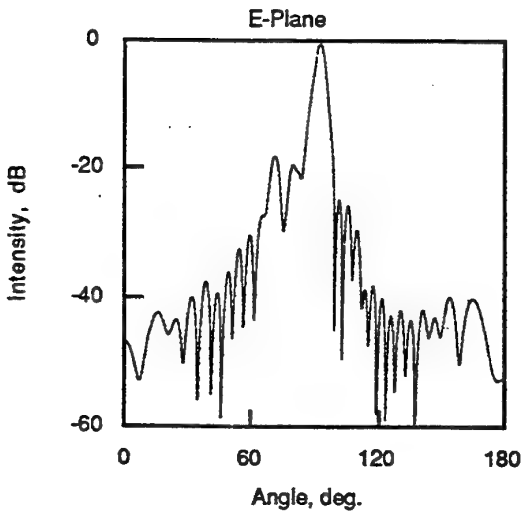

Figure 5

Acknowledgments

Near-field measurements were performed at GM Hughes Radar System Group.

We want to thank Mr. Long Bui of Lear Astronics for helpful discussions.

Stepped Leaky-Wave Antennas for Microwave and Millimeterwave Applications

C. Di Nallo, F. Frezza, A. Galli, G. Gerosa and P. Lampariello

1996 International Workshop on Millimeter Waves - Orvieto, Italy, April 11-12, 1996
Contributed Paper

STEPPED LEAKY-WAVE ANTENNAS FOR MICROWAVE AND MILLIMETERWAVE APPLICATIONS

Carlo Di Nallo, Fabrizio Frezza, Alessandro Galli, Giorgio Gerosa and Paolo Lampariello

"La Sapienza" University of Rome, Rome, Italy - Department of Electronic Engineering
Via Eudossiana 18, 00184 Roma, Italy
Tel: +39-6-44585841 ; Fax: +39-6-4742647
E-mail: plamp@die.ing.uniroma1.it

Abstract

A recently proposed class of leaky-wave antennas, derived by slotted rectangular waveguides with stepped section [1], is here analyzed and developed for advanced applications at microwave and millimeter waves.

The basic advantages of such a novel topology are represented by almost-separated controls of phase and leakage characteristics through different geometric parameters (i.e., the average length and the unbalance of the lateral arms, respectively), and also by compactness and good versatility. These fundamental attractive features have pushed us to further investigate the operational potentialities of the stepped antennas. In addition to the possibility of achieving favorable radiation patterns with controlled sidelobes through simple longitudinal tapering of the basic geometry, we have focused our attention on various other important design aspects.

Concerning the capability of enlarging the pointing angular range via frequency scanning, we have evaluated the effects of the introduction of dielectric materials. The relevant improvements have been quantified for both the uniform and the tapered geometries. In this sphere, also the use of practical radomes to protect the structure has been taken into account.

The achievement of effective pencil-like beams both in elevation and in azimuth is then analyzed by modeling suitably one-dimensional scannable arrays of line sources.

All the relevant theoretical simulations have been based on proper analytical and numerical procedures (transverse-resonance network to calculate the phase and leakage constants, and therefore to evaluate the beam orientation and width; standard tapering and optimization methods to control the sidelobes; unit cell approach to characterize the arrays [2]), suitably implemented in a modular code.

The practical implications related to the effective realization of prototypes of stepped antennas are considered as well, both at microwaves and at millimeter waves. In this connection, specific attention has been paid to the accurate evaluation of the effects of ohmic losses in the dielectric and conductor parts, which can affect the performances of leaky-wave antennas in particular as frequency is increased.

On the basis of such global investigation, this kind of antennas has confirmed excellent performances and perspectives for applications in large ranges of frequency.

References

[1] C. Di Nallo, F. Frezza, A. Galli, and P. Lampariello, "Complete characterisation of leaky-wave antennas based on stepped rectangular waveguides," *Proc. 25th European Microwave Conf.*, Bologna, Italy, pp. 1062-1067, Sept. 1995.

[2] A. A. Oliner, "Leaky-wave antennas," in R. C. Johnson, Ed., *Antenna Engineering Handbook*, 3rd ed., McGraw-Hill, New York, NY, Ch. 10, 1993.

Plane Wave Scattering by a Large and Finite Strip Array on Dielectric Substrate

L. Vegni, A. Toscano and B. Popovski

PLANE WAVE SCATTERING BY A LARGE AND FINITE STRIP ARRAY ON DIELECTRIC SUBSTRATE

L. Vegni, A. Toscano and B. Popovski

I. INTRODUCTION AND PROBLEM FORMULATION

The wave scattering by strip gratings supported by a dielectric slab remains a canonical problem in wave scattering theory. It also find applications in number of areas like frequency selective surface, slow-wave structures, leaky-wave antennas, and microstrip arrays. For instance, frequency selective properties of these screens are exploited for use as components in reflector antenna systems, or to reduce radar cross section (RCS) and at infrared wavelengths as components in optical systems. Hence, wave scattering from strip gratings has been investigated by many authors. However, most works are limited to infinite periodic grating. In such studies, the problem reduces to much simpler investigation of scattering from a single unite cell. Recently, attention has been given to the effects of array truncation [1,2,3].
The purpose of this paper is to extend this technique [1] to more complicated structures, that is scattering from a finite array of strips supported by a dielectric slab, with or without ground plane. Prior solutions for radiating microstrip antenna or scattering problems were primarily concerned with a narrow range of frequencies. If one were to apply this techniques directly to ultra wideband (UWB) scattering problem, the CPU time required would be excessive as to make the analysis impracticable. To avoid this difficulty, the present study utilises a hybrid numerical/analytical technique. This involves application of spectral-domain formulation, with a moment method (MM) solution. Closed form asymptotic expressions are developed for mutual coupling integrals that contain expansion and testing functions separated by 0.1 λ_0 or more. This method leads to highly efficient and accurate procedure with a noteworthy reduction of the CPU time. Both TE and TM strips are examined, and calculated results are compared to the available data in the literature. Comparisons show a very good agreement with the available data in the literature. It has also to be noted that the new formulation, proposed here, can be easily extended to more complicated structures involving biisotropic, anisotropic and bianisotropic grounded slabs and resistive strips.

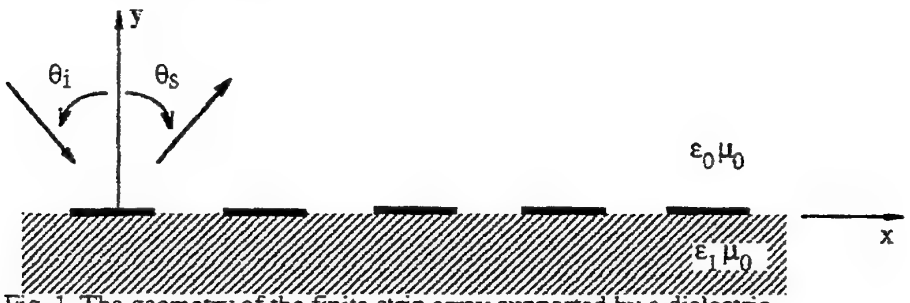

Fig. 1. The geometry of the finite strip array supported by a dielectric slab.

Referring to Fig.1, the surfaces of the strips are assumed to be perpendicular to $\hat{y}$, located at y=0, with strip width W, strip separation D, and the fields in this two-dimensional problem are assumed to be independent of z.
For a plane wave incident obliquely on the strips in Fig.1, the electric field integral equation (EFIE) to be solved is a statement of the boundary condition that the total tangential electric field must vanish on the perfect conductors. The scattered field can be expressed in terms of the dyadic Green's function and surface current, respectively, in the spectral wave number domain. The required component of the spectral domain Green's function for sources and observation points located at y = 0 plane can be found in [4]. The unknown strip currents are expanded into a set of N basis function with unknown coefficients a_k. Discretization of the EFIE results in a system of linear algebraic equations written as: $[Z][I]=[V^i]$. After the decomposition, the impedance matrix elements are determined using Galerkin testing procedure and are given by

$$K_{mk}^{e,h} = \int_c \tilde{G}^{e,h}(k_x) s_m(k_x) s_k(k_x) e^{-jk_x\Delta_x} e^{k_x nW} dk_x \qquad (1)$$

In (1) n is either 0, 1 or -1, $D_x = x_m - x_k$ and function s_k is the slowly varying part of the Fourier transform of the basis function. Integrals (1) can be evaluated most efficiently by mapping the contour of integration along the real axis onto the steepest descent path (SDP). It can be shown that the mutual coupling integral (1) can be written in a closed asymptotic expression [5].

II. NUMERICAL RESULTS

In order to test the validity of the algorithm based on MM and asymptotic solution of the mutual coupling integrals, we computed RCS for number of different array sizes and slab widths. Fig.2 shows calculated RCS versus frequency in the reflected direction for a uniform array of 10 strips on a slab without a ground plane with $\varepsilon_r = 2.57$, $d = 0.171\ \lambda_0$, $W = D$, and E_z incidence at $\theta_i = 30^\circ$. All results in this paper related to the variation of the RCS with frequency are obtained by calculating impedance matrix every 200 MHz in the ultra-wide frequency range, and, then, matrix elements are interpolated to obtain scattered field every 50 MHz. In this case variation of the RCS in the frequency range from 9 GHz to 42 GHz are compared with results obtained by numerical integration of EFIE, and reference [3]. Agreement is very good.

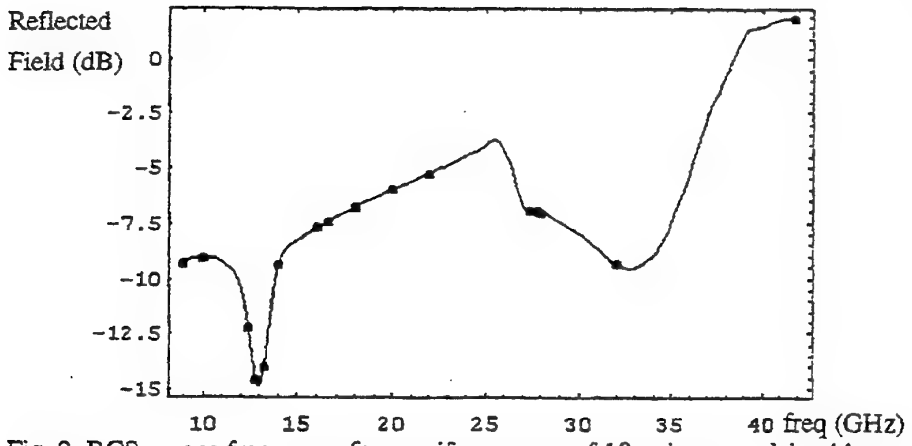

Fig. 2. RCS versus frequency for a uniform array of 10 strips on a slab without a ground plane ($\varepsilon_r = 2.57$, $d = 0.171\ \lambda_0$, $W = D$, and E_z incidence at $\theta_i = 60^\circ$).

— this work
• reference [3]

III. REFERENCES

[1] L.Carin and L.B.Felsen, "Efficient analytical-numerical modelling of ultra-wideband pulsed plane wave scattering from a large strip grating"Int. Jour. of Numerical Modelling: elec. netw.,devices and fields",Vol.6, pp. 3-17, 1993.

[2] T.Cwik and R.Mittra, "The Effects of the Truncation and Curvature of Periodic Surfaces: A Strip Grating", IEEE Trans. Antennas Propagat., vol. 36, pp. 612-622, May 1988.

[3] C.Cheng Lu and W.Cho Chew, "Electromagnetic Scattering of Finite Strip Array on a Dielectric Slub", IEEE Trans. MTT., vol 41, pp. 97-100, January 1993.

[4] L.Vegni, R.Cicchetti and P.Capece, "Spectral Dyadic Green's Function Formulation for Planar Integrated Structures", IEEE Trans. Antennas Propagat., vol. 36, pp. 1057-1065, August 1988.

[5] B.Popovski, A.Toscano and L.Vegni, "Radial and Asymptotic Closed Form Representation of the Spatial Microstrip Dyadic Green's Function", Journal of Electromag. Waves and Applic. vol 9, pp. 97-126, No. 1/2, 1995.

Efficient Analysis of Millimeterwave Transmission Lines and Components by the Method of Lines

L. Vietzorreck and R. Pregla

Efficient Analysis of Millimeterwave Transmission Lines and Components by the Method of Lines

Larissa Vietzorreck and Reinhold Pregla
FernUniversität, Allgemeine und Theoretische Elektrotechnik, D-58084 Hagen, Germany
Tel.: +49 2371 566253 Fax: +49 2371 51898
e-mail: Larissa.Vietzorreck@FernUni-Hagen.de

The application of millimeterwaves to the commercial sector has been increased steadily in the last years, especially on the areas of mobile communication or traffic control. Therefore there is an increasing need of accurate methods for analysis and modeling millimeterwave components or devices.
With increasing frequencies the properties of the material, such as dielectric and ohmic losses or the finite thickness of the metallization, play a more important role than for microwave frequencies. Add to this the investigated structures are 3-dimensional, containing dielectric cavities underneath the transmission lines or metallic air bridges for coplanar waveguides. These features require not only an accurate but moreover a general and flexible method of analysis.
It has been shown in numerous papers, that the Method of Lines (MoL) is highly suitable for analysis of microwave and optical components such as waveguides, filters, discontinuities [1]. The semi-analytical approach guarantees a high accuracy combined with a numerical efficiency. Appropriate to the kind of structure under investigation, a one-dimensional or two-dimensional discretization has to be provided, whereas in the remaining directions the calculation is analytical.
Typical waveguides for millimeterwave technology are different forms of coplanar lines [2], buried microstrip lines (BMSL) [3] (see Fig. 1) or even rectangular waveguides. For an efficient analysis these structures are subjected an investigation using a one-dimensional discretization, where the cross-section is divided in single layers.

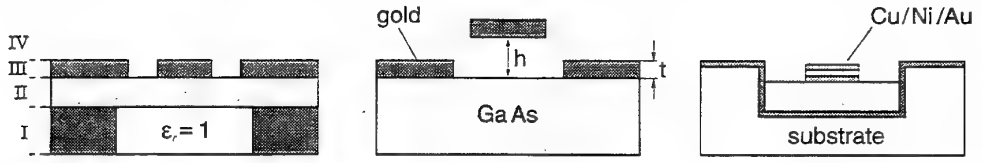

Fig. 1: a) Different types of CPWs b) BMSL

With a generalized impedance transformation in connection with the matrix partition technique [4] all interesting features of the transmission line - propagation constant, attenuation, characteristic impedance - are calculated very accurately with little numerical effort. With the proposed algorithm, where the impedances are transformed from interface to interface analytically, layer thicknesses of extremely different dimensions can be treated in the same way. No complementary effort has to be taken to eliminate disturbing effect by higher order modes. All essential properties such as inhomogeneous dielectric layers, finite thickness of the metallization and losses are taken into account. In this way the influence of the different parameters concerning material and geometry are determined.
For the analysis of circuits and components containing discontinuities a two-dimensional discretization with discretization lines in propagation direction becomes necessary [5]. Here the structure is not divided into layers, but into cascaded sections (see Fig. 2). The analytical calculation is now performed in propagation direction, which makes special boundaries at the input and output unnecessary. The size of the discretization window depends only on the cross-section, which is extremely favorable for long structures or structures with significant differences in the length of the sections. For the cross-section of every section the general formulation allows an inhomogeneous distribution of the dielectric material and a two-dimensional metallization.

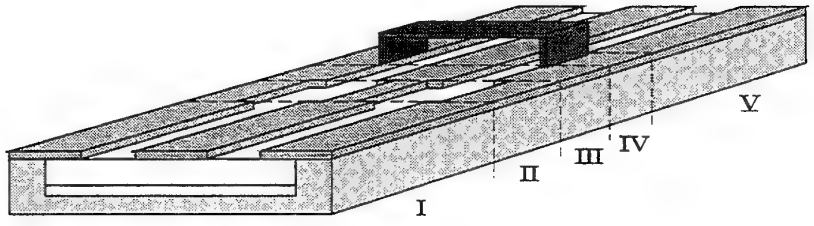

Fig. 2: Cascaded CPW discontinuities

Two examples of millimeter wave components are given. Fig. 3 shows an E-plane filter [6, 7] for which an analysis using a one-dimensional discretization is sufficient. In Fig. 4 the scattering parameters vs. frequency in comparison to calculated and measured values are depicted.

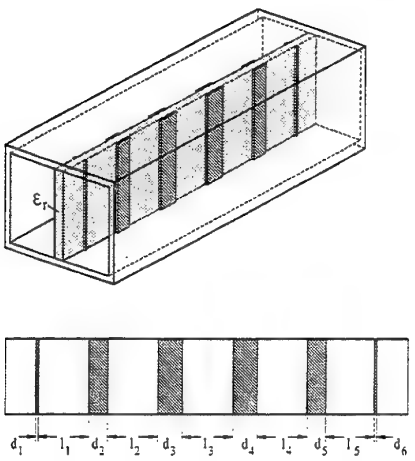

Fig. 3: E-plane filter

$a = 1.651$ mm, $d_{sub} = 0.0762$ mm, $\varepsilon_r = 2.1$, $d_1 = d_6 = 0.03175$ mm, $d_2 = d_5 = 0.3365$ mm, $d_3 = d_4 = 0.887$ mm, $l_1 = l_5 = 0.887$ mm, $l_2 = l_4 = 0.8989$ mm, $l_3 = 0.8992$ mm

As an example for a 3-dimensional structure, analyzed with a 2-dimensional discretization, a coplanar step discontinuity was calculated. The analysis was performed once for an infinitely thin metallization, once for a metallization of the finite thickness of $t = 10$ μm. The amplitudes of the corresponding scattering parameters are compared to results of [8] in Fig. 5. The data of the structure are: $w_1 = 0.2$ mm, $w_2 = 0.8$ mm, $s_1 = 0.1$ mm $s_2 = 0.6$ mm, $\varepsilon = 2.22$, $h = 0.254$ mm. The analysis of these examples shows a good consistency to the results gained by other methods, so that further investigations will be extended to more complex structures.

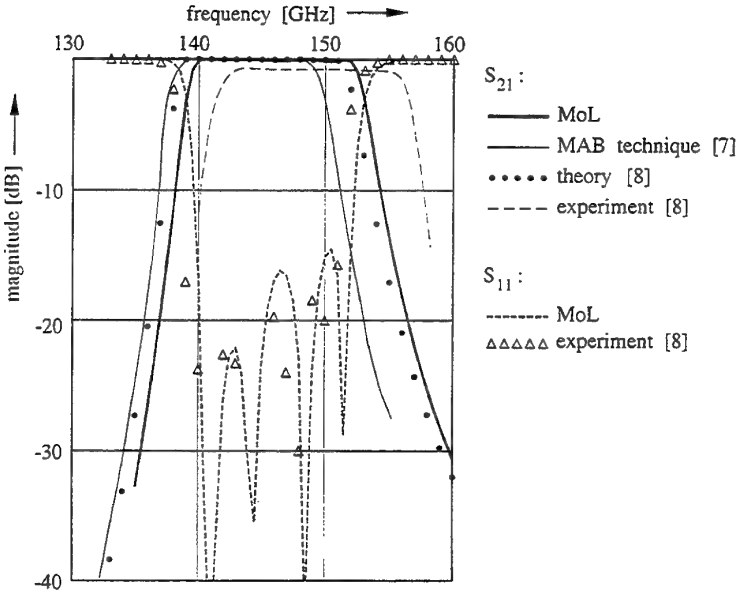

Fig. 4: Scattering parameters S_{11} and S_{21}

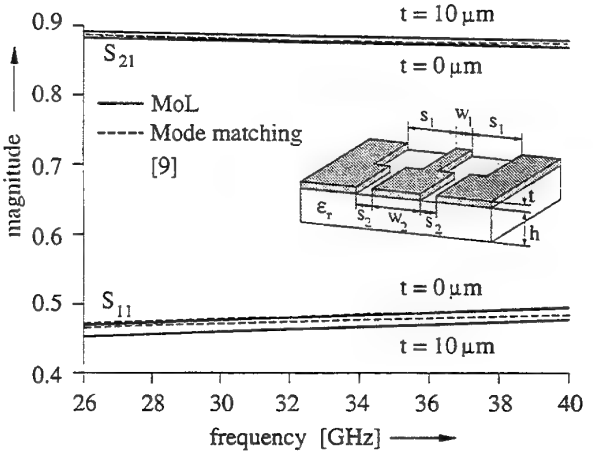

Fig. 5: S-parameter of CPW step-in-width

References

[1] R. Pregla and W. Pascher. The Method of Lines. In *T. Itoh, editor, Numerical Techniques for Microwave and Millimeter Wave Passive Structures*, pages 381–446. J. Wiley Publ., New York, USA, 1989.

[2] S. Hofschen and I. Wolff. Simulation of an Elevated Coplanar Waveguide Using 2 - D FDTD. In: *IEEE Microw. Guid. Wave Lett.*, Vol.6(1), pages 28–30, 1996.

[3] T. Ishikawa and E. Yamashita. Experimental Results on Buried Microstrip Lines for Constructing High - Density Microwave Integrated Circuits. In: *IEEE Microw. Guid. Wave Lett.*, Vol.5(12), pages 437–438, 1995.

[4] R. Pregla. Transformation Matrix Partition Technique and Impedance /Admittance Transfer in the Method of Lines, 1996. in preparation.

[5] L. Vietzorreck and R. Pregla. Analysis of Discontinuities in Microwave Circuits with a New Eigenmode Algorithm Based on the Method of Lines. *Proc. 25th European Microwave Conference*, pages 804–808, Bologna, Italy, Sep. 1995.

[6] J. Macháč. Analysis of Discontinuities in Waveguiding Structures by MAB Method. In: *IEE Proceedings-H*, Vol.139(4), pages 351–357, 1992.

[7] L. Q. Bui, D. Ball, and T. Itoh. Broadband Millimeter-Wave E-Plane Bandpass Filters. In: *IEEE Trans. Microw. Theory Tech.*, Vol.32(12), pages 1655–1658, 1984.

[8] T.W. Huang and T. Itoh. The Influence of Metallization Thickness on the Characteristics of Cascaded Junction Discontinuities of Shielded Coplanar Type Transmission Line. In: *IEEE Trans. Microw. Theory Tech.*, Vol.41(4), pages 693–697, 1993.

Computation of the Characteristic Impedance and Cutoff Frequencies of the Suspended Strip in Elliptical Cross-Section

T. Rozzi, L. Pierantoni, M. Ronzitti

COMPUTATION OF THE CHARACTERISTIC IMPEDANCE AND CUTOFF FREQUENCIES OF THE SUSPENDED STRIP IN ELLIPTICAL CROSS-SECTION

Tullio Rozzi, Luca Pierantoni, Marco Ronzitti

Dipartimento di Elettronica ed Automatica, Università degli Studi di Ancona, Via delle Brecce Bianche, 60131 Ancona, Italy. Tel. +39 71 2204840, Fax +39 71 2804334.

Synthesis - A thin metallic strip centrally suspended in a hollow conductor of elliptical cross-section, as shown in Fig.1, constitutes a coaxial-like TEM transmission line, where TEM characteristic impedance and mode pattern can be controlled by varying the stripwidth and excentricity. Apart from its own merit, it can be found in transitions from ordinary coax to CPW and other planar guides or from coax to TEM cells [1]. Although the fundamental TEM mode of the cross-section of Fig.1 can be analyzed by conformal mapping [2], [3], its higher order TE/TM modes involve solution of the wave equation with boundary conditions on the elliptic conductor and in presence of sharp edge conditions at the strip extremities. The latter problem too is solvible by a variety of methods, such as variational techniques, transverse resonance, or numerical methods such as Finite Elements Method (F.E.M.) as will be done in this paper. This configuration, however, also provides an instructive test-bed for a direct solution of the wave equation by the method of separation of coordinates, once the appropriate system of coordinates is selected. The latter is seen to be the elliptic cylinder system, where the inner strip conductor is seen as the limiting case of an ellipse of unit excentricity. Separation of 'radial' and 'angular' dependences leads to the well known Mathieu equations, whose solutions are fairly well documented [4], [5] and currently avalaible in standard mathematical codes [6]. The closed form analysis very simply produces the fundamental TEM mode, while also highlighting the existence of two types of higher modes, first reported in 1973 in [7] in connection with ridged elliptical waveguides. The first kind is found in closed elliptical waveguides and is perfectly 'regular', that is, it does neither feel the presence of the strip, nor present edge singularities. The latter kind, however, being closely linked to the presence of the strip, displays the typical singular square-root behaviour. Characteristic impedance and mode pattern of the fundamental mode are reported vs. the excentricity, whereas cutoff frequencies and mode patterns of the first few TE and TM modes of both kinds above are compared with the numerical results of the F.E.M. method.

Theory - *Cross Section Geometry.* Let us consider the structure shown in Fig.1, that is cylindrical and uniform along the z-direction of propagation; it consists of an outer conductor of elliptical form, and an inner strip conductor, extending between the two focal points of the ellipse; both conductors are ideal. This cross-section can be described in terms of an elliptical cylindrical coordinate system (ρ, ϕ, z), that is connected to the Cartesian one (x,y,z) by means of the following relationships, [4],[7]: $x = \frac{a}{2}\cosh(\rho)\cos(\phi)$ $y = \frac{a}{2}\sinh(\rho)\sin(\phi)$. The elliptical outer boundary of the guide is described by the locus: $\rho = \rho_0$ $-\pi < \phi < \pi$; whereas the inner strip of width a can be seen as a degenerate ellipse given by: $\rho = 0$ $-\pi < \phi < \pi$. The geometrical characteristics of the section can be usefully summarized by a single parameter, its excentricity e, defined as follows: $e = \frac{a}{A}$; A is the major axis of the elliptical outer conductor that is expressible in terms of a, ρ_0 as: $A = a\cosh(\rho_0)$

I) Solution of the Wave Equation - The electromagnetic wave propagation in the above cylindrical guide can be described in terms of a scalar wave-function Ψ satisfying the Helmholtz equation:

$$\left[\frac{\partial^2}{\partial\rho^2} + \frac{\partial^2}{\partial\phi^2} + \left(\frac{a\cdot k_c}{2}\right)^2\left(\cosh^2\rho - \cos^2\phi\right)\right]\cdot\Psi = 0 \qquad \text{where} \quad k_c^2 = k^2 - \beta^2 \;; k = \omega/c$$

The above equation separates in elliptic cylinder coordinates; as a consequence, the scalar wave function Ψ can be represented as the product $\Psi = \Phi(\phi)\cdot R(\rho)$, where Φ is an angular Mathieu function, R a radial one.

II) Fundamental TEM mode analysis - In order to obtain the TEM mode we set k_c=0; then k=β and the wave equation reduces to the Laplace's equation for the quasi-static potential. If the inner strip potential is set equal to V_0, the solution of the above equation is simply given by :

$\Psi = V_0\left(1 - \frac{\rho}{\rho_0}\right)$. The electric and magnetic fields are derived from the above potential.

Characteristic TEM Impedance - The TEM characteristic impedance is obtained from the computation of the distributed capacitance and inductance of the line per unit length.

Capacitance per unit length - The total charge per unit length on the strip is found as: $Q = \frac{a}{2}\int_0^{2\pi}\sigma|\sin\theta|d\theta = 2\pi\varepsilon\frac{V}{\rho_0}$ (Gauss' law), hence the capacitance per unit length is $C = \frac{Q}{V} = \frac{2\pi\varepsilon}{\rho_0}$ and is plotted in Fig.2. The TEM characteristic impedance is found as : $Z_0 = \sqrt{\frac{L}{C}} = \eta\frac{\rho_0}{2\pi}$ and is plotted in Fig.2 vs. e. Looking at the plot of the characteristic impedance Z_0 versus the excentricity e, we note that as $e \approx 0.8$, $Z_0 \approx 50\ \Omega$, as suitable for applications.

III) Higher order modes analysis - The solutions of the Helmholtz's equation can be separated in the following two sets of modes, each having even/odd symmetry with respect to the y=0 axis :

i) TE modes: for which it is $\Psi = H_z$;

ii) TM modes, for which we have $\Psi = E_z$.

Results - In fig.2 we compare the analytical results with the numerical ones obtained by F.E.M. method of the characteristic impedance and the normalized capacitance vs. excentricity; the two sets of data are in excellent agreement. In figs 3a and 3b we report the cutoff frequencies for the first two modes of each type, evaluated both analytically and by a means of standard F.E.M. program. The normalized wavelengths are plotted versus the excentricity of the cross-section; the normalization constant is the major axis of the ellipse. The Mathieu radial functions involved in the above calculations were computed by utilizing their Bessel expansions [4],[5],[6]. On the computation with the F.E.M. method we note that a 450 elements grid gives an error which is less than 2/3%. The grid topology is the same as the coordinate system with 15 divisions for the radial coordinate and 15 divisions for the azimutal coordinate (using triangular elements this gives: 2*(15*15)=450 elements). The computational time in this case was about 15 minutes for each value of excentrity, against the 5 minutes needed for the analytical computation (the PC used for this computation is equiped with an 486-100MHz processor and 12 Mb RAM, all the programs was implemented in MATLAB).

Conclusions -The suspended strip in elliptical cross-section is solved analytically in elliptical coordinates. For the fundamental TEM mode, field patterns and characteristic impedance vs. excentricity are obtained. Higher order TE and TM modes of two kinds are found: those that would also exist in an empty elliptical guide and those solely due to the presence of the strip conductor, featuring singular behaviour at the strip edges. Cutoff frequencies and mode patterns of the lowest eight modes are in excellent agreement with the results of the F.E.M. analysis.

References

[1] P.Wilson, D.Hansen, and D.Koenigstein, "Simulating open area test site emission measurement based on data obtained in a novel broadband TEM cell", *IEEE Nat. Symp. EMC*, Denver, CO, May 23-25, 1989.

[2] S.Ramo, J.R.Whinnery, T.Van Duzer, *Fields and waves in communication electronics*, -second edition- Cap.7, pp 326-345, John Whiley &Sons.

[3] R.E.Collin, *Foundation for Microwave Engineering*, -second edition- Appendix III McGraw Hill International editions *Electrical Engineering Series.*

[4] P.H.Morse and H.Feshbach, *Methods of Theoretical Physics*, vol. I e II. New York: McGraw-Hill, 1953.

[5] M.Abramowitz and I.A.Stegun, *Handbook of Mathematical Functions.* Dover Publications, 1968.

[6] "Mathieu functions of integral orders and real arguments - computer programs description" vol.MTT-28, no.', March 1980

[7] El-Sherbiny, "Cutoff Wavelenghts of Ridged, Circular and Elliptic Guides",*IEEE Transactions on Microwave Theory and Techniques*, vol. MTT-21, no.1, Jan.1973, pp. 7-12.

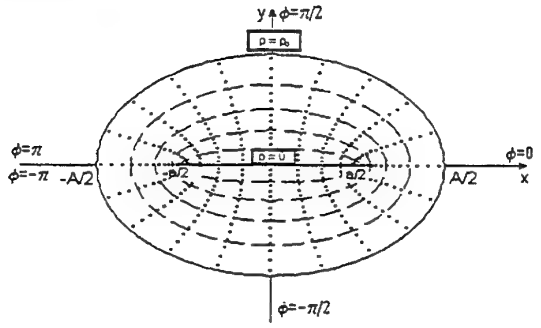

Fig.1: Cross-section geometry and coordinate system (ρ = const. give equipotential lines).

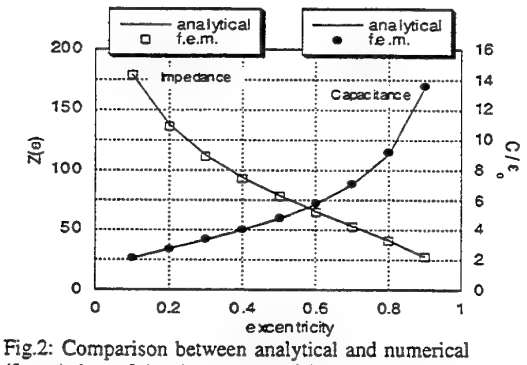

Fig.2: Comparison between analytical and numerical (f.e.m.) data of the characteristic TEM impedance and of the normalized Capacitance (ratio C/ε₀) per unit length, plotted versus the excentricity of the cross section.

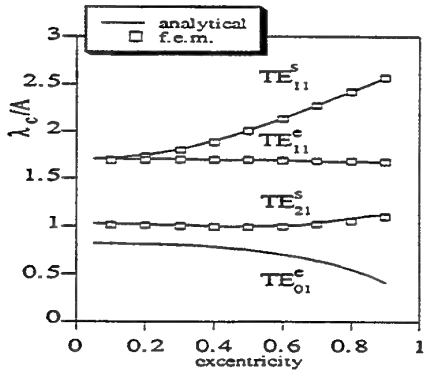

Fig.3a: Comparison between analytical and numerical (f.e.m.) of the normalized Cut-off wavelengths versus the excentricity of the cross-section, for the first higher TE modes.

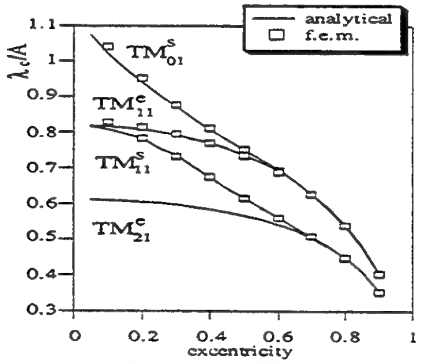

Fig.3b: Comparison between analytical and numerical (f.e.m.) of the normalized Cut-off wavelengths versus the excentricity of the cross-section, for the first higher TM modes.

New Equivalent Circuits for Modal Analysis of Waveguide Discontinuities by Commercial Simulators

M. Mongiardo, A. Weisshaar, and V. K. Tripathi

New Equivalent Circuits for Modal Analysis of Waveguide Discontinuities by Commercial Simulators

M. Mongiardo, A. Weisshaar, and V. K. Tripathi

Abstract—**We introduce a new class of equivalent circuits suitable for performing modal analysis directly by simulators, such as Libra, MDS, etc. Although several equivalent circuits of waveguide discontinuities have been developed in the past, most of them are neither multimodal neither suitable to direct implementation by using the standard element currently provided in the simulators library.**
The new class of equivalent circuits is based on the representation of waveguide discontinuities in terms of controlled sources. By using these equivalent circuits it is possible to perform exactly the same analyses as commonly done with mode-matching techniques but by using commonly available circuit simulators.
The efficiency and accuracy of the proposed approach is highlighted with reference to some specific examples. Noteworthy, while the accuracy is the same as for full-wave mode-matching codes, also the efficiency compares very favorably.

I. Summary

Computer aided design of waveguide components such as filters, junctions, diplexers, couplers. etc. is generally accomplished by using mode-matching routines. The advantages of modal analysis for the above waveguide discontinuities are well known and do not need to be repeated. However, a major drawback is represented by the fact that, in order to develop a mode-matching code, one has to be acquainted with relative convergence phenomena, spectral representations, numerical modeling, etc. Moreover, the resulting code is often a stand-alone application that need to be interfaced to other simulators in order to perform optimizations or to evaluate the overall characteristics of the entire network.

On the other hand, although a fairly large number of equivalent circuit of waveguide discontinuities have been proposed in the past, most of them are of limited use in common practice since they are not multimodal, e.g. the equivalent circuits provided in [1]; or are of difficult implementation in current transmission lines simulators like Libra. MDS, etc.

It is noted that, since waveguide technology is nowadays used mainly in satellite applications requiring a high degree of accuracy, multimodal representations for describing waveguide discontinuities are mandatory. As a consequence, the design of waveguide components with stringent requirements is almost invariably accomplished by using specifically developed mode matching codes.

In this contribution we introduce, both for the E- and H-plane discontinuities, a rigorous multi-mode equivalent circuit model, valid both for single and cascaded steps also including interacting steps such as thick irises, stubs and waveguide bifurcations. Using this new multi-mode equivalent circuit representation, several waveguide components. including filters, phase shifters, couplers, etc., can be analyzed and designed entirely with commercial circuit simulators. Since the equivalent circuit model is rigorously derived from modal analysis, a full-wave analysis of the component can be performed directly by *circuit simulation* thus eliminating the need for additional matrix inversion software.

Let us consider, as an example, the multimodal equivalent circuits of the H-plane interacting step discontinuities shown in Fig. 1 relative to the thick iris and the stub discontinuity of Fig. 2. In order to demonstrate the accuracy of the new equivalent circuit representation we have implemented the above equivalent circuit in the commercial microwave simulator Libra [2] and we have analyzed inductive irises of various thicknesses (Fig. 3), i.e. for various degrees of interaction between the steps via the higher order modes. The results for the transmission coefficient for different thicknesses d of the iris are shown in Fig. 4. Also included in the figure are the results obtained from a mode-matching analysis which considers the correct edge behavior [3]. Perfect agreement between the two methods is noted.

As an example of practical application, we have implemented the equivalent circuit approach to analyze a bandpass filter which was designed in [4] for the Ka-band at 35 GHz and a bandwidth of 1 GHz. The filter dimensions are given in Fig. 5. The results obtained from a circuit simulation on Libra are shown in Fig. 6 and compared with the mode-matching method which includes the correct edge condition. The circuit simulation was done by retaining 10 modes in the wide regions, five modes in the irises of width 3.2mm, and three modes in the irises of width 2.4mm. The results obtained with the two different methods show very good agreement thus validating the equivalent circuit approach for waveguide filter analysis and design.

In summary, the above examples demonstrates the feasibility of performing a full-wave modal analysis of practical microwave components entirely by using general purpose commercial circuit simulators. The potential benefits of using such simulators for the analysis and design of waveguide components include: costumized codes for the design of these components are not required and full advantage can be taken of the available design, optimization, and graphical user interface capabilities of the CAD tools.

References

[1] N. Marcuvitz, *Waveguide Handbook*. Lexington, MA: Boston Technical Publishers, 1964.
[2] HP EEsof, Westlake Village, California, USA.
[3] T. Rozzi and M. Mongiardo, "E-plane steps in rectangular waveguide," *IEEE Trans. Microwave Theory Tech.*, vol. 39, pp. 1279-1288, Aug. 1991.
[4] W. Menzel, F. Alessandri, M. Mongiardo, R. Sorrentino, C. Eswarappa, P. P. M. So, and W. J. R. Hoefer, "Analysis of a Millimeter-Wave Filter Using Transmission Line Matrix and Mode Matching Methods and Comparison with the Measurements," *9th Annual Review of Progress in Applied Computational Electromagnetics*, Proc. pp. 289-296. Monterey. CA, March 1993.

M. Mongiardo is with the Istituto di Elettronica, Universitá di Perugia, I-06100, Perugia, Italy; Ph. 39-75-585 2668. fax 39-75-585 2654, e-mail: mongiardo@istel.ing.unipg.it; on sabbatical at the Department of Electrical and Computer Engineering, Oregon State University, Corvallis, OR 97331, during summer 1995.

A. Weisshaar, and V. K. Tripathi are with the Department of Electrical and Computer Engineering, Oregon State University, Corvallis, OR 97331.

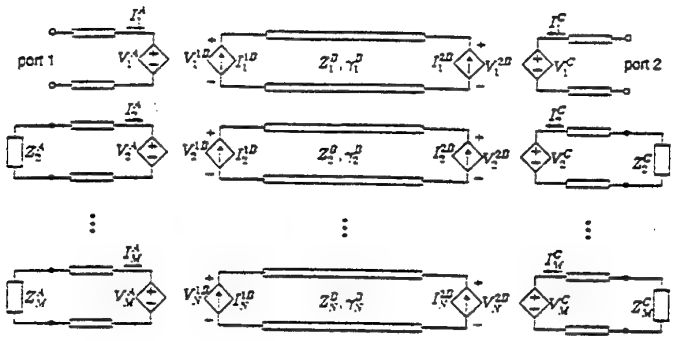

Figure 1: Multi-mode equivalent circuit of a thick iris. The voltages and currents are defined in the paper. The impedance Z_p^q and propagation constant γ_p^q correspond to mode p in region q, respectively.

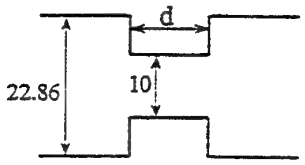

Figure 3: Geometry of an inductive iris of variable thickness d. Dimensions are given in mm.

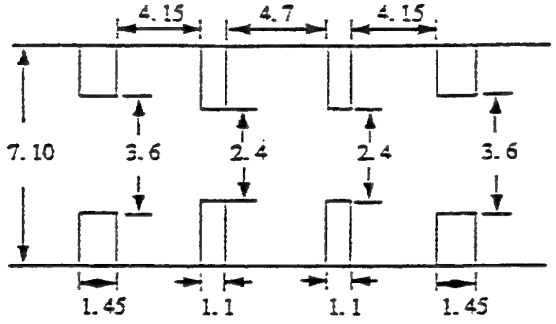

Figure 5: Geometry of a bandpass filter for the Ka-band. Dimensions are given in mm.

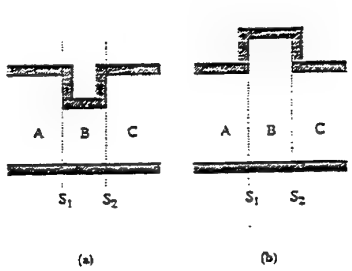

Figure 2: Geometry of (a) a thick iris and (b) a stub discontinuity.

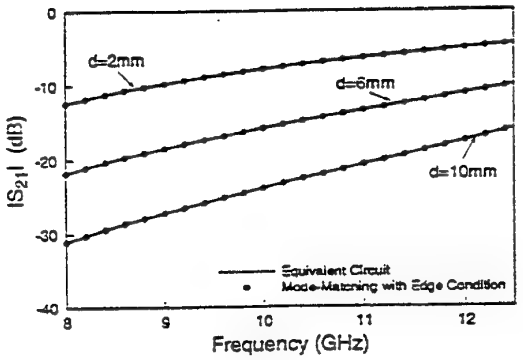

Figure 4: Transmission coefficient of an iris for different thicknesses d as defined in Fig. 3.

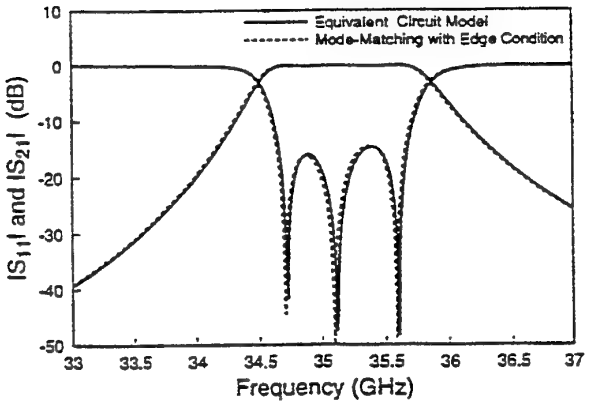

Figure 6: Scattering parameters of a bandpass filter with dimensions given Fig. 5.

Device Modeling at mm-Wave

A. Cappy

DEVICE MODELING AT MM-WAVES

Alain CAPPY
Institut d' Electronique et de Microelectronique du Nord
UMR CNRS 9929
Cite Scientifique
Avenue Poincare- BP 69
59652 Villeneuve d'Ascq Cedex- France
phone 33-20 19 78 59, Fax 33-20 19 78 92,
E.mail Alain.Cappy@IEMN.Univ-Lille1.fr

Abstract: The modeling of devices at mm-waves constitutes a key point to the development of mm-wave circuits 'right first time' . In fact, the term 'device modeling' covers a large area including the physical modeling, the process modeling and the electrical modeling. The aim of this contribution is to review the recent development in the field of physical and electrical modeling of active devices (HEMTS and HBTs) for mm-wave applications. The different operating modes such as small signal, large signal will be considered as well as the specific problem of the noise modeling in devices under linear and non linear operation at mm waves.

Département Hyperfréquences & Semiconducteurs

OUTLINE

1) INTRODUCTION

2) PHYSICAL MODELING FOR MM-WAVES DEVICES

- Physical modeling: why ?
- That are the existing models?
- Relevance and applications of these modelings
- Noise modeling
- New trends

3) ELECTRICAL MODELING

- The small signal equivalent circuit
- Topology and accuracy
- parameter determination from experiments
- noise parameters
- nonlinear modeling
- noise in nonlinear devices

4) CONCLUSION

Objectives of the physical simulations

The structure of mm-wave devices is more and more complicated .
The dimensions of the active regions are smaller than 0.1µm.
The active layer is typically 50nm thick.

→New phenomena occur and must be taken into account.

OBJECTIVES OF PHYSICAL DEVICE MODELING:

- Improvement of the knowledge of devices behaviour by clearly identifying the physical phenomena involved in either the intrinsic behaviour or parasitic effects.

- Accurate prediction of the expected performance for any application (small signal, large signal, noise, linearity...)

- Help the device designer by systematically determining the relation between electrical performance and technological parameters (sensibility analysis).

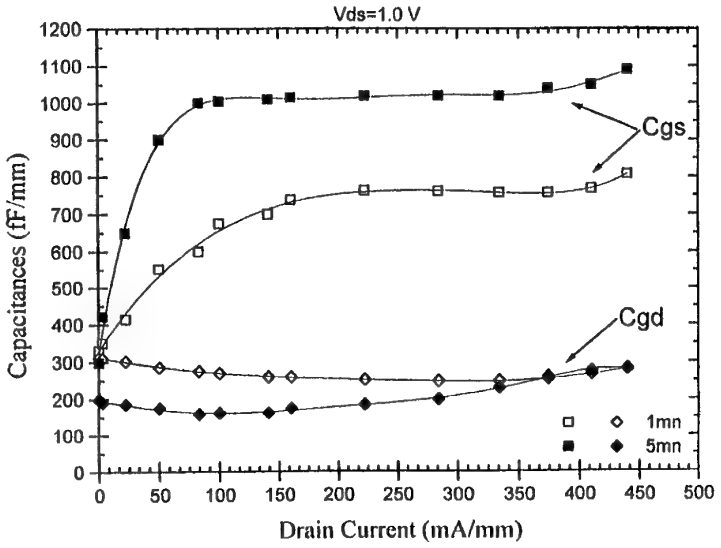

Experimental gate-to-source and gate-to-drain capacitance versus recess width in LM-HEMT on InP

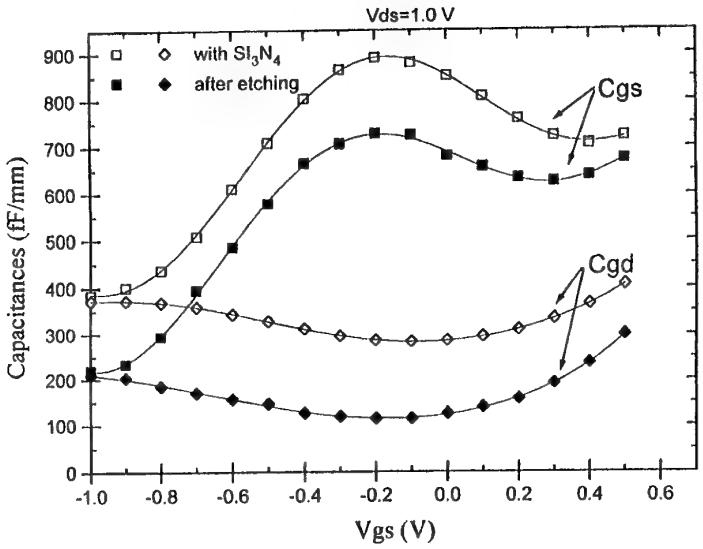

Experimental gate-to-source and gate-to-drain capacitance with and without silicon nitride passivation layer

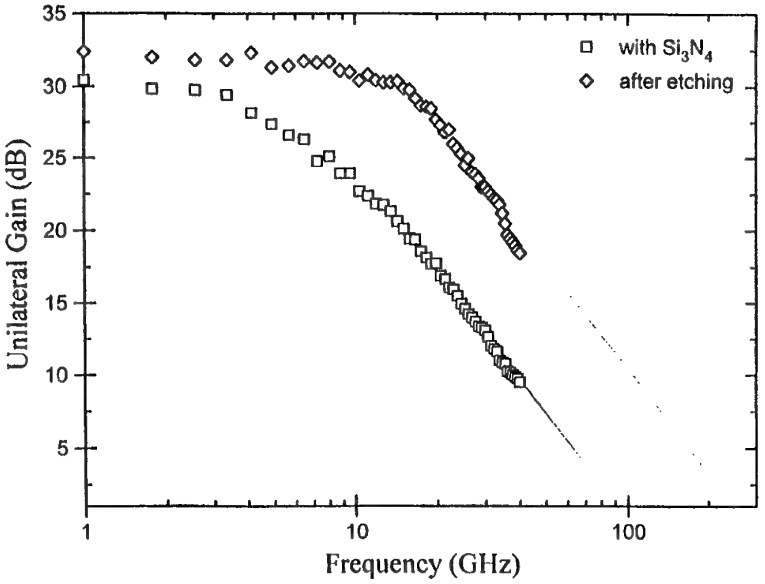

Experimental LM-HEMT Mason's unilateral gain with and without passivation silicon nitride layer versus frequency

iemn Recherche Formation Transfert

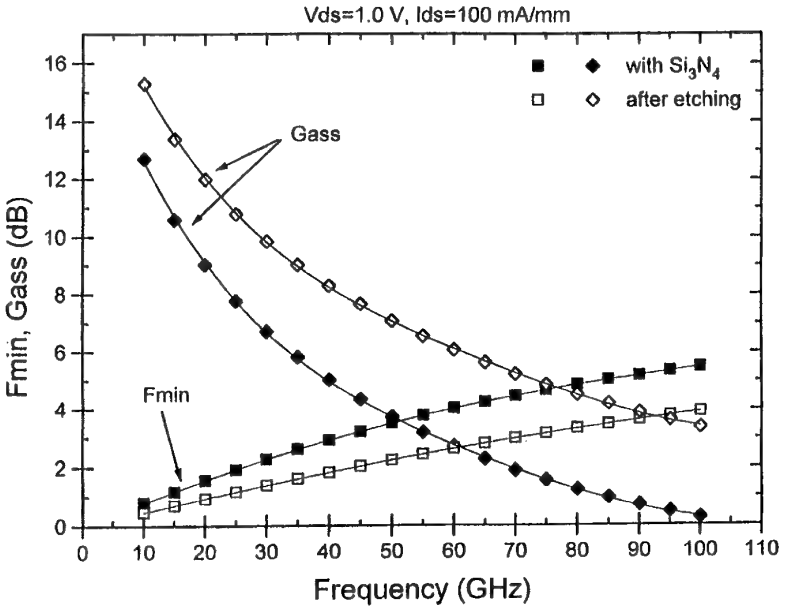

Experimental LM-HEMT minimum noise figure and associtaed gain versus frequency

MONTE CARLO OR PARTICLE MODELS

PRINCIPLE :

The stochastical motion ot the carriers is studied simultaneously :

- In the 3D $\vec{K}$ space : for each time step Δt are considered :
  - * The effect of the driving electric field $\Delta \vec{K} = \frac{q}{h} \vec{E} \Delta t$
  - * the stochastic effect of scattering mechanisms as well as their respective probabilities.
- In the 2D (or 3D!) $\vec{r}$ space : that gives the two (three)dimensional description of :
  - * the carrier positon
  - * the electric field determined from Poisson's equation

    →the external currents and voltages can be deduced at each time. The HF noise analysis is possible.

CAPABILITIES

- calculation of material properties (transport properties)
- study of almost any kinds of device
- validity study of the small signal equivalent circuit

Typical Structure of an InP LM-HEMT

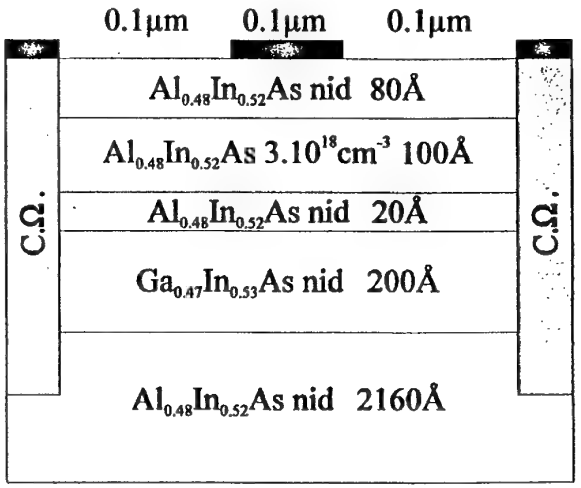

* **Advantages :**
  - Good transport properties in InGaAs
  - High conduction band discontinuity
* **Drawbacks :**
  - $Eg_{InGaAs} = 0.75$ eV
  - Scaling down ==> E↗

    ☛ **impact ionisation**

Limitations :
Low breakdown voltage
Power applications

Electrical Characteristics

AlInAs/GaInAs/InP HEMT performance deduced from Monte Carlo simulation (Fauquembergue et al)

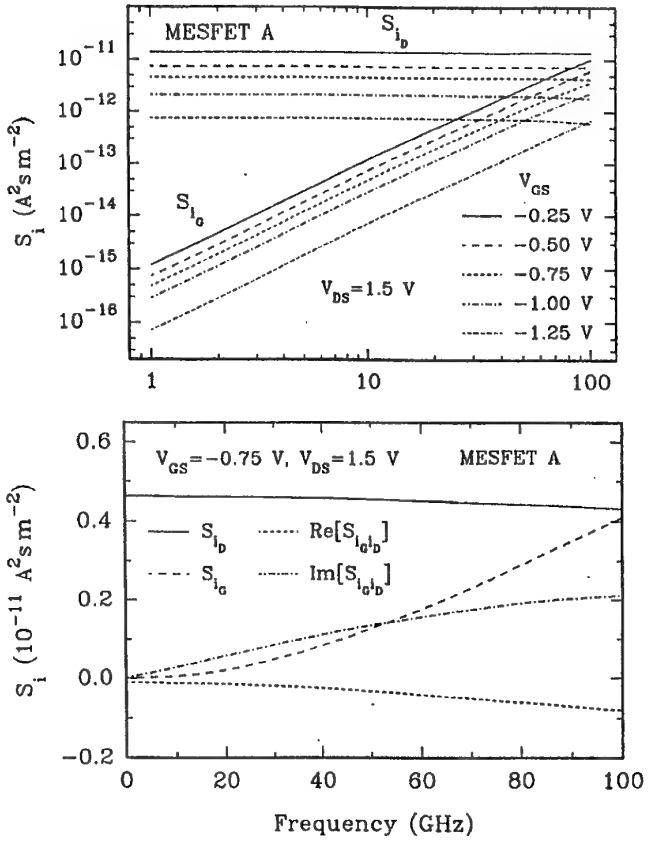

From T. GONZALES et al , IEEE ED 42 ,1995

Hydrodynamic two-dimensional models

MAIN FEATURES :

A large number of physical phenomena can be taken into account for the study of FETs :

* non-stationary electron dynamic effects
* surface depletion effect
* impact ionisation
* gate recess shape
* quantization effect
* screening effects

PRINCIPLE :

2D resolution of semiconductor equations

* particle, momentum and energy conservation equation
* Poisson's equation

CAPABILITIES :

* Description ot the physical behaviour
* Accurate analysis of realistic complex structures
* Determination of the microwave performance, the main limitations (breakdown) and the intrinsic equivalent circuit.

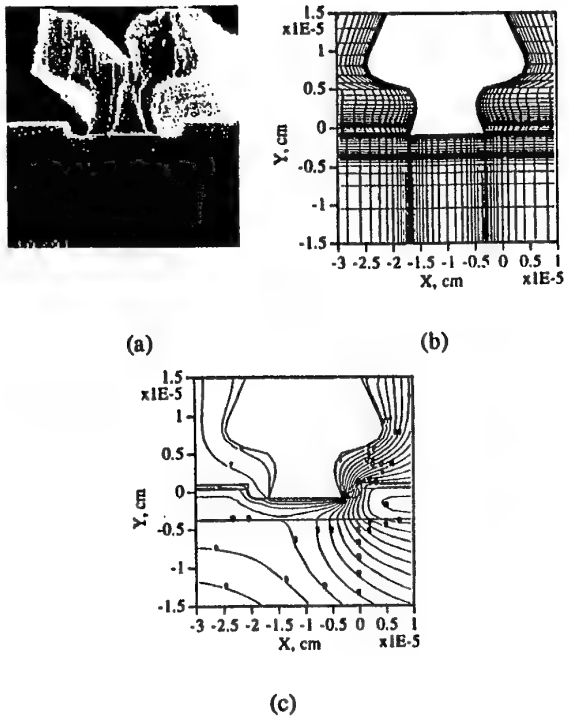

Figure 1. Finite element simulation of a 200 nm gate length MESFET. (a) SEM picture of the device cross sectional view (b) the corresponding H2F grid (c) Potential distribution at VG=-0.4 V and VD=2.5 V.

from A. Azenov et al , Proc SISDEP 1993

GATE RECESS OFFSET INFLUENCE

(R = 100 nm ; Vgs = 0 V ; Vds = 4 V)

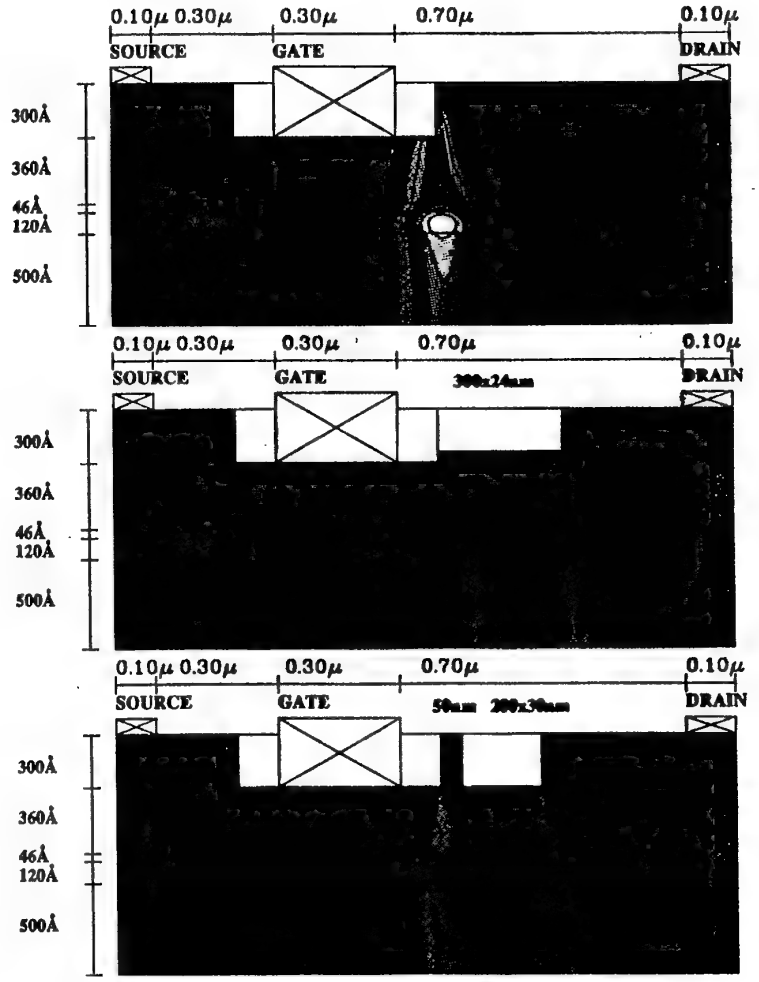

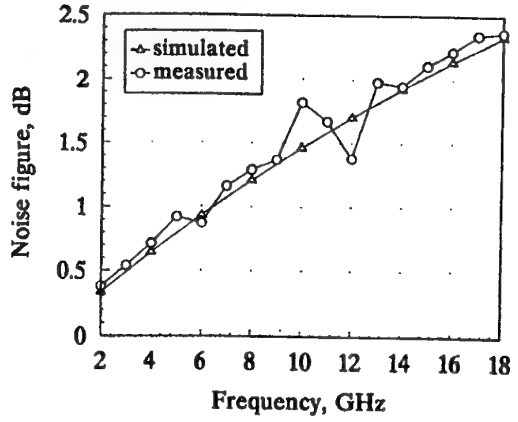

(a)

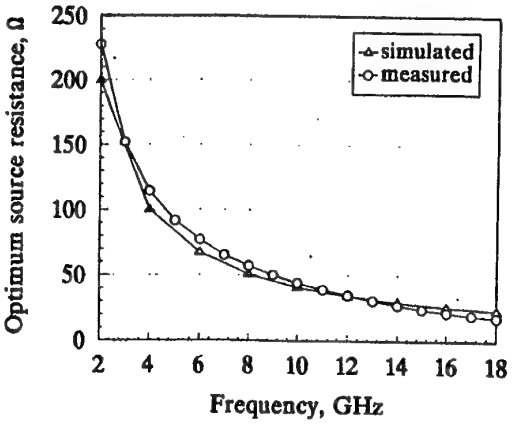

from F. FILICORI et al IEEE ED 40 n7, 1992 et al

QUASI TWO-DIMENSIONAL APPROACH

AIMS

Numerical modeling more simple than full D but more accurate than simple 1D models

PRINCIPLE

A charge control model is combined together with a transport model

carrier injection in the buffer is taken into account

CAPABILITIES

Modeling intented for CAD

Able to give DC, AC, noise and nonlinear properties

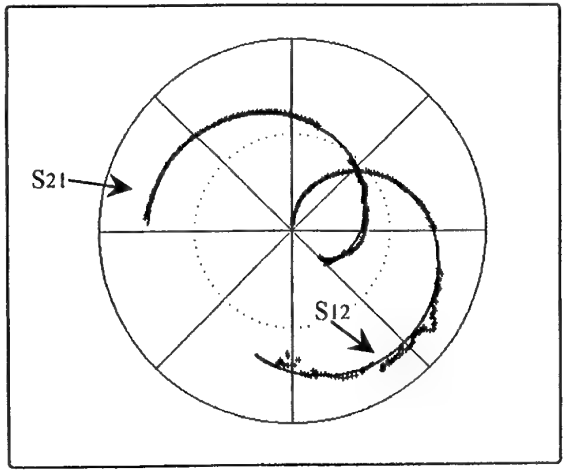

+ Measured 1-110 GHz
__ Extrapolated

Maximum Radius:
S21: 3
S12: 0.3

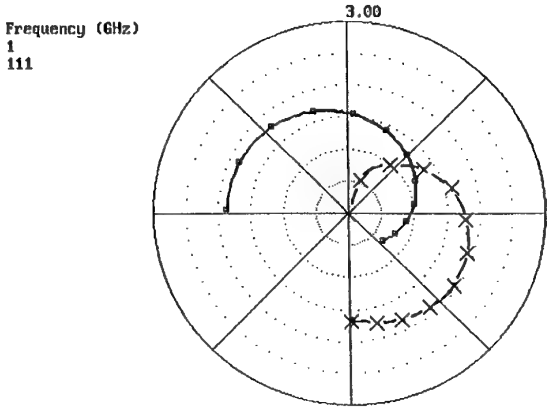

Q 2D model

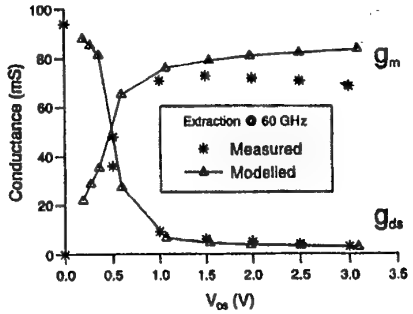

Figure 8: Comparison of modelled and measured conductances extracted at 60 GHz.

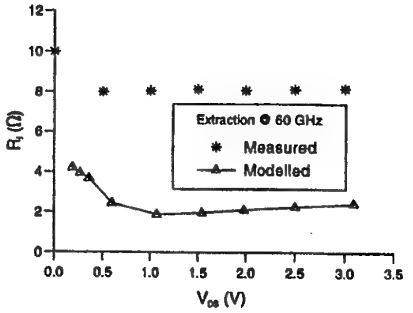

Figure 9: Comparison of modelled and measured R_i extracted at 60 GHz.

from C.G.MORTON et al, Proc Eu MC 1995

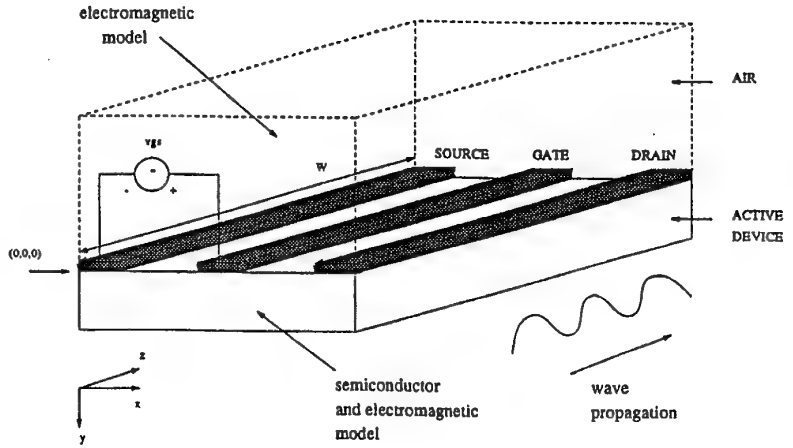

from M.A. ALSUNAIDI et al private communication,
submitted to IEEE MTT

iemn Recherche Formation Transfert

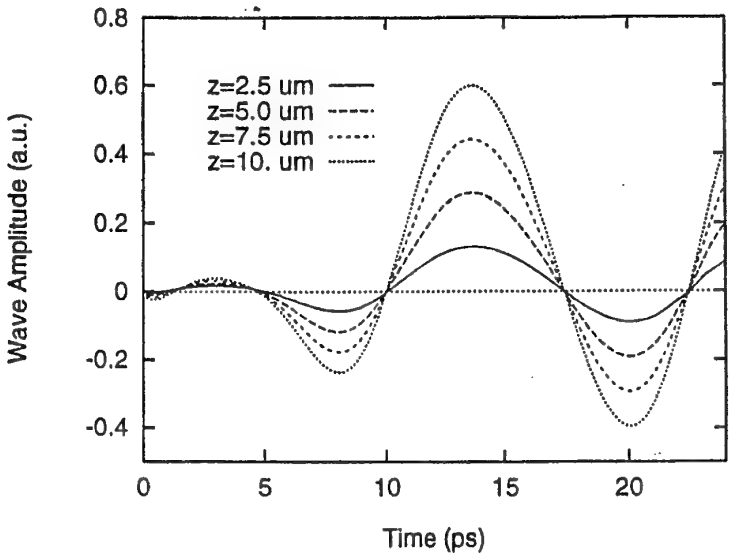

from M.A. ALSUNAIDI et al private communication,
submitted to IEEE MTT

Département Hyperfréquences & Semiconducteurs

SMALL SIGNAL EQUIVALENT CIRCUIT

Two methods are available

* S parameter least square fit
  - ----> very accurate
  - ----> some elements can be unphysical
  - ----> extrapolation is difficult
* Direct measurement in two steps

  Cold measurement ---> exrinsic elements

  hot measurements ----> intrinsic elements

  by matrix manipulation

  ----> very general method for FETs,HEMTs, DGFETs,HBTs

  ----> Device physics has to be known

  ----> extrapolation easy

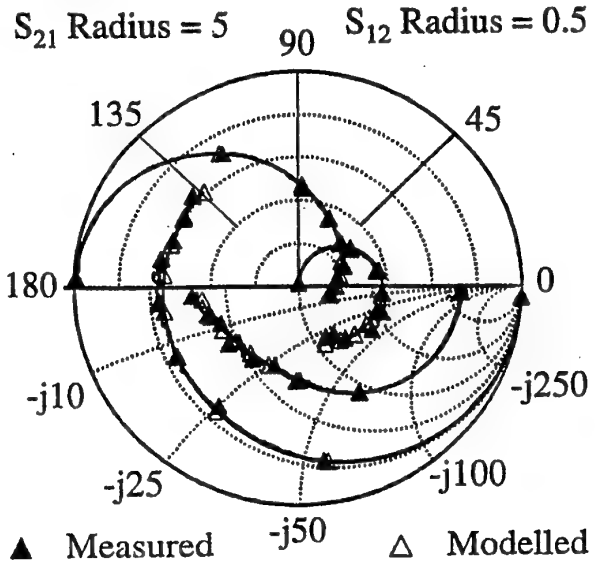

Fig. 7 Comparision between measured and modelled S-parameters of a 0.15 x 100 μm^2 MODFET biased for low noise (V_{ds}=2.5 V I_{ds}=100 mA/mm) from 0.5 GHz to 118.5 GHz (Symbols every 13.5 GHz).

from P.J. TASKER et al, MTT-S digest, 1995

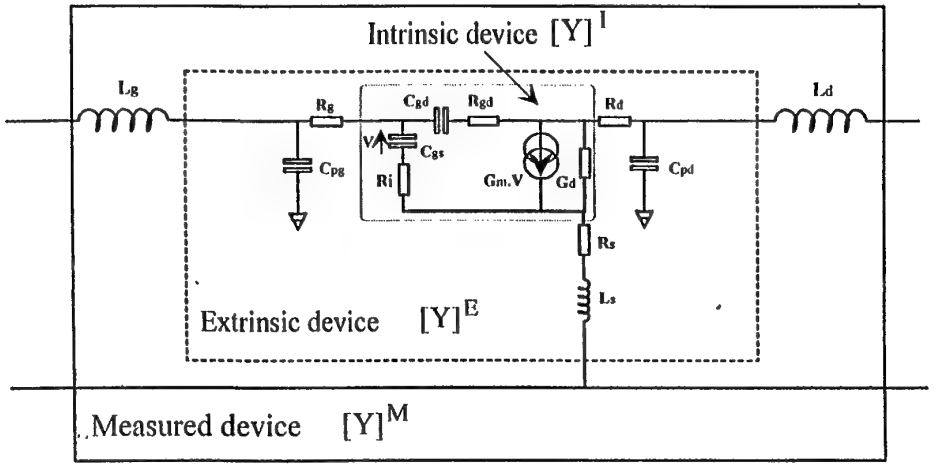

$$[Y]^E \approx \begin{bmatrix} (a_{11}.f^2 + j.b_{11}.f) & (a_{12}.f^2 + j.b_{12}.f) \\ (a_{21_0} + a_{21}.f^2 + j.b_{21}.f) & (a_{22_0} + a_{22}.f^2 + j.b_{22}.f) \end{bmatrix}$$

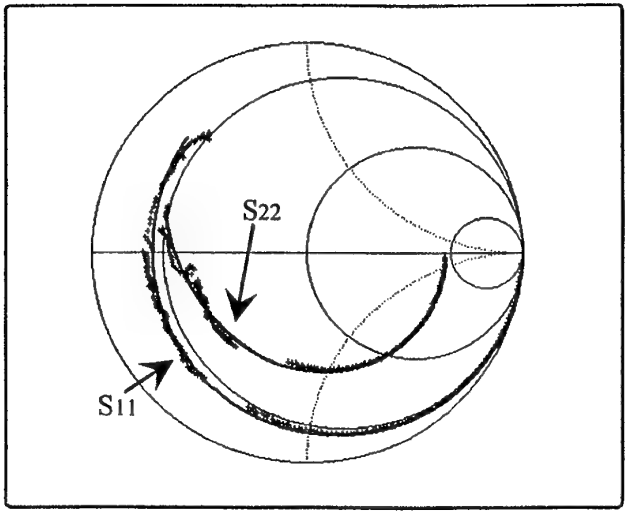

Comparison between the extrinsic model and experimental data from 1 to 110 Ghz. S21 radius =3, S12 radius =0.3. PM-hemt with 2x25x0.15 µm2 gate geometry. Ids= 300mA/mm (gm max)

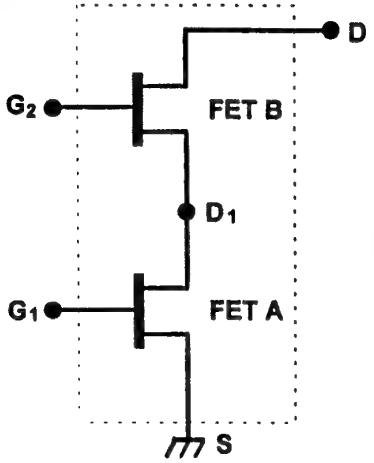

Equivalent scheme of a Dual Gate FET deduced from the Cascode configuration

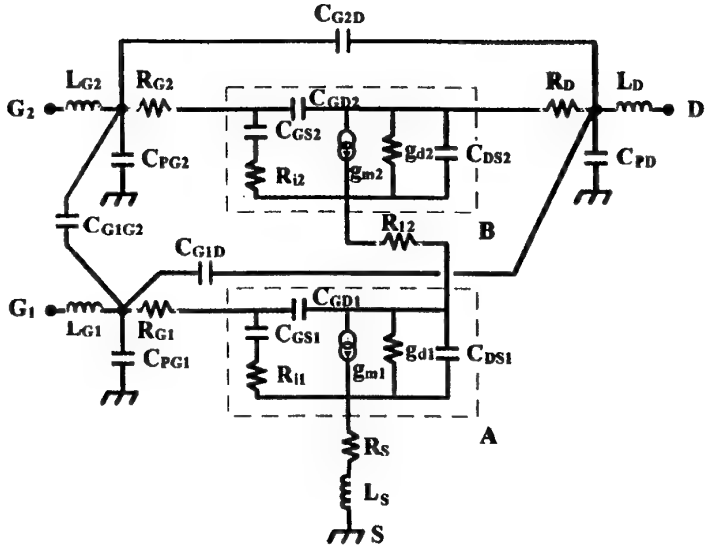

Institut d'Electronique et de Microélectronique du Nord
Cité scientifique
Avenue Poincaré - B.P. 69 - 59652 Villeneuve d'Ascq Cédex
Téléphone : 20 19 78 93 - Télécopie : 20 19 78 88
Standard : Téléphone : 20 19 79 79 - Télécopie : 20 19 78 96

iemn Recherche Formation Transfert

Dual Gate PHEMT

Variation of intrinsic elements :

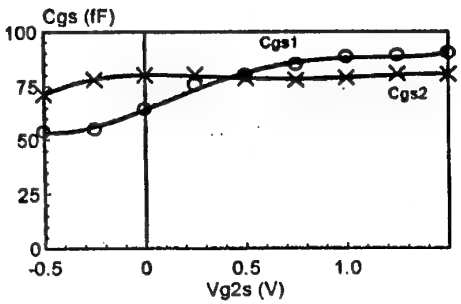

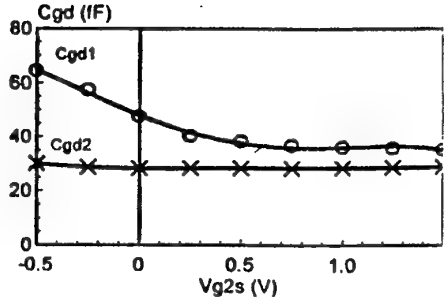

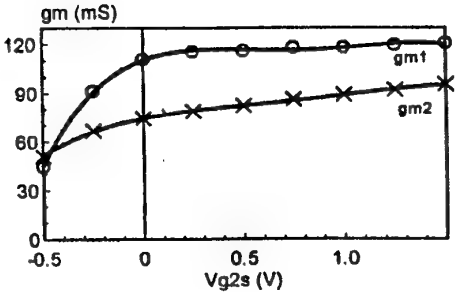

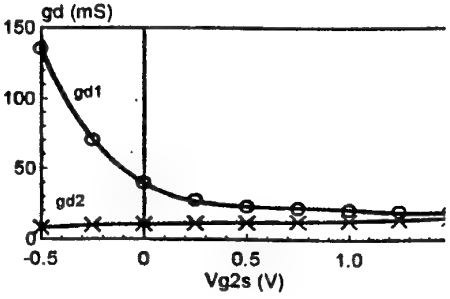

DGPHEMT (3x0.15µmx50µm) intrinsic elements versus Vg_2s (Vds = 3V, Vg_1s = 0V)

NOISE PARAMETERS

mm-waves Low noise amplifier design needs four noise parameters but the four noise parameters are difficult to measure directly in V or W band.

PROPOSED METHOD

1) the four noise parameters are determined at low frequency (1-26 GHz) using a commercial equipment or the F50 method.

2) Check the validity of the four noise parameters by F50 noise figure at some spot frequency (40 GHz, 60 GHz and 94 GHz in our Lab)

3) Determine the four noise parameters and the associated gain by extrapolation at the frequency of interest

iemn Recherche Formation Transfert

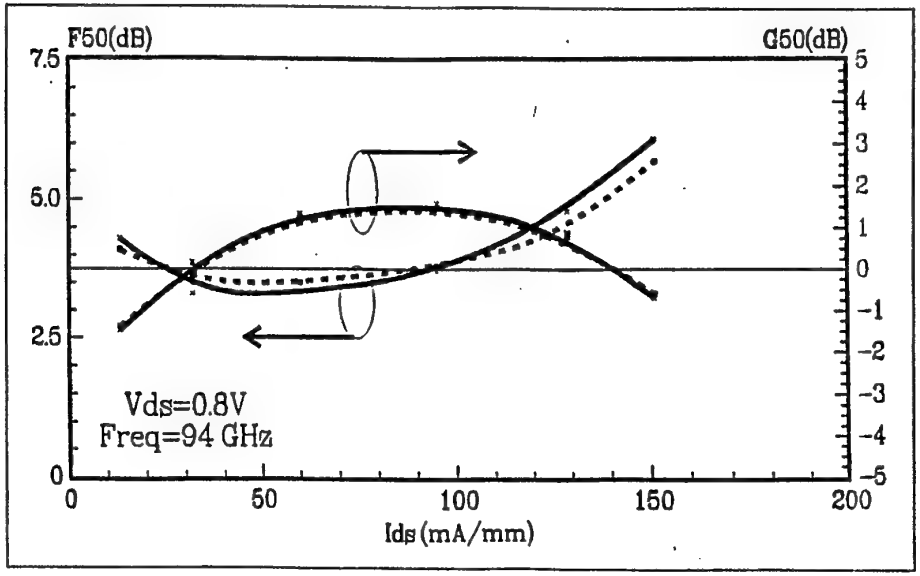

Comparison between measured and calculated noise figure F50 and G50 at 94 Ghz. the measurement is done on wafer. The noise model is extracted from 6 to 20 GHz noise measurements.

COMPARISON BETWEEN THE EXPERIMENTAL RESULTS AND HE RESIMULATION FOR A DUAL GATE MIXER (Kolanowski et al

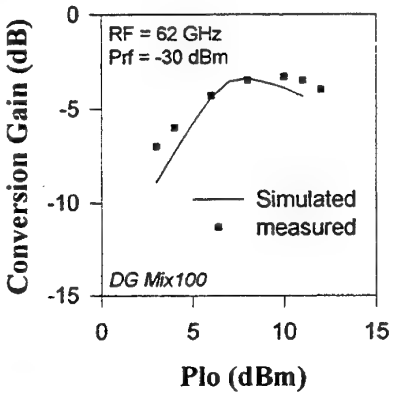

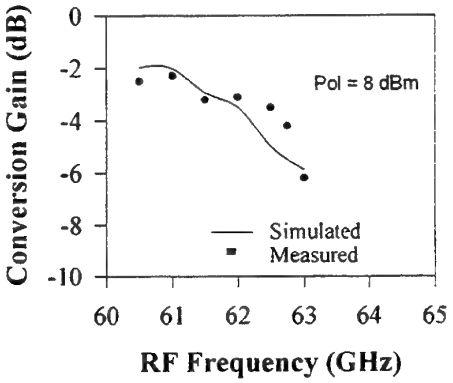

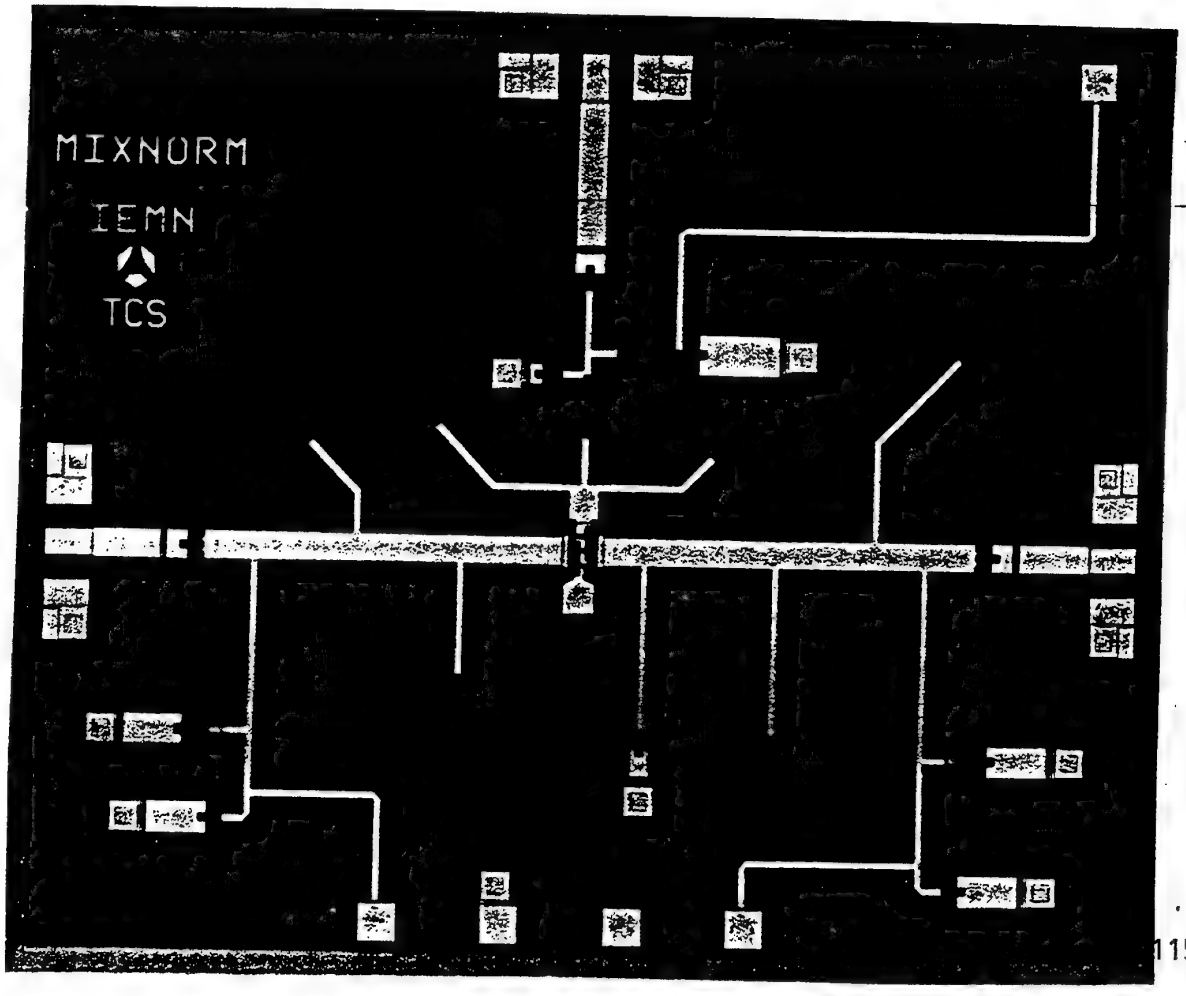

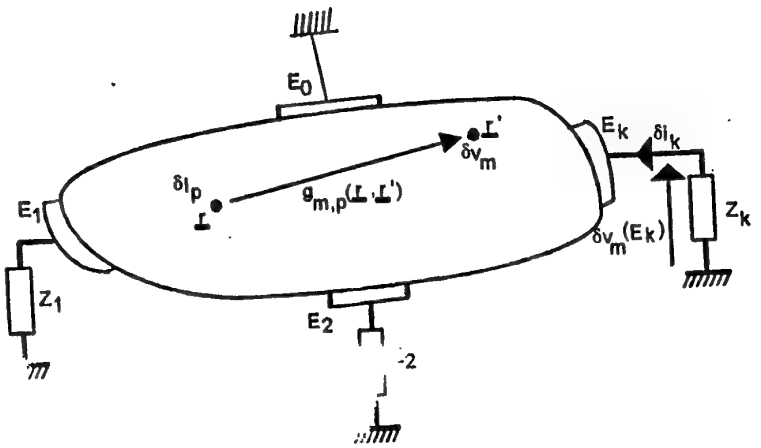

Modeling of the noise in devices under non linear operation

Noise modeling in devices under nonlinear operation

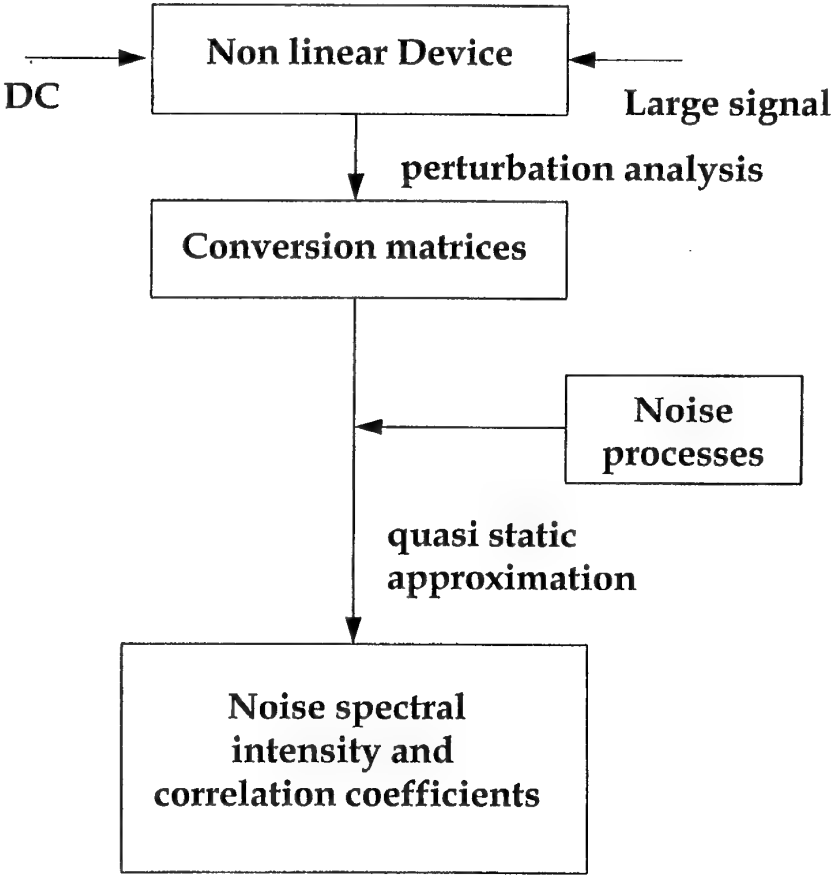

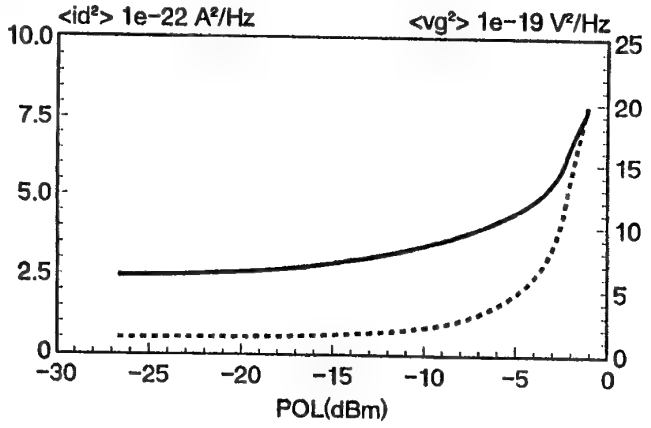

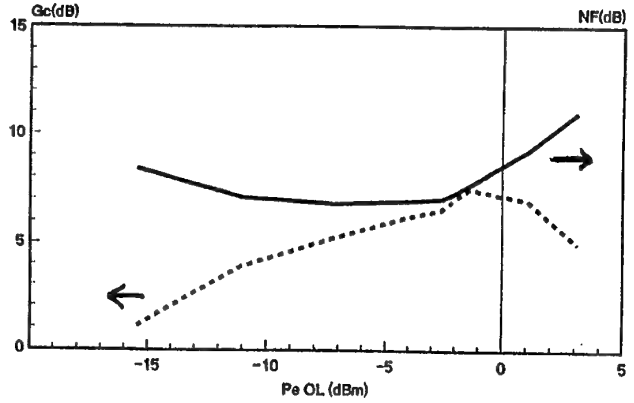

Modeling of the noise mixer noise performance

CONCLUSION

- The device performance in the mm-wave range is strongly dependent to the parasitic elements (Gd, Cgd, ionization, coprrelation between Rg and Cgd .....). The device performance can be optimized by physical modeling.

- The noise performance can be obtained from 2D modelings (Monte carlo or hydrodynamic)

- First results using full wave high frequency time-domain model .

- validity of the conventional small signal equivalent circuit and two temperatures noise model shown up to 110 Ghz.

- First results on the noise modeling of HEMTs under nonlinear operation.

Design of Millimeter-Wave Solid State Circuits

P. Briere, M. Camiade, I. Telliez, P. Quentin, P. Bourne-Yaonaba, C. Rumelhard

DESIGN OF MILLIMETER-WAVE SOLID STATE CIRCUITS

P. BRIERE - M. CAMIADE - I. TELLIEZ - P. QUENTIN - P. BOURNE-YAONABA
Thomson-CSF Semiconducteur Spécifiques - Route Départementale 128 - Boite postale 46 - 91401 ORSAY CEDEX - FRANCE

C. RUMELHARD
CNAM - Laboratoire de Physique des Composants Electroniques
292, rue Saint-Martin - 75141 PARIS CEDEX 03 - FRANCE

I. ABSTRACT

Recognised advantages of millimetre-waves are the basis for the development of large volume applications in the recent and near future years. This paper review some of the major trends in millimetre-wave monolithic circuit design, shows the emergence of multifunction circuits illustrated by some recently developed millimetre-wave chip sets for various millimetre-wave applications : millimetre-wave phase locked oscillator, transmit and receive sections of millimetre-wave radio link, automotive and radiometry W-band applications.

II. INTRODUCTION

The advantages of millimetre-waves can be listed in a general way as :

- high directivity for small antennas,
- high security,
- wide bandwidths allowing high information content,
- miniaturisation and low power consumption,
- possible integration of the radiating element with the transmit/receive circuits,
- discrete communications by proper choice of the frequency versus atmospheric absorption curve,
- low sensitivity to climatic conditions (as compared to infrared) and relatively low interference,
- reduced area of circuitry allows for more compacity and multifunctionality and ultimately lower cost.

These advantages of millimetre-wave are the basis for the development of civil applications (table 1) in the recent and near future years. The traditional millimetre-wave activity relying on the heavy and bulky wave guide based circuitry is being progressively replaced by combination of the low weight and cost integrated and hybrid circuit technologies and this transition open the door to volume applications in the millimetre-wave field.

On the following table, the various applications, either under development or envisaged, which rely on millimetre-wave GaAs IC's, are briefly presented. (from ref. [1])

	20-45 GHz	58-66 GHz	78-100 GHz
AUTOMOBILE			
2-way Communication		X	
Collision Avoidance	X		X
Tolling		X	
Road/Tunnel surveillance	X	X	X
RAILWAY			
Control	X		
Location	X	X	
AIRPORTS			
Airport Surveillance	X		X
AIRCRAFT			
Helico Anticollision	X		X
Radio Altimeter	X	X	
SPACE			
V-Sat	X		
Inter Sat Comm		X	
Radiometry	X	X	X
COMMUNICATIONS			
Mobile links	X	X	
Fixed Radio links	X	X	
Local Area Networks	X	X	
Point/Multipoint Distribution	X		
INDUSTRIAL			
Robotics	X		X
REMOTE CONTROL	X		

Table 1

In order to support these new applications, specific design methodology, design expertise, and CAD tools are being developed and various set of chips specifically design for millimetre-wave applications have been fabricated. In the following, we will describe some of general trends in millimetre-wave circuit design and report examples of some millimetre-wave chip sets developed at Thomson-CSF Semiconducteurs Spécifiques.

III. TRENDS IN MILLIMETRE-WAVE MONOLITHIC CIRCUIT DESIGN

A number of configurations of monolithic circuits and of types of components are specific for frequencies above 30 GHz. These particularities constitute the beginning of a set of design rules for millimetre-wave monolithic circuits.

Types of lines

In the lower part of microwave region, microstrip type of line is currently used; When going up in frequency, coplanar waveguide lines appear as an attractive alternative solution and many circuits at these frequencies are realised in coplanar lines. This solution decreases the cost of the chips by reduction of process complexity and avoids higher order modes in the line itself.

For multifunction chips, many connections to the ground are necessary and the best way to realise these connections is to use via holes. To make via holes, the height of the substrate is usually 100 µm. This gives the possibility to have microstrip lines working at very high frequencies without any higher order mode.

A complete comparison remains to be done to know in which case microstrip or coplanar lines would be the best.

Passive components

At 60 GHz, in a GaAs microstrip line, a quarter wavelength is about 350 µm. So, many distributed components which could not be used at lower frequencies because of their size, except in hybrid circuits, can now be used in monolithic circuits.

These components are : stubs, radial lines, combinations of quarter wavelengths for biasing circuits of filters, Lange couplers, coupled lines for band-pass filters or to replace DC isolation capacitors between different transistors.

All these components were already used in hybrid circuits, but the necessity to decrease the surface area of monolithic chips will imply that the coupling between these components is taken into account in the simulations. This is, in fact a key issue in millimetre-wave GaAs IC's designs.

Active components

At these frequencies, there is no more competition between GaAs and silicon. The substrate which is mainly used is GaAs, with heterojunction FETs-either lattice matched or pseudomorphic. The gate lengths of these transistors are between 0.3 and 0.1 µm which meant many developments in technologies. Higher gains or the same gain with larger gate lengths can be obtained with heterojunction FETs on InP substrates with lattice matched or pseudomorphic GaInAs layers. But the corresponding technologies are not stabilised at the present state of the art.

Another technology in development is HBT (Hereto Bipolar Transistor) which can be used at these frequencies to realise low 1/f noise oscillators.

Another way to get higher gains is to use dual gate transistors or cascode mountings. For HBT the Darlington configuration can be used, but up to now there is no realisation in the millimetre-wave regions.

All these components are to be characterised and modelled until very high frequencies in small or large signals, in noise, etc... This implies complex measurements equipments and large amount of measured data.

These different active components appear in the table 2 showing different types of small signal amplifiers realised recently in Europe and which is taken from [2].

F GHz	Gain dB	stage numb.	NF dB	Technology	Institution
2 - 52	9	matrix	7	0.25 µ HFET	F-IAF + Alcatel SEL
2 - 28	13	distribut.	6	0.25 µ HFET	Dassault Electronique + TH-CSF
5 - 80	9	cascode	3.5	0.25 µ HFET	F-IAF
28.6 - 38	13	2	3.5	0.25 µ HFET	Thorn-EMI + GMMT
24 - 30	16	3	4	0.2 µ P-HFET	Alcatel + PML
28.5	13.5	2	3.2	0.25 µ HFET	Daimler-Benz
34.7	18	3	3	0.25 µ HFET	+ TH-CSF
62 - 69	10	3	-	0.15 µ HFET	TH-CSF
5 - 50	11.5	dual-gate	-	0.25 µ HFET	IMEC + ESAT/TELEMIC

Table 2 : Examples of distributed and low noise amplifiers

Specific circuits

As the working frequencies are near the cut-off frequencies of transistors, several specific circuits are also to be used. These circuits are for instance, frequency doublers based on transistors, sub harmonic pumped mixers, push-push oscillators. The mixers are rather realised with cold FETs (no arain bias) to have a better matching or with biased FETs to have a conversion gain.

Another type of circuit which can be designed, is the balanced amplifier which can be realised with Lange couplers, whose dimensions at millimetre-waves do not increase too much the chip area.

Multifunction chips

There is a continuous trend, in IC technology towards higher integration level. Since at millimetre-waves, all the bonding between different chips introduce uncertainties in the reflection coefficients, gains, and so on... there is a large interest in using multifunction chip. This allows for a better control of the matching circuits, reduces the number of test and assembly operations and increases the overall reliability of the function. An additional advantage is a substantial cost reduction. Multifunction circuits are a key issue in millimetre-wave IC's and are opening the way towards the "subsystem on a chip" which appears feasible in a near future for very specific, high volume applications (i.e. automotive).

However, coupling effects between circuit elements through the substrate have to be precisely simulated.

This call for 3D electromagnetic simulators really suitable for MMIC design.

Packaging

A big problem appearing in the packaging is the presence of parasitic resonances in the metallic boxes surrounding the chips. Thanks to the electromagnetic numerical simulators which are now available, it is now possible to have an idea of the behaviour of these resonances.

VI. EXAMPLES OF RECENTLY DEVELOPED MILLIMETRE-WAVE SHIP SETS

a) 38 GHz radiolink

The chip set, which has been developed at Thomson-TCS combines four different chips. This set is shown on Figure 1.

The down link utilises two tiny chips :

A four stage low noise amplifier exhibiting 25 dB of gain and a noise figure of 3.5 dB associated with an image rejection mixer using cold FET and lange coupler achieving a total conversion gain higher than 16 dB for a 0.5 GHz IF.

The uplink is composed of three chips and delivers more than 20 dBm at 38 GHz with a conversion gain higher than 25 dB.

b) Millimetre-wave phase locked oscillator

This three chips subsystem has been developed under the Race project 2067 "MBS". The architecture of the oscillator is shown in figure 2 circuits and results have already been published in [3].

The multifunction chip concentrates the following functions : a buffered frequency multiplier, filter, power divider and two chains of three stage amplifiers in a 6 mm^2 chip.

c) W-band radiometer

Three millimetre-wave chips have been developed under an ESA Project for a W-band radiometer. The architecture which has been chosen for this application take advantage of the specific circuits mentioned in section II : analogue frequency multiplier and sub harmonically pumped cold FET mixer. A 90 GHz LNA using 0.15 µm gatelength pseudomorphic HEMT has been developed in this project. The architecture of the receiver is shown on figure 3.

Again circuit layouts and electrical results have been published in [4]. Conversion gain of the receiver is higher than 20 dB with a noise figure around 6 dB for a 0.1 to 0.7 GHz IF band.

d) 77 GHz automotive radar chip set

The MMIC chip set developed in this project has been partly supported by the French MOI.

The architecture of the various chips developed is shown on figure 4. The same type of design principles mentioned in the previous circuits are used : frequency generation using half-frequency fundamental oscillation and frequency multiplication, to achieve good stability and phase noise trade off. Results of these various circuits have been presented in [5].

V. CONCLUSION

As the GaAs millimetre-wave IC technology has now entered in a relatively mature stage, using 0.25 µm and 0.25 µm HEMT processes, design principles and techniques at frequencies between 30 GHz and 100 GHz are becoming more and more standardised and large demonstration of various types of multifunction MMIC's have been made. The challenge now for the millimetre-wave GaAs circuit manufacturers is to enter into volume production for cost driven applications such as automotive radars and point to point/multipoint data distribution.

REFERENCES

[1] P. BRIERE - "Recent European Development Programmes for Volume Application of Millimetre-waves IC's" - EUMC, Cannes, 1994.

[2] C. RUMELHARD, "R/D Activities on MMICs in Europe", International Symposium on Signals, Systems and Electronics, San Francisco, October 25-27, 1995.

[3] I. TELLIEZ, M. CAMIADE, P. SAVARY, P. BOURNE-YAONABA - "Millimetre-wave Phase locked Oscillator for Mobile Communications Systems" - MMWMCS, Orlando, May 1995.

[4] M. CAMIADE, C. DOURLENS, V. SERRU, P. SAVARY, J.C. BLANC - "Highly Integrated and Compact W-band Front-end for Radiometry Applications" - Workshop ESA, Dec. 1995.

[5] M. CAMIADE and al. - "Generic MMIC Chip Set for Automotive Radar Application at 77 GHz" - Workshop ESA, Dec. 1995.

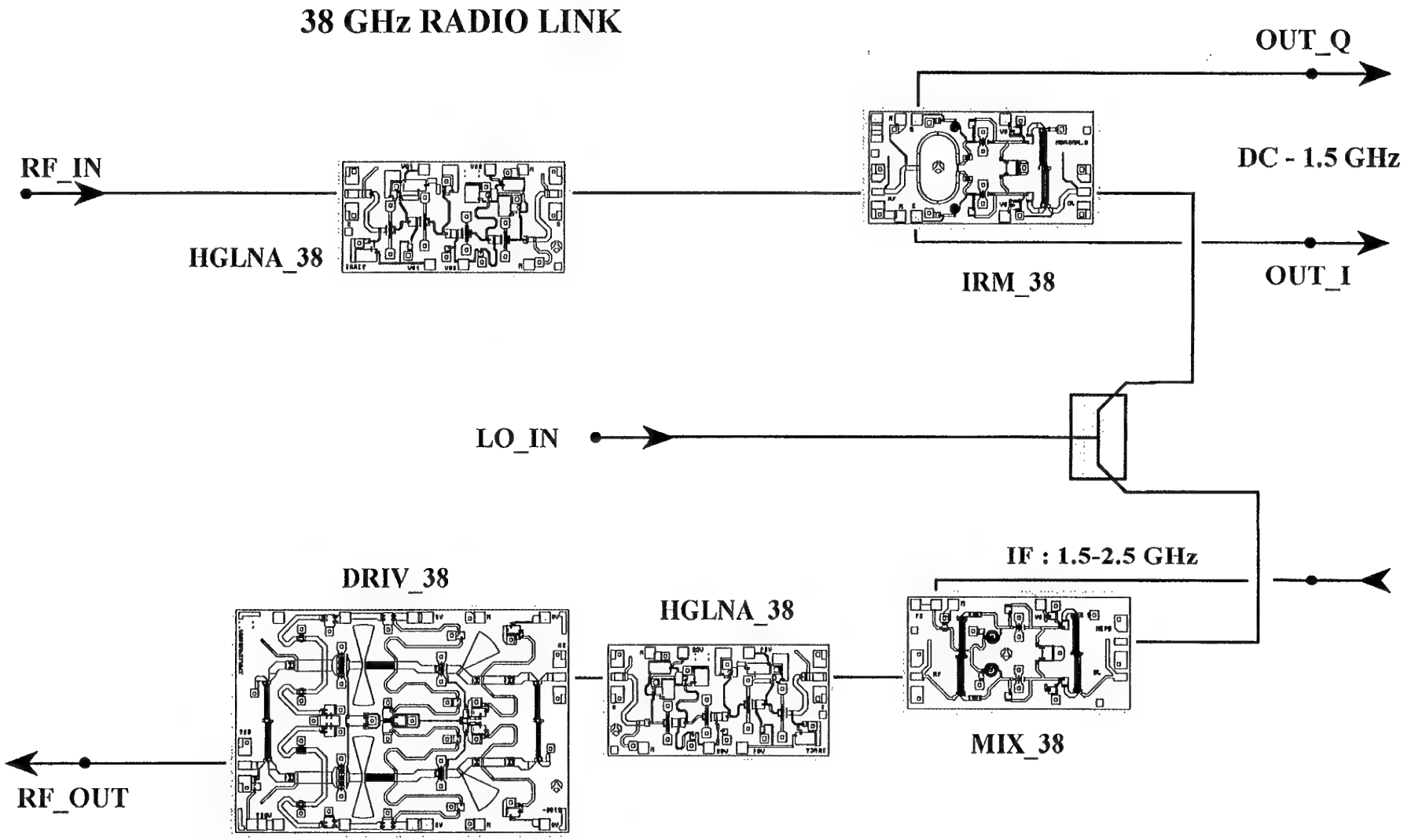
38 GHz RADIO LINK
OUT_Q
RF_IN
DC - 1.5 GHz
HGLNA_38
IRM_38
OUT_I
LO_IN
IF : 1.5-2.5 GHz
DRIV_38
HGLNA_38
MIX_38
RF_OUT

Figure 1

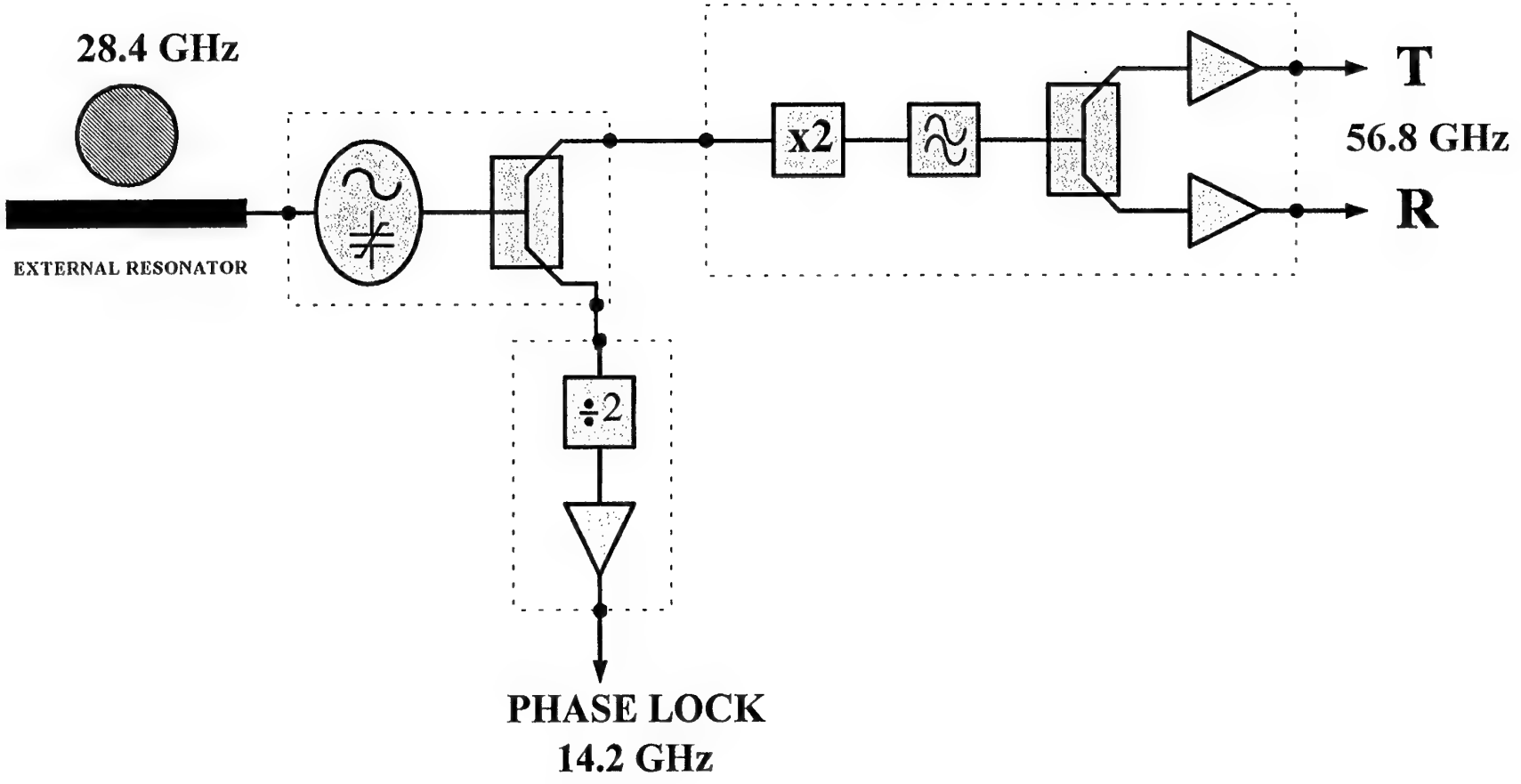

Block diagram of the phase locked oscillator at 60GHz
Figure 2

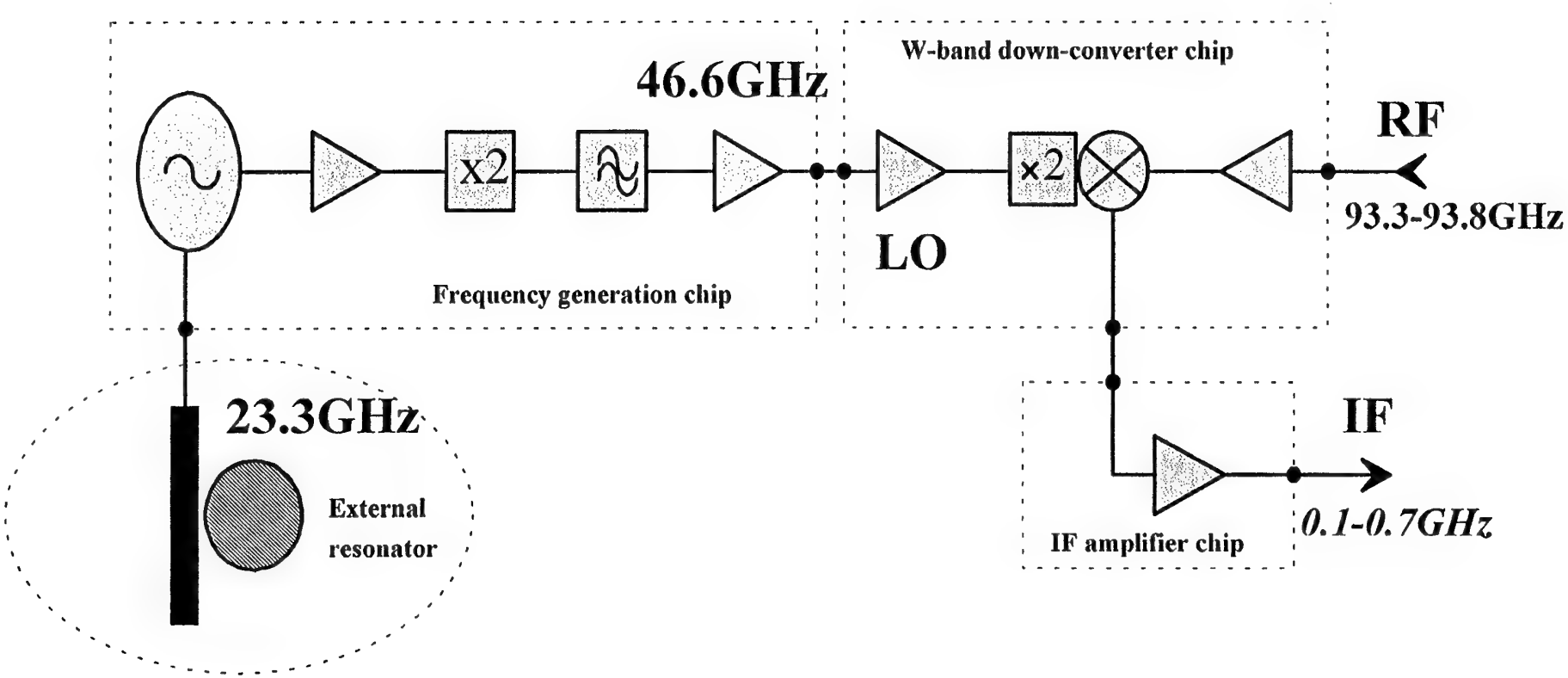

Block diagram of the W-band receiver front-end
Figure 3

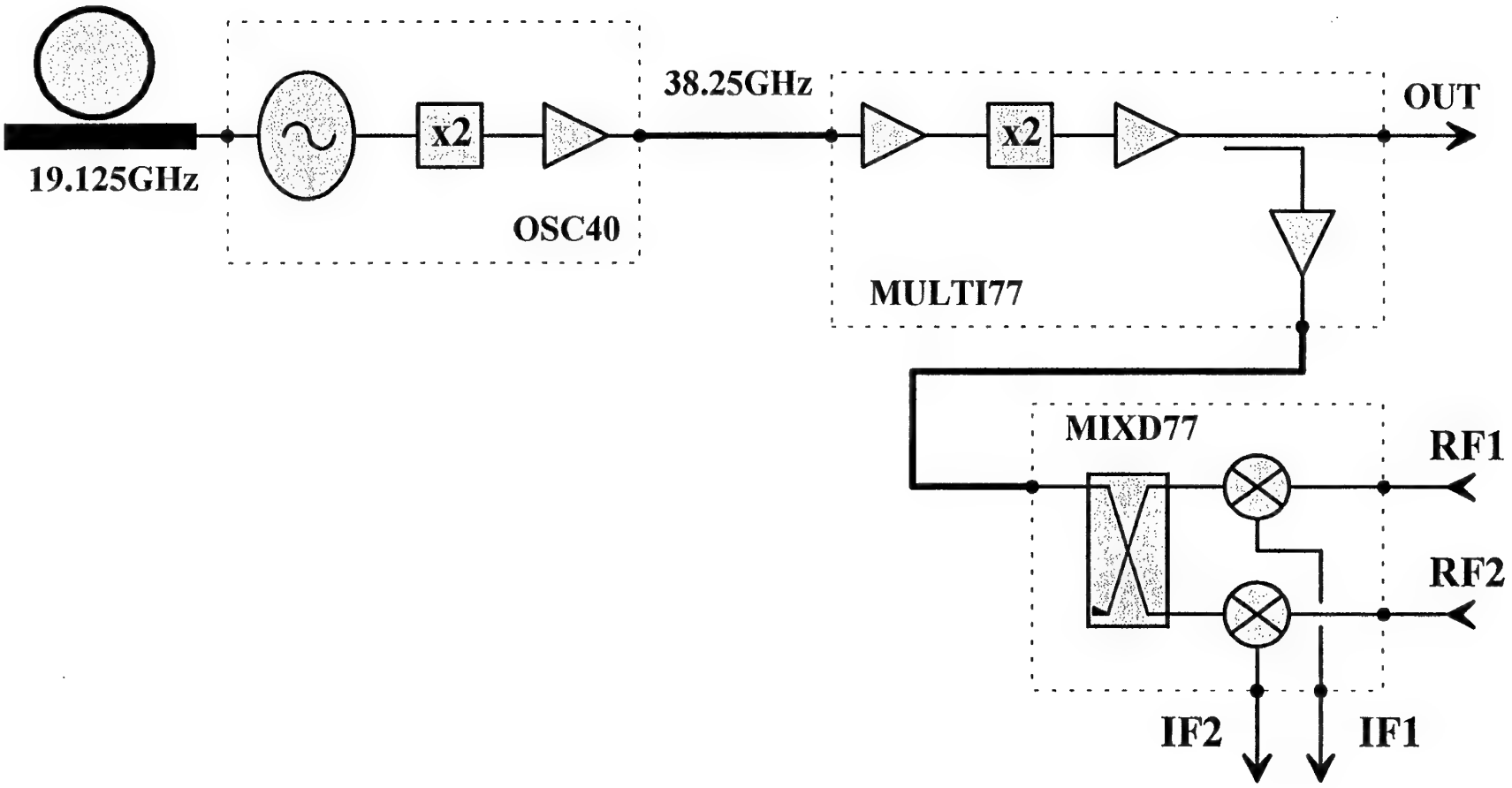

Block diagram of the radar front-end at 77GHz
Figure 4

Identification of the Noisy Parts of mm-wave FETs

A. Abdipour, A. Pacaud

Identification of the Noisy Parts of mm-wave FETs

A. ABDIPOUR, and A. PACAUD
Service Radioélectricité et Électronique, École Supérieure d'Électricité (SUPÉLEC)
Plateau de Moulon-91192 GIF-SUR-YVETTE Cédex FRANCE
Tel: (33-1) 69.85.14. 48, Fax: (33-1) 69.85.12.34. E-mail ABDIPOUR@SUPELEC.FR

Abstract
In this paper we describe a method to identify the noisy parts of the full semidistributed model of mm-wave FETs [2]. The noise contributed by passive parts and each active slice, on final two-port noise can be easily evaluated and identified to optimised the device structure for low noise applications.

Introduction
With recent developments in MMIC and MIMIC applications [3], and the influence of the wave propagation in FET's performances, a CAD routine for noise parameters study (F_{min}, R_n, $|\Gamma_{opt}|$, and Φ_{opt}) of such devices is necessary to optimize the noise performances of low noise FETs at millimeter-wave frequencies.

1. Determination of the full semidistributed model
By dividing the FET into many cells (6-port) cascaded together, the full semidistributed model based on distributed theory and experimental results was presented [1], [2]. Each cell contains the coupled electrode transmission lines, resistance and internal inductance of the electrodes, and active coupling elements. For noise modelling the approach adopted by Pospiezalski [4] was used in a distributed form.

2. Simultaneous determination of the correlation noise wave matrix and scattering matrix of final two-port.
The correlation noise wave matrix and the scattering matrix of the full semidistributed FET model, at each temperature and each frequency and bias point can be determined as follows :

$$C_s^M(V_{gs},\ V_{ds},\ f,\ T) = kT_0 df.\Delta(\mathbf{I}_{3N+M} - S^p S^{p\dagger})\Delta^\dagger + \Omega C_s^a \Omega^\dagger$$
$$S_M(V_{gs},\ V_{ds},\ f,\ T) = S_{ee}^p + \Omega S^a S_{ie}^p \qquad (2)$$

where $\Omega = S_{ei}^p(\mathbf{I}_M - S^a S_{ii}^p)^{-1}$; $\Delta = \left[\mathbf{I}_M \ \vdots \ \Omega S^a\right]$; $S^p = \begin{bmatrix} S^p_{ee} & \vdots & S^p_{ei} \\ \cdots & \vdots & \cdots \\ S^p_{ie} & \vdots & S^p_{ii} \end{bmatrix}$

S^p : is the partitioned scattering matrix of the passive multiport where subscripts e and i denote a reference to external and internal waves, respectively.

C_s^a and S^a : are the block-diagonal matrices with 3x3 normalized noise wave correlation matrices $C_{sa}^{(k)}$ and scattering matrices $S_a^{(k)}$ of active three-ports (Slice) located on the main diagonal. C_s^M and S_M : are the noise wave correlation matrix and scattering matrix at external ports, respectively. I is an identity matrix.

3. Results
Using full semidistributed approach, the identification of noisy parts of NE710 transistor has been studied. The transistor was biased at Vds=3 V, Ids=10 mA and the S- parameters were measured in 2-26 GHz band using the HP 8510 C Network analyzer and the noise parameters were measured in 2-18 GHz band by means of a specialized computer-controlled noise test set. When considering device's gate width (4x70=280 micron) four slices were sufficient for full semidistributed modelling Fig. 1 (external ports are not shown). In Fig. 2 we show the noise parameters of the transistor : (1) considering only noisy passive part, (2) considering only noisy active part, (3) considering both noisy passive and active parts, (4) considering only noisy slices at end of electrodes, and (5) considering only noisy slices at center of electrodes. Firstly, one can find that the contributed noise of passive parts is less important in the total noise of devices and secondly in mm-wave frequency the contribution of each slice is not the same for device's noise performances. These results show the importance of the full semidistributed modelling in mm-wave frequency ranges.

4. Conclusion
In this paper it has been shown that the noisy parts of the full semidistributed model of mm-wave FETs can be identified by a simultaneous signal and noise determination CAD routine. This approach can be used to control the influence of the parasitic elements on device's noise performance at mm-wave frequency.

5. References

[1] A. Abdipour, and A. Pacaud," A new semidistributed model for the noise and scattering parameters of the M(H)MIC FETs" *1995 SBMO/IEEE MTT-S* , Rio de Janeiro- Brazil, vol. 2, pp. 755-760, July 1995.

[2] A. Abdipour, A. Pacaud, " Complete sliced model of microwave FETs and comparison with lumped model and experimental results." *IEEE Trans. on Microwave Theory and Techniques* , pp. 4-10, January 1996.

[3] M. Parisot," Practical design and test of monolithic microwave integrated circuits" *Ecole d'été, Circuits Intégrés Micro-ondes (MMIC) et Applications*, Orsay, Université de Paris XI, 19-23 Sept. 1994.

[4] M.W. Pospieszalski, " Modeling of noise parameters of MESFET's and MODFET's and their frequency and temperature dependence,"*IEEE Trans. MTT*, Vol. 37, No. 9, pp 1340-1350, Sept. 1989.

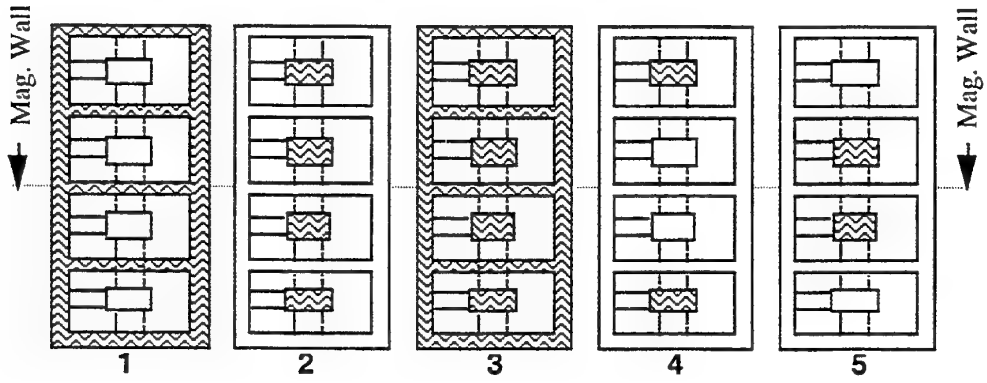

Fig. 1- Contribution of the passive and active parts on device's noise performances.

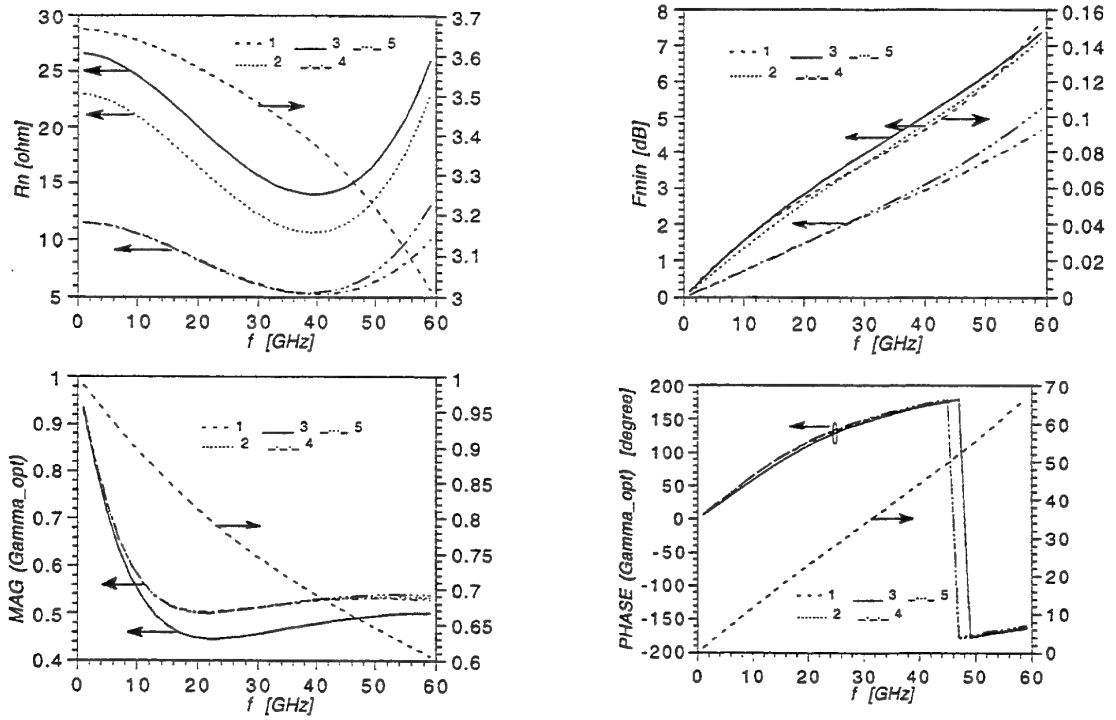

Fig. 2- Identification of the noisy parts of mm-wave FET's model.

On the Validity of a New Extrinsic Model of HEMTs Required for Millimeter Wave Circuit Design

G. Dambrine, J. M. Belquin, F. Danneville and A. Cappy

ON THE VALIDITY OF A NEW EXTRINSIC MODEL OF HEMTs REQUIRED FOR MILLIMETER WAVE CIRCUIT DESIGN

G. DAMBRINE, Member IEEE, J.M. BELQUIN, F. DANNEVILLE and A. CAPPY, Member IEEE.

Institut d'Electronique et de microelectronique du Nord (I.E.M.N.)

UMR CNRS N° 9929 Avenue Poincare B.P. 69 59652 Villeneuve d'Ascq CEDEX

Tel: (33) 20 19 78 61; Fax: (33) 20 19 78 92

E-Mail: Gilles.Dambrine@iemn.univ-Lille1.fr

Abstract:

In this paper, we propose a reliable extrinsic equivalent circuit of HEMT to determine both the [S] and noise parameters in the millimeter wave range from characterizations below 40 GHz. We show the validity of such equivalent circuit by S-parameters and noise measurements up to W band.

INTRODUCTION

Two main solutions are conceivable to obtained the microwave and noise parameters of HEMTs for the design of low noise circuits in millimeter wave.

First we can directly use the values of [S] and noise parameters measured in the millimeter wave range. However it is very difficult, for instance, to accuratly measure, in the millimeter wave range, the four noise parameters of HEMT's using conventional noise measurement methods. Moreover these measured [S] and noise parameters can not be extrapolated both as function of the frequency and the gate width.

Second we can use an equivalent circuit with associated intrinsic noise sources. The intrinsic and extrinsic elements of such equivalent circuit are determined from characterizations at relatively low frequencies. Many works [1], [2] have shown that such equivalent circuits remain valid up to W band (75-110 GHz). Nevertheless, the main drawback of such method is that the [S] and noise parameters calculated in the millimeter wave range are very sensitive to the value of some intrinsic and extrinsic elements of the equivalent circuit.

For instance, to increase the good agreement between measured and calculated S-parameters up to 120 GHz, [1] increases the complexity of the equivalent circuit by adding input and output LC distributed networks. However, the determination, of each elements of such complex circuit in relatively low frequencies, is very sensitive to uncertainty of measurements. An other example concerns the commonly used Pospieszalski T_g/T_d intrinsic two equivalent noise temperatures model [2]. This noise model necessitates the accurate knowledge of the value of some intrinsic element like R_i or G_d, but it is well known that the determination of R_i is particulary inaccurate.

To avoid the drawbacks of these preceeding equivalent circuits, we develop a new methodology to obtain both the [S] and noise parameters up to W band.

NEW METHODOLOGY

In a first step, we determine the elements of an extrinsic equivalent circuit including two uncorrelated noise sources or extrinsic equivalent noise temperatures from S-parameters and noise measurements up to 40 GHz. Using this method only three extrinsic elements (L_g, C_{pg} and L_d) have to be accuratly determined instead of eight (at least) in the case of the commonly used equivalent circuit.

Experimental data and simple equivalent circuit study prove that the extrinsic equivalent noise temperatures, used in this extrinsic equivalent circuit, are almost independant of the frequency and the gate width.

Using such extrinsic equivalent circuit, we can calculate both the S-parameters and the four noise parameters up to W band.

In a second step, we prove the reliability and the accuracy of such extrinsic equivalent circuit by S-parameters and noise measurements in the millimeter wave range. For instance figure 1. shows, in the case of a P-HEMT, the good agreement between measured and calculated S-parameters using this model up to W band.

To show the validity of the calculated noise parameters using the extrinsic equivalent circuit, we have developed narrow band on-wafer noise measurement set-up. Using such benches, we accuratly measure the noise figure under 50 Ω impedance of generator (F_{50}) at 60 and 94 GHz. The efficiency of the comparison

between measured and calculated F_{50} at 60 and 94 GHz is due to the fact that F_{50} depends of all the four noise parameters. Figure 2. shows the good agreement of the measured and calculated F_{50} and G_{50} versus the drain current in the case of a 2x50x0.1 μm^2 LM-HEMT at 94 GHz. On the same figure, we represents the variation of the calculated F_{min} and G_{ass} versus the drain current.

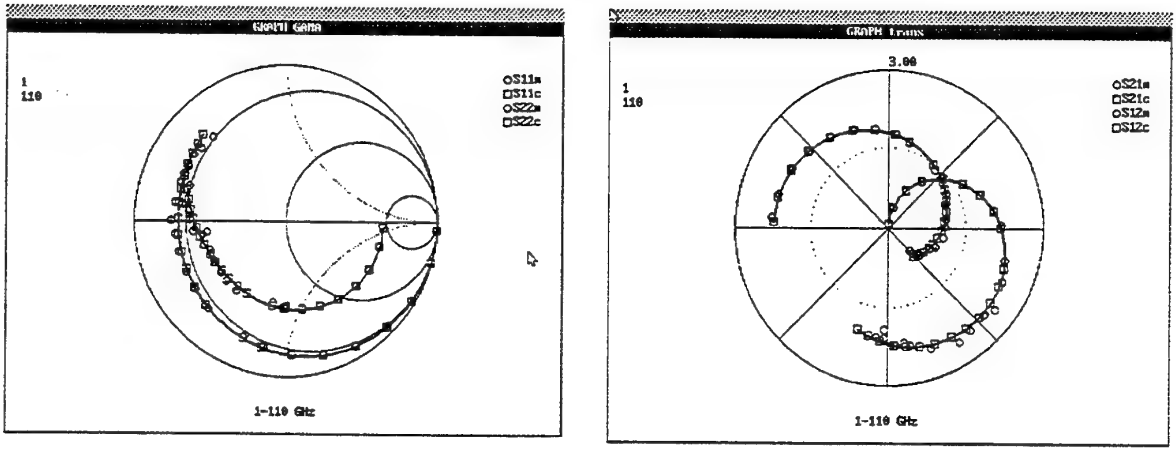

Fig. 1 Comparison of measured and calculated scattering parameters in the 1 to 110 GHz frequency range.
P-HEMT 0.15x2x25 μm^2; V_{ds}=2V, V_{gs}=0V
$S_{ij\,m}$ are measured parameters and the $S_{ij\,c}$ are extrapolated parameters.
The modulus of S_{12} is multiplied by 10 as a matter of clarity of the graph.

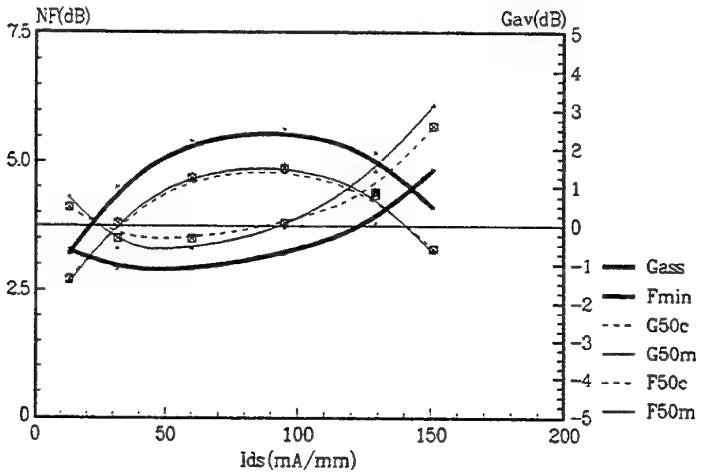

Fig.2 *Comparison between measured and calculated noise figure and available gain with a 50 Ω source impedance as a function of Ids at 94 GHz. The device is a 2x50x0.1 μm^2 LM-HEMT; Vds=0.8V.*
full lines correspond to the measured data
dashed lines correspond to the calculated data
thick full lines correspond to the calculated F_{min} and G_{ass}.

REFERENCES:

[1] P.J. TASKER, J. BRAUNSTEIN « New MODFET small signal circuit model required for millimeter-wave MMIC design: Extraction and validation to 120 GHz »
IEEE MTT-S Digest 1995 pp.661-614.

[2] M.W. POSPIEZALSKI, "Modeling of Noise Parameter of MESFETs and MODFETs and their Frequency and Temperature Dependence." *IEEE Trans. Microwave Theory Tech.*, vol. 37, no. 9, September 1989.

Noise Parameter Determination of Active Devices at Microwave and Millimeter Wave Frequencies

A. Caddemi, S. Castiglia and M. Sannino

NOISE PARAMETER DETERMINATION OF ACTIVE DEVICES AT MICROWAVE AND MILLIMETER WAVE FREQUENCIES

A. Caddemi, S. Castiglia (student) and M. Sannino

Dipartimento di Ingegneria Elettrica - Università di Palermo
Laboratorio di Elettronica delle Microonde
Viale delle Scienze - 90128, Palermo - ITALY
TEL.++39-91-6566275 / FAX ++39-91-488452

1. INTRODUCTION

Accurate noise parameter determination of active devices at microwave and millimeter wave frequencies is of primary importance for either the design of low-noise amplifiers and the noise modeling aimed at the extraction of equivalent noise sources.
The experimental determination of the noise parameters ({N}) is based on a complex procedure which still requires a great deal of operator expertise, despite the fact that automated systems are now commercially available.
On the contrary, the measurement of two-port scattering parameters ([S]) vs. frequency and bias is handled easily by use of the modern automatic network analyzers (ANA) operating up to the millimeter wave range (50 GHz).
On the basis of our work in the field of noise measurements and modeling of low-noise transistors, we here present the results of the complete characterization of pseudomorphic high electron mobility transistors (HEMT) over the 6-18 GHz frequency range with the new version of our noise figure measuring system driven by a proprietary procedure [1].
Such results are compared with the noise parameters predicted by computer analysis of a noisy circuit model previously extracted from measured [S] plus one noise figure measurement in input matched condition (i.e. @ noise source impedance value of 50 Ω).

2. EXPERIMENTAL PROCEDURE

At microwave and millimeter wave frequencies, the noise parameters of devices are more conveniently expressed in the reflection coefficient form as follows

$$F(\Gamma_S) = F_O + 4\, r_n \frac{|\Gamma_S - \Gamma_O|^2}{|1 + \Gamma_O|^2 (1 - |\Gamma_S|^2)} \qquad (1)$$

where F_O (optimum noise figure), $|\Gamma_O|$ and $/\Gamma_O$ (optimum value of Γ_S) and r_n (equivalent noise resistance) are the four noise parameters, F and Γ_S are the noise figure and the relevant input termination reflection coefficient of the DUT, respectively.
Therefore, the determination of the noise parameters has to be accomplished by measuring the variations of the device noise figure F as a function of Γ_S and by processing the output data by means of proper procedures. By means of an automatic system whose measuring procedure has been developed in our lab, we perform measurements of the noise figure at the system output for either some properly selected values of Γ_S and , at each Γ_S value, for different values of the *receiver* noise figure realized by a high repeatability step attenuator. From these noise data we derive all the noise and the scattering parameters of the device by applying appropriate data

This work was supported by Italian Space Agency (ASI), National Research Council (CNR) and Ministry of University, Science and Technology Research (MURST).

processing techniques without the need for separate measurements with the network analyzer (see [1] and references therein). The system is now operating in the updated version up to 50 GHz vs. bias and temperature (-100 ÷ 100 °C). A block diagram of the computer-driven set-up is shown in Fig.1.
However, with a view to obtaining a set of {N} which is self-consistent and representative of the device noise behavior to a good degree of approximation, an easy-to-use method has been tested and its accuracy verified for packaged HEMT's. This method makes use of a single-parameter noise model associated with the equivalent circuit of a microwave FET for predicting the device noise behavior. Such noise fitting factor can be derived from the noise figure measurement in input matched conditions, namely F_{50} (i.e., @ $\Gamma_S = 0$), which does not require to run the complete determination procedure since it is performed by an adequate use of a commercial noise figure meter [2].

3. Results

We have tested a set of packaged pseudomorphic HEMTs (NE20283A, by NEC) first in terms of [S] over the 2-18 GHz range and extracted a circuit model which is statistically representative of the measured transistor performances. Next, we derived the noise model by measuring and fitting F_{50} vs. frequency [3]. The noise parameters have then been computed by circuit analysis. As a second step, we have performed the complete characterization of the devices over the 6-18 GHz frequency range with our noise figure measurement system.
Finally, we have compared a) the measured noise parameters with the simulated ones; b) the scattering parameters measured by the ANA with the scattering parameters measured by our system through noise figure measurements only; c) the noise figure F_{50} measured by the noise figure meter with the F_{50} values computed from the measured noise parameters by use of eq.(1) evaluated @ $\Gamma_S = 0$. Sample plots reporting such comparison are shown in Fig.2 a-d.

4. Concluding Remarks

The above results exhibit a high degree of consistence concerning either the different measurement procedures and the model performance determined on the basis of a single noise fitting factor.
Clearly, the simplified method can be employed vs. frequency as long as the device lumped element model has a reasonable physical meaning (about 30 GHz), whereas the complete experimental determination is limited only by the performance of the available instrumentation and by application of an accurate *deembedding* procedure for the correct placement of the measurement reference planes as close as possible to the device under test (presently, 50 GHz).

References

[1] G. Martines and M. Sannino, "The determination of the noise, gain and scattering parameters of microwave transistors (HEMTs) using only an automatic noise figure test-set", *IEEE Trans. Microwave Theory Tech.*, vol. MTT-42, pp.1105-1113, July 1994.
[2] A. Caddemi, M. Sannino, " Comparison between complete and simplified methods for determining the microwave noise parameters of HEMTs", *Proceedings of the 43rd Conference of the Automatic Radio Frequency Techniques Group*, San Diego, USA, May 1994.
[3] A. Di Paola and M. Sannino, "Determination of gain of microwave amplifying devices through noise figure measurements", *Proceedings of the IEEE Instrumentation and Measurement Technology Conference*, Waltham, USA, pp. 526-529, April 1995.

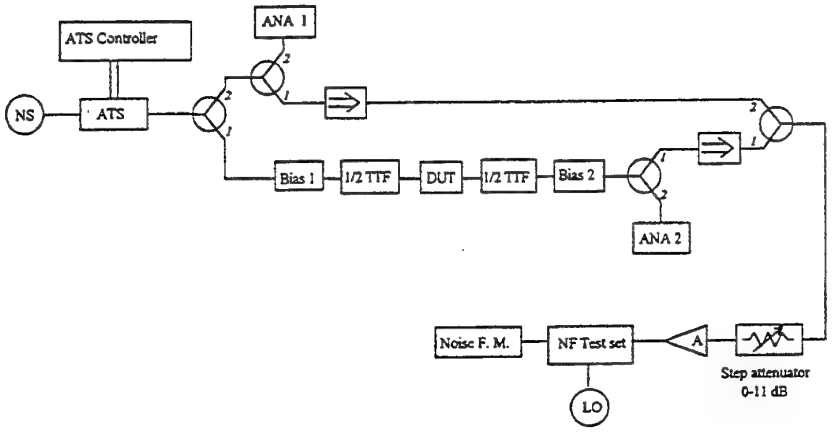

Fig.1 - Block diagram of the system for the complete characterization of low-noise transistors by means of noise figure measurements only

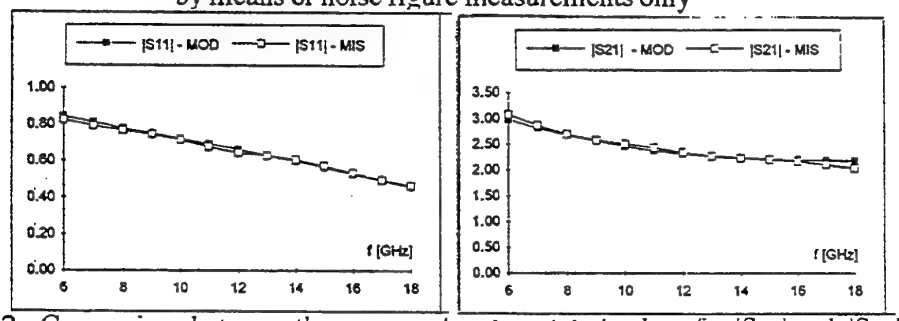

Fig.2 - Comparison between the measured and modeled values for $|S_{11}|$ and $|S_{21}|$

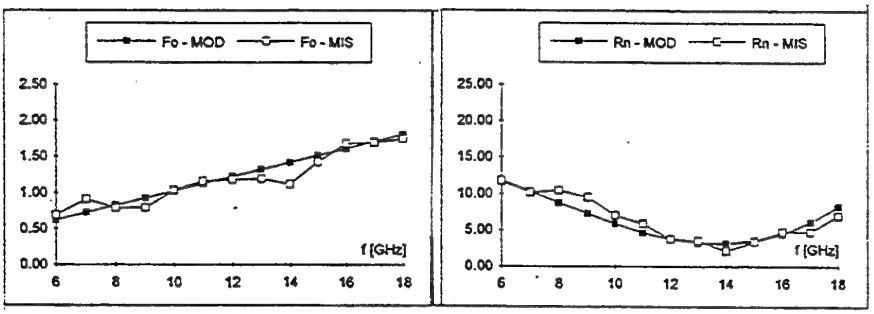

Fig.3 - Comparison between the measured and modeled values for F_O and R_n

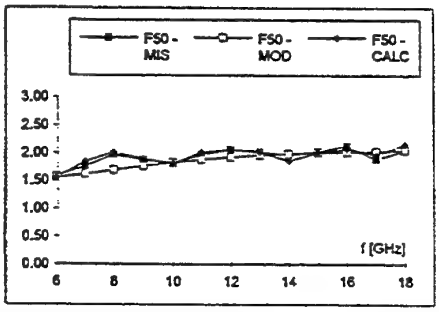

Fig.3 - Comparison among the values of F_{50} obtained from: a) measurements, b) modeling, c) computation from the measured noise parameters

A New Global Finite Element Analysis of Planar Balanced Mixers

K. Guillouard, M. F. Wong, V. Fouad Hanna, J. Citerne

A New Global Finite Element Analysis of Planar Balanced Mixers

K.Guillouard*, M.F. Wong*, Member IEEE, V. Fouad Hanna*, Fellow IEEE,
J. Citerne**

*France Telecom - CNET Paris B
**INSA, CNRS, URA 834

INTRODUCTION

The planar microwave circuit technology is now well-known to provide compact, low weight, low cost and easy to fabricate components, replacing the conventional waveguide configurations. But the recent widespread use of extremely complex and highly integrated devices, composed of various transmission lines, discontinuities and lumped elements like resistors, capacitors or other active linear and non linear elements, has increased the need of accurate fullwave electromagnetic (EM) modelling tools. Especially, the electromagnetic coupling due to the insertion of lumped components has to be taken into account to provide precise analysis of such circuits at frequencies in the millimetric range.

For this purpose, our paper presents a new 3D Finite Element Method (FEM) analysis, using edge elements, applied on the study of a planar balanced mixer that can be hardly simulated by available commercial electromagnetic or circuit simulators, since there is no separation between the lumped non linear element and the distributed circuit.

OUTLINE OF THE TECHNIQUE

The 3D FEM analysis, using edge elements, is very suitable for simulating fields in complex EM structures without having parasitic solutions [1]. The edge elements allow a space discretization of the field : the degrees of freedom (dof's) are directly the circulations of the field along the edges. This formulation can be put in matrix form as :

$[Y].[e]=[i]$, where [e] is the vector of dof's (in Volts), [i] is the excitation current vector (in Amperes) and [Y] is an admittance matrix which relates the interaction between edges. According to circuit definitions, one edge can be directly compared to an internal port whose own voltage and current characteristics are respectively e_e and i_e. We can write :

$i_e = \sum_{k=1}^{M} Y_{ek}\, e_k$, where M is the number of dof's.

If a lumped component is connected to this internal port, the Kirchhoff's laws can be written as :

$\sum_{k=1}^{M} Y_{ek} \cdot e_k = -i_e$, where i_e is the current in the lumped component.

The inclusion of the lumped element is taken into account in the excitation current vector. In a first step, the edge corresponding to the location of the component becomes an internal port that has to be considered like other usual external ports. It is either connected to a current source or open-circuited. This operation provides an impedance matrix which represents the distributed part of the circuit. In a second step, the obtained matrix is connected to the lumped element using a circuit simulation software like the commercial circuit analysis software Hewlett Packard (MDS).

This technique presents several advantages. Indeed, its formulation is quite simple, direct and general : the insertion of any linear or non linear, passive or active components can be considered (we note that the method used for the analysis of non linear circuits is the Harmonic Balance Method (HBM)). Moreover, the lumped components can be as close as desired to circuit discontinuities, since electromagnetic coupling is taken into account. Finally, the use of the FE discretization allows a locally fine meshing of zones, where the variations of the EM field are important.

Thanks to these properties, our simulator is well adapted for studying planar mixers operating in millimetric band.

RESULTS

Our analysis is used for analysing two planar balanced mixers : the first one is operating in the X-band (fig.1) and the second one given in (fig.3) is operating in the 26.5-40 GHz band [3]. We give here the results for the first mixer fabricated on a 0.635mm thick alumina substrate using a planar magic tee composed of a coplanar waveguide - slotline junction [2]. Two beam-lead Schottky-barrier diodes are directly soldered on the junction (fig.1). The mixer operates at a LO frequency of 8 GHz and a LO level of 10dBm and for a RF signal at a frequency of 10 GHz and a level of -10dBm.

The frequency spectrum given by our FEM-MDS simulations and that obtained by measurements are given in (fig.2). The differences of the magnitude of the output mixer products between our simulation results and measurements ones are mainly due to a non perfect symmetry of the measured structure whereas the FEM meshing of the mixer used in the simulation is rigorously symmetric. However, the comparison shows a good agreement between the simulation and the measurements for the very low levels of the harmonics at 4 GHz ($2f_{RF}$-$2f_{LO}$) and at 16 GHz ($2f_{LO}$) because the mixer is a balanced one. Moreover, the Image frequency is present at the RF port and is at a very low level (-108dB and -41dB resp. for simulation and measurements) at the output port, compared to the IF level (-32dB and -26dB resp.). The comparison can be judged to be satisfactory.

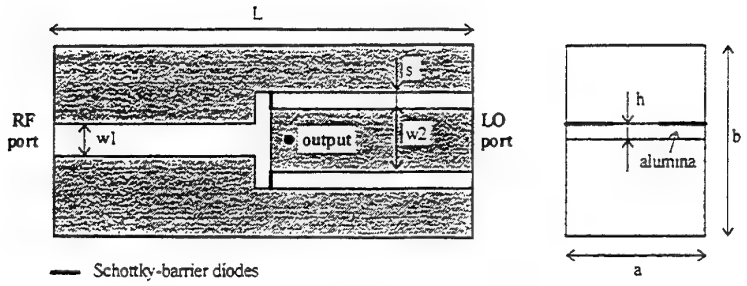

Figure 1 : Planar balanced mixer for use at X-band.
(w1=1.21mm, w2=1.668mm, s=0.436mm, h=0.635mm, a=9.525mm, b=19.05mm, L=7.99mm).

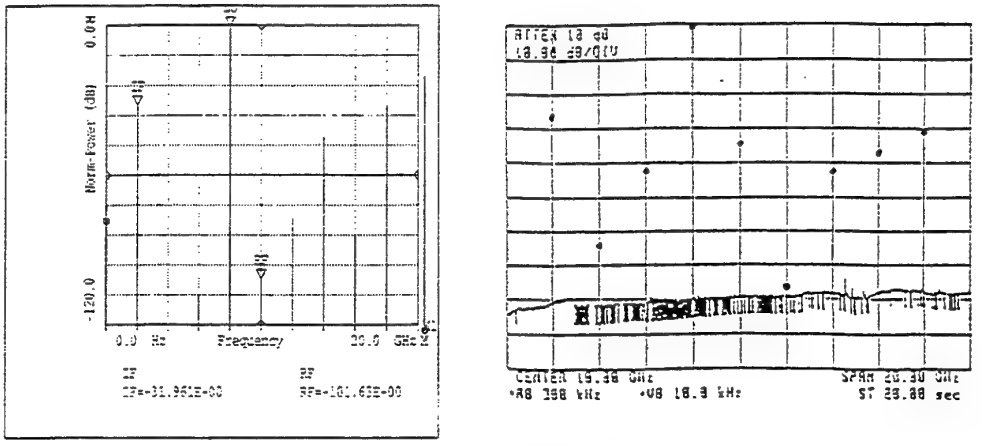

(a) *(b)*

Figure 2 : Mixer normalised output power.
(a) computed results by FEM-MDS. (b) experimental results.

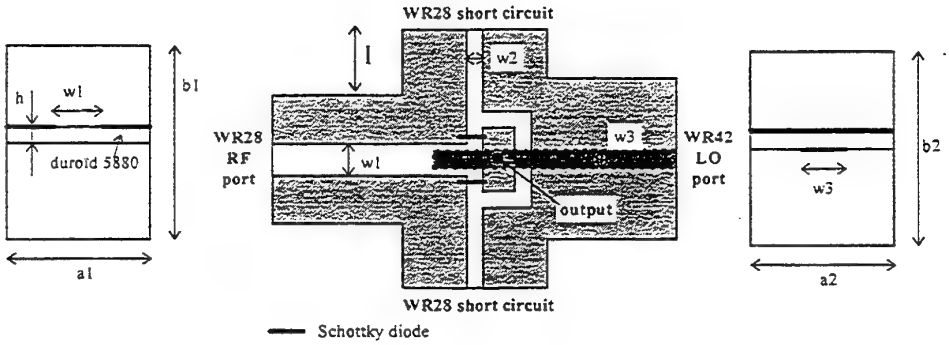

Figure 3 : 26.5-40 GHz band balanced finline mixer.(a1=3.556mm, b1=7.112mm, a2=4.318mm, b2=10.668mm, h=0.254mmw1=0.603mm, w2=0.05mm, w3=0.572mm, l=1.172mm)

CONCLUSION

A new global electromagnetic analysis is presented for the simulation of non-linear regions embedded in distributed circuits. It relies on the use of a rigorous 3D FEM simulator combined with an efficient simulator using the harmonic balance method. The comparison between our simulation and measurements results confirms the adaptability of our technique for the treatment of difficult problems like that of balanced mixers as the effect of the insertion of the lumped elements, which becomes important in the millimetric range, is taken into consideration.

REFERENCES

[1] M.F. Wong, O. Picon, V. Fouad Hanna, « Three dimensional finite element analysis of N-port waveguide junctions using edge elements », IEEE MTT-S Digest, pp. 417-420, 1992.

[2] O. Picon, V. Fouad Hanna, J. Citerne, J.-P. Lefevre, « Exact calculation of scattering parameters of the coplanar-slot transition in unilateral finline technology », IEEE Trans. MTT, vol.35, pp. 1408-1413, Dec 1987.

[3] V. Fouad Hanna, L. Ramboz « Mélangeur équilibré dans la bande de 26.5 à 40 Ghz en technologie de la ligne à ailettes ». Annales Télécommunications, 43, n° 5-6, 1988, pp. 282-286.

Modelling the Potential of Novel 3-D Integraded RTD/HFET Frequency Multiplier Circuits

G. Janßen, W. Prost, R. Reuter, U. Auer, W. Schroeder, and F. J. Tegude

submitted to *1996 International Workshop on Millimeterwaves*
Orvieto, 11-12. April 1996

MODELLING THE POTENTIAL OF NOVEL 3-D INTEGRATED RTD/HFET FREQUENCY MULTIPLIER CIRCUITS

G.Janßen, W. Prost, R.Reuter, U. Auer, W. Schroeder[1], and F. J. Tegude

Gerhard-Mercator-University-Duisburg, Solid State Electronics Department, Kommandantenstr. 60,
[1] Allgemeine und Theoretische Elektrotechnik
D-47057 Duisburg, Germany, (Fax: +49-203-3793400, Tel: +49-203-3792989, email prost@hlt.uni-duisburg.de)

ABSTRACT: Very recent work demonstrated that the ultimate performance limits of resonant tunneling diodes (RTD) are not reached (cf. [1]) and that there may be solutions for the power/stability/frequency trade off's (e.g. [2]). We focus on the possible benefits which are attainable by an efficient combination negative differential resistance due to a two-terminal and amplification due to a three terminal device. In this contribution we discuss a RTD/HFET circuitry for high performance frequency multiplication in the (sub-) millimeter wave range. Our approach consists on the following items:

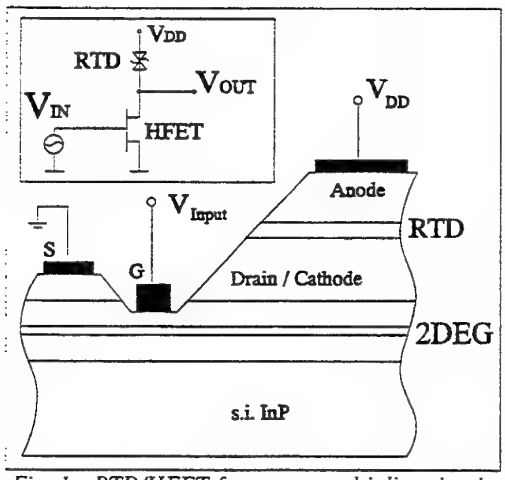

Fig. 1 :RTD/HFET frequency multiplier circuitry in a 3D monolithic integrated version

(i) Proposed circuitry:
We will present the proposed circuit design and topology (cf. fig.1). A 3-dimensional integration is choosen in order to avoid any additonal series inductance and to reduce parasitic resistances to its minimum. The RTD design for frequency multiplication with optimization of output power will be addressed. The technological litmits will be discussed on the basis of realized InGaAs/InAlAs devices fabricated on s.i. InP:Fe substrate by MBE. A highly strained InAs-well has been choosen which enables an extremely broad voltage swing with negative differential resistance. The resulting triangular shape of the I-V characteristic favours the generation of odd harmonics for frequency multiplication. A self-alignment technology was used to realize the three mesa-topology with extremly low parasitics. An InGaAs/InAlAs/InP Heterostructure field-effect transistor (HFET) with a gate lengt of 0.8 µm is choosen which can be easily realized by optical lithography. The gate width and the RTD anode area were designed such that the HFET provides at zero gate bias more current than the RTD peak current (cf. fig.2).

(ii) RTD and HFET small signal parameters:
Scattering parameters were measured on-wafer from 45 MHz to 45 GHz of both types of devices. The HFET exhibits cut-off frequencies of f_t= 39 GHz and f_{max} = 119 GHz. The small signal parameters of the RTD are discussed in more detail. It is worth noting that an excellent agreement with the measured data has been achieved with frequency independent parameters in the whole frequency range. The negative differential resistance $-R_P$ is unchanged from DC to 50 GHz. Due to an optimized contact topology the capacitance scales geometrically down to the lowest realised areaof the device mesa. In combination with the low series resistance an extremely low $R_S \cdot C = 0.3 \cdot 10^{-12}$s is achieved on a s.i. substrate. Special care was taken on the physical interpretation of the series inductance in the RTD which is of pronounced interest for the power/stability versus frequency trade-off. A field-theoretical analysis is added to evaluate the theoretical limits for the series inductance in the intrinsic RTD device. Although the bias dependence of the inductance is still under discussion it is assumed that the equivalent circuit should be extended by means of an inductance in the NDR-branch which represents the bias

dependent current delay due to the RTD. The series inductance should be bias independent and is determined by the air-bridges and the interconnects between the mesas.

iii) Modelling the output spectrum of the frequency multiplier:

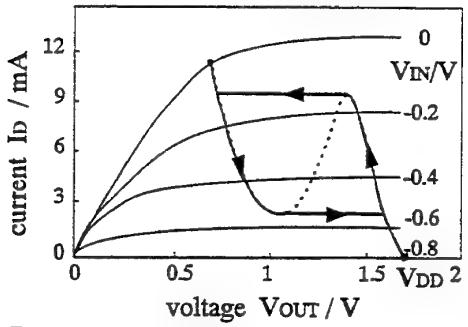

Fig. 2: Typical DC load characteristics of a RTD/HFET frequency multiplier

The frequency multiplier circuit was modeled using the HP-"microwave design system" circuit simulator (MDS) on an UNIX-workstation. A combination of a one-port nonlinear symbolic device model for the I-V-characteristic of the RTD and small signal elements for the parasitic device elements formed the RF and large signal RTD-model. The nonlinear symbolic device contained a measured data set of the I-V-characteristic and its bias dependence. The parasitic elements series resistance R_S= 20 Ω, the series inductance L_S= 38 pH and the RTD-capacitance C= 10 fF were held constant each at its largest value. The HFET was modeled by the EEHEMT1-HFET-model which describes the transistor for RF and large signal simulation as well. In a first step we have evaluated the DC load characteristic (cf. fig. 2). The negativ differential resistance results in rectangular type output voltage at DC. At higher frequencies the output voltage is no longer rectangular (c.f. fig. 3a). We calculated the spectrum of the output voltage V_{out} with a fast fourier transformation after a time domain simulation of the circuit.

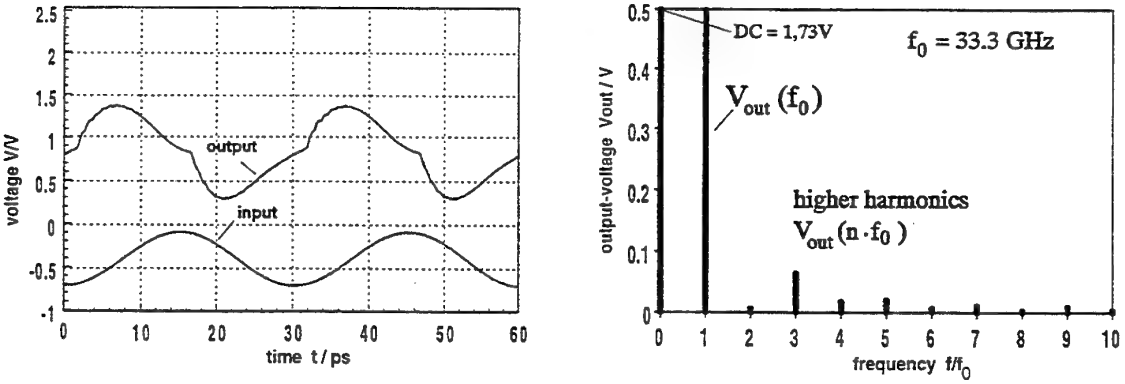

Fig. 3: Modeled output voltage left) vs. time and right) vs. frequency for a DB-RTD-HFET combination.

In fig. 3 the input voltage was set at a frequency of 33.3 GHz. The preferred generation of odd higher harmonic is clearly demonstrated. At 100 GHz the output voltage is about 1/5 of the fundamental which is still quite close to maximum of 1/3 in case of a pure rectangular output voltage.

The potential of this approach for sub-millimeter wave generation will be addressed. In addition first results from heterobipolar-transistor (HBT) devices will be shown.

[1] N.Shimizu. T.Nagatsuma. M.Shinagawa, T.Waho, "Picosecond-switching time of $In_{0.53}Ga_{0.47}As/In_{0.52}Al_{0.48}As$ resonant tunneling diodes measured by electro-optic sampling technique", IEEE Electron Device Lett., vol. 16, pp.262-264, June 1995.

[2] R.Sun, O.Boric-Lubecke, D.-S.Pan, T.Itoh, "Considerations and simulations of subfrequency excitation of series integrated resonant tunneling diodes oscillator", IEEE Trans. Microwave Theory and Techniques, vol. 43, pp2478-2485, October 1995.

Steady-State Simulation of mm-Wave Multiple-Device Oscillators

T. Bauer and J. Freyer

Steady-state simulation of mm-wave multiple-device oscillators

T.Bauer and J. Freyer

14.2.1996

The realisation of multiple-device oscillators, i. e. addition of output power from several active devices in a coupled system, is one way to increase power output at mm-wave frequencies, where the power capability of single devices is relatively poor. The combining efficiency of such oscillators mainly depends on the coupling network between the individual active devices and the load resistance, where the sum of the power is extracted. This coupling network has to be mode-selective to avoid out-of-phase operation of the devices. Selectivity can be achieved by an appropriate design of the resonator, so that oscillation is only possible in the one mode with the highest combining efficiency. It can be shown, that for optimum combining efficiency in this so-called desired mode, the admittance matrix of the coupling network must possess special symmetry properties [1]. For mm-wave resonators, the symmetry of the coupling network depends on the geometry of the cavity and the tuning elements.

The purpose of this paper is to provide a general procedure for the computer-aided analysis of multiple-device oscillators and to give design criteria for the coupling network in order to optimise the combining efficiency. The theoretical results are compared to those achived experimentally from a three-diode Impatt oscillator at 90 GHz.

A generalized scheme for an N-device oscillator is given in Fig. 1. In the frequency-domain, the active devices are represented by two-terminal admittances $Y_{D,i}(A_i,f)$ with negative real part, where A_i is the i-th rf-amplitude and f the common oscillation frequency. The linear circuit consists of the coupling network between the active devices and the load resistance (from which the power is extracted) and may depend on an additional tuning parameter λ (generally, λ can be a vector). It is described by its scattering matrix $S(f, \lambda)$ or admittance matrix $\mathbf{Y}(f, \lambda)$, both N*N. The voltage at each port is given in eq. (1) as a sinusoidal oscillation, where φ_i is the i-th phase. The load admittance $Y_{circ,i}$ at port i , given by eq. (2) [2], is readily available from the Y-parameters Y_{ij} and depends on amplitudes and phases of the voltages at all network ports.

$$u_i(t) = A_i \exp(j2\pi ft+\varphi_i) \quad (1)$$

$$Y_{circ,i} = \sum_{j=1}^{N} Y_{ij} \frac{u_j}{u_i} \quad (2)$$

Under steady-state conditions, the sum of the device admittance and the circuit load at each port has to vanish:

$$Y_{D,i}(A_i, f) + Y_{circ,i}(A_1, \ldots, A_N, \varphi_1, \ldots, \varphi_N, f, \lambda) = 0 \qquad i = 1 \ldots N \quad (3)$$

As the system from Fig.1 is autonomous, one of the phases can arbitrarily be chosen, here φ_1 is set to 0. The 2N equations for real- and imaginary part of (3) then compose a nonlinear system for 2N unknowns $A_1, \ldots, A_N, \varphi_2, \ldots, \varphi_N, f$. Using simplifications for devices and coupling (e.g. quadratic dependence of device admittance on amplitude,nearest-neighbour coupling, weak broadband coupling networks), direct expression of (3) for some practical examples can be given [2]. In the general case, however, this system must be solved using a continuation method, which takes the solution of (3) at $\lambda=\lambda_k$ as a predictor for the Newton-algorithm at $\lambda=\lambda_{k+1}$. Starting values at $\lambda=\lambda_0$ can be obtained from the analytical solution of (3) for a simplified linear circuit.

For the Newton-iteration, the values of Y_D and Y_{circ} as well as their derivatives with respect to amplitudes, phases and frequency must be provided at arbitrary values of amplitude and frequency. Usually both, the linear circuit and the nonlinear devices are described by systems of partial differential equations. Because of the complexity of the problem only discrete frequency- or amplitude points can be calculated in finite time (respectively measured). Therefore, an appropriate interpolation scheme is necessary. Cubic spline interpolation proved effective, as it provides continuous values of the interpolated function as well as of its first and second derivatives. The device admittances are interpolated versus frequency and amplitude using two-dimensional cubic splines. Complex cubic spline interpolation of the S-parameters gives values for S and dS/df, from which **Y** and d**Y**/df and, using (2), $dY_{circ,i}/df$ can be calculated analytically. Analytical derivatives with respect to amplitudes and phases are readily available from (2). With this knowledge, the system of nonlinear equations (3) can be solved for amplitudes, phases and frequency.

A three-device oscillator realized with GaAs Impatt diodes under a common resonant cap in waveguide technique [3] is chosen to prove the validity of the described theory. The linear circuit can be tuned with a single sliding short in order to accomplish impedance matching of all three devices. Compared to a single

device, from this oscillator about three times the output power (500 mW at 90 GHz) could be achieved experimentally, indicating high combining efficiency.
For the applied resonator structure, the S-parameters at discrete frequencies are determined using a commercial finite-element program [4]. The nonlinear devices are described by the help of a large-signal drift-diffusion model [5]. The above described procedure gives theoretical values for rf-amplitude and phase of each diode as well as common frequency as a function of the sliding short position. From these data output power and combining efficiency can be calculated and compared to the experiment. The theoretical results show that the phase differences between the individual diodes are negligible, despite the principal unsymmetries of the rectangular waveguide/cylindrical resonant cap mount. Considering the negligible phase differences and a lossless reactive coupling network, the realized high combining efficiency can easily be explained.Also all other experimental data are in good agreement with the theory.
To investigate the influence of larger disturbances of the symmetry, which can arise during the technological fabrication of the oscillator, a change of 20 % in diode parameters is considered. The results indicate that the used resonator with three active diodes is relatively insensitive to disturbances in the symmetry. The applied change of 20 % theoretically only leads to a reduction of the combining efficiency from about 100 % to 98 %. Even for D-band frequencies, where the probability of unsymmetries in resonator structure and diodes is higher due to the absolute smaller dimensions, the drop in the combining efficiency is not severe. This predicts that the used type of multiple-device oscillator is also suitable for application at higher frequencies.

Conclusion:
A procedure for the numerical analysis of general multiple-device oscillators has been presented, based on a frequency-domain description of nonlinear active devices and linear coupling network. Steady-state frequency, amplitudes and phase-differences of the devices and related output power and combining efficiency can be calculated. Application of the theory to a three-diode oscillator confirmed the experimental result that even in the presence of moderate unsymmetries, excellent combining efficiencies can be obtained.

References:

[1] Kurokawa, K.: `The single-cavity multiple-device oscillator', IEEE Trans. Microwave Theory Tech., 1971, vol. MTT-19, pp.793-801
[2] York, R. A., Liao, P. and Lynch, J. L.: `Oscillator Array Dynamics with Broadband N-Port Coupling Networks', IEEE Trans. Microwave Theory Tech., 1994, vol. 42, pp.2040-2045
[3] Bauer, T. and Freyer, J.: `Analysis of a new millimetre wave power combiner', Proc. 25th European Microwave Conf., 1995, Vol.1, pp.470-473
[4] Freyer, J., Mayer, B. and Tschernitz, M.: `CAD for mm-wave resonators', Proc. 24th European Microwave Conf., 1994, Vol.1, pp.273-278
[5] Gaul, L.: `Großsignal- und Stabilitätsanalyse von GaAs-Lawinendioden für Puls-Leistungsoszillatoren im Millimeterwellen-bereich', PhD thesis, Technische Universität München, 1993

Fig. 1: Generalized scheme for an N-device oscillator

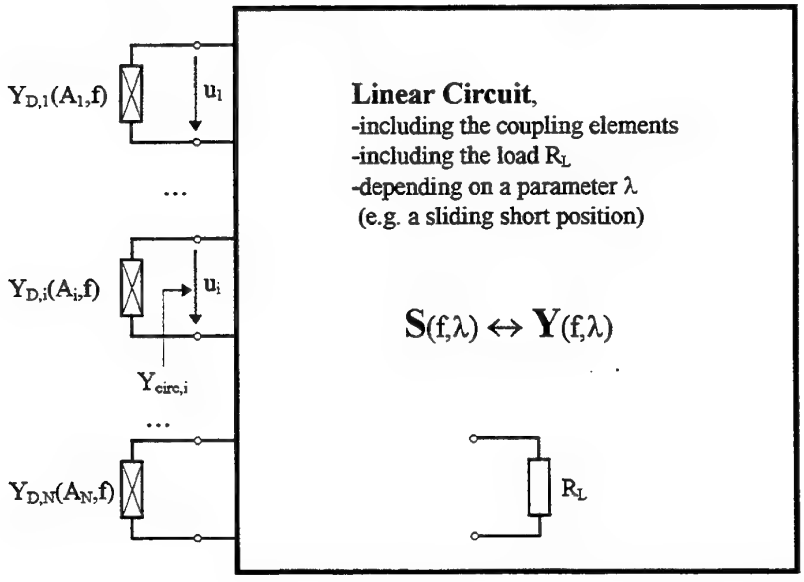

Silicon-Based Integrated Millimeterwave Monolithic Circuits

P. Russer

Silicon-Based Integrated Millimeterwave Monolithic Circuits

Peter Russer

Lehrstuhl für Hochfrequenztechnik, Technische Universität München
Arcisstr. 21, 80333 München, Germany
phone: +49-89/2105 3379, fax: +49-89/2105 3365, e-mail: russer@hft.e-technik.tu-muenchen.de

1 Introduction

Investigations of silicon–based planar circuits have already been reported as early as 1965 [1, 2]. Silicon as a substrate for millimeter–wave monolithically integrated circuits has been suggested in 1981 by the RCA group of A. Rosen et al [3]. Since 1986 in the field of silicon monolithic millimeterwave integrated circuits (SIMMWICs) there are increasing research activities at the former AEG–Telefunken Research Institute which has merged now into the Daimler–Benz Research Center [4]–[19]. Up to now SIMMWICs for frequencies up to above 100 GHz already have been fabricated, and the suitability of silicon as the base material for monolithic integrated millimeterwave circuits has been successfully demonstrated. Monolithic integration of solid–state devices provides the possibility of low–cost production, improved reliability, small size and light weight, and easy assembly.

Since the high–field drift velocity of Si and GaAs are in the same order silicon is suited for IMPATT diodes as well as GaAs. For SIMMWICs the IMPATT diode provides high oscillator output power combined with high efficiency. Also the SiGe heterojunction bipolar transistor is a promising candidate for silicon based monolithic integrated millimeterwave circuits.

The linear passive parts of SIMMWICs may be realized in planar circuit technology. The fundamental transmission line structures used in SIMMWIC design are microstrip lines, slot lines, coplanar lines, coplanar strip lines, and microshield lines. Based on these fundamental geometric structures the planar circuit elements are designed. These planar circuit elements include transmission line discontinuities, planar resonators and antennas as the basic structures.

In the frequency region above 60 GHz SIMMWICs with only a few millimeters dimensions may also include planar antenna structures. The integration of the antenna structures allows the direct coupling of SIMMWICs to the radiation field. Complete receiver or transmitter circuits may be realized monolithically on chips with a few millimeters dimension. The antenna gain of the chips may be increased if necessary using lenses and mirrors. The base–band signal processing circuits can be integrated on the SIMMWIC.

Table 1 gives a comparison of the data of Si and GaAs. The dielectric constant of both materials is comparable. At 90 GHz also the dielectric loss tangents of Si and GaAs are within the same order of magnitude. Today, silicon substrate material with a specific resistance of 10,000 Ωcm is available. For this material, in planar circuits the conductor losses due to the skin effect dominate the loss contributions whereas the substrate losses in the silicon account only for a minor part. The electron mobility of GaAs is six times higher than the electron mobility of Si. This yields a correspondingly higher f_T value for bipolar transistors and field effect transistors. On the other hand, the high field drift velocity of Si and GaAs are in the same order. The higher thermal conductivity of silicon is advantageous for power circuits.

	Si	GaAs
Diel. Const.	$\epsilon_r = 11.7$	$\epsilon_r = 12.9$
Specific Resist.	$> 10^4$ Ω cm	$> 10^6$ Ω cm
Dielectric Loss Factor (90 GHz)	$1.3 \cdot 10^{-3}$	$0.7 \cdot 10^{-3}$
Thermal Cond.	1.45 W $cm^{-1}K^{-1}$	0.46 W $cm^{-1}K^{-1}$
Electron Mobility	700 cm^2/Vs	4300 cm^2/Vs
High Field Drift Velocity	10^7 cm s^{-1}	$6 \cdot 10^6$ cm s^{-1}
Density	2.33 g cm^{-3}	5.32 g cm^{-3}

Table 1: Parameters of Si and GaAs

A unified SiGe/SIMMWIC technology allows also to incorporate SiGe heterojunction bipolar transistors [19]. This unified technology allows the fabrication of Schottky diodes, IMPATT diodes, SiGe heterojunction bipolar transistors and PIN diodes (Fig. 1).

2 Passive Circuits on Silicon

2.1 Planar Circuits

Since for highly insulating silicon material for millimeterwave frequencies the dielectric losses in the silicon play a minor role compared with conductor loss, the use of silicon yields no drawback. Experimental investigations have shown, that on substrates with 195 μm thickness microstrip lines with an attenuation as low as 0.6 dB/cm can be realized [5]. Epitaxial layers have to

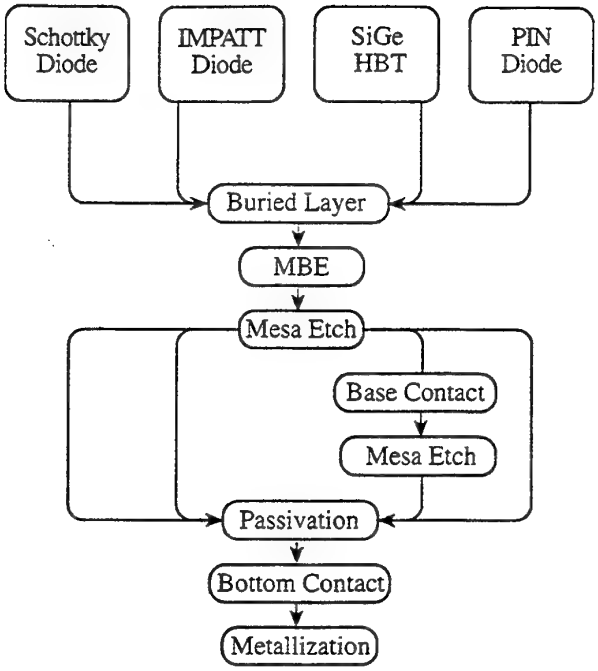

Fig. 1: Steps of a unified SiGe/SIMMWIC technology.

be removed by etching in the areas of planar circuits in order to obtain these low attenuation values. Parasitic effects induced by passivation of high–resistivity silicon substrates play an important role and have to be minimized in order to obtain low loss [20]. The common types of planar transmission lines are summarized in Fig. 2.

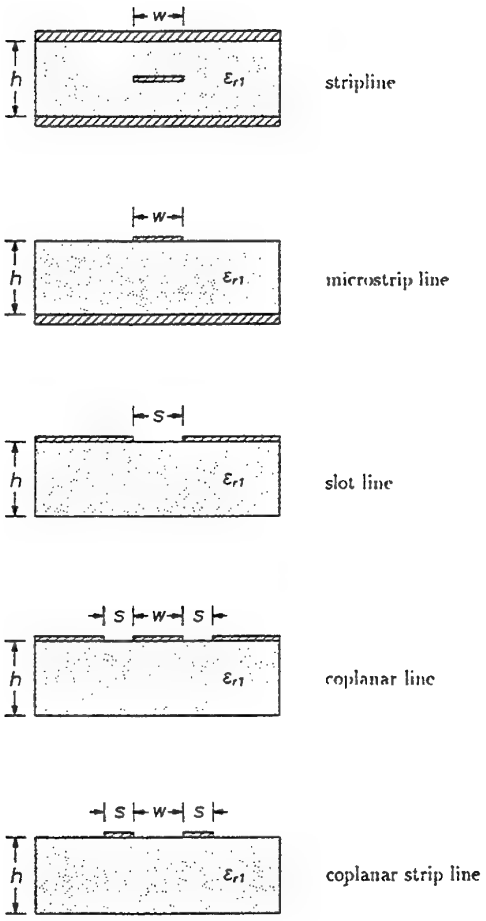

Fig. 2: Planar transmission lines.

2.1.1 Microstrip Lines

Microstrip lines are most commonly used in monolithic integrated circuits. Due to the back side metallization the substrate can easily be fixed on a metallic mount providing an efficient heat sink. Mounting of lumped elements in series configuration is very easy. Mounting of lumped elements in shunt configuration and fabrication of shorts requires via holes, which are in monolithic integrated circuits technologically expensive.

The maximum frequency of operation with a microstrip is mainly limited by the excitation of spurious modes, namely higher-order hybrid microstrip modes, trapped surface waves, and radiating waves. The cutoff frequency $f_{c,HE1}$ of the first order hybrid microstrip mode is given by [24]

$$f_{c,HE1} \doteq \frac{c_0 Z_0}{2\eta_0 h}. \qquad (1)$$

For a $Z_0 = 50\,\Omega$ microstrip line on a $h = 100\,\mu$m thick silicon substrate with 80μm width (1) yields a cutoff frequency $f_{c,HE1} \doteq 200$ GHz.

2.1.2 Slot Lines

Unlike the stripline and the microstrip line, the slotline is a balanced transmission line. Slotlines suffer from high dispersion, high radiation loss, and low power handling capabilities. They find, however, interesting applications as resonators [16] and resonant antennas [21, 22, 25]. The fundamental mode of the slotline is a quasi–TE mode. For transverse dimensions below the wavelength the structure supports a quasi–TEM type of mode similar to that of the coplanar strip line [26].

2.1.3 Coplanar Lines and Coplanar Strip Lines

Coplanar lines have been investigated theoretically and experimentally [27, 28] and particularly with respect to applications in hybrid and monolithic integrated circuits [29]–[34]. They extend substantially the flexibility in the circuit design and exhibit some distinctive advantages. Mounting of components in shunt and series configuration is equally easy and no via holes

are needed. The fundamental mode propagating along coplanar lines at low frequencies is quasi–TEM. With increasing frequency the fields and surface currents concentrate around the slots and finally the quasi–TE slotline mode occurs. The coplanar strip line is due to its balanced nature ideally suited as a feed line for printed dipole antennas [23]. Passive elements for coplanar MMICs are reported in [20].

2.1.4 Transmission Line Discontinuities

For a variety of stripline and microstrip line discontinuities equivalent circuits and closed form expressions for the reactances have been found [36, 37]. In [38] open circuits, short circuits, and step changes in width of coplanar waveguides have been investigated. In [39]–[42], simple models for coplanar stubs and T-junctions were developed.

Radiation losses of short circuited coplanar waveguides have been investigated in [43]. At coplanar waveguide discontinuities substantial mode conversion can occur [31, 40].

2.1.5 Planar Resonators

Planar resonators are open structures and suffer from energy leakage into radiating and surface wave modes. This radiation can be utilized if the resonator is also used as an antenna. The rectangular planar resonator consists of a planar transmission line of length l. For an open microstrip resonator resonance occurs for

$$l + 2\Delta l = n\frac{\lambda_g}{2}, \qquad n = 1, 2, 3, \ldots \qquad (2)$$

with the guide wavelength λ_g and the the length extension Δl of the open microstrip line.

With dual fed coplanar resonators very low radiation losses are achieved. In this configuration at each end of a $\lambda/2$ coplanar line resonator an IMPATT diode is integrated. The generated power is delivered to another coplanar line, which is capactively coupled at the center of the resonator [44].

2.2 Planar Antennas

In the millimeterwave region with small antenna dimensions a considerable antenna gain may be achieved. This allows to include planar antenna structures into SIMMWICs. An overview over planar antennas is presented in [47, 49]. Using integrated antennas as the radiating structures, feed lines and associated components, such as oscillators, detectors and mixers may be combined. Planar antennas with 36 elements and with 96 elements have been designed and fabricated [5, 9]. In this section, we discuss basic design concepts of planar millimeter wave antennas. For a comprehensive review on millimeterwave antennas in general we refer to [45]–[50]. The design of planar antenna arrays in the millimeterwave region involves new problems, since substrate surface waves may increase mutual coupling between the antenna elements, and losses in the feed lines limit the array size. However in order to minimize the SIMMWIC chip size the combination of a single patch or slot antenna element on the chip with mirrors or dielectric lenses may be preferable.

2.2.1 Patch Antennas

The microstrip patch is the most commonly used planar millimeterwave antenna and the basic antenna element for antenna arrays. The application of these antennas, however, is limited by their narrow bandwidth. At millimeterwave frequencies they suffer from excitation of surface wave modes and from losses in the feed lines. Excitation of surface wave modes results in poor radiation efficiency and in mutual coupling of antenna elements in antenna arrays.

Fig. 3 shows an asymmetric patch antenna, the magnitude of the 2-D surface current distribution at 76 GHz, and resistance and reactance as a function of the frequency [51]. The diode feeding the patch antenna is located at the point of the highest surface current density – the junction between the patches – resulting in a minimal resistance of only 2.1 Ω. The first parallel resonance at 64 GHz is caused by the longer patch, the second at 95 GHz by the shorter one. By varying the length of the patches the Q-factor of the radiating oscillator can be influenced. As can be seen, there are two possible frequencies at 37 GHz and 76 GHz at which the diode can compensate the input impedance of the antenna.

2.2.2 Slot Antennas

Compared with patch antennas slot antennas exhibit a higher bandwidth. The slot length equals one line wavelength. Coplanar active devices can be placed within the radiating aperture and the slot simultaneously acts as a resonator. In [52] and [53] results of a rigorous full wave analysis of half–wavelength and full–wavelength slot antennas are reported. Fig. 4 presents the surface current distribution and the impedance of a slot-line oscillator at 76 GHz [51]. Measurement results are provided in Fig. 5. In the left part the measured radiated power of the slot oscillator in cw mode is drawn versus the feeding current of the diode. A maximum power of 1 mW at 79.7 GHz is achieved. The noise-to-carrier ratio reached an excellent value of 81.7 dBc/Hz at an offset of 100 kHz. On the right hand, the measured spectrum in cw mode is shown at a bandwidth of 1 MHz. At the frequency of 79.4 GHz we measured a radiated power of – 2 dBm.

The metalization containing the radiating slot on the top of the substrate and the ground metalization at the bottom provides a parallel plate waveguide. In this configuration parallel plate waveguide modes are excited efficiently resulting in substrate resonances and parasitic radiation at the substrate edges. A slot antenna on a monolithically integrated cavity resonator exhibits a very large radiation efficiency of about 50% [54, 55].

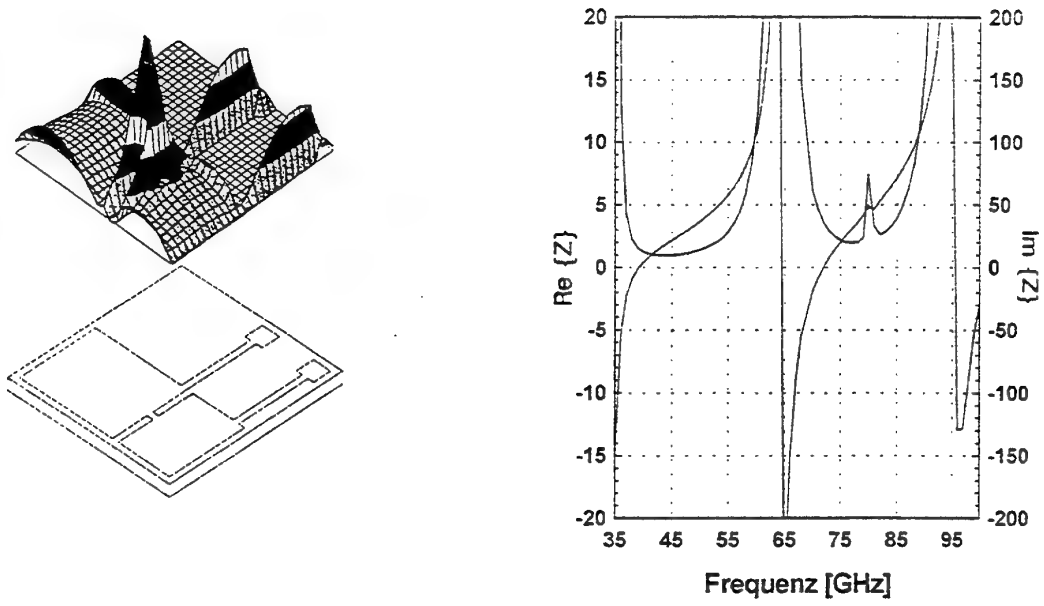

Fig. 3: Patch antenna: surface current distribution at 76 GHz (left) and calculated input impedance (right).

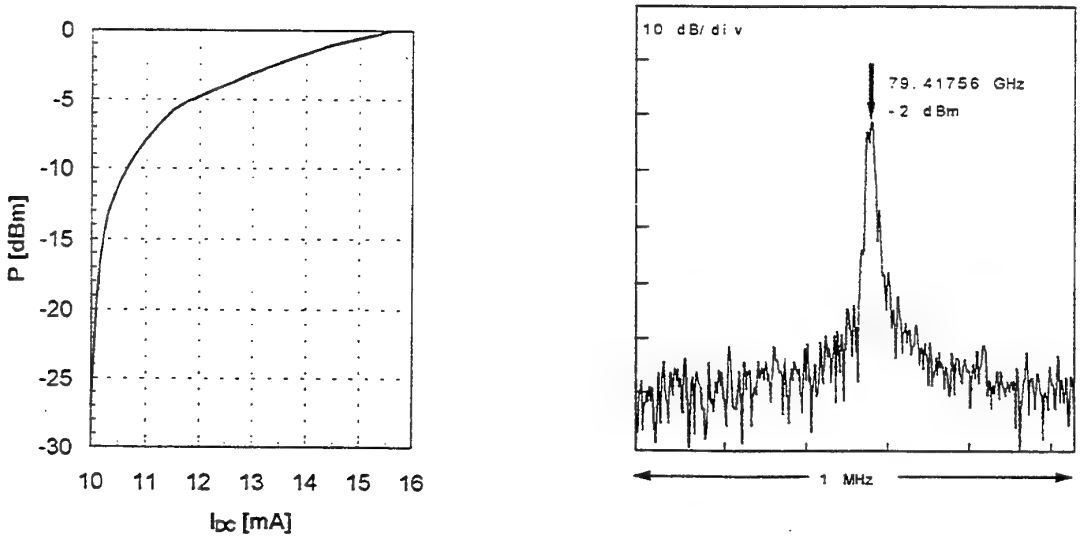

Fig. 4: Slot antenna: surface current distribution at 76 GHz (left) and calculated input impedance (right).

2.3 Micromachined Circuits

Besides their advantages of high design flexibility, reduced area and simple integration with active devices planar circuits suffer from undesirable electromagnetic effects and parasitics limiting their electrical performance. These frequency dependent parasitic effects are due to the losses in the conductors and in the dielectric material as well as the radiation losses of the open planar structures. The radiation effects may be reduced by sophisticated packaging techniques. A very promising attempt to overcome the drawbacks of planar circuits are the microshield line concept and the suspended membrane microstrip (SMM) line concept [57, 58, 59, 60]. The advantages of the microshield line and SMMs are low dielectric losses and low radiation losses at discontinuities. Both transmission line types are fabricated by micromachining techniqes on a $SiO_2 - Si_3N_4 - SiO_2$ membrane, grown on a silicon substrate. Fig. 6 shows the cross section of a microshield line. The membrane thickness is 1.5 μm. Standard lithographic processing techniques are used for the metal pattern definition and cavity etching. The depth of the ground plane cavity is controlled by timing the etch. The microshield line has properties similar to a coplanar line without dielectric support. In copla-

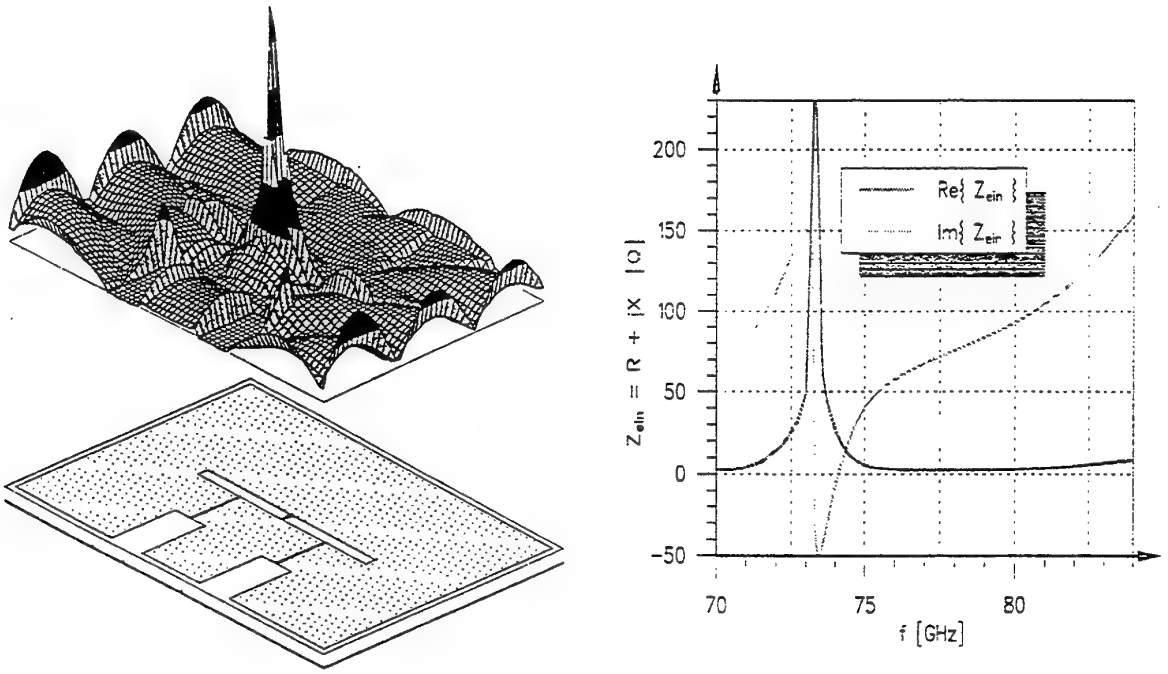

Fig. 5: Slot antenna: Measured radiated power of slot oscillator in cw mode versus feeding current of the diode (left) and measured spectrum in cw mode at a bandwidth of 1 MHz (right).

nar waveguides the radiation loss into parasitic modes is a function of both f^3 and $(\epsilon_r - 1)^2$ where f is the frequency and ϵ_r is the relative permittivity of the substrate [49, 61]. Therefore, although radiation loss is increasing strongly with frequency it may be eliminated completely by removing the dielectric. At 35 GHz losses as low as 0.03 dB/mm have already been measured [62].

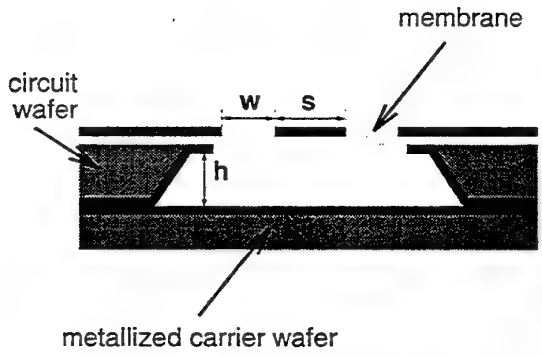

Fig. 6: Cross section of the microshield line

The SMM line, depicted in Fig. 7 is essentially a shielded microstrip line with an air dielectric [59, 63]. The fabrication of the SMM line requires multiple micromachining steps. The shield is formed by a second micromachined wafer.

Micromachined techniques already have been applied to the development of circuits. Stripline resonators

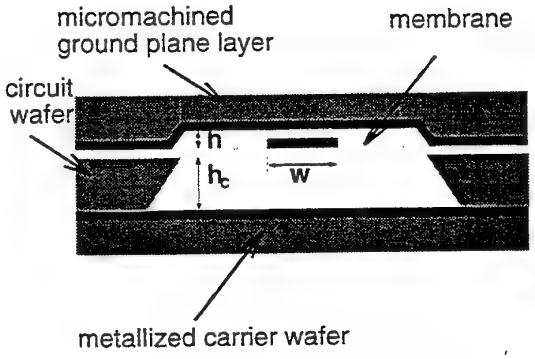

Fig. 7: Cross section of the SMM line

on thin dielectric membranes exhibited dispersion–free, conductor loss limited performance at 13.5 GHz, 27.3 GHz and 39.6 GHz [64]. The fabrication of microshield filters at 30 GHz and 90 GHz, microstrip bandpass filters at 94 GHz, and a 250 GHz bandpass filter with 1.0 dB – 1.5 dB insertion loss has been reported [62].

The fabrication of micromachined circuits requires a higher technological effort than the fabrication of planar circuits. However since micromachined circuits can be self–packaged it may be cost–competitive with packaged planar circuits.

3 Diodes and Transistors

3.1 Schottky Diodes

Schottky diodes are used for detector and mixer applications in SIMMWIC receivers [66]. Monolithically integrated Schottky diodes have been realized in a coplanar configuration [15, 67]. For the fabrication of coplanar Schottky diodes on highly insulating silicon substrates the substrates first are thermally oxidized and highly doped n^+ regions are defined by As or AsP implantation and subsequent diffusion. After this a 100 nm thick lightly doped semiconductor n layer is deposited by silicon molecular beam epitaxy. The Schottky anode finger is defined by photolithography or by x-ray lithography and a lift off process. For the Schottky anode metalisation Ti/Pt/Au is used. Then the ohmic contact is formed by a further lift off process and gold is electroplated.

With coplanar AsP doped Schottky diodes and the n epitaxial layer grown by low temperature doping at 300°C and a junction area of 33 μm a series resistance of 2.6 Ω and a junction capacity of 59 fF were measured. From these values a cutoff frequency greater than 1 THz is evaluated. Coplanar Schottky diodes allow a coplanar circuit design without via holes through the substrate. The air–bridge technology provides a lower parasitic capacitance and a lower leakage current.

3.2 IMPATT Diodes

IMPATT diodes are junction devices, operated in the reverse direction. The diode is biased above the threshold for impact ionisation. The carrier generation in connection with the transit time delay arising from the drift process, causes a dynamic negative resistance [68, 69, 70]. The IMPATT diode provides high oscillator output power combined with high efficiency. Efficiencies higher than 10 % may be achieved at 100 GHz. Since monolithic integrated circuits usually exhibit a higher thermal resistance, the high efficiency of IMPATT diodes is advantageous.

The negative real part of the IMPATT diode impedance is in the order of 1 Ω to 10 Ω. For this reason a low impedance termination of the IMPATT diode is required in order to achieve oscillator operation [71]. Especially in the case of planar resonators, due to the low Q value of these resonators a careful oscillator design is required. Usually IMPATT diodes have to be thinned to a few micrometer in order to obtain a low series resistance and a good thermal conductivity. In the case of discrete IMPATT diodes the electrical contacts are formed on both sides of the contact. Using this geometry in monolithic circuits requires substrate thinning in the region of the IMPATT diode. This can be done in principle by selective etching.

For monolithic integration of IMPATT diodes a coplanar device structure is advantageous [10, 16]. Fig. 8 shows the cross section of a coplanar IMPATT diode in a coplanar oscillator. The pnn^+ layers of the

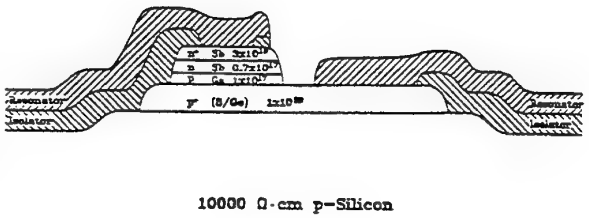

Fig. 8: Cross section of a coplanar IMPATT diode.

double drift region diode is grown by molecular beam epitaxy on a highly p^+ doped edge stop and contact layer. This layer has been grown epitactically on high resistivity silicon. In order to obtain a low series resistance large p^+ contact areas are defined in a photoresist process. After passivation of the individual diodes and opening of the contact windows the contact and planar circuit metalisation is formed by evaporating gold and increasing the thickness of the gold layer to 3 μm by electroplating.

For SIMMWIC applications the double low–high–low (DLHL) diode following the original Read diode approach is very promising [19]. Compared with conventional IMPATT diodes the absolute value of the (negative) real part of the DLHL diode impedance is increased by more than a factor of two. This will improve the matching of the diode to planar resonators.

3.3 SiGe–Base HBTs

Although silicon bipolar transistors with transient frequencies above 50 GHz are possible in principle, these devices would exhibit a too high base resistance and too low breakdown voltages. A promising device for millimeterwave applications is the Si–Ge–base heterojunction bipolar transistor. The heterojunction bipolar transistor first has been suggested in 1957 by Kroemer [72]. A first suggestion for a SiGe–base heterojunction bipolar transistor (HBT) for high frequency applications has been made in 1977 [73, 74]. Detailed investigations of the millimeterwave Si–Ge–base heterojunction bipolar transistor were presented by [75]–[78]. Fig. 9 shows the cross section of a heterojunction bipolar transistor. In the Si–Ge–base heterojunction bipolar transistor the base is formed by an epitactically grown Si–Ge layer between the adjacent silicon layers. By this way the band gap in the base region is reduced compared with the band gap in the emitter region. The current gain β of a conventional bipolar transistor is given by

$$\beta = \frac{D_{nE}\, N_E\, w_E}{D_{pB}\, P_B\, w_B}\,, \qquad (3)$$

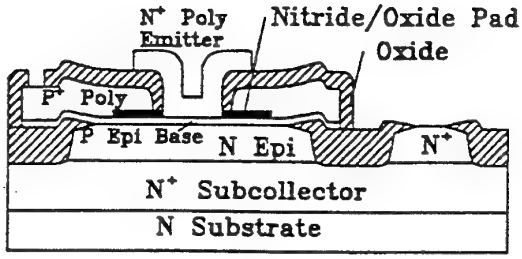

Fig. 9: Cross section of Si-Ge HBT.

where D_n and D_p are the diffusion constants of electrons and holes in the emitter and base regions respectively, N_E and P_B are the emitter and base doping concentrations, w_E is the emitter thickness and w_B is the base thickness. For the HBT after Kroemer [72] the current gain β is given by

$$\beta = \frac{D_{nE}\, N_E\, w_E}{D_{pB}\, P_B\, w_B}\, e^{\Delta E/kT}\,, \qquad (4)$$

where ΔE is the bad gap difference between Si and SiGe. The exponential dependence of the minority carrier injection rate across the emitter base barrier on the band gap difference yields already at Ge contents of 20 % a value of the exponential term of more than 1000. This allows to obtain a high base efficiency also in the case of a high emitter doping. Due to the high base doping low base sheet resistances with base width down to 10 nm are attainable. A typical high–frequency silicon bipolar transistor with a base width of less than 100 nm exhibits base sheet resistances in the order of 10 k$\Omega/2$, whereas SiGe–HBTs reach base sheet resistances as low as 1 k$\Omega/2$ for a 20 nm doped base [19]. A high current gain and a low base resistance may be combined therefore also in the case of extremely low base widths.

The maximum oscillation frequency f_{max} of the HBT is given by

$$f_{max} = \sqrt{\frac{f_T}{8\, pi\, C_{BC}\, R_B}}\,, \qquad (5)$$

where f_T is the transit frequency, R_B is the base resistance, and C_{BC} is the base collector capacity. The fabrication of a heterojunction bipolar Si–Ge–transistor with f_T values above 100 GHz has already been reported [19, 74, 78, 79, 80]. For most circuit applications f_{max} is the more important parameter [19, 74]. Coplanar MMICs baed on SiGe–HBTs with f_{max} values as high as 80 GHz are under development [20, 35].

4 Active and Nonlinear Circuits

4.1 Amplifiers

A monolithic SiGe HBT Ka–Band amplifier has been reported in [35]. Its design is based on coplanar structures. Slot–line modes are suppressed by air bridges. As the passive circuit elements coplanar lines. metal–insulator–metal capacitors and spiral inductors were used. The amplifier exhibits a gain of 4 dB in the frequency range from 20 GHz to 24 GHz.

4.2 Oscillators

As active elements for planar millimeterwave oscillators IMPATT diodes yield high cw output power at frequencies up to above 100 GHz. In order to obtain both high output power and a narrow spectrum IMPATT diodes must be connected with a low impedance series resonant circuit. Since for planar resonators, the quality factors that can be achieved typically range below 100 one must take care in order to obtain a low impedance planar resonator design. Best results were obtained using a planar circular disk resonator with the IMPATT diode in the center and a through contact beyond the IMPATT diode to the circuit ground plane [5, 9, 11, 12, 81].

Based upon optimized circuit layouts cw power output values as high as 20 mW at 93 GHz [9] and 200 mW at 73 GHz [11, 12] were achieved. Fig. 10 shows the layout of the 200 mW oscillator. The circuit dimensions

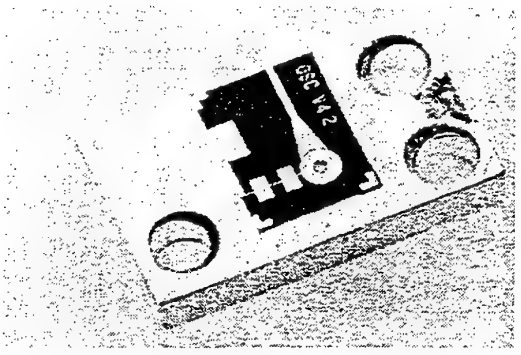

Fig. 10: The planar 200 mW IMPATT oscillator.

are $6 * 4.5$ mm^2. The substrate thickness is 110 μm. The through-metallization beyond the IMPATT diode has been realized using a hybrid technology. The planar circuit has a hole in the center of the disk resonator. Within this hole the IMPATT diode is mounted on a cylindric heat sink continuation reaching into the hole. A double drift IMPATT diode is used in this circuit. At the oscillation frequency of 73 GHz in continuous wave operation 200 mW output power at an efficiency of 4.5 % was achieved. The dependence of the output power and the efficiency on the dc bias current and the measured power spectrum of the planar 200 mW oscillator is shown in Fig. 11. The substrate thickness of

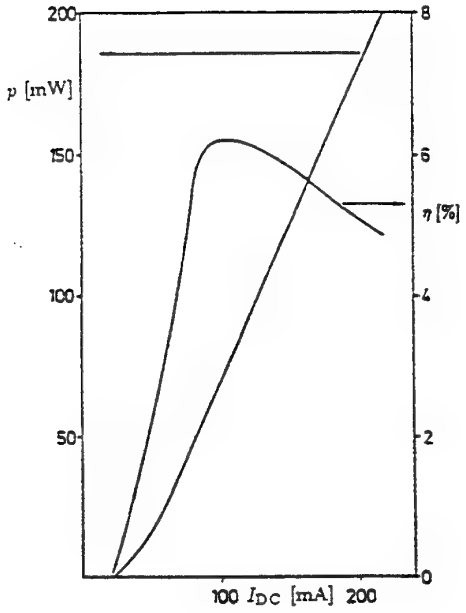

Fig. 11: Bias dependence of the cw output power P and the efficiency η.

only 110 μm minimizes the resonator impedance and is necessary to achieve a high output power level without the occurrence of bias oscillations [11, 12].

A fully monolithic integrated planar disc resonator oscillator with an output power of 1.8 mW at 61 GHz has already been reported [82]. The IMPATT diode is located at the side of the substrate with the ground metallization. The diode connected to the disc metallization via an etched and metallized conical hole (Fig. 12).

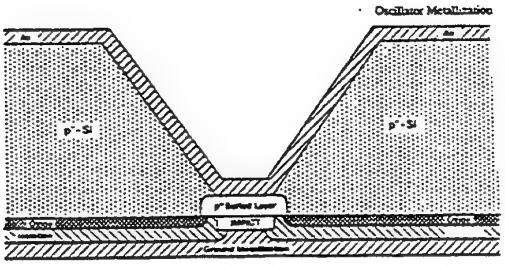

Fig. 12: Cross section through the disc oscillator.

Many applications of millimeterwave oscillators require electronic frequency tuning. Fig. 13 shows a varactor diode tunable planar IMPATT oscillator [13]. The oscillator output power is 18 mW at 80.2 GHz. A tuning range of 425 MHz has been achieved.

Using coplanar IMPATT diodes no via holes are required. Several coplanar oscillator designs have already been discussed [10]–[16]. Fig. 14 shows a coplanar IMPATT oscillator. The coplanar IMPATT diode is connected to the center of a slot line [16]. The oscillator was fabricated on a 100 μm substrate in order to minimize the surface wave losses. The slot length is 1.12 mm and the slot width is 80 μm. The IMPATT diode diameter is 20 μm. A radiated output power of 7 mW was measured at 109 GHz. The required frequency stabilization is achieved by means of subharmonic injection locking [83]. The design of planar IMPATT oscillators is very sensitive with respect to the matching of the IMPATT diode to the planar resonato–antenna structure [84, 84].

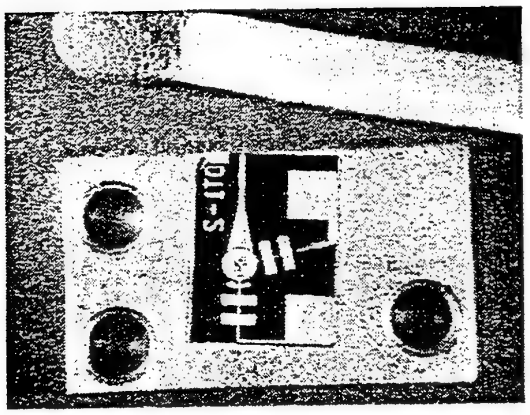

Fig. 13: Voltage controlled IMPATT oscillator.

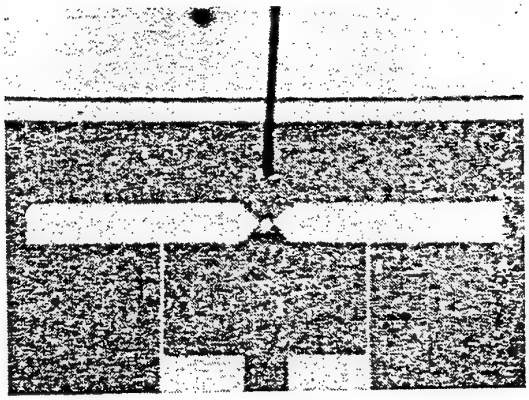

Fig. 14: Coplanar IMPATT oscillator.

4.3 Transmitters and Receiver Circuits

4.3.1 Receiver Circuits

A 93 GHz SIMMWIC receiver with a planar 36 element antenna and a Schottky diode has been realized [9, 12]. Fig. 15 shows the receiver. A coplanar Schottky diode is connected to the antenna via a strip line. The Schottky diode is terminated by a $\lambda/4$ line. The dc bias lines include low pass filters. The receiver has been integrated monolithically on a highly insulating silicon substrate. The antenna dimensions are $5.4 * 5.6$ mm^2. The Schottky diode exhibits 4 Ω series resistance and a junction capacity of 0.1 pF. The measured receiver sensitivity is $65\mu V\mu W^{-1}cm^2$.

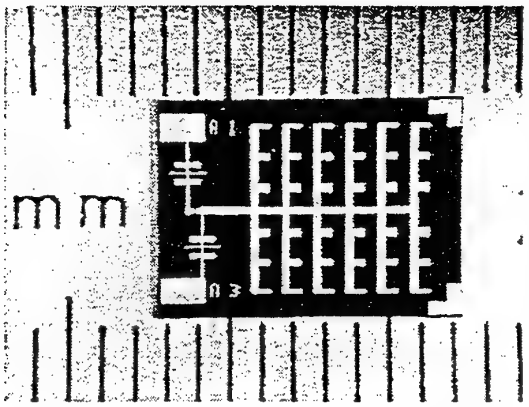

Fig. 15: SIMMWIC receiver.

5 Applications and Outlook

The feasibility of silicon monolithic millimeterwave integrated circuits for frequencies up to 100 GHz has been demonstrated. Complete receivers and transmitters may be integrated monolithically using IMPATT diodes, SiGe-HBTs, PIN diodes and Schottky diodes. The SiGe HBT provides a three-terminal device which, of course, offers many advantages compared to the diode circuits. Simulation results show also the possibility of future high frequency applications of Si/SiGe MODFETs and MOSFETs [86]. The advantages of millimeter waves are high bandwidth for communication applications, high resolution for sensor applications, and high antenna gain also with small antennas. Various applications of SIMMWICS have already been investigated [87, 88, 89]. For near range sensor applications SIMMWICs with IMPATT diodes operated in a self–oscillating mixer mode allow the realization of cost effective near range sensor applications. The distance to be covered is limited by the coherence length of the free–running IMPATT oscillators [87]. An integrated transmitter for automotive applications delivered a radiated power of 1 mW at 79 GHz [89]. An excellent carrier–to–noise ratio of 81.7 dBc/Hz at an offset of 100 kHz has been achieved. Fundamental or subharmonic injection locking using an HBT oscillator improves the coherence length of the transmitter [83]. The future availability of low–cost millimeterwave components and millimeterwave monolithic integrated circuits (MMICs) will stimulate the penetration of millimeterwave technology into commercial and consumer electronics [90].

6 Bibliography

[1] T. M. Hyltin, "Microstrip transmission on semiconductor dielectrics," *IEEE Trans. Microwave Theory Tech.*, vol. MTT-13, pp. 777–781, June 1965.

[2] H. Storck, "Streifenleitungen auf Halbleitermaterialien," Dissertation an der Rheinisch–Westfälischen Technischen Hochschule Aachen, 1971.

[3] A. Rosen, M. Caulton, P. Stabile, A. M. Gombar, W. M. Janton, C. P. Wu, J. F. Corboy, and C. W. Magee, "Silicon as a millimeter–wave monolithically integrated substrate," *RCA Review*, vol. 42, pp. 633–660, Dec. 1981.

[4] K. M. Strohm, J. Büchler, P. Russer, and E. Kasper, "Silicon high resistivity substrate millimeter-wave technology," *IEEE Microwave and Millimeter-Wave Monolithic Circuits Symp. Digest*, (Baltimore, MD), pp. 93–97, June 4–5, 1986.

[5] J. Büchler, E. Kasper, P. Russer, K. M. Strohm, "Silicon high–resistivity–substrate millimeter-wave technology," *IEEE Trans. Microwave Theory Tech.*, vol. MTT-34, pp. 1516–1521, Dec. 1986, also published in: *IEEE Trans. Electron Devices*, vol. ED-33, pp. 2047–2052, Dec. 1986.

[6] P. Russer, "Silicon monolithic millimeterwave integrated circuits" *Proc. of the 21st Europ. Microwave Conf.*, (Stuttgart, Germany), pp. 55–71, 9–12 Sep. 1991.

[7] J.–F. Luy, P. Russer,"Silicon–based millimeter–wave devices", Springer Series in Electronics and Photonics 32, Springer, Berlin Heidelberg New York 1994.

[8] P. Russer, E. Biebl, "Fundamentals", In: "Silicon–based millimeter–wave devices", Springer Series in Electronics and Photonics 32, pp.1–46, Springer, Berlin Heidelberg New York 1994.

[9] J. Büchler, E. Kasper, J. F. Luy, P. Russer, and K. M. Strohm, "Silicon millimeter-wave circuits for receivers and transmitters," *IEEE Microwave and Millimeter-Wave Monolithic Circuits Symp. Digest*, (New York), pp. 67–70, May 24–25 1988.

[10] J.–F. Luy, K. M. Strohm, and J. Büchler, "Monolithically integrated coplanar 75-GHz silicon IMPATT oscillator," *Microwave and Optical Technology Letters*, vol. 1, pp. 117–119, June 1988.

[11] J. Büchler, E. Kasper, J. F. Luy, P. Russer, and K. M. Strohm, "70 GHz integrated silicon oscillator," *Electronics Letters*, vol. 24, pp. 977–978, July 1988.

[12] J. Büchler, E. Kasper, J. F. Luy, P. Russer, and K. M. Strohm, "Planar W-band receiver and oscillator," *18th European Microwave Conf. Digest*, (Stockholm, Sweden), pp. 364–369, Sep. 12–16 1988.

[13] J. Büchler, J.–F. Luy, and K. M. Strohm, "Varactor-tuned planar W–band oscillator," *Proc. 1989 IEEE MTT-S Int. Microwave Symp. Dig.*, (Long Beach, CA), pp. 1205–1206, June 1989.

[14] P. Russer, "Millimeterwave integrated circuits", *9th National Meeting on Electromagnetics*, (Assisi, Italy), 5–8 Oct. 1992.

[15] K. M. Strohm, J.–F. Luy, J. Büchler, F. Schäffler, A. Schaub, "Planar 100 GHz silicon detector circuits," Microelectronic Engineering, vol. 15, pp. 285–288,1991.

[16] J. Buechler, K. M. Strohm, J.–F. Luy, T. Goeller, and P. Russer, "Coplanar monolithic silicon IMPATT transmitter," *21th European Microwave Conf. Digest*, (Stuttgart, Germany), pp. 352–357, Sep. 9–12, 1991.

[17] J. Buechler, "Silicon millimeter–wave integrated circuits", In: "Silicon–based millimeter–wave devices", Springer Series in Electronics and Photonics 32, pp.193–214, Springer, Berlin Heidelberg New York 1994.

[18] K.M. Strohm, "Silicon millimeter–wave integrated circuit technology", In: "Silicon–based millimeter–wave devices", Springer Series in Electronics and Photonics 32, pp.241–284, Springer, Berlin Heidelberg New York 1994.

[19] J.–F. Luy, K.M. Strohm, H.–E. Sasse, A. Schüppen, J. Büchler, M. Wollitzer, A. Gruhle, F. Schäffler, U. Güttich, A. Klaassen, "Si/SiGe MMIC's," *IEEE Trans. Microwave Theory Tech.*, vol. MTT-43, pp. 705–714, April 1995.

[20] R. Doerner, J. Gerdes. C. Rheinfelder, F.J. Schmückle, W. Heinrich, K. Strohm, F. Schäffler, J.–F. Luy, "Modelling of passive elements for coplanar SiGe MMIC's," *Proc. 1995 IEEE MTT-S Int. Microwave Symp. Dig.*, (Orlando, Fl), pp. 1187–1190, May 1995.

[21] Y. Yoshimura, "A microstripline slot antenna," *IEEE Trans. Microwave Theory Tech.*, vol. MTT-20, pp. 760–762, Nov. 1972.

[22] J. Zmuidzinas and N. G. LeDuc, "Quasi-optical slot antenna sis mixers," *IEEE Trans. Microwave Theory Tech.*, vol. MTT-40, pp. 1797–1804, Sep. 1992.

[23] D. F. Filipovic, W. Y. Ali-Ahmad, and G. M. Rebeiz, "Millimeter-wave double-diploe antennas for high-gain integrated reflector illumination," *IEEE Trans. Microwave Theory Tech.*, vol. MTT-40, pp. 962–967, May 1992.

[24] R. K. Hoffmann, *Handbook of microwave integrated circuits*, Norwood: Artech House, 1987.

[25] K. Itoh, N. Aizawa, and N. Goto, "Circularly polarized printed array antennas composed of strips and slots," *Electr. Lett.*, vol. 15, pp. 811–812, Dec. 1979.

[26] W. Heinrich, "The slot line in uniplanar MMIC's: propagation characteristics and loss analysis," *1990 IEEE MTT-S Digest*, Vol. I, S. 167-170.

[27] V. Fouad Hanna, D. Thebault, "Theoretical and experimental investigation of asymmetric coplanar waveguides," *IEEE Trans. Microwave Theory Tech.*, vol. MTT–32, pp. 1649–1651, Dec. 1984.

[28] A. Gopinath, "Losses in coplanar waveguides," *IEEE Trans. Microwave Theory Tech.*, vol. MTT–30, pp. 1101–1104, Dec. 1982.

[29] G. Ghione and C. Naldi, "Coplanar waveguides for MMIC applications: Effect of Upper Shielding, Conductor Backing, Finite Extent Ground Planes, and Line–to–Line Coupling," *IEEE Trans. Microwave Theory Tech.*, vol. MTT-35, pp. 260–267, Mar. 1987.

[30] R. W. Jackson, "Considerations of the use of coplanar Waveguide for Millimeter–Wave Integrated Circuits," *IEEE Trans. Microwave Theory Tech.*, vol. MTT-34, pp. 1450–1465, Dec. 1986.

[31] R. W. Jackson, "Mode conversion due to discontinuities in modified coplanar grounded waveguide." *IEEE MTT-S Microwave Symp. Digest*, (New York), pp. 203–206, May 24–25 1988.

[32] W. Heinrich, "Full-wave analysis of conductor losses on MMIC transmission lines," *IEEE Trans. Microwave Theory Tech.*, vol. MTT-38, S. 1468-1472, Oct. 1990.

[33] W. Heinrich, "Conductor loss on transmission lines in monolithic microwave and millimeter-wave integrated circuits," *Int. Journal of Microwave and Millimeter-Wave Computer-Aided Engineering*, Vol. 2, No. 3, S. 155-167, 1992.

[34] W. Heinrich, "Quasi-TEM description of MMIC coplanar lines including conductor-loss effects," to be presented at the *IEEE MTT-S Microwave Symp.*, Orlando, May 16–18, 1995.

[35] K.M. Strohm, J.–F. Luy, F.n Schäffler, H. Jorke, H. Kibbel, C. Rheinfelder, R. Doerner, J. Gerdes, F.J. Schmückle, W. Heinrich, "Coplanar Ka–band SiGe–MMIC amplifier," *Electronics Letters*, vol. 31, pp. 1353–1354, Aug. 1995.

[36] K. C. Gupta, "Transmission-line discontinuities," in *Handbook of Microwave and Optical Components, Vol. 1*, (K. Chang, ed.), ch. 2, New York: Wiley, 1989.

[37] I. J. Bahl, "Transmission lines and lumped elements," in *Microwave Solid State Circuit Design*, (I. Bahl and P. Bhartia, eds.), ch. 2, New York: Wiley, 1988.

[38] M. Naghed and I. Wolff, "Equivalent capacitances of coplanar waveguide discontinuities and interdigitated capacitors using three-dimensional finite difference method," *IEEE Trans. Microwave Theory Tech.*, vol. MTT-38, pp. 1808–1815, Dec. 1990.

[39] K. Beilenhoff, W. Heinrich, and H.L. Hartnagel, "The scattering behaviour of air bridges in coplanar MMIC's", *21st European Microwave Conference Digest*, Vol. 2, 1991, pp. 1131-1135

[40] K. Beilenhoff, W. Heinrich, and H.L. Hartnagel, "Finite-Difference analysis of open and short circuits in coplanar MMIC's including finite metallization thickness and mode conversion," *1992 IEEE Int. Microwave Symposium Digest*, Vol. I, pp. 103-106

[41] K. Beilenhoff, H. Klingbeil, W. Heinrich, and H.L. Hartnagel, "Open and short circuits in coplanar MMIC's", *IEEE Trans. MTT*, Vol. 41, No. 9, 1993, pp. 1534-1537

[42] K. Beilenhoff, W. Heinrich, and H.L. Hartnagel, "Analysis of T-junctions for coplanar MMICs," *1994 IEEE Int. Microwave Symposium Digest*, Vol. II, pp. 1301-1304

[43] M. Drissi, F. Hanna, and J. Citerne, "Analysis of radiating end effects of symmetric and asymmetric coplanar waveguide using integral equations technique," in *IEEE MTT-S Int. Microwave Symp. Digest*, (Long Beach), pp. 791–794, June 1989.

[44] A. Stiller, M. Thieme, E.M. Biebl, W. Wollitzer, and J.-F. Luy, "A dual fed coplanar resonator for monolithic integration," *International Workshop of the German IEEE Joint MTT/AP Chapter on Silicon Based High Frequency Devices and Circuits*, (Günzburg, Germany), 10./11. November 1994, pp. 24–27.

[45] P. Bhartia and I. J. Bahl, "Millimeter wave engineering and applications", ch. 9, pp. 477–616. New York: Wiley, 1984.

[46] R. J. Mailloux, F. K. Schwering, A. Oliner, and J. W. Mink, "Antennas III: Array, millimeterwave, and integrated antennas," in *Handbook of microwave and optical components, Vol. 1*, (K. Chang, ed.), ch. 12, New York: Wiley, 1989.

[47] R. J. Mailloux, J. F. McIlvenna, and N. P. Kernweis, "Microstrip array technology," *IEEE Trans. Antennas Propagat.*, vol. AP-29, pp. 25–37, Jan. 1981.

[48] G. M. Rebeiz, "Millimeter-wave and terahertz integrated circuit antennas," *Proc. IEEE*, vol. 80, pp. 1748–1770, Nov. 1992.

[49] D.B. Rutledge, D.P. Neikirk, D.P. Kassiligam, "Integrated–circuit antennas," in *Infrared and Millimeter Waves, vol. 10*, (K.J. Button, ed.), pp. 1–90, Academic Press, 1983.

[50] F. K. Schwering, "Millimeter wave antennas," *Proc. IEEE*, vol. 80, pp. 92–102, Jan. 1992.

[51] P. Russer, E. Biebl, W. Heinrich, "Planar millimeterwave circuits on silicon," *International Workshop of the German IEEE Joint MTT/AP Chapter on Silicon Based High Frequency Devices and Circuits*, (Günzburg, Germany), 10./11. November 1994, pp. 1–15.

[52] E. M. Biebl, J. Müller, and H. Ostner, "Analysis of planar millimeter wave slot antennas using a spectral domain approach," *IEEE MTT-S Int. Microwave Symp. Digest*, (Albuquerque), pp. 381–384, June 1992.

[53] H. Ostner, T. Ostertag, and E. M. Biebl, "Calculation of the impedance of planar slot antennas," in *IEEE Asia-Pacific Microwave Conf. Digest*, (Adelaide), pp. 137–140, 1992.

[54] M. Singer, J. Buechler, and E.M. Biebl, "Slot antenna in a monolithically integrated dielectric-filled cavity resonator," *International Workshop of the German IEEE Joint MTT/AP Chapter on Silicon Based High Frequency Devices and Circuits*, (Günzburg, Germany), 10./11. November 1994, pp. 24–27.

[55] G. L. Friedsam, E. M. Biebl, "Analysis of Planar Slot Antennas Backed by Rectangular Cavities", *PIERS 95, Seattle, 24. – 28.7.95*, p. 165, July 1995.

[56] N. I. Dib, L.P.B. Katehi, "study of a novel planar transmission line," *IEEE MTT-S Int. Microwave Symp. Digest*, (Boston), pp. 623–626, June 1991.

[57] N. I. Dib, L.P.B. Katehi, "Impedance calculation for the microshield line," *IEEE Microwave and Guided Wave Letters*, vol. 2, pp. 406–408, Oct. 1992.

[58] L. P. B. Katehi, "Novel transmission lines for the submillimeter-wave region," *Proc. IEEE*, vol. 80, pp. 1771–1787, Nov. 1992.

[59] R.F. Drayton, T.M, Weller, L.P.B. Katehi, "Development of miniaturized Circuits for high–frequency applications using micromachining techniques," *Int. J. of Microcircuits and Electronic Packaging*, vol. 18, pp. 217–222, 1995.

[60] R.F. Drayton, T.M., Weller, L.P.B. Katehi, "Development of self–packaged high frequency circuits using micromachining techniques," to be published in: *IEEE Trans. Microwave Theory Tech.*

[61] R.Y. Yu, M. Reddy, J. Pusl, S.T. Allen, M. Case, M.J.W. Rodwell, "Millimeter–wave on–wafer wafeform and network measurements using active probes," *IEEE Trans. Microwave Theory Tech.*, vol. MTT-43, pp. 721–729, April 1995.

[62] T.M. Weller, L.P.B. Katehi, G.M. Rebeiz, "High–performance microshield line components," *IEEE Trans. Microwave Theory Tech.*, vol. MTT-43, pp. 534–543, March 1995.

[63] C.–Y. Chi, G.M. Rebeiz, "Planar microwave and millimeter–wave lumped elements and coupled –line filters using micro–machining techniques," *IEEE Trans. Microwave Theory Tech.*, vol. MTT-43, pp. 730–738, April 1995.

[64] C.–Y. Chi, G.M. Rebeiz, "Conductor–loss limited stripline resonators," to be published in: *IEEE Trans. Microwave Theory Tech.*, vol. MTT-44, April 1996

[65] G.M. Rebeiz, L.P.B. Katehi, T.M. Weller, C.–Y. Chi, S.V. Robertson, "Micromachined filters for microwave and millimeter–wave applications," to be published in: *Int. J. Microwave and Millimeterwave Computer Aided Engineering*, February 1996

[66] J.H. Werner, U. Rau, "Schottky contacts on silicon", In: "Silicon–based millimeter–wave devices", Springer Series in Electronics and Photonics 32, pp.89–148, Springer, Berlin Heidelberg New York 1994.

[67] K.M. Strohm, J.–F. Luy, J. Büchler, "Technologien für integrierte Silizium–Millimeterwellenbauelemente," In: *ITG–Fachbericht Vol. 114, Mikroelektronik für die Informationstechnik*, Berlin, Oct. 2–4, 1990.

[68] K. Chang, H.J. Kuno "Impatt and related transit–time devices," In: *K. Chang, "Handbook of Microwave and Optical Components"*, Vol. 2, Wiley, 1990, pp. 305–391.

[69] E. Kasper, J.–F. Luy, "State of the art and future development in silicon IMPATT diodes for mm wave seeker requirements," *1990 Military Microwave Conference Digest*, London, 1990, pp. 293–298.

[70] J.–F. Luy, "Transit–time devices", In: "Silicon–based millimeter–wave devices", Springer Series in Electronics and Photonics 32, pp.47–88, Springer, Berlin Heidelberg New York 1994.

[71] J.–F. Luy, J. Büchler, M. Thieme, and E. Biebl, "Matching of active millimetre-wave slot-line antennas," *Electron. Lett.*, vol. 29, no. 20, pp. 1772–1774, 1993.

[72] H. Kroemer, "Theory of a wide–gap emitter for transistors," *Proc. IRE*, Vol. 45, No. 11, 1957, pp. 1535–1537.

[73] E. Kasper, P. Russer, "Verfahren zur Herstellung von bipolaren Hochfrequenzschaltungen," *German Disclosure* , P 27 19 464.5, April. 30, 1977.

[74] A. Gruhle, "SiGe heterojunction bipolar transistors", In: "Silicon–based millimeter–wave devices", Springer Series in Electronics and Photonics 32, pp.149–192, Springer, Berlin Heidelberg New York 1994.

[75] S.A. Campbell, A. Gopinath, "Possibility of Silicon Monolithic Millimeterwave Integrated Circuits," *Proc. 1989 IEEE MTT-S Int. Microwave Symp. Dig.*, (Long Beach, CA), June 1989, pp. 817–819.

[76] M. Karlsteen, M. Willander, "Optimized frequency characteristics of Si/SiGe heterojunction and conventional bipolar transistors," *Solid State Electronics*, Vol. 33, No 2. pp. 199-204, 1990

[77] T. Won, H. Morkoc, "High–speed pPerformance of $Si/Si_{1-x}Ge_x$ heterojunction bipolar transistors," *IEEE Electron Device Letters* Vol. 10, No. 1, pp. 33–35, Jan. 1989.

[78] G.L.Patton,J.H.Comfort,B.S.Meyerson, E.F. Crabbe, G.J. Scilla, E. de Fresart, J.M.C. Stork, J.Y.–C. Sun, D.L. Harame, J.N. Burghartz, "75–GHz f_T SiGe–base heterojunction bipolar transistors," *IEEE Electron Device Letters*, Vol. 11, No. 4, pp. 171–173, Jan. 1990.

[79] E. Kasper, A. Gruhle, H, Kibbel, "High speed SIGe–HBT with very low base sheet resistivity," *Proc. IEDM'93*,, pp. 79–81. 1993.

[80] E.F. Crabbe, B.S. Meyerson, J.M.C. Stork, D.I. Harame, "Vertical profile optimization of very high frequency epitaxial Si–, and SiGe–base bipolar transistors. *Proc. IEDM'93*,, pp. 73–86. 1993.

[81] J.–F. Luy, K. M. Strohm, and J. Büchler, "Silicon monolithic millimeter wave IMPATT oscillators," *18th European Microwave Conf. Digest*, (Stockholm, Sweden), pp. 382–387, Sept. 12–16, 1988.

[82] K.M. Strohm, J. Buechler, E. Sasse, F. Schäffler, J.–F. Luy "Monolithic integrated radiating 55–72 GHz disc oscillators," *International Workshop of the German IEEE Joint MTT/AP Chapter on Silicon Based High Frequency Devices and Circuits*, (Günzburg, Germany), 10. – 11. November 1994, pp. 16–18.

[83] M. Wollitzer, J. Büchler, and E. Biebl, "Subharmonic injection locking of slot oscillators," *Electron. Lett.*, vol. 29, no. 22, pp. 1958–1959, 1993.

[84] A. Stiller, M. Singer, K. M. Strohm, E. M. Biebl, "Characterization of Planar Resonators by Means of Integrated Schottky Diodes", *MTT-Symposium, Orlando, 16.– 20.5.95*, pp. 1151–1154, May 1995.

[85] A. Stiller, M. Singer, K. M. Strohm, E. M. Biebl, "Charakterisierung der Eingangsimpedanz planarer Antennenstrukturen mit Hilfe von Schottky Dioden", *Mikrowellen und Optronik, 8. Kongreßmesse für Hochfrequenztechnik, Sindelfingen, 30.5. – 1.6.95*, pp. 517–522, May 1995.

[86] M. Willander, "Future devices", In: "Silicon–based millimeter–wave devices", Springer Series in Electronics and Photonics 32, pp.285–322, Springer, Berlin Heidelberg New York 1994.

[87] J. Buechler, J.F. Luy, K.M. Strohm, "V and W band MMIC sensors for mobile applications", *International Workshop of the German MTT/AP Chapter 'Microwave Sensing', Ilmenau*, pp. 34–41, 1993.

[88] J. Buechler, "Two frequency multifunctional radar for mobile application", *1995 IEEE Microwave Systems Conference* pp. 125–128, 1995.

[89] A. Stiller, E.M. Biebl, J.-F. Luy, K.M. Strohm, J. Buechler, "A Monolithic Integrated Millimeter Wave Transmitter for Automotive Applications", *IEEE Transactions on Microwave Theory and Techniques*, Vol. 43, No. 7, pp. 1654–1658, July 1995.

[90] W. Menzel, "Future applications", In: "Silicon–based millimeter–wave devices", Springer Series in Electronics and Photonics 32, pp.323–338, Springer, Berlin Heidelberg New York 1994.

New Devices for mm-Wave Applications

H. L. Hartnagel

New Devices for mm-Wave Applications

H. L. Hartnagel
Technische Hochschule Darmstadt
Institut für Hochfrequenztechnik
Merckstr. 25, 64283 Darmstadt
Germany
Tel.: 06151-16-2162
Fax: 06151-16-4367
E-mail: HFmwe001@hrz2.hrz.TH-Darmstadt.de

Contents:

Indroductory Remarks

Mm Wave Devices are influenced by a number of factors

1) Heterostructure-Epitaxy Capabilities
2) Nanometric Structuring
3) Quantum Effects

Therefore totally new concepts can emerge with improved performance or even new properties for further market challenge.

The Material Concepts

Heteroepitaxy based on

- Si
- GaAs
- InP
- GaSb

Type II heterojunction : new device concepts of

- 2 DEG and 2 DHG
- interband tunnelling

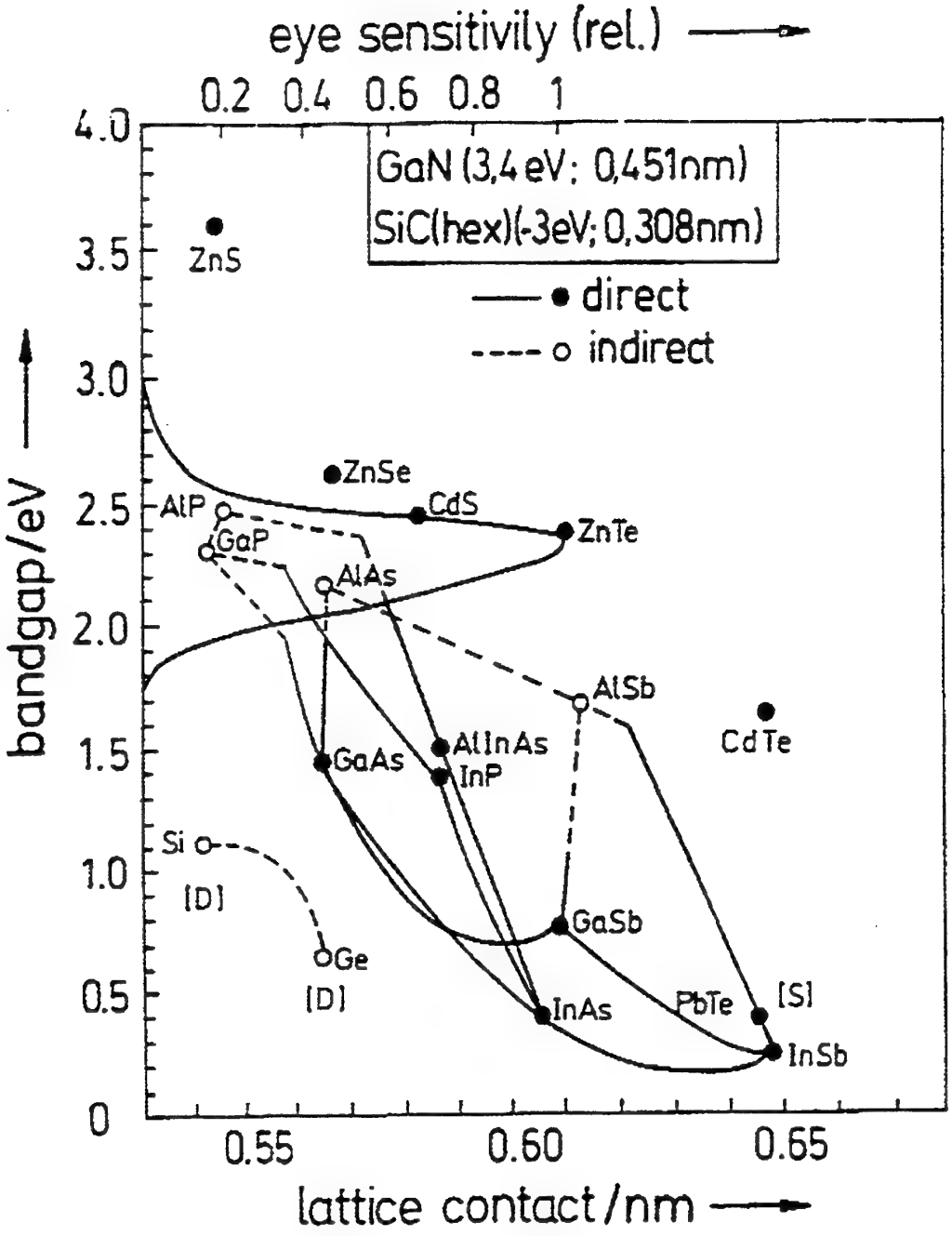

D - diamond lattice crystal

S - NaCl-type lattice

all others: zincblende lattice

Fig. 3

Discontinuity references (T=300K)

Lattice constant of group (Å)	Material system	ΔE_g (eV)	ΔE_c (eV)	ΔE_v (eV)
5.44	GaP/Si	1.148	0.798	0.35
5.66	GaAs/Ge	0.758	0.268	0.49
	AlAs/Ge	1.48	0.55	0.93
	$Ga_{0.7}Al_{0.3}As$/GaAs	0.395	0.263	0.132
	AlAs/GaAs	0.73	0.29	0.44
	$Ga_{0.51}In_{0.49}P$/GaAs	0.463	0.223	0.24
5.87	$Al_{0.48}In_{0.52}As$/InP	0.106	0.30	−0.194
	InP/$Ga_{0.47}In_{0.53}As$	0.600	0.20	0.40
	$Al_{0.48}In_{0.52}As$/$Ga_{0.47}In_{0.53}As$	0.706	0.50	0.206
6.10	AlSb/GaSb	0.887	0.487	0.40
	GaSb/InAs	0.370	0.88	−0.51
	AlSb/InAs	1.257	1.367	−0.11

Sources

- Transistor oscillators with active inductor for compact layout:

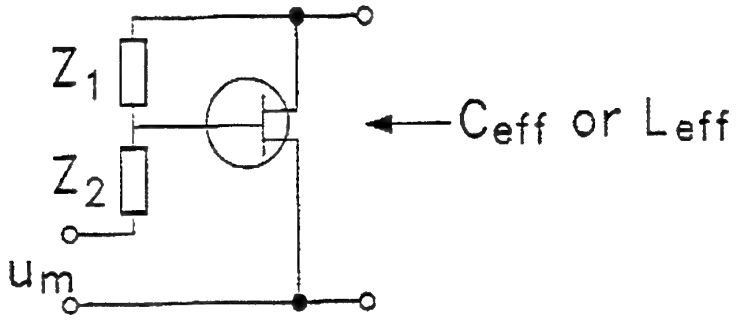

1) $Z_1 = \frac{1}{j\omega c}$, $Z_2 = R \rightarrow C_{eff} = RCg_m$

2) $Z_1 = R$, $Z_2 = \frac{1}{j\omega c} \rightarrow L_{eff} = \frac{RC}{g_m}$

where u_m modulates $g_m = \frac{dI_{DS}}{dV_{GD}}$ and therefore L_{eff} and C_{eff}.

- RTD: Interband tunnelling

either:

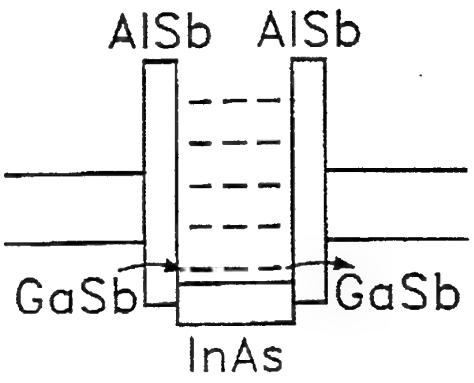

or:

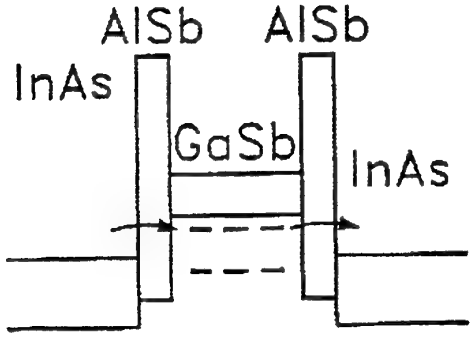

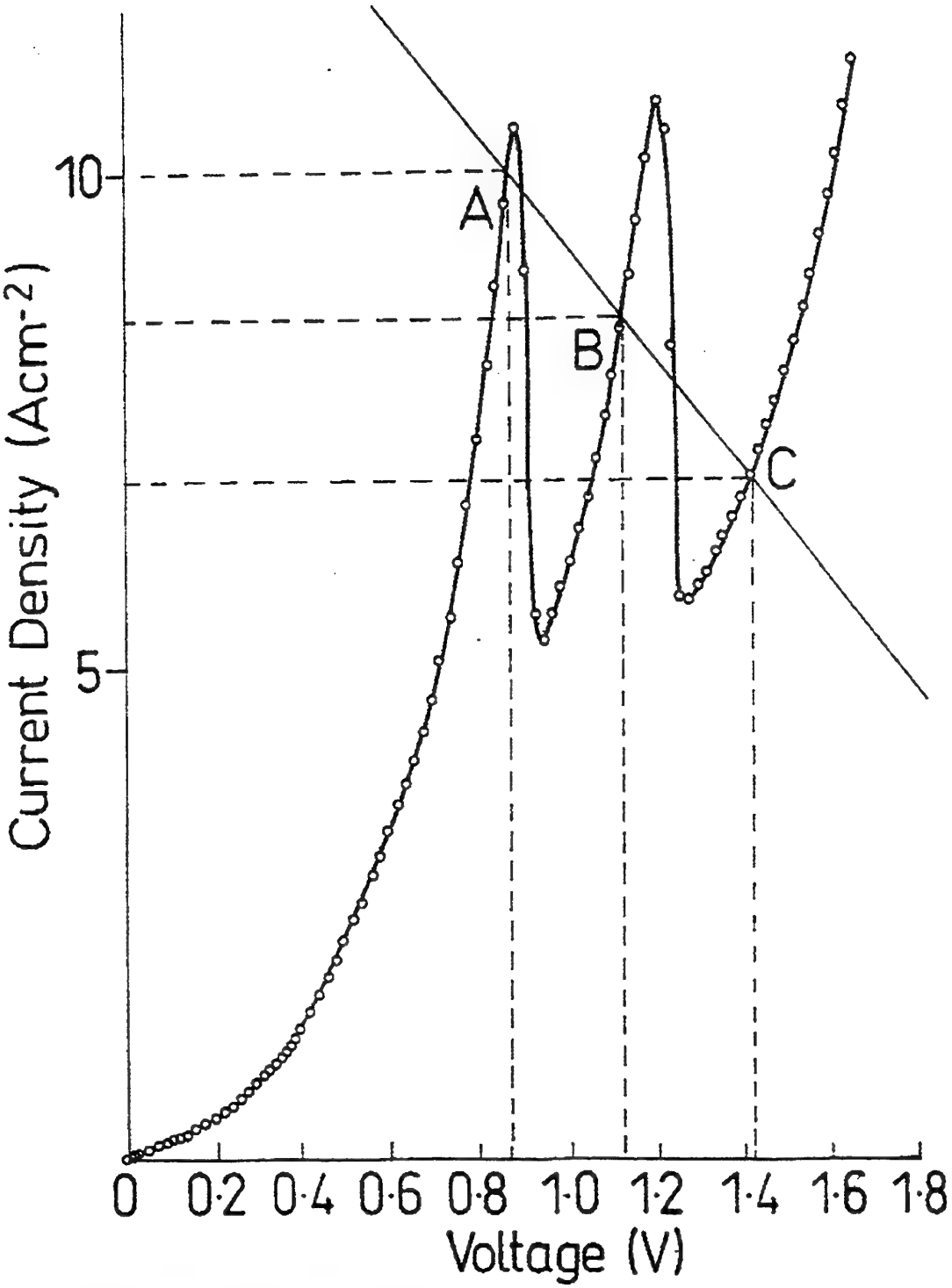

Modelled room-temperature I/V characteristic of two series RTDs with load line and operating points, GaSb, AlSb (5nm), InAs (5nm), AlSb (5nm), GaSb.

Amplifiers

- HEMT and HBT with led

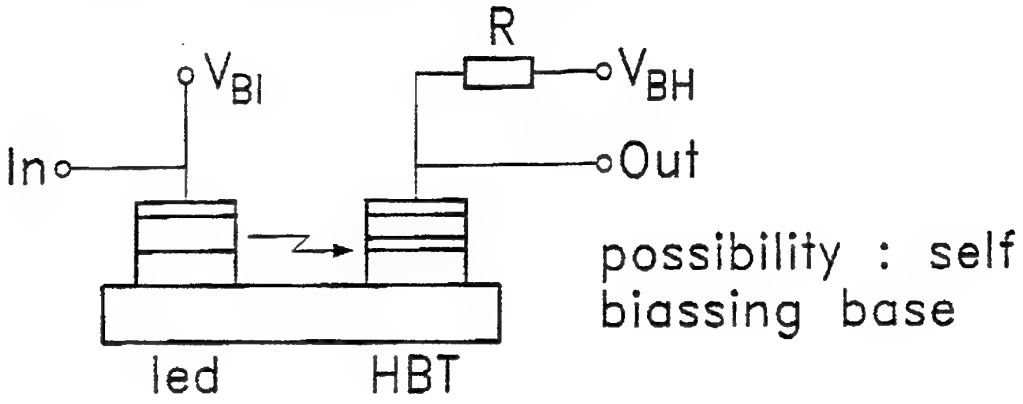

similarly with HEMT
Advantages: low feedback,
gate-access resistor small

- Cascode, Darlington etc for impedance optimization

- Field-emitter triodes with quasivacuum conditions built into semiconductor chip by new micro structuring techniques

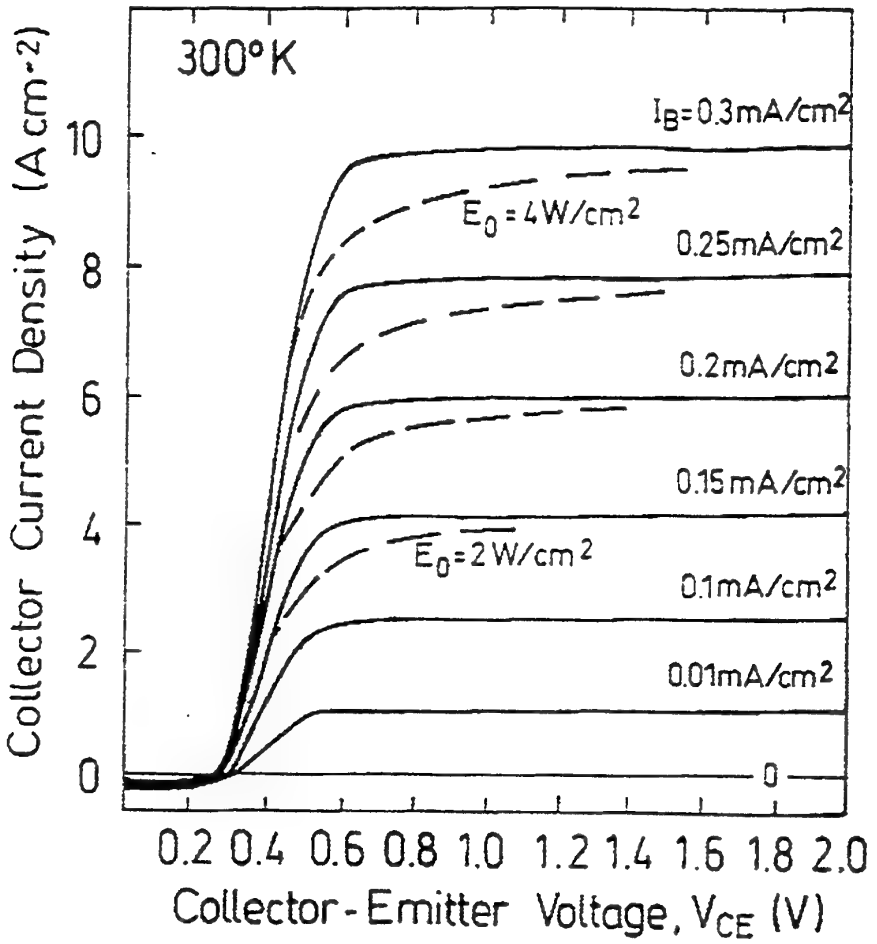

Simulated collector current I_C as a function of collector-to-emitter voltage V_{CE} with I_B in current per cross-sectional area of transistor (——) and opt. illumination power density (- - -) as parameters.
(The illumination is assumed to be uniform over the trasistor junctions).

Small signal equivalent circuit model of (a) common-source, (b) common-gate, and (c) cascode HEMT's.

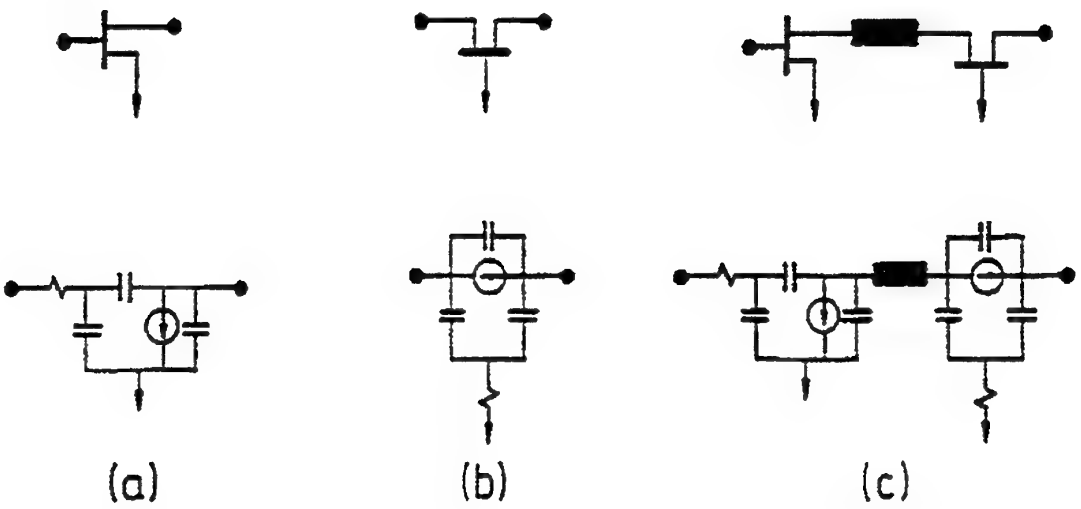

Darlington configuration increases the stage bandwidth by providing a low-impedance drive to the (capacitive) input of the common-emitter device (Q2).

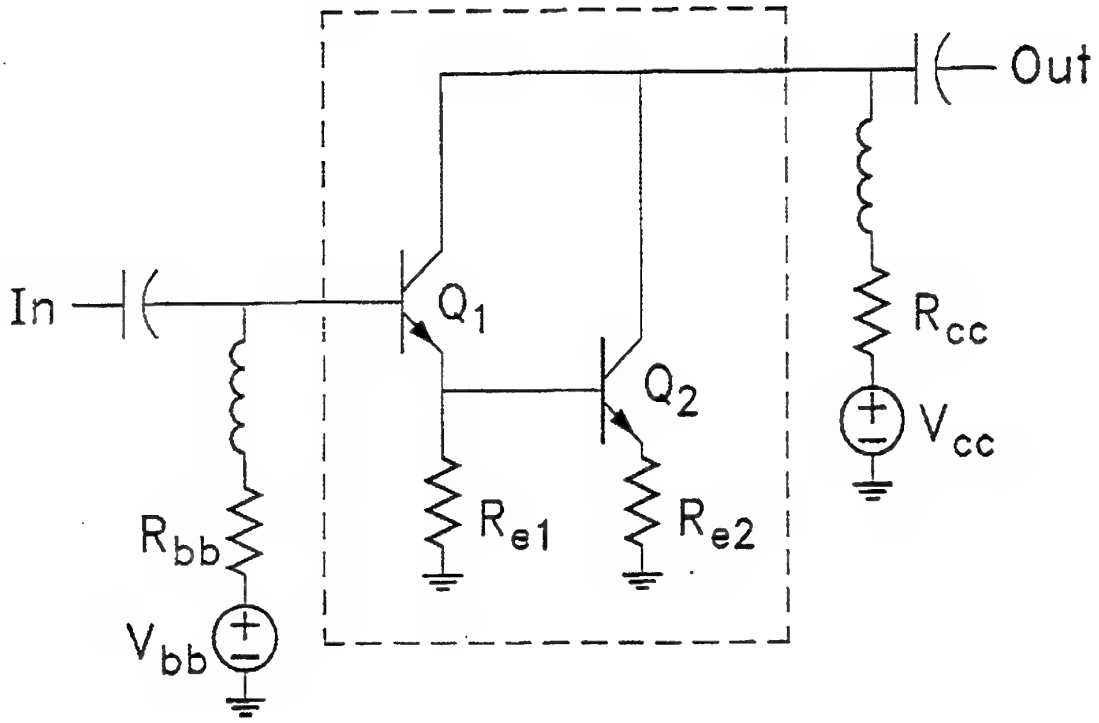

Cascode, base bypass capacitance with large gain bandwidth, using HBT.

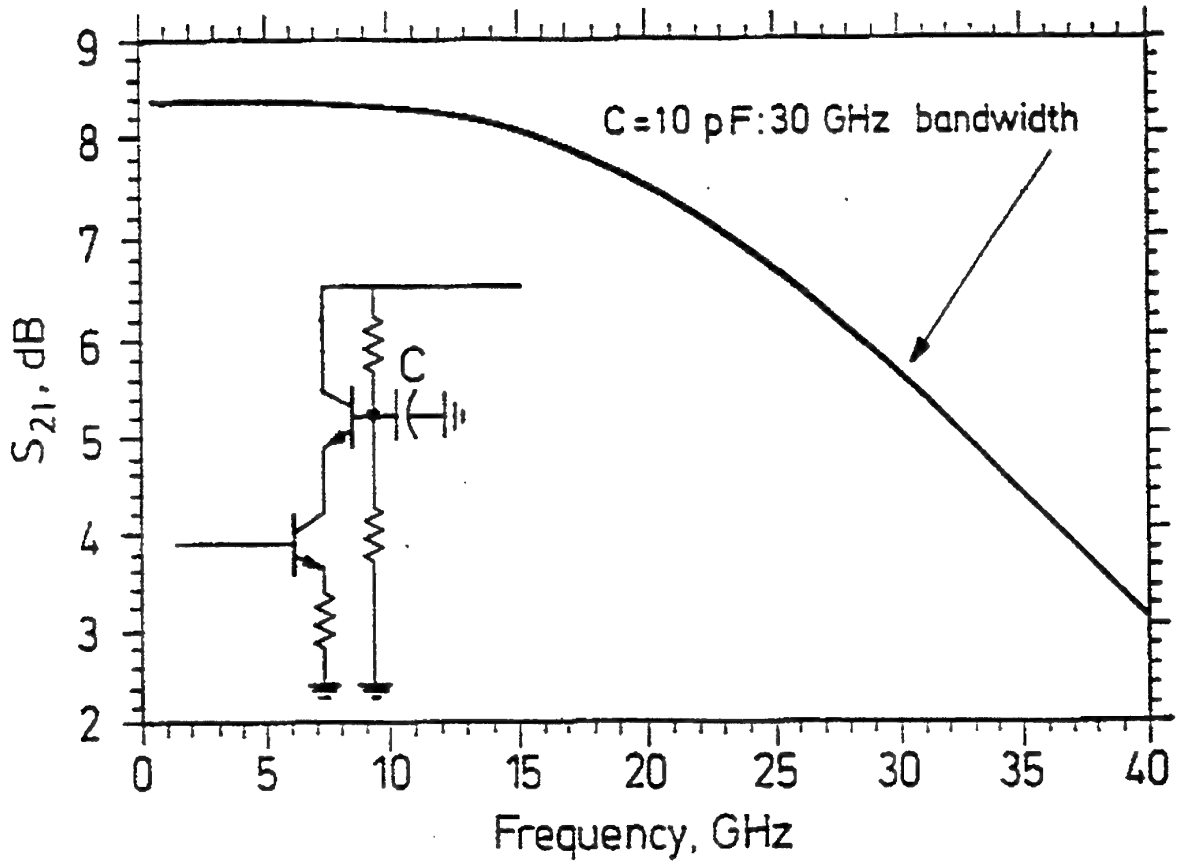

Cascode-Amplifier Integration involving dual-gate FET to be considered as new component, advantages:

- higher RF power gain
- higher output impedance
- reduced feedback capacitance

Schematic of Circuit

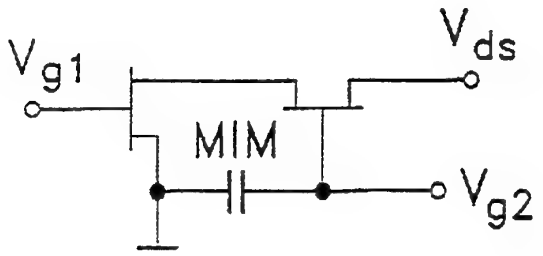

Second-gate electrode is internally RF-grounded via two parallel MIM capacitors resulting in a compact cascode unit.

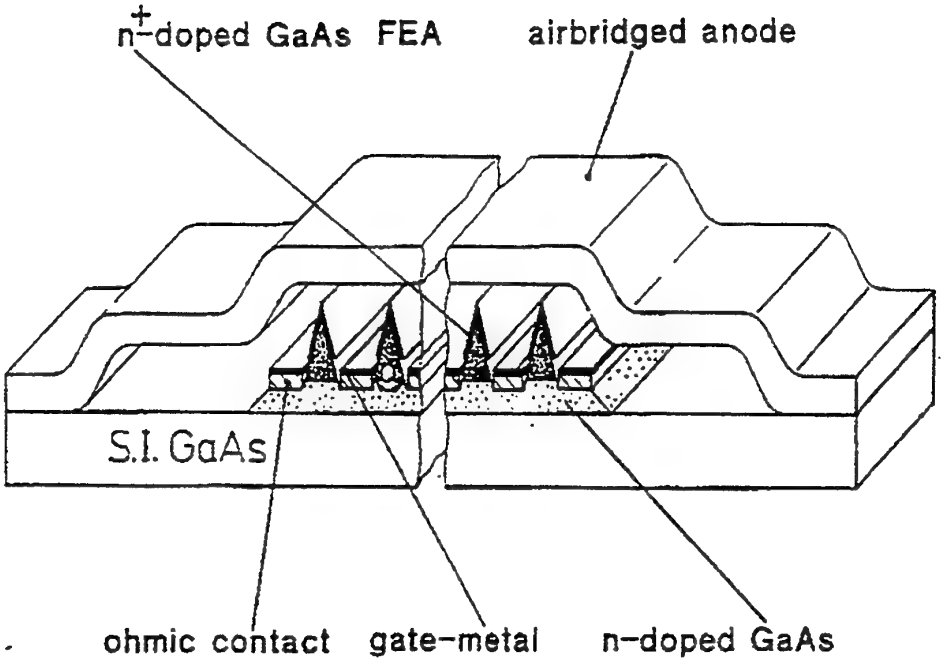

Fig. 3.2.9.1 Drawing of the multi-wedge ESD-protection switch (diode)

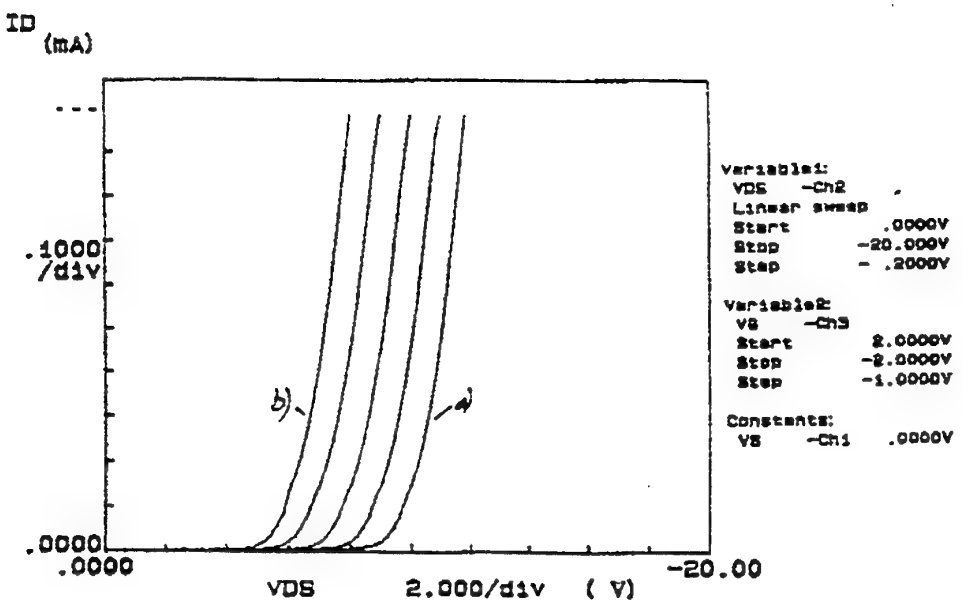

Fig. 3.4.7.2 variation of turn-on point of four wedge field-emission triode versus gate voltage a) V_G=-2V b) V_G=2V

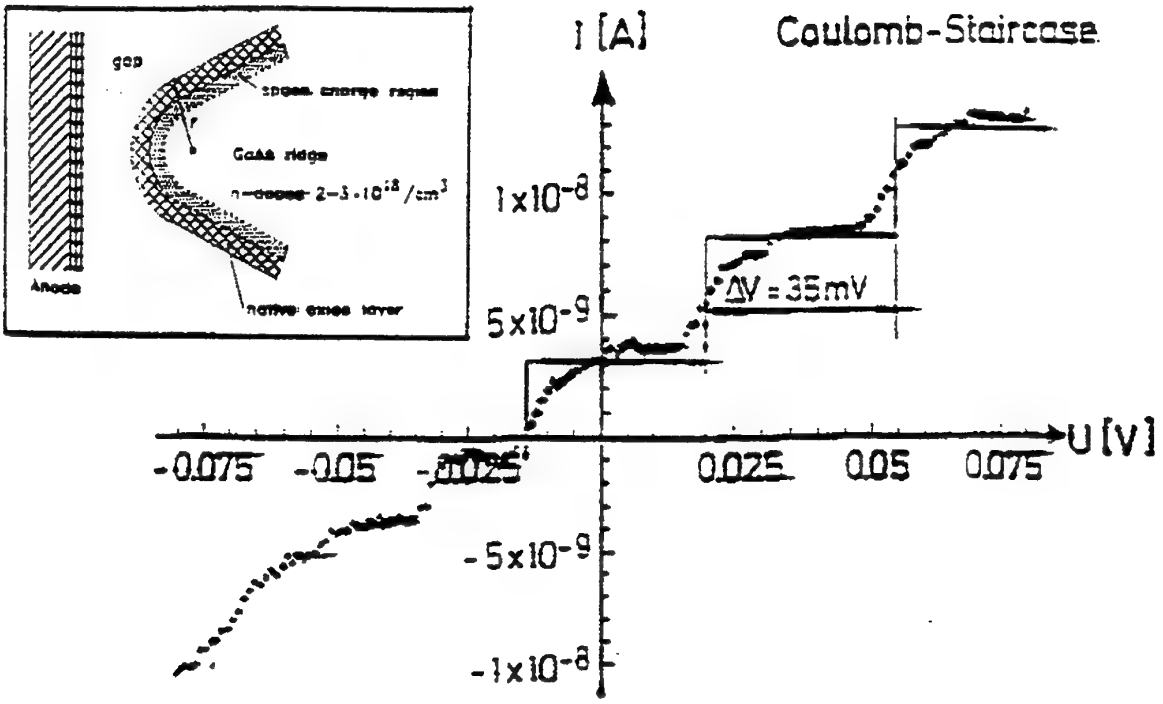

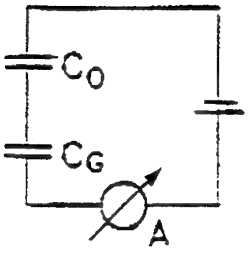

$$C_\Sigma = \frac{1}{\frac{1}{C_O} + \frac{1}{C_G}}$$

$$C_\Sigma = \frac{e}{\Delta V} = 0.5 \cdot 10^{-17} F$$

C_O - oxide capacitance

C_G - gap capacitance

C_Σ - parallel capacitance as "experienced" by trapped electron charge

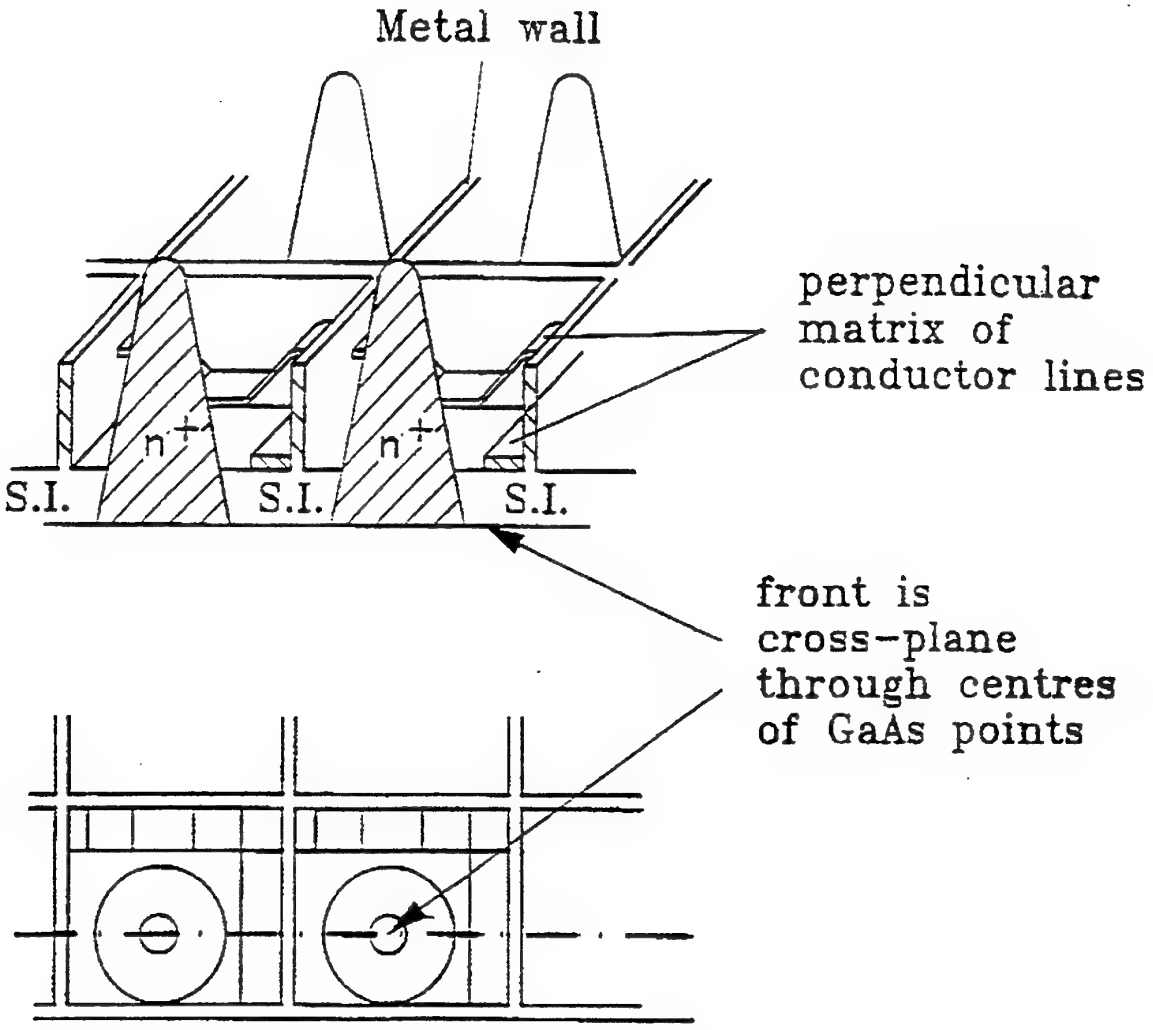
Metal wall
perpendicular
matrix of
conductor lines
n+
n+
S.I.
S.I.
S.I.
front is
cross-plane
through centres
of GaAs points

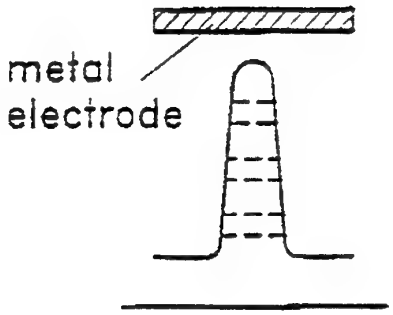

zerovoltage applied:

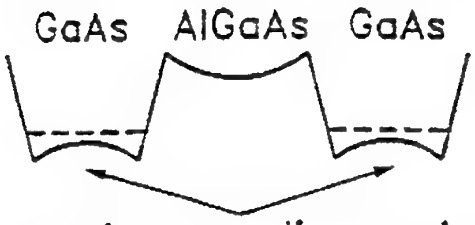

quasi–zero–dimensoinal
electron gas

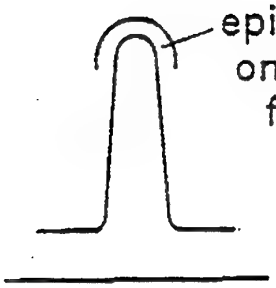

ext. voltage applied:

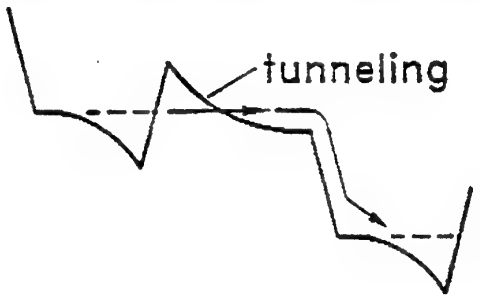

Mixing

Nonlinearity to be achieved by:

- Schottky contacts with large airbridges giving planarization for monolithic integration for frequencies above 100 GHz, replacing old whisker structures; here new types of transmission lines on membranes and thick polyimide insulators with low ε_r.

- Tunneling devices, possibly directly associated with transistors (multiple gate or base electroding)

- Field emitter, possibly based on quasi-single electron Coulomb blockade.

Conclusions and Outlook

- So far, many mm-wave diodes and transistors commonly involved with MMICs up to 100 GHz.

- Improvement of performance can be envisaged with new concepts.

- New capabilities for applications above 100 GHz.

Millimeter Wave Generation of Nonlinear Transmission Lines

R. Hülsewede, V. K. Mezentsev, S. L. Musher, I. V. Ryzhenkova, S. K. Turitsyn, and D. Jäger

1996 International Workshop on Millimeter Waves, April 11-12, Orvieto, Italy, 1996

Millimeter Wave Generation on Nonlinear Transmission Lines

R. Hülsewede+, V. K. Mezentsev*, S.L.Musher*, I. V. Ryzhenkova*, S. K. Turitsyn*,and D. Jäger+

+:*Fachgebiet Optoelektronik, Universität Duisburg,*
Kommandantenstrasse 60, 47048 Duisburg, Germany
*:*Institute of Automation and Electrometry,*
Universitetskii pr.1, 630090 Novosibirsk, Russia

In recent years, nonlinear transmission lines (NLTLs) have successfully been used to form ultrashort electrical pulses (solitons) or transients (shock waves) from an sinusoidal input signal [1,2]. In the frequency domain, this pulse compression results from the generation of a large number of harmonics with suitable phase relationships.

In this paper, two examples of NLTLs are discussed which are capable to produce millimeter wave signals at selected frequencies, here by third harmonic generation and nonlinear active wave propagation effects, respectively. For that purpose, we present numerical results for distributed circuits consisting of a periodic arrangement of quantum barrier varactor diodes QBVD [3] or tunnelling diodes TD [4], respectively, loading a coplanar transmission line. Wave propagation has been studied by using experimental data for the device and relevant transmission line equations derived from suitable equivalent circuits, as outlined in [5].

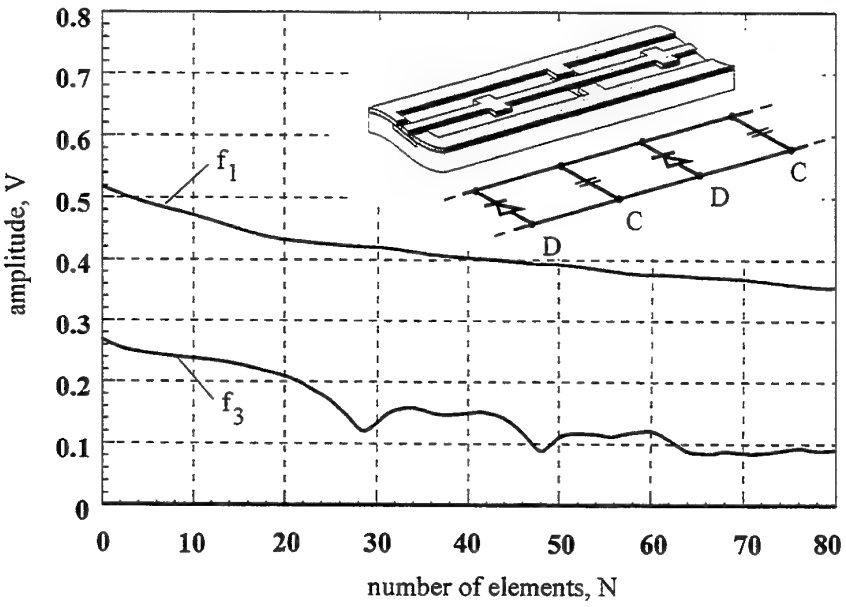

Fig.1: Third harmonic generation on a varactor diode NLTL. The inset shows a schematic structure of the periodic circuit, consisting of varactor diodes D and capacitances C loading a coplanar transmission line [5].

In Fig. 1, a bi-modal NLTL is shown where the periodic structure provides a suitable filter and dispersion characteristic for phase matching between a fundamental wave and its third harmonic [5]. Simultaneously, the generation of other harmonics is almost prevented. Additionally, the third harmonic is a backward wave leading to a maximum amplitude at the input of the NLTL [6]. As can bee seen from Fig. 1, a f_1 = 68 GHz input signal is converted into a f_3 = 204 GHz signal with a power efficiency of approximately 25%. Fig. 2 shows the results for a distributed oscillator which results from a periodic arrangement of TDs and short circuits at both ends. In this case selfgenerated oscillations are observable where a sinusoidal signal is produced after about 700 ps which is the

switch-on time. The frequency of 170 GHz is determined by the standing wave inside the resonator where multimode behaviour is again prevented by the filter structure.

In summary, this paper presents two examples of MMIC compatible NLTLs to generate millimeter wave signals with high efficiencies.

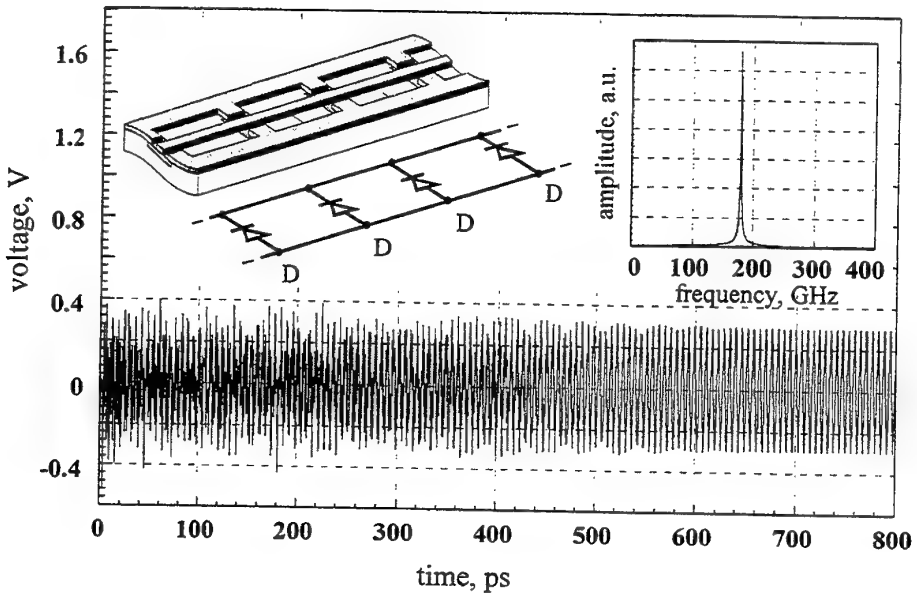

Fig. 2: Generation of a 170 GHz signal on a tunnelling diode NLTL. Outline of the circuit and spectrum are shown in the inset. The tunneling diodes, loading a coplanar transmission line, are marked by D

References

[1] M.J.W. Rodwell, S.T. Allen, R.Y.Y. Yu, M.G. Case, U. Bhattacharya, M.Reddy, E. Carman, M. Kamegawa, Y. Konishi, J. Pusl, R. Pullela, "Active and nonlinear wave propagation devices in ultrafast electronics and optoelectronics", *IEEE Proc.*, vol. 82, no. 7, pp. 1037-1059, 1994 (invited paper)

[2] M. Dragoman, R. Kremer, and D. Jäger, "Pulse generation and compression on a travelling-wave MMIC Schottky diode array", in: Ultra-Wideband, Short-Pulse Electromagnetics, H.L. Bertoni, L. Carin, and L.B. Felsen, eds., Plenum Press, New York, pp. 67-74, 1993

[3] M.A. Frerking, J.R. East, "Novel heterojunction varactors", *IEEE Proc.*, vol. 80, no. 11, pp. 1853-1860, 1992

[4] R.Y.Y. Yu, Y. Konishi, S.T. Allen, M. Reddy, M.J.W. Rodwell, "A travelling-wave resonant tunnel diode pulse generator", *IEEE Microwave and Guided Wave Lett.*, vol. 4, no. 7, pp. 220-222, 1994

[5] D. Jäger, "Characteristics of travelling waves along nonlinear transmission lines for monolithic integrated circuits: A review", Int. J. Electron. 58, 649-669 (1985) (invited paper)

[6] B. Wedding and D. Jäger, "Phase-matched second harmonic generation and parametric mixing on nonlinear transmission lines", Electron. Lett. 17, 76-77 (1981)

CAD Techiques for MMICs

I. D. Robertson, U. Karacaoglu and D. Sánchez-Hernández

CAD Techniques for MMICs

I. D. Robertson, U. Karacaoglu and D. Sánchez-Hernández

MMIC Research Team. Centre for Telecommunications Research
Department of Electronic & Electrical Engineering
King's College, Strand London WC2R 2LS
Tel: + 44 171 873 2523
Fax: + 44 171 873 2081
e-mail: ianr@orion.eee.kcl.ac.uk

1. Introduction

This paper reviews the different CAD packages that are available and describes how these are used in conjunction with foundry models in the MMIC design process. It is shown that there are a wide range of different component models that can be used, the choice of which depends on the level of foundry characterisation and the specific CAD package that is available. At one end of the scale it is possible to design a simple MMIC using a basic PC simulator with simple equivalent circuit models. At the other end of the scale, it is possible to use a fully integrated MMIC CAD workstation which has SMART™ libraries for layout automation and direct integration of electromagnetic simulation for non-standard structures. The degree to which the design process can be integrated and even automated depends on how much your company/institution can afford to spend on CAD and on which foundry you are using: CAD packages can cost over £50k per seat, and relatively few foundries have developed the necessary SMART™ library elements.

2. Types of Microwave Simulator

The key players in the major microwave CAD business are listed in Table I. HP/EEsof still has two product lines, but is working towards a unified product using the best elements of the HP and EEsof products. There is a wide range of software on offer, and the function of each of the different types of microwave CAD package is now described.

Linear Frequency-Domain

This type of simulator generally uses Y-parameter matrix techniques to solve for the steady-state frequency response of linear circuits, and Touchstone™ is the most familiar example. Since individual components are treated essentially as frequency-dependent admittance's within a nodal matrix, solution for the overall circuit response is a case of using matrix reduction techniques to end up with an overall set of Y-parameters. These can then be converted to S-parameters, etc., for display. The simulator does not need to calculate the currents or voltages in the circuit, and the analysis is very fast as a result. In particular, working in the frequency-domain means that only the steady-state response of distributed elements (transmission-lines) needs to be considered. This is very important, because the multiple reflections encountered in a microwave circuit would take a lot of time to solve in the time-domain. Furthermore, frequency-dependence of transmission-line parameters (e.g. dispersion, resulting in a change of Z_0 with frequency) can easily be handled. However, non-linear

elements cannot be modeled since the currents and voltages in the circuit are not calculated.

Non-Linear

In order to calculate the true response of non-linear components such as transistors it is necessary to work in the time-domain. This is because the equivalent circuit elements vary with signal amplitude, and are thus functions of time. Direct time-domain methods are generally based on SPICE, with more convenient display options added to create programs such as MICROWAVE SPICE™ (now known as the Time Domain Test Bench in Series IV).

The handling of transmission-line elements is difficult in the time-domain because of the long time taken to reach a steady state and the need to consider dispersion. Some of the newer time-domain simulators use a convolution technique which does makes it possible to handle dispersion (e.g. Impulse™). For steady-state large-signal analysis (such as gain compression of a power amplifier) the harmonic balance technique is faster than time-domain methods. This uses a combination of time- and frequency-domain analysis. The voltages & currents in the non-linear components are calculated in the time domain. The linear elements are treated in the frequency domain. Fourier transformation is then used to compare the currents and voltages of the non-linear components with the terminating impedance's presented by the linear components at all the harmonic frequencies used in the analysis. Any error is reduced by successive iterations, as shown in Fig. 1. The signals must be periodic in order to use the Fourier transform. Due to the enormous number of calculations required, and the need for iterations to ensure convergence, this type of analysis requires a fast computer with a lot of memory. These requirements go up dramatically as the number of harmonics increases. Examples of harmonic balance programs are Libra™, Harmonica™, and MNS™ (Microwave Non-linear Simulator, within MDS™). Currently, MDS™ appears to have the best harmonic-balance algorithm, which is able to handle three independent frequencies with 12 harmonics in the analysis. However, as much as 300 Mb of RAM may be required for such an analysis!

Planar Electromagnetic

These programs are intended to solve for the S-parameters of arbitrarily shaped microstrip or CPW structures. Usually, the circuit conductors are divided into subsections and the method of moments is used for the electromagnetic analysis. Examples of this type of simulator are *em*™, Explorer™, and Momentum™. Often, many metal and dielectric layers can be handled, but these are assumed to be planar, and so the term 21/2-D has been coined (2-D currents but 3-D fields). These simulators cannot analyse true 3-D structures, such as microstrip-to-stripline transitions where the dielectric are not planar. Yet, when the current on the third dimension can be used to represent, for example, vias, but the analysis allows only layered dielectric, the term 3-D planar is more appropriate. 21/2-D and 3-D planar simulators are used extensively in MMIC design to analyse non-standard microstrip structures such as coupled bends and meandered lines. Fig. 2. shows the layout of a CPW Tee-junction on *xgeom* ™ by Sonnet Software. The 3-D planar simulator *em*™ can handle any number of ports and metal or dielectric layers.

3D Electromagnetic

The High Frequency Structure Simulator (HFSS™) by HP (3-D arbitrary) has dominated this market for several years. This uses finite element techniques to analyse completely arbitrary metal and dielectric structures and can thus be used for analysing components such as waveguide-to-microstrip transitions and MMIC packages. However, this type of analysis is extremely demanding of CPU time and memory: HP currently recommend around 300Mb of RAM. Since most MMIC components are at present basically planar in nature, 3-D simulation is not used extensively. More recently, some other companies have introduced 3D simulators: for example the MacNeal-Schwendler Corporation (MSC) has introduced "MicroWaveLab" and KCC has introduced "Microstripes". Microstripes uses the transmission-line matrix (TLM) method which is a fast technique requiring less memory than finite element methods. The TLM method simulates the propagation of electromagnetic waves in any medium where both space and time are discretised. The space is modeled by a transmission line bounded network which allows the description of 3-D structures made up of dielectric substrates and metallic strips with finite dimensions. The effects of the limited ground plane are shown on spatial representations of the electromagnetic fields. For all these numerical methods the most time consuming step is the solving of the matrix ($O(n^3)$), while the building of the matrix is $O(n^2)$. Recently, however, a fast iterative matrix solver where solution time increases only as the square of the number of unknowns rather than the traditional cubic technique has been developed by Ansoft Corporation for its 3-D planar *Maxwell-Strata* electromagnetic simulator.

System Block Diagram

These programs treat individual circuits as black boxes with some kind of describing function (not just S-parameters). This enables complex subsystems, such as complete transmitters and receivers, to be designed at a high level. An example of this is Omnisys™ by HP/EEsof. Whilst packages such as MDS™ can analyse complex subsystems with its standard simulators, there is a need for component-oriented methods which are easier to use for complex subsystems. Since systems are becoming increasingly complex, and as digital signal processing becomes closely integrated with microwave hardware, system level simulation is becoming more important and is receiving a great deal of attention. The Communications Design Suite by HP/EEsof currently represents the state-of-the-art in the field.

Filter / Matching network synthesis

These programs, such as E-Syn™ and Matchnet™, carry out the design of filters and matching networks using established synthesis techniques. Amplifiers and matching network designs should definitely be based on this type of synthesis program, rather than trying to blindly optimise previous designs or adding elements by trial and error. They should be used with caution, however: Too tight a specification (ripple, bandwidth, etc.) leads to over complex networks with extreme component values.

Schematic Capture Front-ends

These are a means of entering designs directly into a circuit diagram using symbols. This is now a fundamental part of most of the major CAD packages, and the old "net-list" is often not accessible. The advantages of schematic capture are that it is easy to visualise your circuit and prevent mistakes. Designs should use hierarchy extensively in order to keep them tidy and easy to follow. Fig. 3 shows the Academy™ schematic of

a rat-race coupler; each CAD element has its own symbol and these are wired together on the circuit page.

Layout and Design Rule Checking

MMIC layout is still a mostly manual procedure. In the early days, layouts were often carried out by specially trained operators on dedicated systems such as CALMA™. The CALMA™ GDSII file is still the industry standard, but layout packages are now available on the designer's own workstation or even his PC. The best example of this is WAVEMAKER™ Layout, which offers a tremendous range of powerful layout commands yet is economical and can run on anything from a modest PC upwards. This type of dedicated program is often superior to the layout facilities in other CAD packages, which were developed for hybrid-MIC layouts. Fig. 4 shows a screen shot of an MMIC oscillator on WAVEMAKER™. For the layout and design-rule checking of complete mask-sets, powerful packages such as CADENCE™ or MENTOR GRAPHICS™ are important. Many CAD packages now offer their simulator "engines" for use with these industry standard interfaces.

Fully Integrated Design Packages

These offer a truly integrated suite of the above types of program. The "MMIC Workstation" is becoming increasingly important as chip complexity increases. Customisation of these packages for a particular foundry is possible, and this is discussed in Section 4.

3. Types of Component Models

Foundry S-parameters

Often, foundries supply a large number of S-parameter files to cover the most commonly used components. For example, data for 1 turn, 1.5 turn.....up to 6 turn spiral inductors may be provided. If the measured data has been de-embedded accurately, and the reference planes defined properly, then this data should be very reliable. However, it is often the case that, for example, a non-standard number of turns is required. This data-file approach has clear limitations for design and optimisation.

Foundry equivalent circuit models

In this approach a wide range of components are measured, and an equivalent circuit model is fitted to each one. Then, equations can be generated which give the values for the equivalent circuit as a function of either the layout dimensions or other parameter (such as the number of turns). This approach has the advantage that the model is not limited to discrete values of standard elements. Optimisation can therefore be used. However, care must be exercised to ensure that the models are not used outside their range of validity and that they are accurate at high frequency. The most common problems are encountered with lumped spiral inductor models, since these are often inaccurate past the self-resonant frequency of the inductor.

Standard CAD elements

The standard elements from the CAD package can be used (e.g. the microstrip lines in Touchstone™). However, these are often outside their range of validity for the small dimensions of MMIC components. GEC-Marconi use a "fiddle-factor" to enable the

standard microstrip line models to be used for their multi-dielectric process: The dielectric constant and loss parameters are made functions of the line width.

Special CAD elements
Many CAD packages now include special library elements which have been developed for MMICs. An example is the 3-port capacitor in LINMIC+™, shown in Fig. 5. These elements are often based on rigorous theoretical treatment of the component, resulting in an accurate model which requires many input parameters. These can be expected to be more accurate than foundry equivalent circuit models when distributed effects in the component are important (e.g. at 20 GHz).

S-parameters from EM simulation
Electromagnetic simulation of arbitrary planar structures is now a reality. This is particularly useful for microstrip circuitry where standard CAD elements are invalid due the close proximity of bends, Tee-junctions, etc. So, after the bulk of the design has been carried out using CAD elements, the initial layout is carried out. Once the required geometry of the microstrip is known, the layout (of a meandered line, for example) can be imported directly into the em analysis package. The S-parameters are calculated and the new circuit response checked. This process is now transparent with some of the latest CAD packages. OSA have gone one stage further to enable optimisation of the microstrip geometry to take place (EMPIPE™).

Active Device Models
For linear simulations these can be S-parameters, equivalent circuits for a fixed device and bias point, or scaleable/bias-dependent equivalent circuits. A scaleable model is one which can model different gate-widths. A bias-dependent model is one in which the small-signal equivalent circuit elements vary with a bias parameter. For example, the drain current of a FET might be a parameter: This allows the designer to see how the bias affects the gain of an amplifier, but it is not a large-signal model.

Large-signal device models (transistors and diodes) are ones in which the DC and RF parameters are all calculated dynamically for the instantaneous voltages applied to the device. As a result, when using a large-signal model the DC bias supplies must be added to the simulation as voltage or current sources. Many different large-signal models exist for FETs, such as the Curtice Cubic, Triquint's Own, HP Root, etc. Most foundries provide at least one large-signal model type. The better foundries will offer a model optimised for your particular simulator. The accuracy of large-signal models still leaves a lot to be desired, especially for highly non-linear circuits such as mixers.

4. Simulator Customisation: SMART Libraries

In a fully integrated CAD package there is seamless integration of the schematic and layout. In order to achieve this level of design integration, the simulator must be customised to the foundry. This means that the foundry's models and layout library elements form a core part of the simulator's element library. In this way the layout and schematic can be linked together: A change made in the layout window will automatically result in a change of the parameters in the schematic. For example, if you edit the length of a microstrip line in the layout editor then the new length information is passed to the schematic, and the simulation can be re-run directly. This

transfer of information directly between the layout and the schematic/simulation is called back annotation. The ability to edit the layout (i.e. the artwork) of a particular library element and then re-simulate directly has led to the phrase **S**imulateable **M**icrowave **ART**works, which was coined by EEsof. These SMART™ library elements have the component model and layout integrated, so the design becomes partially automated. This is illustrated in Fig. 6. It should be noted, however, that there is a limit to the complexity of a layout which can be created in this way. Apart from fairly simple circuits most MMICs are too complicated to make full use of the automated layout facility. As an example, the Libra™ schematic of an MMIC amplifier using GMMT-SMART™ Library is shown in figure 7.

5. Some examples

The need for electromagnetic simulators is outlined in the examples of figures 8 to 11. Figure 8 shows a meandered line on xgeom™ (Sonnet Software). The designer might expect that the parasitic coupling between the arms of the meandered line may degrade the final results. A comparison between the libra_3.0 model, SMART™ Library model, and two electromagnetic simulations, one using the so-called breaking-down technique and a full electromagnetic simulation, is given in figure 9. Another interesting example of the extensive use of electromagnetic simulators on MMIC design is the monolithic ring filter of figure 10. The simulation of the polyimide overlay capacitors is crucial to achieve accurate prediction of the transmission response, as depicted in figure 11. A detailed description of these two examples will be given in the presentation.

6. Summary

In summary, MMIC CAD has advanced tremendously in the last 5 years. The latest generation of integrated MMIC design environment offers the ability to use a number of different types of simulation and component model within a single design file. Electromagnetic modeling and SMART library elements stand out as two particularly important developments for the MMIC designer. However, it is as important as ever for the designer to be aware of the limitations of the models that he is using. Furthermore, the treatment of component interactions (e.g. coupling between spiral inductors) is still limited. However, as workstation performance increases electromagnetic modeling will be able to handle larger portions of the circuit. Eventually, it is likely that accurate electromagnetic modeling of reasonably complex circuits will be possible directly from the layout. Unfortunately, as always, the pressure to make MMICs with higher levels of integration and increased functionality means that CAD capabilities and computer speed will probably always trail behind what is required to some extent.

TABLE I

COMPANY	PRODUCT (all trademarks acknowledged)	TYPE
HP-EEsof (HP range)	MDS	Integrated package
	MLS	Linear simulator
	MNS	Harmonic balance
	Impulse	Time-domain
	Momentum	3D Planar eletromagnetic
	HFSS	3D Arbitrary electromagnetic
	MW Artwork Generator	Layout
HP-EEsof (EEsof range)	Touchstone	Linear
	Libra	Harmonic balance
	Microwave Spice (now in Libra)	Time-domain
	E-SYN	Filter synthesis
	Omnisys	System simulation
	EMSim	21/2D Electromagnetic
Compact Software	EASi	Integrated suite
	Serenade	Schematic capture
	SuperCompact	Linear
	Harmonica	Harmonic balance
	SuperSpice	Time-domain
	Success	System simulation
	Explorer	3-D Planar electromagnetic
Sonnet Software	em	3-D Planar electromagnetic
	xgeom	Layout entry
	emvu	Current display
	patgen/patvu	Patch antenna patterns
Jansen Microwave	LINMIC+	Linear (integrated suite)
	LINMIC+/N	Non-linear
	UNISYM	3D Planar electromagnetic
	SFPMIC	3D Planar electromagnetic
Ansoft Corporation	Maxwell-Strata	3D Planar electromagnetic
	Maxwell SI Eminence	High speed circuitry/EMI/EMC
	Maxwell SI Spicelink	High speed digital design
ArguMens	Octopus	Linear
	Stingray	3D Planar electromagnetic
	Shark	Layout
Barnard Microsystems	WAVEMAKER	Layout, linear simulation, schematic capture, device modelling (Modules).
UC Boulder	PMESH	21/2D electromagnetic
GaAs Code		Device modelling
OSA	HOPE	Linear/Non-linear
	HARPE	Parameter extraction
	EMPIPE	Sonnet em optimisation
MSC	MicroWaveLab	3D Arbitrary electromagnetic
KCC	MicroStripes	3D Arbitrary electromagnetic (TLM)
Optotek	MMICAD	Linear simulator

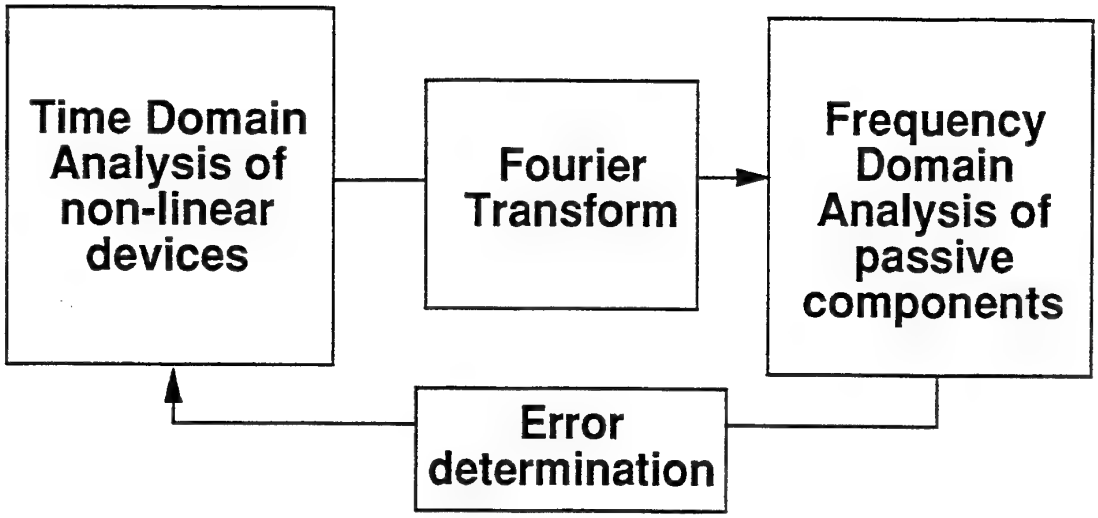

Fig. 1. The harmonic balance technique

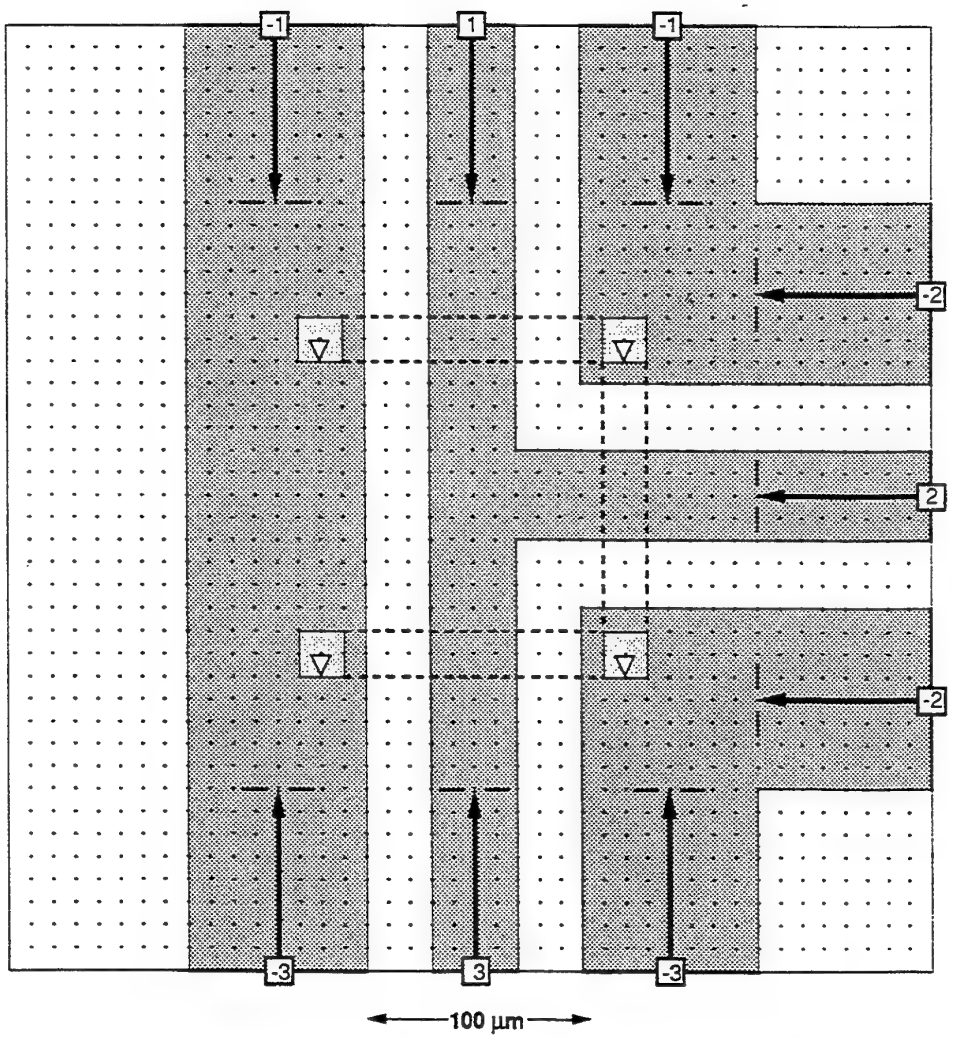

Fig. 2. CPW T-junction on *xgeom*™

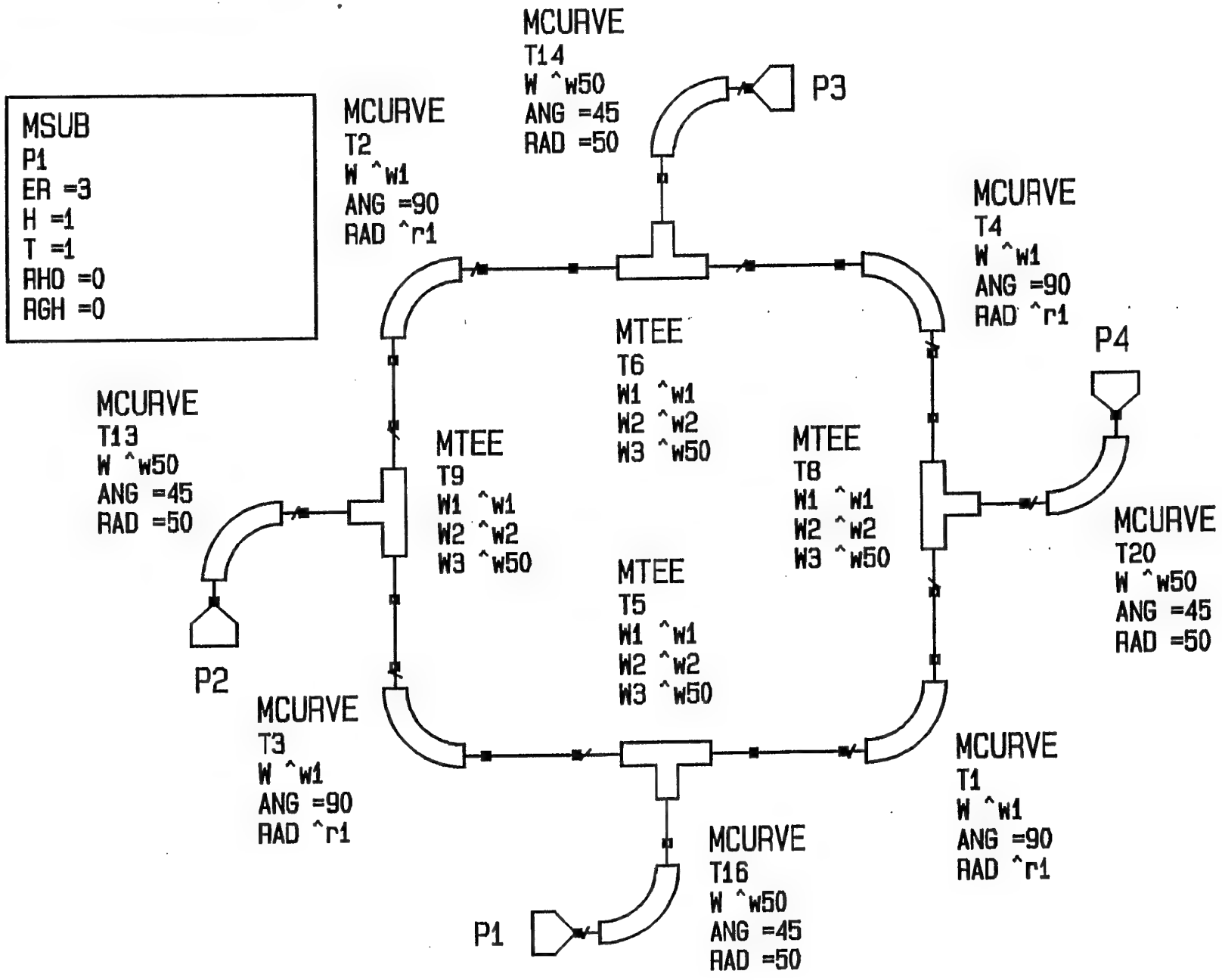

Fig. 3. Academy™ schematic of a rat-race coupler

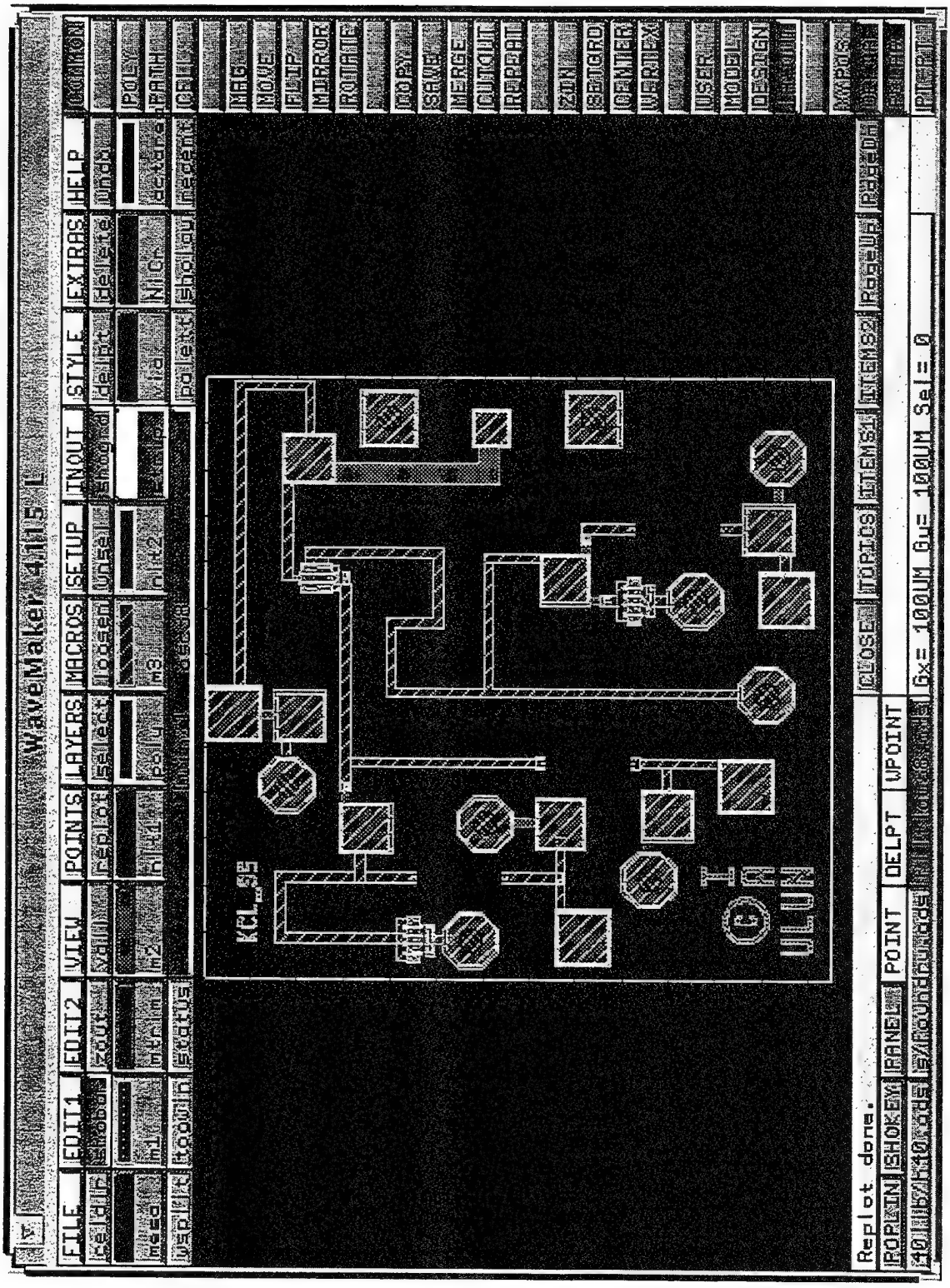

Fig. 4. WAVEMAKER: Oscillator layout

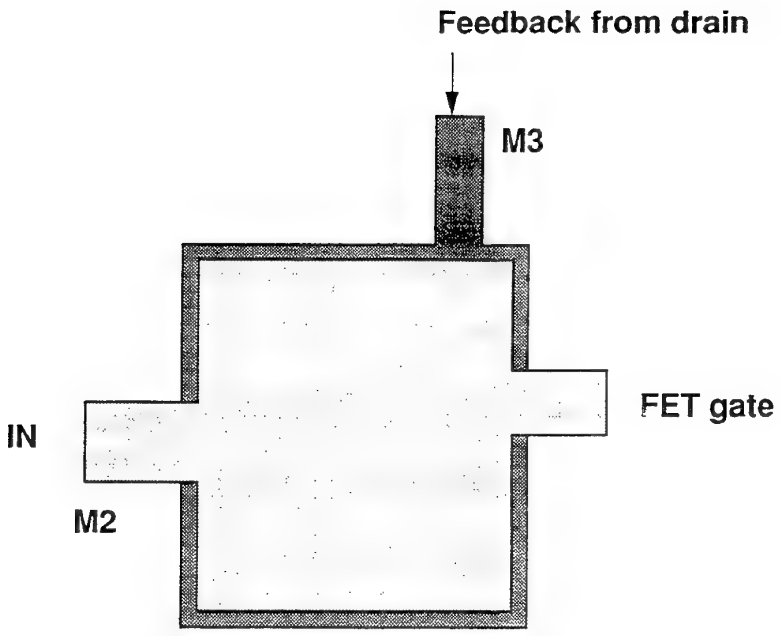

Fig. 5. Three-port capacitor (e.g. in a feedback amplifier)

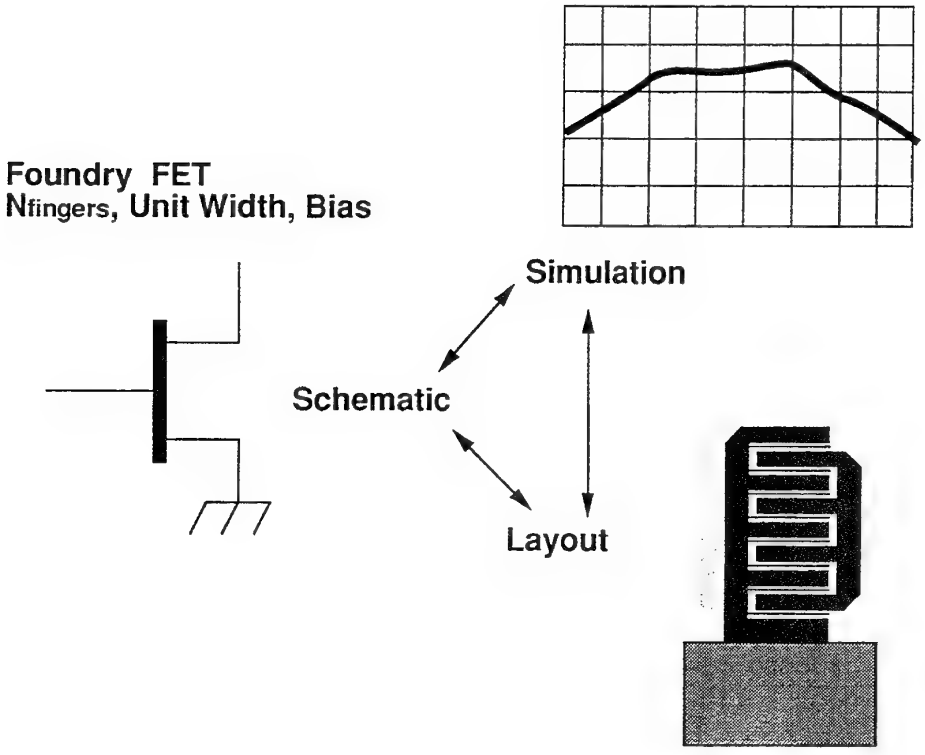

Fig. 6. SMART library elements

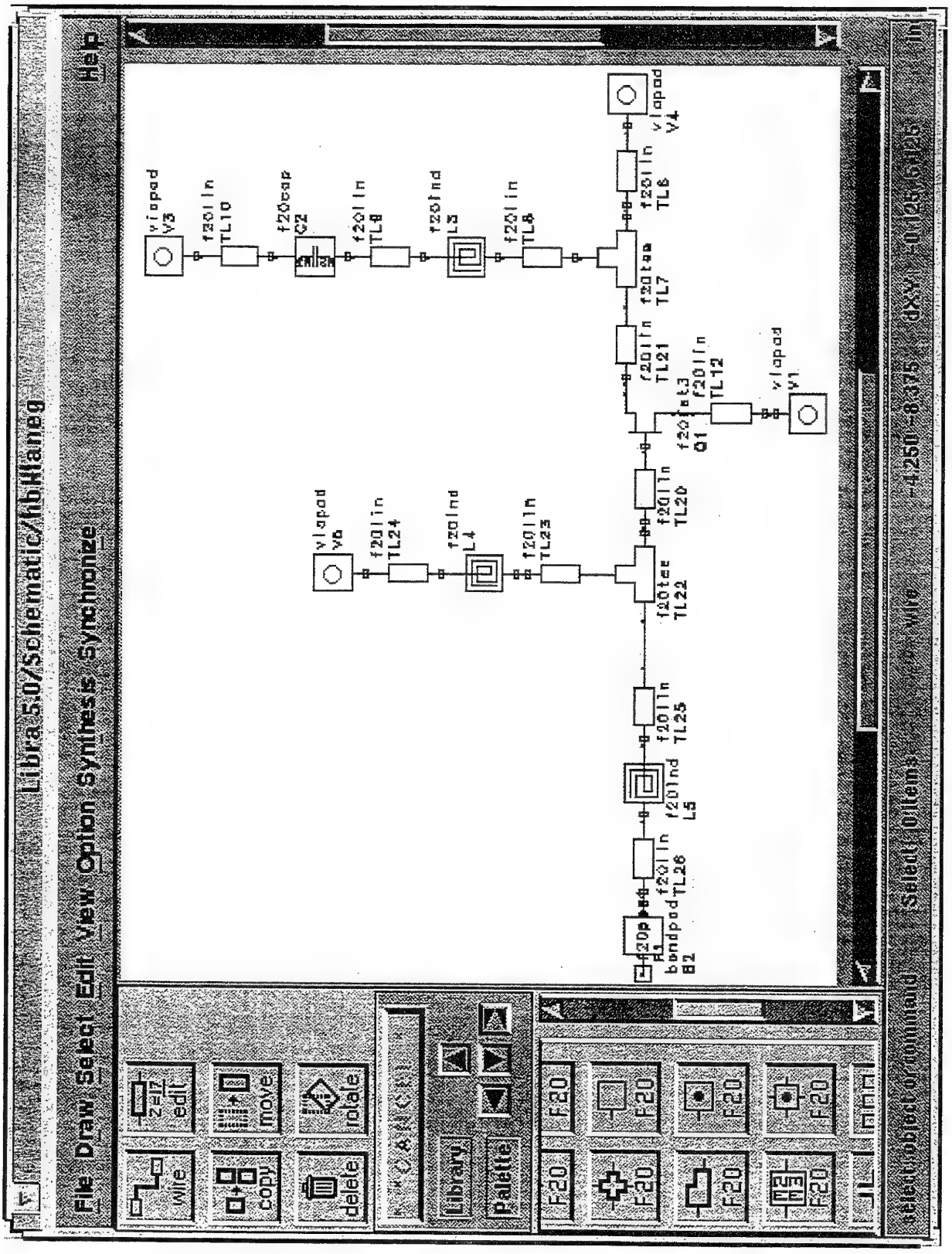

Fig. 7. Libra™ schematic of MMIC amplifier using GMMT-Smart™ Library

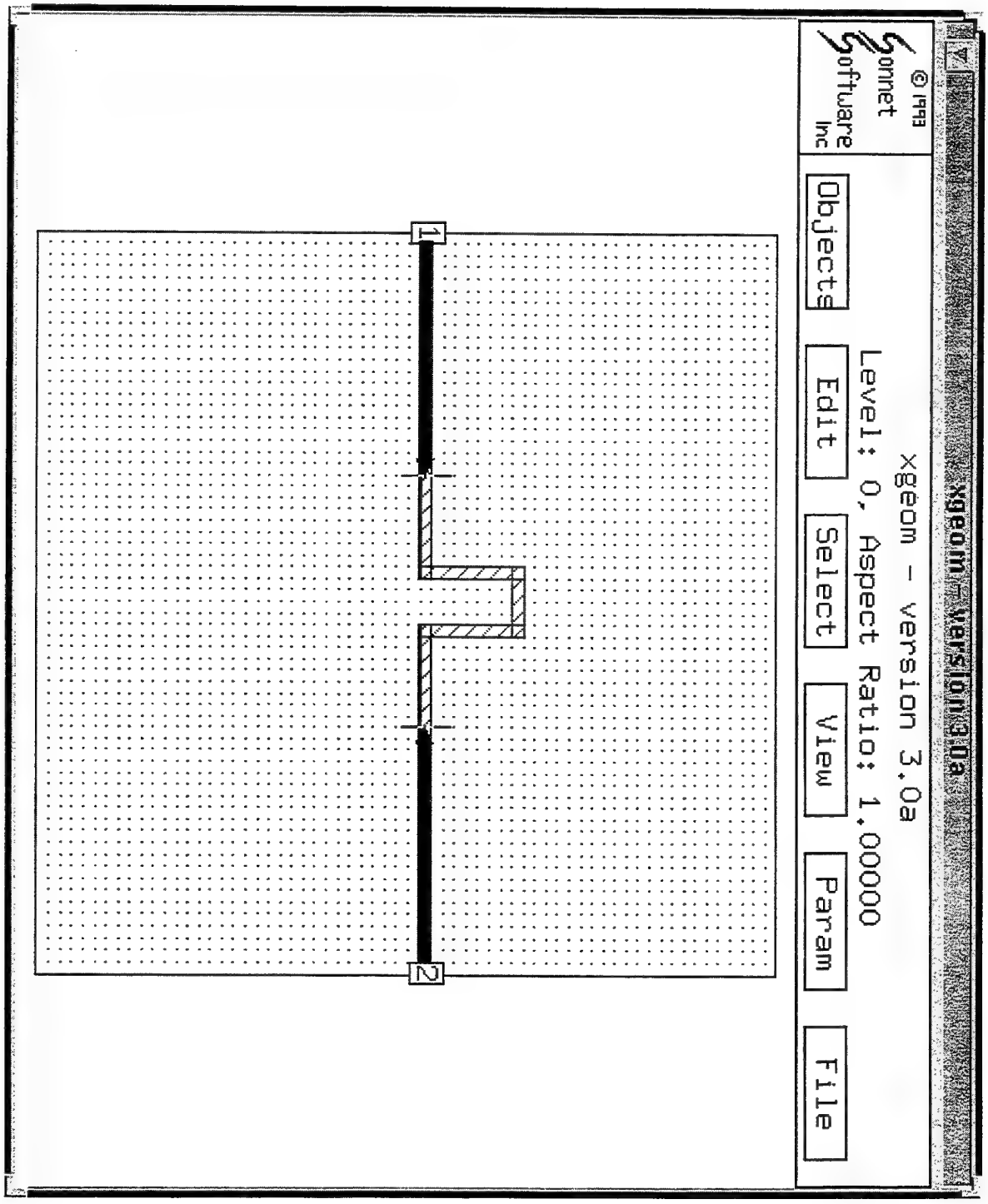

Fig. 8. Meander line on xgeom™.

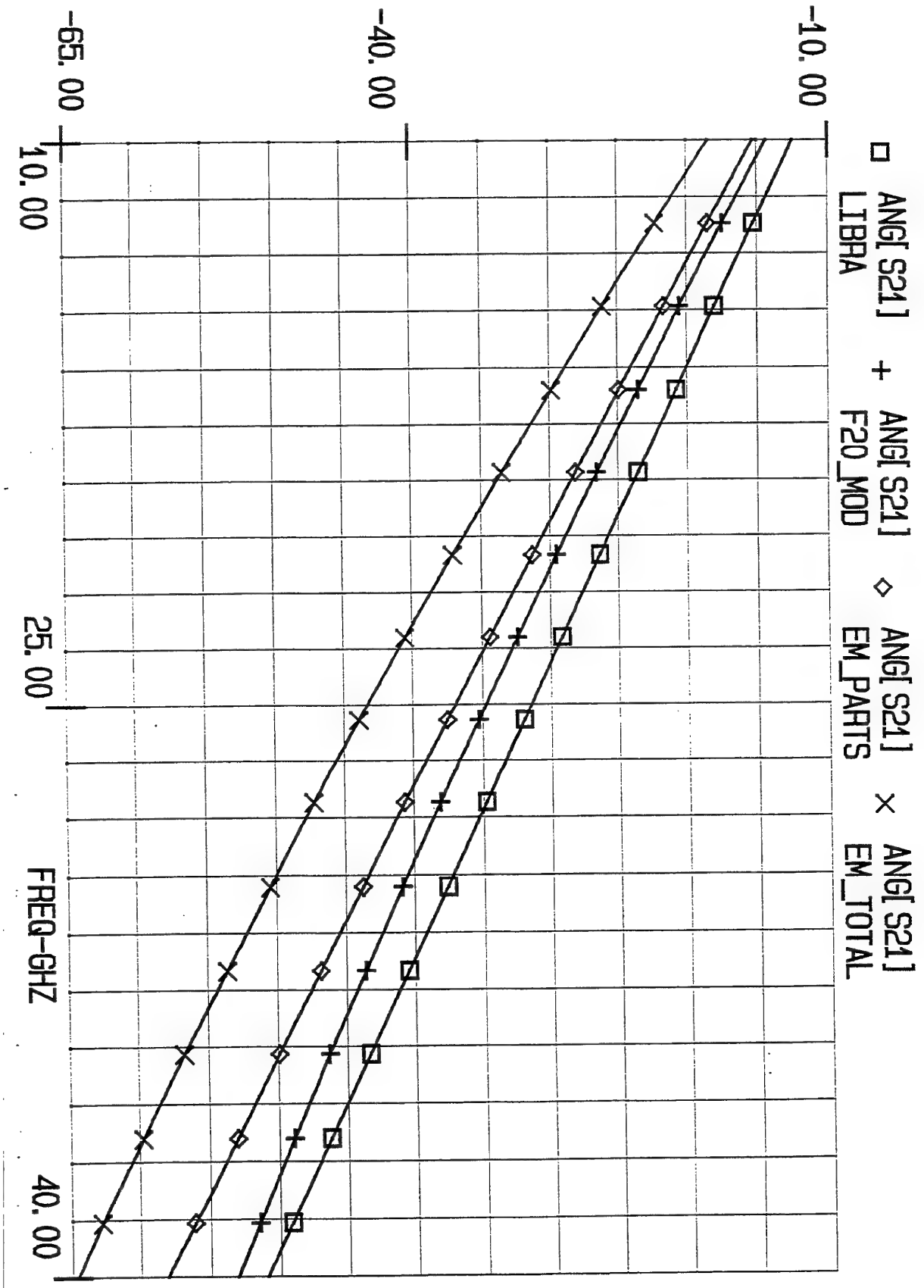

Fig. 9. A comparison between models for S21 phase of meander line.

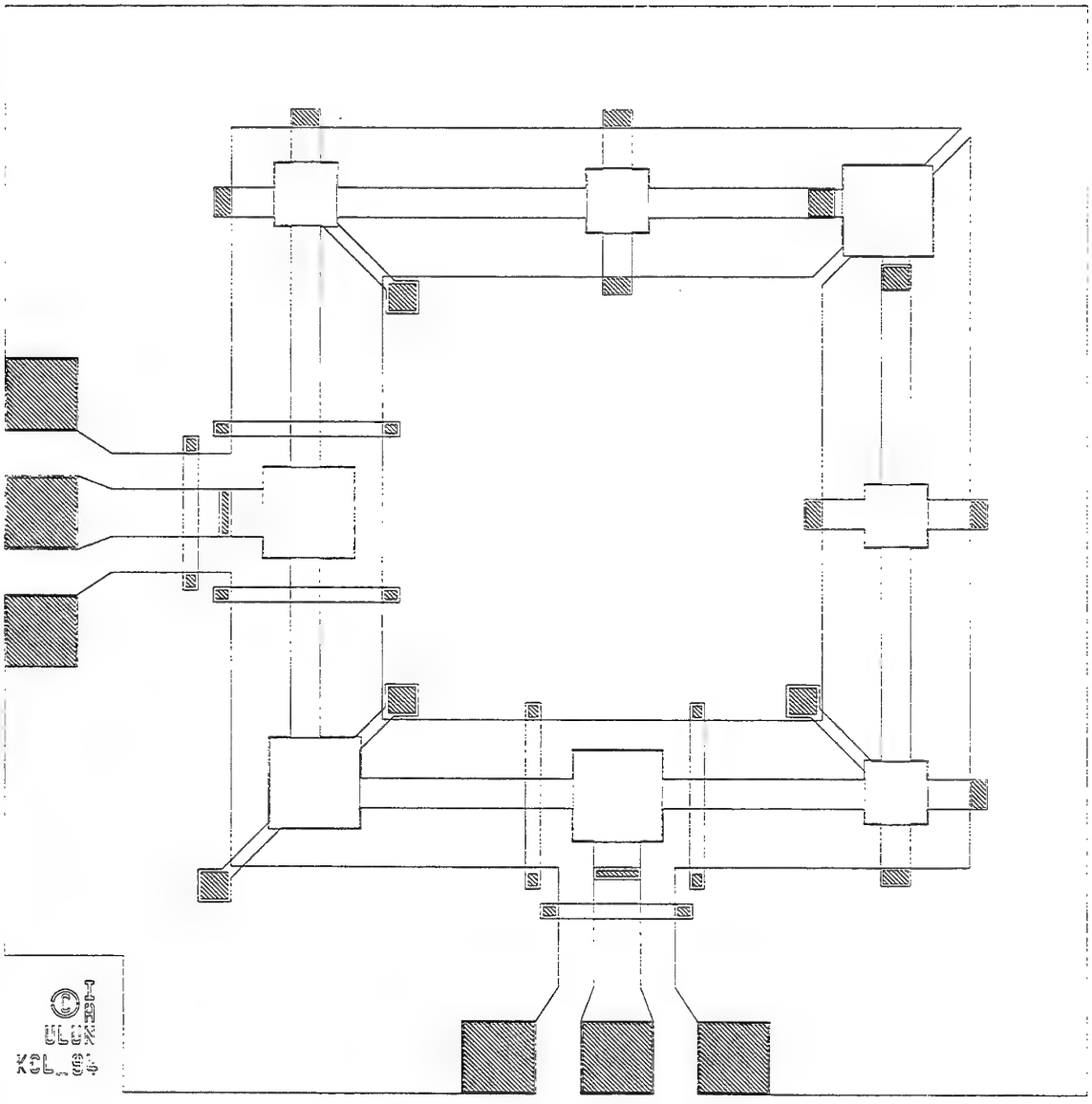

Fig. 10. Layout of MMIC ring resonator filter.

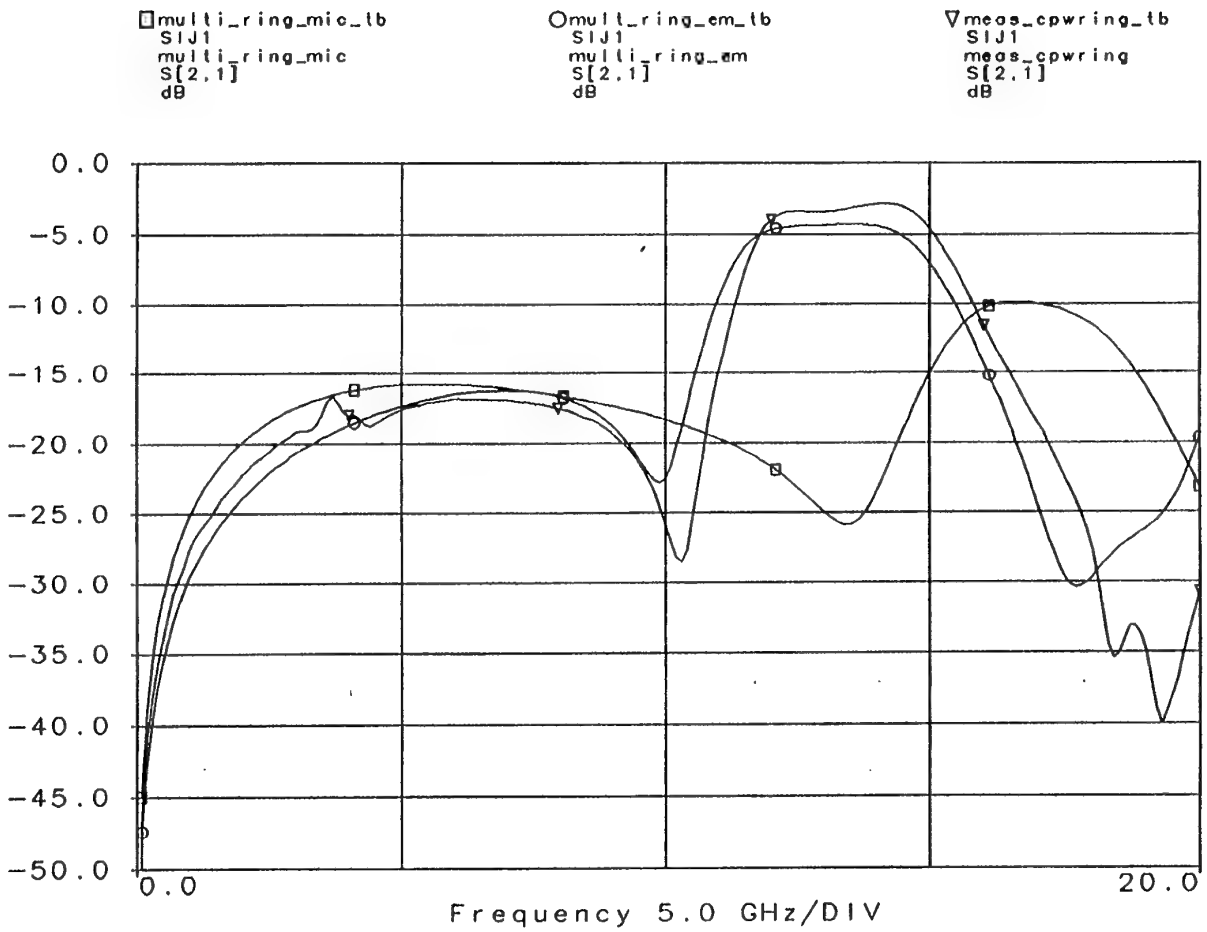

Fig. 11. Transmission response of MMIC ring with a) em™ and b,c) Smart™ Library.

Design-Oriented Full-Wave Modeling of Passive MMIC Structures

P. Bernardi, R. Cicchetti, and A. Faraone

Design-Oriented Full-Wave Modeling of Passive MMIC Structures

P. Bernardi, R. Cicchetti, and A. Faraone

Department of Electronic Engineering, University of Rome "La Sapienza"
Via Eudossiana 18, I-00184 Roma, Italy
Phone: +39 6 44585 855; Fax: +39 6 4742647; E-mail: bernardi@tce.ing.uniroma1.it

ABSTRACT

A full-wave modeling of passive MMIC structures has been carried out to predict the actual behavior of electronic circuits operating at microwave and millimeter wave in high package-density circuitry. A particular effort has been devoted to the simulation of medium complexity circuits in realistic exciting/loading situations. The prediction of undesired EMI effects, a widely addressed problem in high-density circuitry, can be performed by accounting for coupling and surface and volume wave radiation through the use of the electrodynamic dyadic Green's function.

I Introduction

Given the growing packaging density of modern electronic devices, a reliable characterization of microwave and millimeter wave planar integrated circuits and antennas requires the inclusion of all physical phenomena that affect their performance. These phenomena, frequently related with the excitation of volume and surface waves, remarkably influence the behavior of the circuits, especially when substrates with high dielectric permittivity (e.g., GaAs) are employed, as in MMIC's. As a matter of fact, a degradation of system performance may occur if the effects associated with these phenomena are not properly taken into account during the design stage, frequently resulting in EMC intrasystem problems and longer design practices. In this context, full-wave methodologies are presently gaining wider interest as reliable prediction tools for MIC's and MMIC's design, given their capabilities of handling structures with complex geometries within reasonable simulation times [1]. In particular, methodologies based on integral equation formulations [2]-[5] that employ the dyadic Green's function to express the electromagnetic field [6] are well suited for the frequency-domain analysis of planar microstrip circuits and antennas.

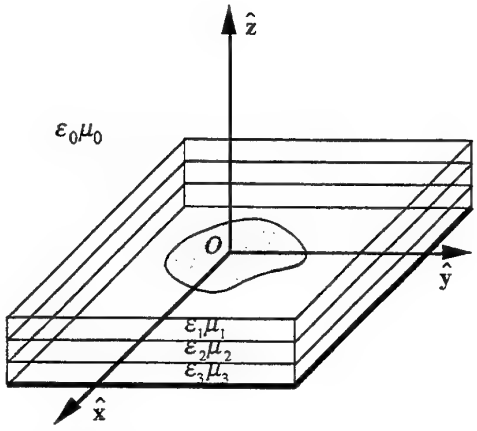

Fig. 1 *A planar multi-layer structure.*

In this contribution, a full-wave modeling approach based on the SDA, suitable for the electrodynamic characterization of wide classes of planar structures (including antennas) working in the microwave and millimeter wave frequency range, as well as to predict their EMC characteristics in realistic circuital configurations, is presented. This methodology, besides accounting for all the electrodynamic phenomena that influence the system performance, allows the inclusion of discontinuity effects and of eventual passive and active loads in the analysis of complex interconnecting structures. Planar multi-layer structures (Fig. 1) are easily accounted for by adopting the appropriate dyadic Green's function. Therefore, the electrical behavior of circuital layouts of medium complexity can be predicted in realistic operation with a high degree of reliability, so that possible EMI problems can be individuated and reduced already during the design stage.

II Formulation

The derivation of a set of coupled Electric Field Integral Equations (EFIE's), that enforce the appropriate boundary conditions on the metallizations, is performed by expressing the total electric field as a superposition of an exciting field $\mathbf{E}_I$ (impressed) and a scattering field $\mathbf{E}_S$ via the electric dyadic Green's function $\underline{\mathbf{G}}$ as follows

$$\mathbf{E}(\mathbf{r}) = \mathbf{E}_I(\mathbf{r}) + \mathbf{E}_S(\mathbf{r}) = \\ = \mathbf{E}_I(\mathbf{r}) + \int_{V'} \underline{\mathbf{G}}(\mathbf{r}|\mathbf{r}') \cdot \mathbf{J}_S(\mathbf{r})\, dV' \quad . \qquad (1)$$

The scattering current $\mathbf{J}_S$, excited on the metallizations at $z = z_j$, is then expanded in terms of appropriate basis functions Λ_j as follows

$$\mathbf{J}_S(\mathbf{r}) = \Sigma_j I_j \Lambda_j(\mathbf{r})\, \hat{\mathbf{t}}_j\, \delta(z - z_j), \quad \left(\hat{\mathbf{t}}_j = \hat{\mathbf{x}}, \hat{\mathbf{y}}\right) \qquad (2)$$

where $\delta(\cdot)$ represents the Dirac *delta* distribution. In the particular case of microstrip discontinuities, traveling wave modes and higher-order mode currents excited near the discontinuities must be employed [7]-[8]. Then, Galerkin's procedure (quasi-Galerkin when traveling current modes are involved) is adopted to enforce a vanishing field on the metallic domains D_k, thus leading to the mentioned set of coupled EFIE's, which are reduced to a linear equation system, through the method of moments, as follows

$$\begin{aligned} 0 &= \int_{D_k} \mathbf{W}_i(\mathbf{r}) \cdot \mathbf{E}(\mathbf{r})\, dV \\ &= \sum_j I_j \tfrac{1}{4\pi^2} \int \tilde{\mathbf{W}}_i^*(\xi) \cdot \underline{\tilde{\mathbf{G}}}\left(\xi; z_i | z_j\right) \cdot \hat{\mathbf{t}}_j \tilde{\Lambda}_j(\xi)\, d\xi \\ &\quad + \tfrac{1}{4\pi^2} \int \tilde{\mathbf{W}}_i^*(\xi) \cdot \tilde{\mathbf{E}}_I(\xi)\, d\xi \\ &= -\sum_j Z_{ij} I_j + V_i \end{aligned} \qquad (3)$$

where $\xi = \hat{\mathbf{x}}\alpha + \hat{\mathbf{y}}\beta$ is the spectral variable corresponding to the transverse Cartesian coordinates, and $\mathbf{W}_i$ is the weighting function. The solution of the linear system (3) allows the determination of the actual current distribution

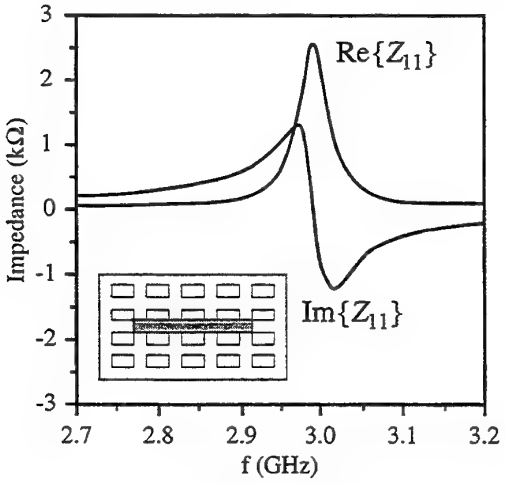

Fig. 2 *Frequency behavior of the Z_{11}-parameter.*

and the extraction of the current scattering coefficients. Moreover, the methodology leads to the computation the Z-matrix parameters of an arbitrary circuital structure [9]-[10]. This feature allows the analysis of a multi-port circuit behavior in realistic exciting/loading configurations, taking into account dispersion and coupling effects, as well as surface and volume wave radiation.

III Numerical Example

In order to show the modeling capabilities of the mentioned full-wave methodology, in Fig. 2 the frequency behavior of the Z_{11}-parameter corresponding to the gridded ground interconnecting structure analyzed in [10] is shown. The gridded ground, featuring 20 rectangular slots of $5.08\,mm \times 2.54\,mm$, has dimensions $40.64\,mm \times 22.86\,mm$. The substrate has dielectric permittivity $\varepsilon_r = 4.7$ and thickness $d = 1.4\,mm$. The planar interconnecting strip has length $l = 25.4\,mm$ and width $w = 2.54\,mm$.

From Fig. 2, it can be observed that radiating effects occur near the first resonance frequency of the structure. Due to the full-wave methodology adopted in the analysis, radiative and reactive phenomena are included in the Z-parameters, so that an accurate prediction of the structure's behavior in realistic exciting/loading configuration can be achieved via straightforward circuit theory.

REFERENCES

[1] J. X. Zheng, "Three-Dimensional Electromagnetic Simulation of Electronic Circuits of General Shape," *Int. J. MIMICAE,* Oct. 1994, pp. 384-395.

[2] T. Itoh, "Spectral Domain Immittance Approach for Dispersion Characteristics of Generalized Printed Transmission Lines," *IEEE Trans. Microwave Theory Tech.*, July 1980, pp. 733-737.

[3] R. H. Jansen, "The Spectral Domain Approach for Microwave integrated Circuits," *IEEE Trans. Microwave Theory Tech.*, Oct. 1985, pp. 1043-1056.

[4] J. R. Mosig, "Arbitrarily Shaped Microstrip Structures and Their Analysis with a Mixed Potential Integral Equation," *IEEE Trans. Microwave Theory Tech.*, Feb. 1988, pp. 314-323.

[5] *Numerical Techniques for Microwave and Millimeter-Wave Passive Structures*, Edited by T. Itoh, New York: John Wiley & Sons, 1989.

[6] P. Bernardi, R. Cicchetti, "Dyadic Green's Functions for Conductor-Backed Layered Structures Excited by Arbitrary Tridimensional Sources," *IEEE Trans. Microwave Theory Tech.*, Aug. 1994, pp. 1474-1483.

[7] R. Cicchetti, A. Faraone, "An Expansion Function Suited for Fast Full-Wave Spectral-Domain Analysis of Microstrip Discontinuities," *Int. J. MIMICAE,* July 1994, pp. 297-306.

[8] R. Cicchetti, A. Faraone, "A Full-Wave Spectral Domain Analysis of an Asymmetric Gap Microstrip Discontinuity," *Microwave Opt. Tech. Letters*, Aug. 1995, pp. 356-358.

[9] P. Bernardi, R. Cicchetti, D. S. Moreolo, "A Full-Wave Model for EMI Prediction in Planar Microstrip Circuits Excited in the Near-Field of a Short Electric Dipole," *IEEE Trans. on Electromag. Compat.*, May 1995, pp. 175-182.

[10] P. Bernardi, R. Cicchetti, A. Faraone, "A Full-Wave Characterization of an Interconnecting Line Printed on a Dielectric Slab Backed by a Gridded Ground Plane," to be published on Special Issue on *IEEE Trans. on Electromag. Compat.*.

Small-Sized Coplanar MMIC Amplifiers in V-Band Using InP-Based Dual-Gate HEMTs

Y. Bayens, D. Schreurs, B. Nauwelaers, K. Van der Zanden
M. Van Hove, W. De Raedt and M. Van Rossum

Small-sized coplanar MMIC amplifiers in V-band using InP-based dual-gate HEMTs

Y. Baeyens, D. Schreurs and B. Nauwelaers
K.U.Leuven, div. ESAT-TELEMIC, Kardinaal Mercierlaan 94, B-3001 Leuven, Belgium

K. Van der Zanden, M. Van Hove, W. De Raedt and M. Van Rossum
IMEC, Kapeldreef 75, B-3001 Leuven, Belgium

GaAs and InP-based HEMTs with very short gatelengths have demonstrated excellent performance in a variety of analog and digital applications [1]. The use of dual-gate HEMTs connected in a cascode configuration with the second gate RF grounded gives additional advantages such as a higher and controllable gain [2]. In this paper, we report the state-of-the art performance of single-stage smallband amplifiers fabricated using 0.15μm gatelength dual-gate HEMTs with a layerstructure lattice-matched grown on InP.

For InP-based HEMTs the gain can be further increased by changing from a single-gate to a dual-gate cascode topology, although this increase is less pronounced in comparison with GaAs-based PHEMTs [3]. InP-based devices have already a low feedback capacitance which can be further reduced by putting two devices in cascode, but is ultimately limited by the parasitic feedback from the first gate to the drain. At 10GHz, a gain of 24.1 and 27.0dB is measured for respectively GaAs and InP-based dual-gate HEMTs. The use of these dual-gate HEMTs in MMIC amplifiers up to Ka-band was demonstrated in [3].

To show the potential of our InP-based dual-gate HEMTs also in millimetrewave applications, different amplifiers operating in Q-, V- and W-band were designed and fabricated. A single-stage reactively matched V-band amplifier is discussed here in more detail. The layout of this amplifier with a total size of $0.9\text{x}0.7\text{mm}^2$ is shown in Fig.1. The input is matched by a series transmission line and a lumped MIM parallel groundcapacitor placed underneath the T-junction connecting the quarter wavelength bias-stub. For the output matching, which is quite critical due to the high output impedance of the cascode FET, the combination of a series transmission line and a double stub RF shorted on top of a MIM capacitor is used. In this coplanar layout, airbridges were extensively used in order to suppress slotline modes at bends and other discontinuities [4]. Their influence is small due to the very small ground-to-ground separation of 50μm.

Measurements on this V-band amplifier are shown in Fig.2 as a function of the frequency. At 58.5 GHz, a maximal gain of 16.4dB is measured, to our knowledge the highest gain reported for a single-stage MMIC amplifier in V-band. At this frequency, also an excellent input and output reflection of less then -20dB is obtained. The amplifier is unconditionally stable from 1GHz up to the highest measurement frequency. For a similar single-stage Q-band amplifier, a gain of more than 17dB is obtained at 42GHz. In general, the characteristics measured on all the fabricated dual-gate amplifiers are in very good agreement with the simulated curves apart from a small and consistent shift (2-4%) of both the reflection and gain towards the lower frequencies. This shift is caused by the slightly higher feedback capacitance of the devices processed in this first run. The extremely high gain which is obtained shows clearly the potential of these devices for amplification beyond 100GHz.

ACKNOWLEDGEMENTS

IMEC wishes to acknowledge the financial support of ESA/ESTEC for its research activities on GaAs and InP-based HEMT technology. Measurements up to 67 GHz were performed at the IMST in Kamp-Lintfort, Germany.

REFERENCES

[1] L. D. Nguyen, L. E. Larson and U. K. Mischra, "Ultra-High-Speed Modulation-Doped Field-Effect Transistors: A Tutorial Review," Proceedings of the IEEE, Vol. **80**, No. **4**, pp. 494-518, 1992

[2] J. Wenger, P. Narozny, H. Dämbkes, J. Splettstoßer and C. Werres, "Low-Noise Pseudomorphic Dual-Gate Cascode HEMT's with Extremely High Gain," IEEE Microwave and Guided Wave Letters, Vol. **2**, No. 2, pp. 46-48, 1992

[3] Y. Baeyens, K. Van der Zanden, D. Schreurs, B. Nauwelaers, W. De Raedt, M. Van Hove and M. Van Rossum "High-gain coplanar amplifiers using InP-based dual-gate cascode HEMT's," Proc. of the IEEE International Topical Meeting on Nomadic Microwave Techn. and Techniques for Mobile Comm. and Detection, pp. 127-130, Arcachon, 1995

[4] I. Wolff, "Design rules and realisation of coplanar circuits for communication applications", Proc. of the 23rd European Microwave Conference, pp. 36-41, Madrid, 1993

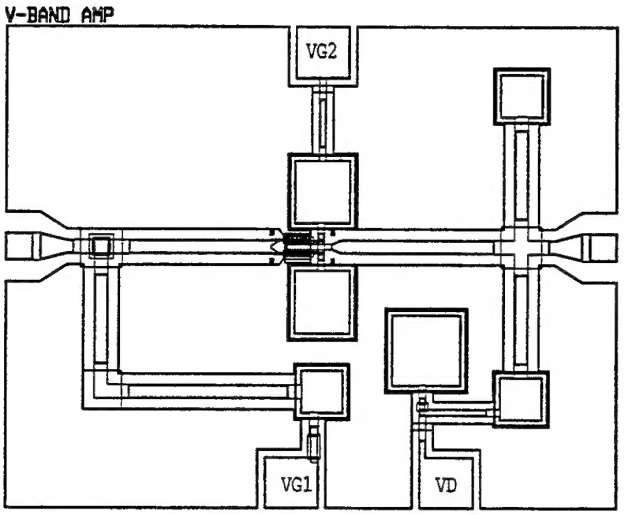

Figure 1: Layout of a single-stage coplanar InP-based V-band amplifier.

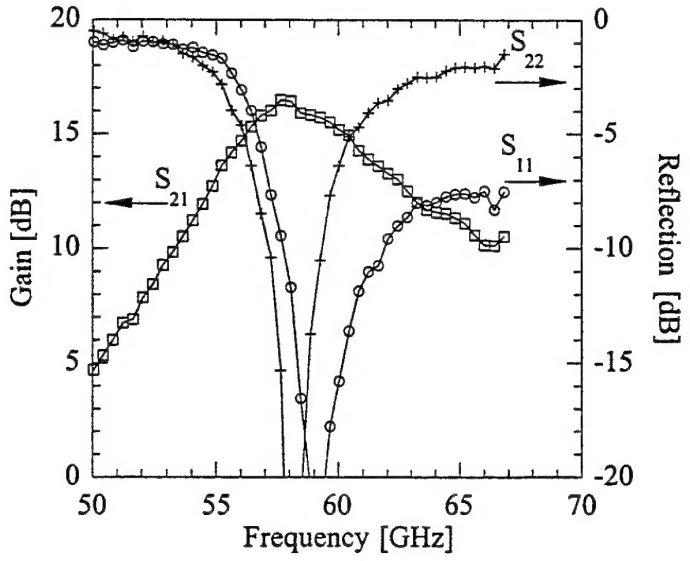

Figure 2: Measured gain and reflection of the V-band single-stage dualgate amplifier.

MMW Hybrid and Monolithic Technology Active Mixer and Amplifiers

V. Alleva, A. Buonocore

MMW HYBRID AND MONOLITHIC TECHNOLOGY

ACTIVE MIXER AND AMPLIFIERS

Vincenzo ALLEVA - Alberto BUONOCORE

ELETTRONICA S.p.A. - Via Tiburtina Valeria, Km 13700 00131 ROMA ITALY

ABSTRACT

A 30-40 GHz low-noise reactive match amplifier, a 0.5-30 Ghz travelling amplifier and a 32-38 GHz RF to 2-8 GHz IF active mixer have been designed both on conventional microstrip substrate, relying on commercially available components, and on monolithic GaAs technology. The hybrid mixer exhibits a very low conversion loss of about 0 dB and a noise figure below 8 dB with an LO power of 10 dBm at 30 GHz, togheter with interesting performances in terms of intermodulation; the low noise amplifier has 4 dB noise figure with gain in excess of 9 dB over the whole 30-40 GHz band; the amplifiers have been designed in monolithic form, while the mixer is presently under design.

INTRODUCTION

Millimeter wave frequencies are increasingly being proposed for high volume, low cost, miniaturized applications in the fields of communication, radar and automotive traffic control. Apart from their propagation behaviour, millimeter waves can achieve good angular resolution within small sized, light weight equipment. Integrated millimetric front end receivers constitute an interesting application where compact design, low cost and high volumes are key factors to competitiveness. The use of up to date HEMT technology allows the integration of low noise amplifiers, oscillators, mixers and other active circuits on the same wafer, resulting in outstanding performances, reduced cost and development time.

Two millimeter waves amplifiers, a 0.5-30 Ghz distributed and a 30-40 Ghz reactively matched, and a 32-38/2-8 Ghz active mixer are described in the following paragraphs, as they constitute the two main active building blocks for the aforementioned RF systems.

AMPLIFIERS DESCRIPTION

The first circuit is a 0.5-30 Ghz monolithic travelling wave amplifier, based on the 100 μm low noise Alenia S.p.A. hemt process. Both linear and non linear models have been extracted and extensive simulation of the circuit has been performed. The expected linear gain from three of the previously mentioned devices is 5.5 dB, with an associated 1 dB compression point output power above 10 dBm at 2 V, 50% Idss bias. Non linear simulation has also shown excellent gain versus gate bias control characteristics, which makes this component suitable also for wide band gain control applications.

The second circuit is a 30-40 Ghz low noise amplifier, which employs two cascaded devices with reactive matching and on chip biasing network. The first device is biased and matched for minimum noise figure, including an input section of coupled lines designed to limit the bandwidth, improve frequency stability and for DC decoupling; the interstage network matches the output impedance of the first fet to the input of the second, which is biased and matched for maximum gain. The circuit has been designed in hybrid version, realized on 0.254 mm alumina substrate using two Mitsubishi MGFC 4418D InGaAs mushroom gate HEMT and successfully tested: it exhibits gain in excess of 9 dB, about 4 dB noise figure and 10 dBm output power.

About 11 dB is the gain expected from the monolithic realization of this amplifier; two such chips will then be embedded between two alumina substrate rat races, which have already been tested alone, to realize a balanced amplifier, so as to improve return loss performances and power capabilities in the full 30-40 Ghz band.

The MMIC circuits are presently under construction at Alenia S.p.A. facilities in Rome.

MIXER DESCRIPTION

An hybrid HEMT transconductance mixer has been designed and tested, adopting the same active device already used in the amplifiers. The RF band (32-38 Ghz) is coupled to the LO power (10 dBm @ 30 Ghz) via a 10 dB coupled lines directional coupler and fed to the gate electrode of the active device; the 2-8 Ghz IF signal is extracted from the drain via a Hi-Low low pass filter, so as to get full advantage of the amplifying properties of the non linear device, which are enhanced by careful selection of the input/output matching networks. To maximize the time variation of gm(t) at the fundamental frequency of the L.O. signal and to minimize all the other non linearities a circuit achieving a short at the drain at the LO frequency, its harmonics and in the RF band, and a low impedance at the gate in the IF band has been developed. A coupled line 29.5-38 GHz band-pass filter section has been included in the input matching network to minimize down-conversion of the unwanted image band noise, being the hemt conjugate matched over the whole RF and LO frequency band but still amplifying in the lower image band.
Conversion loss about 0 dB and noise figure below 9 dB respectively, 30 dB spurious free dynamic range up to -10 dBm RF input power realized in conventional hybrid technology make this component a very interesting building block for mmW down converters.
Non linear modeling, with efficient representation of harmonic behaviour of the active device, is required for the design of the MMIC version of the mixer and is currently under course.

CONCLUSIONS

The designs and performances of hybrid and monolithic technology active mixer and amplifiers have been described. These are the two main building blocks needed in mmW receiving systems, and have been designed with good electrical features, small dimensions and low cost, and are easily integrable with lower frequency circuits.